PNNL-14850

Pacific Northwest
National Laboratory
Operated by Battelle for the
U.S. Department of Energy

Effects of Hyporheic Exchange Flows on Egg Pocket Water Temperature in Snake River Fall Chinook Salmon Spawning Areas

T. P. Hanrahan
D. R. Geist
E. V. Arntzen
C. S. Abernethy

September 2004

Prepared for the U.S. Department of Energy
under Contract DE-AC06-76RL01830

DISCLAIMER

PACIFIC NORTHWEST NATIONAL LABORATORY
operated by
BATTELLE
for the
UNITED STATES DEPARTMENT OF ENERGY
under Contract DE-AC06-76RL01830

PNNL-14850

Effects of Hyporheic Exchange Flows on Egg Pocket Water Temperature in Snake River Fall Chinook Salmon Spawning Areas

T. P. Hanrahan E. V. Arntzen
D. R. Geist C. S. Abernethy

September 2004

Prepared for
Bonneville Power Administration
Portland, Oregon
BPA Project No. 2002-078-00
BPA Contract No. 00000652-00023
under a Related Services Agreement with
the U.S. Department of Energy
under Contract DE-AC06-76RL01830

Cost-shared by

IDAHO POWER
An IDACORP Company
Boise, ID

and

U.S. Department of Energy
Energy Efficiency and Renewable Energy

Wind and Hydropower Technologies

Bringing you a prosperous future where energy is clean, abundant, reliable, and affordable

Washington, DC

Pacific Northwest National Laboratory
Richland, Washington 99352

Summary

The development of the Snake River hydroelectric system has affected fall Chinook salmon smolts by shifting their migration timing to a period (mid- to late-summer) when downstream reservoir conditions are unfavorable for survival. Subsequent to the Snake River Chinook salmon fall-run Evolutionary Significant Unit being listed as Threatened under the Endangered Species Act, recovery planning has included changes in hydrosystem operations (e.g., summer flow augmentation) to improve water temperature and flow conditions during the juvenile Chinook salmon summer migration period. In light of the limited water supplies from the Dworshak reservoir for summer flow augmentation, and the associated uncertainties regarding benefits to migrating fall Chinook salmon smolts, additional approaches for improved smolt survival need to be evaluated.

This report describes research conducted by the Pacific Northwest National Laboratory (PNNL) that evaluated relationships among river discharge, hyporheic zone characteristics, and egg pocket water temperature in Snake River fall Chinook salmon spawning areas. This was a pilot-scale study to evaluate these relationships under existing operations of Hells Canyon Dam (i.e., without any prescribed manipulations of river discharge) during the 2002–2003 water year. The project was initiated in the context of examining the potential for improving juvenile Snake River fall Chinook salmon survival by modifying the discharge operations of Hells Canyon Dam. The potential for improved survival would be gained by increasing the rate at which early life history events proceed (i.e., incubation and emergence), thereby allowing smolts to migrate through downstream reservoirs during early- to mid-summer when river conditions are more favorable for survival.

PNNL implemented this research project at index sites throughout 160 km of the Hells Canyon Reach (HCR) of the Snake River. The HCR extends from Hells Canyon Dam (river kilometer [rkm] 399) downstream to the upper end of Lower Granite Reservoir near rkm 240. We randomly selected 14 fall Chinook salmon spawning locations as study sites, which represents 25% of the most used spawning areas throughout the HCR. Interactions between river water and pore water within the riverbed (i.e., hyporheic zone) at each site were quantified through the use of self-contained temperature and water level data loggers suspended inside of piezometers. Surrounding the piezometer cluster at each site were 3 artificial egg pockets. In mid-November 2002, early-eyed stage fall Chinook salmon eggs were placed inside of perforated polyvinyl chloride (PVC) tubes, along with a temperature data logger, and buried within the egg pockets. Fall Chinook salmon eggs were also incubated in the laboratory for the purpose of developing growth curves that could be used as indicators of emergence timing. The effects of discharge on vertical hydrologic exchange between the river and riverbed were inferred from measured temperature gradients between the river and riverbed, and the application of a numerical model.

The hydrologic regime during the 2002–2003 sampling period exhibited one of the lowest, most stable daily discharge patterns of any of the previous 12 water years. The vertical hydraulic gradients (VHG) between the river and the riverbed suggested the potential for predominantly small magnitude vertical exchange. The VHG also showed little relationship to changes in river discharge at most sites. Despite the relatively small vertical hydraulic gradients at most sites, results from the numerical modeling of riverbed pore water velocity and hyporheic zone temperatures suggested that there was significant

vertical hydrologic exchange during all time periods. The combined results of temperature monitoring and numerical modeling indicate that only 2 of 14 sites were significantly affected by short-term (hourly to daily) large magnitude changes in discharge. Although the two sites exhibited acute flux reversals between river water and hyporheic water resulting from short-term large magnitude changes in discharge, these flux reversals had minimal effect on emergence timing estimates. Indeed, the emergence timing estimates at all sites were largely unaffected by the changes in river stage resulting from hydropower operations at Hells Canyon Dam. Our results indicate that the range of emergence timing estimates due to differences among the eggs from different females can be as large as or larger than the emergence timing estimates due to site differences (i.e., bed temperatures among sites).

We conclude that during the 2002–2003 fall Chinook salmon incubation period, hydropower operations of Hells Canyon Dam had an insignificant effect on fry emergence timing at the study sites. It appears that short-term (i.e., hourly to daily) manipulations of discharge from the Hells Canyon Complex during the incubation period would not substantially alter egg pocket incubation temperatures, and thus would not affect fry emergence timing at the study sites. However, the use of hydropower operational manipulations at the Hells Canyon Complex to accelerate egg incubation and fry emergence should not be ruled out on the basis of only one water year's worth of study. Further investigation of the incubation environment of Snake River fall Chinook salmon is warranted based on the complexity of hyporheic zone characteristics and the variability of surface – subsurface interactions among dry, normal, and wet water years.

Acknowledgments

This project was funded by the Bonneville Power Administration (BPA) under the Northwest Power and Conservation Council's Fish and Wildlife Program solicitation for Innovative Projects during calendar year 2002. We thank BPA staff Bill Maslen and Tracy Noice for their involvement and oversight of this project.

Co-funding was provided by the Idaho Power Company. We wish to extend our gratitude to the Idaho Power Company and its staff for their cooperation and collaboration on the research project. Those staff deserving special thanks include Brad Alcorn, Mike Butler, Jim Chandler, Phil Groves, and Tim Stuart. Without the cooperation of these staff, and the Idaho Power Company in general, this project would have been very difficult to implement.

Additional funding was provided by the U.S. Department of Energy's Advanced Hydropower Program. We would like to express our gratitude to Dennis Dauble (PNNL) for his guidance of this research project on behalf of the Hydropower Program. We also thank additional PNNL staff for assisting with this study, especially Kate Deters, Kris Hand, and Fenton Khan.

Additional thanks go to the Washington Department of Fish and Wildlife and the staff at Lyons Ferry Hatchery for providing us with fall Chinook salmon eggs. Their cooperation and accommodation with our study plans was appreciated.

Contents

Figures

Tables

1.0 Introduction

Prior to the construction of the Hells Canyon Complex of dams on the Snake River, fall Chinook salmon (*Oncorhynchus tshawytscha*) migrated to their primary production areas between Marsing, Idaho, and Swan Falls, Idaho, approximately 300 river kilometers (rkm) upstream of the present spawning areas in Hells Canyon (Dauble et al. 2003). Current fall Chinook salmon spawning areas in the Snake River occur downstream of Hells Canyon Dam, which now is the upstream terminus for anadromous fish migration in the Snake River Basin. The historic spawning areas contained different water temperature regimes than the present spawning areas. Consequently, water temperatures during the egg incubation period (~December–May) may have been relatively warmer in the historic production areas than in the current spawning areas. This difference in temperature regimes may be the reason that fall Chinook salmon from current production areas in the Hells Canyon Reach arrive at the Lower Granite Dam section of the Snake River 1 to 4 weeks later than they did before development of the Hells Canyon Complex and the four lower Snake River projects operated by the U.S. Army Corps of Engineers (NMFS 2000a; Connor et al. 2001).

The shift toward later emergence and migration requires smolts to migrate through downstream reservoirs during mid- to late-summer when environmental conditions are unfavorable for survival (Connor et al. 2001). The differential survival among cohorts of wild Snake River subyearling juvenile Chinook can be traced back to emergence timing, with earlier emerging fish migrating earlier through Lower Granite Reservoir under conditions of higher flows and cooler water temperatures than later emerging fish (Connor 1999). Later migration puts juvenile migrants in reservoirs during periods when water temperatures approach Chinook salmon's thermal tolerance (NMFS 2000a). The delay also places late arriving fall Chinook in unsuitable reservoir environments, and may increase their susceptibility to predation.

Subsequent to the Snake River Chinook salmon fall-run Evolutionary Significant Unit being listed as Threatened under the Endangered Species Act (NMFS 1992), recovery planning has included changes in hydrosystem operations to improve water temperature and flow conditions during the juvenile Chinook salmon summer migration period (NMFS 2000b). One such measure (summer flow augmentation) involves releasing water during mid-June to late-August from the reservoir created by Dworshak Dam on the North Fork of the Clearwater River to increase flow and decrease water temperature in the lower Snake River reservoirs. The volume of water available for summer flow augmentation is very limited, which results in an interagency management team meeting weekly in mid- to late-summer to plan the most effective distribution of water during the late-summer migration period. In addition to concerns over limited water availability for flow augmentation, there are concerns within the scientific community regarding the effectiveness of summer flow augmentation for survival of fall Chinook salmon smolts. Much of the uncertainty is focused on the relationships between increased flows and migration travel times of subyearling Chinook salmon smolts (Berggren and Filardo 1993; Giorgi et al. 1997; Dreher 2000), and the risks associated with migration timing, such as thermally induced mortality (Connor et al. 1998). Because of the difficulty in obtaining flows to augment flow and reduce water temperature, more information is needed on measures that could facilitate earlier movement of fish from the production areas to Lower Granite Dam.

Recent research in the Hells Canyon Reach of the Snake River indicates that warm hyporheic water upwells into fall Chinook salmon spawning areas (Geist et al. 1999; Arntzen et al. 2001). The magnitude and duration of hyporheic water upwelling into these fall Chinook salmon spawning areas is inversely related to discharge from Hells Canyon Dam. During the October – December period when flows are held stable to allow fall Chinook salmon to spawn, the water temperature of the hyporheic zone is up to 2°C warmer than the river water, and hydraulic gradients suggest upwelling potential into the river channel. Under current operations by Idaho Power Company (IPC) and beginning in mid-October, the discharge from Hells Canyon Dam is lowered and daily fluctuations are minimized to benefit spawning fall Chinook salmon within the mainstem Snake River. As discharge decreases, the magnitude of hyporheic upwelling potential at these areas increases (Geist et al. 1999). The period of low, stable discharge from Hells Canyon Dam terminates at the end of the fall Chinook spawning period and the discharge pattern reverts to those of prior operations (i.e., large, variable discharge caused by power-peaking operations). By early December (i.e., early in the egg incubation period), the upwelling hyporheic water was 2°C warmer than the river water (Geist et al. 1999). It is likely that as incubation progresses into February and March, the difference in temperature between the hyporheic zone and the river becomes greater than 2°C. However, there are currently no empirical data quantifying the surface water–ground water interactions occurring during the fall Chinook salmon incubation and emergence periods within Hells Canyon, and thus no way to substantiate this hypothesis.

Resolution of this hypothesis has major implications for juvenile salmon survival in the Snake River system. This is because the survival of downstream migrants ultimately depends upon when they emerge, and the emergence timing is directly related to the temperature at which the eggs are incubated. For all species of Pacific salmon, there is an inverse relationship between temperature and time to hatching and emergence (Weatherly and Gill 1995). Where warm hyporheic water is upwelling into spawning areas within Hells Canyon, it is possible that emergence may occur 2–4 weeks earlier than in spawning areas dominated by cooler surface water. Temperature data from one spawning area in winter 2001 indicates that 19 consecutive days of low and steady discharge from Hells Canyon Dam would result in 50% fry emergence (based on 1140 accumulated temperature units at 6°C) occurring 14 days earlier for eggs incubating in upwelling hyporheic water versus those incubating in egg pockets dominated by cooler surface water (TP Hanrahan, unpublished data). However, because of the current operations of Hells Canyon Dam, these warmer water temperatures within the egg pocket are likely not realized. As the Hells Canyon Dam discharge pattern reverts to that of the pre-fall Chinook spawning period, the magnitude of hyporheic upwelling decreases in response to the increased discharge, likely causing the cooler river water to reduce egg pocket temperatures.

We hypothesize that flows from Hells Canyon Dam could be manipulated to accelerate egg incubation and fry emergence, thereby shifting the smolt emigration from the Hells Canyon Reach to a period when downstream reservoir water temperatures are more conducive to survival. Earlier emergence would presumably result in fish migrating downstream earlier, arriving at Lower Granite Dam earlier than currently observed. This would reduce the need to rely on summer flow augmentation to move fish downstream.

The objective of this study was to evaluate the relationships among river discharge, hyporheic zone characteristics, and egg pocket water temperature in Snake River fall Chinook salmon spawning areas

during a period extending through the spawning and incubation periods. This was a pilot-scale study to evaluate these relationships under existing operations of Hells Canyon Dam (i.e., without any prescribed manipulations of river discharge). Specific research hypotheses were 1) water temperature at egg pocket depth (20–50 cm) and deeper within the hyporheic zone (100+ cm) is warmer than the river water during the spawning and incubation periods, and 2) the vertical hydrologic exchange between the river and the hyporheic zone is inversely related to river discharge.

2.0 Methods

2.1 Study Area

This research was conducted throughout 160 km of the Hells Canyon Reach (HCR) of the Snake River. The HCR extends from Hells Canyon Dam (river kilometer [rkm] 399) downstream to the upper end of Lower Granite Reservoir near rkm 240. This reach of the Snake River is narrowly confined by valley walls, and is generally controlled by large-scale geologic and geomorphic controls, resulting in a lack of floodplain development. The upper section of the HCR (rkm 399–306) is situated in a deep and narrow gorge entrenched in erosion-resistant basalt and metamorphic bedrock. Although when viewed in planform the HCR exhibits a meandering course, geomorphically it is a straight or slightly sinuous river. The river possesses the characteristics of passive meandering, where the planform pattern is imposed by the local landform. While large alluvial terraces exist along the river, they are remnant deposits of the Pleistocene Lake Bonneville Floods, and are located tens of meters above contemporary flood stages (O'Connor 1993). Alluvial deposits within the bankfull channel from these and other flood events are actively reworked by the contemporary flow regime, resulting in a longitudinal pool-riffle bedform morphology, despite the valley confinement. Due to the lack of floodplain development, interactions between the river and its banks are limited to small lateral bars, terraces, and fans inundated by contemporary flow regimes. The lower HCR (rkm 306–240) exhibits more floodplain development than the upper HCR, owing mostly to a geologic fault zone near rkm 306 and the influence from three major tributaries – the Imnaha River at rkm 307, the Salmon River at rkm 300 and the Grande Ronde River at rkm 269. However, even the lower HCR is considered narrowly confined within the valley walls.

The Hells Canyon Complex (Hells Canyon, Oxbow, and Brownlee dams) controls nearly all of the flow through the upper HCR, and just over 50% of the flow in the lower HCR. Immediately downstream from Hells Canyon Dam at U.S. Geological Survey (USGS) gage 13290450, mean daily discharge has averaged 589 m^3/s since 1965. Over this same time period, mean daily discharge in the lower HCR has averaged 1035 m^3/s (USGS gage 13334300, rkm 269). Inputs from the Imnaha, Salmon, and Grande Ronde rivers (USGS gages 13292000, 13317000, and 13333000, respectively) during this period make up a mean daily discharge of 426 m^3/s, resulting in a residual input of approximately 20 m^3/s from tributaries between Hells Canyon Dam (rkm 399) and the Imnaha River confluence (rkm 307). From mid-October to early-December, the Hells Canyon Complex maintains low and stable hourly discharges (e.g., 255 m^3/s) for the benefit of spawning fall Chinook salmon. During the remainder of the year, power peaking operations cause large daily fluctuations in discharge (240–800 m^3/s), resulting in stage changes of over 2.0 m in the upper HCR.

Study sites were selected by stratified random sampling of fall Chinook salmon spawning locations. The HCR was stratified into three segments based on longitudinal valley slope and the confluence with major tributaries. The upper segment extends from Hells Canyon Dam (rkm 399) downstream to a fault zone near Pine Bar (rkm 364), and has a longitudinal slope of 0.002. The middle and lower segments are separated just downstream of the Salmon River confluence (near rkm 298), where the longitudinal gradient changes from 0.001 (middle segment) to 0.0007 (lower segment). Fall Chinook salmon redd counts from 1997 to 2001 were used to identify the 56 most used spawning sites. Of the 56 spawning

sites, 20% were in the upper segment, 48% in the middle segment, and 32% in the lower segment. Fourteen study sites (25% of the total) were randomly selected, with the number in each segment corresponding to the proportion of spawning sites within each segment (Table 1, Figure 1).

Table 1. Hells Canyon Study Sites

River mile[1]	River kilometer	Segment
148.5	239.0	lower
149.2	240.1	lower
152.3	145.3	lower
156.8	252.5	lower
196.0	315.4	middle
198.2	319.0	middle
198.8	319.9	middle
211.9	341.0	middle
218.7	351.8	middle
219.3	352.9	middle
222.7	358.4	middle
238.6	384.0	upper
240.6	387.2	upper
244.5	393.5	upper

[1.] River mile numbers will be used as site identifiers throughout this report.

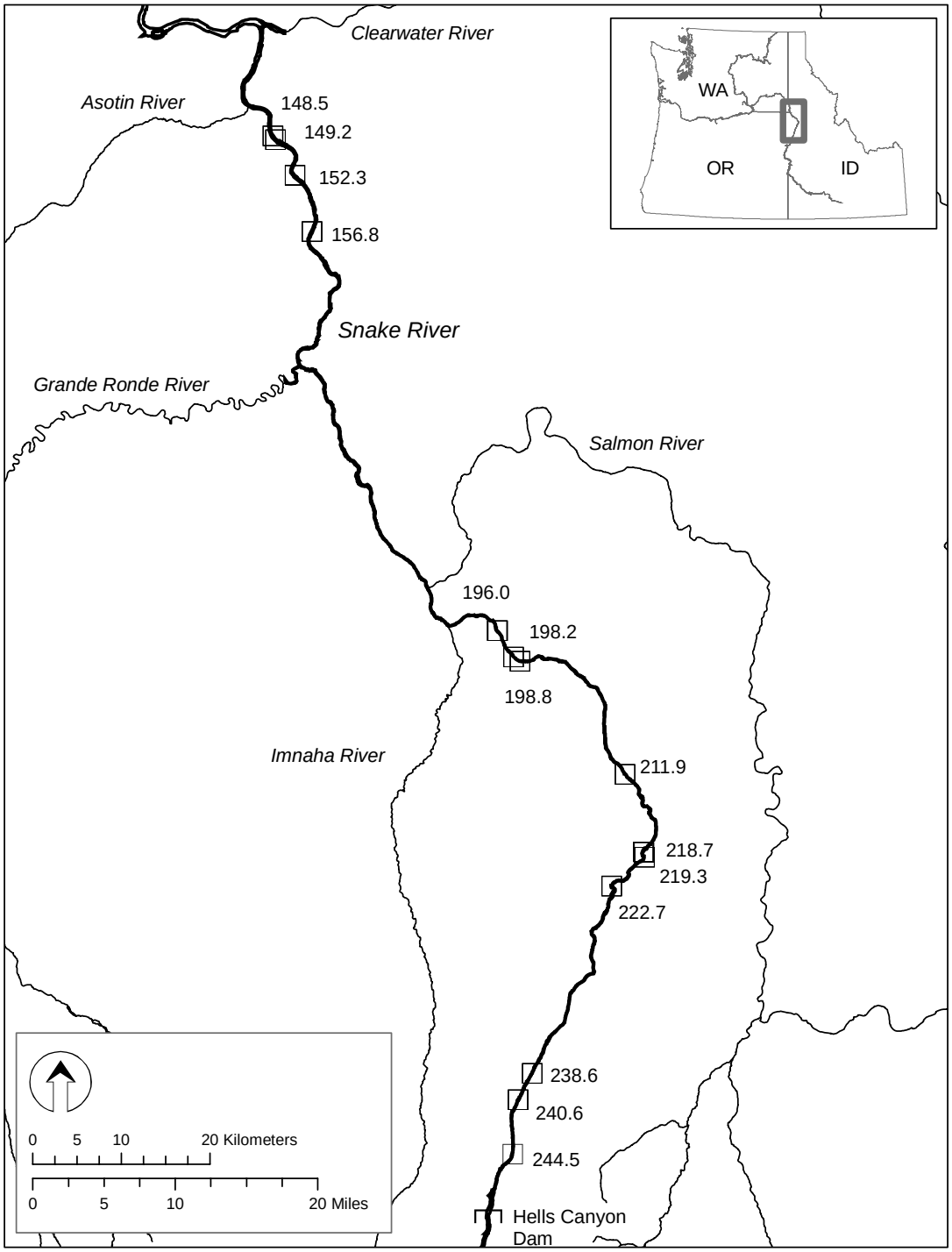

Figure 1. The study area extended from Hells Canyon Dam downstream to near the confluence with the Asotin River. Study sites (□) are identified by their river mile location.

2.2 Site-Scale Study Design

Interactions between ground water and surface water at each site were quantified through the use of self-contained temperature and water level data loggers suspended inside of piezometers. Each site contained one cluster of two piezometers and one river standpipe spaced within 1.0 m of one another. One piezometer monitored egg pocket depths (20–50 cm) while the other monitored the deeper hyporheic zone (50+ cm). Each piezometer consisted of a 31.0 cm length of well screen with a 3.2 cm inside diameter. The screen was welded on one end to a 12.0 cm solid drive point and welded on the other end to a variable length section of unscreened stainless steel pipe. The river standpipe was constructed from an unscreened section of galvanized pipe threaded at one end onto a solid drive point and on the other end to an 18.0 cm section of PVC screen open to the river. The piezometers were driven into the riverbed until the top of one piezometer screen reached approximately 30.0 cm below the riverbed surface (average 30.5 cm) and the other piezometer screen reached approximately 60.0 cm below the riverbed surface (average 60.4 cm) (Table 2). The river standpipe was driven into the riverbed until the top of the PVC screen was approximately 20.0 cm above the riverbed surface (average 20.9 cm). The elevations of the piezometers and the standpipe were surveyed relative to local arbitrary benchmarks using differential leveling. Relative elevations were surveyed from multiple stations until the differences among the results from three stations did not exceed 0.2 cm.

Data loggers were suspended inside the pipes by non-stretch stainless steel cable attached to a water-tight cap at the top of the pipe. The temperature and pressure sensor end of the data loggers was placed near the top of the piezometer screens, just above the riverbed surface inside the river standpipe. Data loggers were programmed to record temperature and absolute pressure (cm of water) every 20 min. Four additional data loggers were distributed throughout the entire study area to record atmospheric pressure at the same time intervals. Atmospheric pressure was subtracted from the absolute pressure readings in the piezometers to determine the gage pressure (cm of water) due to river stage changes every 20 min. According to calibration certificates provided by the data logger manufacturer, the instruments are accurate to ±0.1 °C and ±0.7 cm of water. The data loggers were deployed in October 2002 and retrieved in March 2003.

Surrounding the piezometer cluster at each site were three artificial egg pockets spaced 3–5 m apart. Each egg pocket was dug within a 1.0 m diameter PVC standardizing template using a hydraulic pump and hand tools. Egg pockets were excavated until the bottom of the egg pocket was approximately 25.0 cm (average 23.0 cm) beneath the riverbed surface (Table 2), which is within the range (19–37 cm) of Chinook salmon egg pocket depths in the Columbia River (Chapman 1988). In mid-November 2002, 50 early-eyed (315 accumulated temperature units (ATU) °C, where ATU is the sum of the daily average temperatures exceeding 0°C) Chinook salmon eggs were placed inside a perforated PVC tube (30.0 cm length x 3.2 cm i.d.) and buried within the egg pocket. Each egg pocket contained 1 tube with 50 eggs from one of three females. Thus, each site contained the eggs of three different females. Temperature data loggers were place inside of each egg tube, and were programmed to record at the same 20 min time interval as the data loggers inside the piezometers. According to calibration certificates provided by the temperature data logger manufacturer, the instruments are accurate to ±0.17°C. The egg tubes were

retrieved early in the estimated emergence period (late-February–early-March) and the alevins and dead eggs were counted. The contents of each tube were placed in 5% neutral buffered formalin (NBF) and returned to the laboratory for analysis.

Table 2. Summary of distances beneath the riverbed surface to the top of the piezometer screens in the hyporheic zone, and to the bottom of the artificial egg pockets. Egg pocket depths represent the average depth of three artificial egg pockets at each site.

Site	Artificial egg pockets Depth (cm)	Shallow hyporheic zone Depth (cm)	Deep hyporheic zone Depth (cm)
148.5	22.0	29.0	59.0
149.2	22.7	28.0	61.0
152.3	24.0	37.0	70.0
156.8	23.0	30.0	55.0
196.0	21.0	31.0	63.0
198.2	22.7	30.0	59.0
198.8	23.3	31.0	62.0
211.9	22.0	29.0	60.0
218.7	24.7	25.0	54.0
219.3	24.3	33.0	63.0
222.7	22.0	32.0	61.0
238.6	21.3	30.0	58.0
240.6	26.3	32.0	60.0
244.5	27.3	30.0	60.0

2.3 Laboratory Analysis

Fall Chinook salmon eggs were incubated in the laboratory for the purpose of developing growth curves that could be used as indicators of emergence timing (e.g., ATU at maximum alevin wet weight). One-hundred early-eyed stage (315 ATU) eggs from each of the three females used for the egg tubes were returned to the laboratory. An additional one-hundred early-eyed stage (315 ATU) eggs from each of three additional females were also taken to the laboratory. The eggs from each of the six females were placed into partitioned incubation trays that were floating in recirculating tanks. Two tanks were used, with each tank containing the eggs from three females. Fifty eggs from each female were immediately sampled for egg mass and diameter, and then returned to the incubation trays. The initial temperature of each incubation tank was set at approximately 10°C. The temperature regime during the incubation period followed one of two patterns. One tank followed a 10 y (1991–2000) average surface water temperature within the Hells Canyon reach of the Snake River, while the other tank followed a 10 y (1991–2000) average surface water temperature within the Swan Falls reach of the Snake River (Idaho

Power Company, unpublished data). Temperature within the incubation tanks was logged in 20 min intervals with an instrument accurate to ±0.17°C.

Embryos and alevins were sampled at periodic intervals from 18 November 2002 until 9 April 2003. The sample frequency was adjusted to account for the rate at which development progressed with the sampling occurring approximately every 1 to 2 weeks for a total of 11 samples. At each sampling, five embryos or alevins (depending on development) were randomly removed from each female's lot, euthanized (if necessary), measured for length (nearest mm) and mass (nearest mg), photographed, and preserved in 5% neutral buffered formalin. The samples were preserved for at least 80 days to ensure that tissue weights stabilized. The samples were then individually re-measured to the nearest 1.0 mm with calipers. Weights were taken by blotting excess moisture and weighing the entire group (n=5 alevins) to the nearest 1.0 mg. The yolk and tissue were separated by dissection, dried in an oven at 60°C for 2 d, and then reweighed to the nearest 1.0 mg.

2.4 Data Analysis

The hydrologic regime during the study period was summarized using daily mean discharge values from just downstream from Hells Canyon Dam (USGS gage 13290450). Exceedence probabilities were calculated for the daily mean discharge values that were exceeded 10%, 50%, and 90% of the time (Q10/Q50/Q90). Discharge values from the study period were compared with the 12 previous water years.

The vertical hydraulic gradient (VHG) at each site was determined from the gage pressure readings as

$$\mathrm{VHG} = \frac{dh}{L} \tag{1}$$

where *dh* is the hydraulic head (cm) inside the piezometer minus the hydraulic head (cm) of the river, and *L* is the distance (cm) from the top of the piezometer screen to the riverbed surface. The VHG represents a potential for upwelling from the hyporheic zone (positive VHG) or downwelling into the hyporheic zone (negative VHG). Analyses of hydraulic gradients between the river and riverbed were primarily based on *dh* values. The *dh* values were used so that hydraulic gradients could be evaluated relative to the uncertainty error of the instruments (±1.4 cm), which does not vary over the range of depths for which they were used in this study. Differences in mean *dh* among sites and time period (spawning, early incubation, late incubation) were evaluated through one-way analysis of variance. Differences in mean *dh* between individual sites were identified using Tukey's HSD post-hoc multiple comparison test.

The effects of discharge on vertical hydrologic exchange between the river and riverbed were evaluated through measured temperature gradients between the river and riverbed, and the application of a numerical model. Lapham (1989) presented an explicit finite-difference approximation to Stallman's

(1965) equation describing the steady, one-dimensional, vertical flow of fluid and heat through homogenous, porous media. We used Lapham's equation as

$$T_{i,n+1} = \frac{k\Delta t}{\rho c \Delta z^2}\left(1 + \frac{\rho_w c_w v_z \Delta z}{2k}\right)T_{i-1,n} + \frac{k\Delta t}{\rho c \Delta z^2}\left(1 - \frac{\rho_w c_w v_z \Delta z}{2k}\right)T_{i+1,n} + \left(1 - \frac{2k\Delta t}{\rho c \Delta z^2}\right)T_{i,n} \qquad (2)$$

where

$T_{i,n+1}$ = temperature at node i (shallow hyporheic zone) at time step n+1
$T_{i-1,n}$ = temperature at node i-1 (deep hyporheic zone) at time step n
$T_{i+1,n}$ = temperature at node i+1 (river) at time step n
$T_{i,n}$ = temperature at node i at time step n
Δt = time increment (s) between steps
Δz = spacing (cm) between nodes
k = thermal conductivity (cal s^{-1} cm °C) of the rock-fluid matrix
ρ = wet bulk density (g cm^{-3}) of the rock-water matrix
ρ_w = density of water (g cm^{-3})
c = volumetric heat capacity (cal cm^{-3} °C) of the rock-water matrix
c_w = volumetric heat capacity (cal cm^{-3} °C) of the water
v_z = vertical component of darcian water velocity (cm s^{-1})

At every 20-min time step, Equation (2) was used to estimate the temperature in the shallow hyporheic zone given the time-varying upper thermal boundary condition of the river temperature and the lower thermal boundary condition of the deep hyporheic zone temperature. The magnitude and direction of vertical flux (i.e., apparent darcy velocity v_z) between the river and the riverbed was determined by adjusting v_z until the model-simulated shallow hyporheic zone temperature matched the observed temperature at the same depth and over time. Because this model assumes that water flow occurs under steady-state conditions, the v_z value was not adjusted at every time step. Rather, the v_z was held constant for periods of days to weeks until there was a relatively large deviation between modeled and observed temperatures. At that point, v_z was adjusted until modeled temperatures again closely matched observed temperatures. The matching of modeled and observed temperature was done by trial-and-error, using time-series plots of the two temperatures and minimizing the mean absolute error (MAE) over time.

Model performance was evaluated using the MAE, which is the average prediction error taken as the average difference between predicted and actual values:

$$MAE = \frac{|m_1 - e_1| + |m_2 - e_2| + \ldots + |m_n - e_n|}{n} \qquad (3)$$

where m is model temperature value, e is empirical temperature value, and n is number of cases (time steps). The root mean-squared error (RMSE) was used to identify model runs where the average prediction error was especially large at some time steps. The RMSE was calculated as

$$RMSE = \sqrt{\frac{(m_1 - e_1)^2 + (m_2 - e_2)^2 + \ldots + (m_n - e_n)^2}{n}} \tag{4}$$

The application of Equation (2) required estimates of the physical and thermal properties of the riverbed materials. Estimates of the grain size distribution of the riverbed material were derived from the results of freeze coring at sites 152.3 and 222.7 (Arntzen et al. 2001), which represent the range of grain sizes at all the study sites. Characteristic particle sizes (d_i) from these distributions were a d_{10} range of 0.5–3.0 mm and a d_{60} range of 40.0–95.0 mm (where d_i is the grain size in mm at which i% of the sample is finer than). The porosity λ of the riverbed was estimated using the empirical relation (Schalchli 1995).

$$\lambda = 0.486 \cdot \left(\frac{d_{60}}{d_{10}} \right)^{-0.20} \tag{5}$$

Particle densities ρ_p ranging from 2.65 g cm^{-3} to 2.80 g cm^{-3} were used in the following relation to estimate dry bulk density ρ_b (Fetter 1994)

$$\lambda = 100 \left[1 - \left(\frac{\rho_b}{\rho_p} \right) \right] \tag{6}$$

The resulting dry bulk densities ranged from 2.01 g cm^{-3} to 2.23 g cm^{-3}. Using Figure 2 in Lapham (1989) these dry bulk densities correspond to thermal conductivity k values of 0.007–0.0088 cal s^{-1} cm °C and volumetric heat capacity c values of 0.53–0.56 cal cm^{-3} °C. Initial model runs were insensitive to this small range in k and c, so constant values were chosen. Because the k and c values in Lapham (1989) are based on empirical relationships with reconstituted mixtures of much smaller grain sizes (Lunardini 1981) than the present study, it was necessary to adjust the k and c values to correspond to a higher dry bulk density. The final values used for all model runs include k = 0.0112 cal s^{-1} cm °C, ρ = 2.9 g cm^{-3}, ρ_w = 1.0 g cm^{-3}, c = 0.51 cal cm^{-3} °C, and c_w = 1.0 cal cm^{-3} °C.

For those sites where the solution to Equation (2) resulted in large estimates of downward flux (positive v_z), the solutions were compared with those obtained from an alternative procedure. Stallman's (1965) equation describing the steady, one-dimensional, vertical flow of fluid and heat through homogenous, porous media can be approximated as a travel time model:

$$v_z = V_T \left(\frac{\rho \cdot c}{\rho_w \cdot c_w} \right) \tag{7}$$

where V_T is the measured vertical velocity of the temperature peak (Constantz and Thomas 1996). Application of Equation (7) requires meeting the assumption of nonisothermal, downward flow of water

into the streambed at a sufficient velocity such that conductive heat transport is negligible relative to advective heat transport. Thus, Equation (7) was only applied to the sites meeting this assumption.

Laboratory egg/alevin data were analyzed using analysis of variance at an alpha level of 0.05. Development index (kd) was calculated as described in Bams (1970). Relationships between growth metrics and time (days post-fertilization) were estimated by fitting the data to either a linear or polynomial regression. Maximum alevin wet weights (MAWW), maximum tissue weight (MTW), maximum fork length (MFL), and minimum Kd values were estimated by taking the first derivative of the various polynomial equations and solving for the maximum.

3.0 Results

3.1 Hydrologic Regime

The hydrologic regime during the 2002–2003 sampling period exhibited one of the lowest, most stable daily discharge patterns of any of the previous twelve water years (Figure 2). The median daily discharge (Q50) during this period was 310 m^3 s^{-1}, which was 210 m^3 s^{-1} lower (or 40% less) than the mean Q50 of the twelve previous water years (Table 3). The low, stable discharge that is provided for spawning fall Chinook salmon during the months of October and November extended approximately 35 days beyond the typical cessation period of those flows (Figure 2). The stability of the hydrologic regime during the 2002–2003 sampling period is indicated by the low range between the Q90 (low) and Q10 (high) discharges, resulting in a low slope of the cumulative probability plot (Figure 3).

The water depth of the river at each site showed little variation during the 2002–2003 spawning and early incubation periods, while much greater fluctuations were observed during the late incubation period (Figures 4 and 5). During the spawning period water depths fluctuated over an average range of 17.2 cm in the lower segment sites, 7.4 cm in the middle segment sites, and 11.7 cm in the upper segment sites (Table 4). The range of water depth fluctuations increased during the early incubation period, with an average range of 34.6 cm in the lower segment sites, 38.6 cm in the middle segment sites, and 43.3 cm in the upper segment sites. During the late incubation period water depths fluctuated over an average range of 143.1 cm in the lower segment sites, 150.8 cm in the middle segment sites, and 141.6 cm in the upper segment sites.

Table 3. Discharge (m^3 s^{-1}) for selected exceedence probabilities based on mean daily discharge in the Snake River near the study sites (USGS gage 13290450) during the period from 1 October to 1 May for the water years 1990—2003. The Q10/50/90 discharge represents the flow that was equaled or exceeded 10/50/90%, respectively, of the days during the period.

Water year	Q10	Q50	Q90
1990-91	433	297	224
1991-92	416	292	268
1992-93	915	314	260
1993-94	521	334	269
1994-95	716	467	261
1995-96	1603	702	273
1996-97	1710	1161	270
1997-98	895	733	343
1998-99	1407	753	271
1999-2000	841	595	351
2000-01	462	283	249
2001-02	586	309	248
2002-03	506	310	245

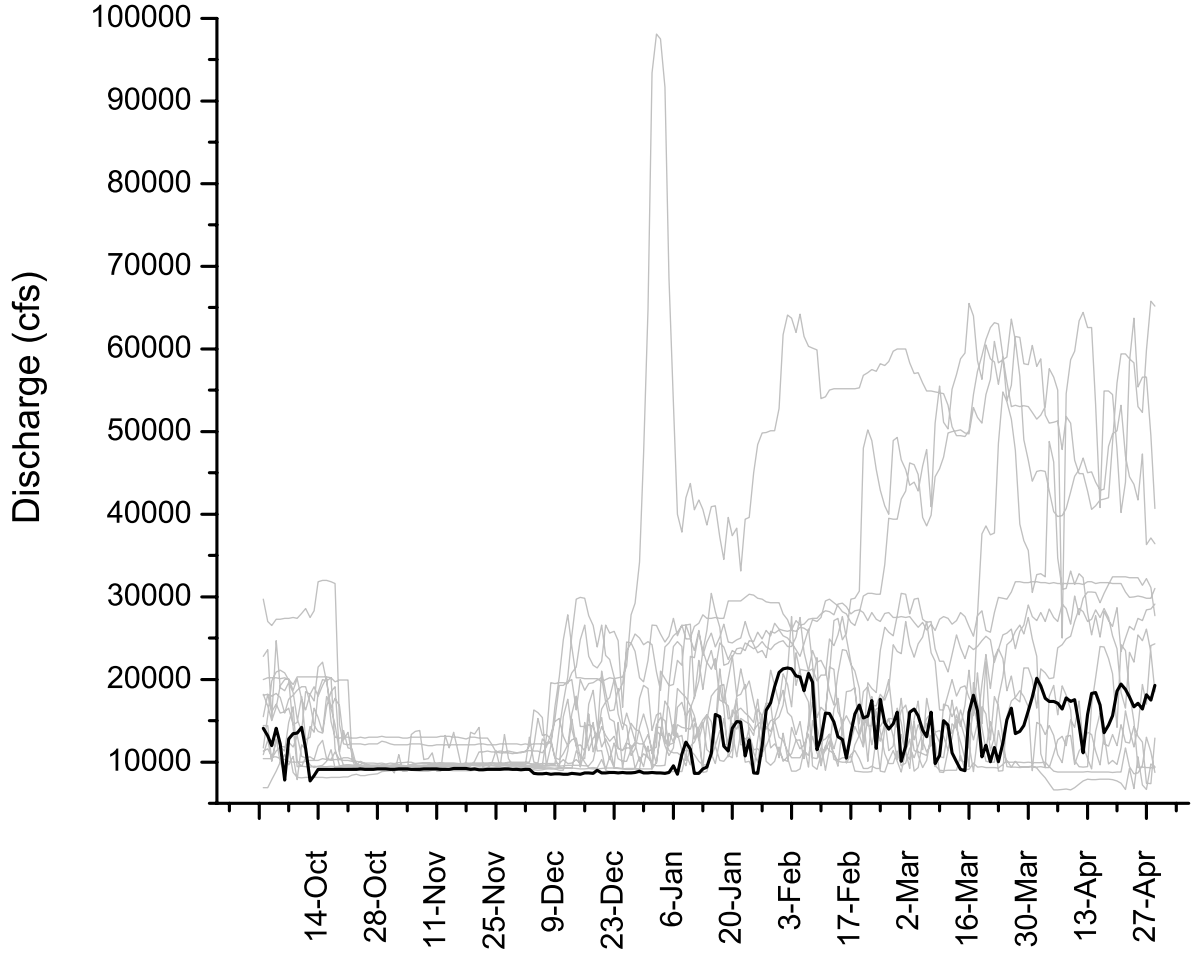

Figure 2. Mean daily discharge in the Snake River downstream from Hells Canyon Dam (USGS gage 13290450) during the period from 1 October to 1 May for the water years 1990–2003. Discharge during the sampling period (2002–2003) is shown as a solid black line, while all other water years are shown in gray. Time periods used in the analyses include the spawning period (20 October 2002 – 2 December 2002), the early incubation period with low, stable discharge (19 November 2002 – 7 January 2003), and the late incubation period with variable discharge (8 January – 2 March 2003).

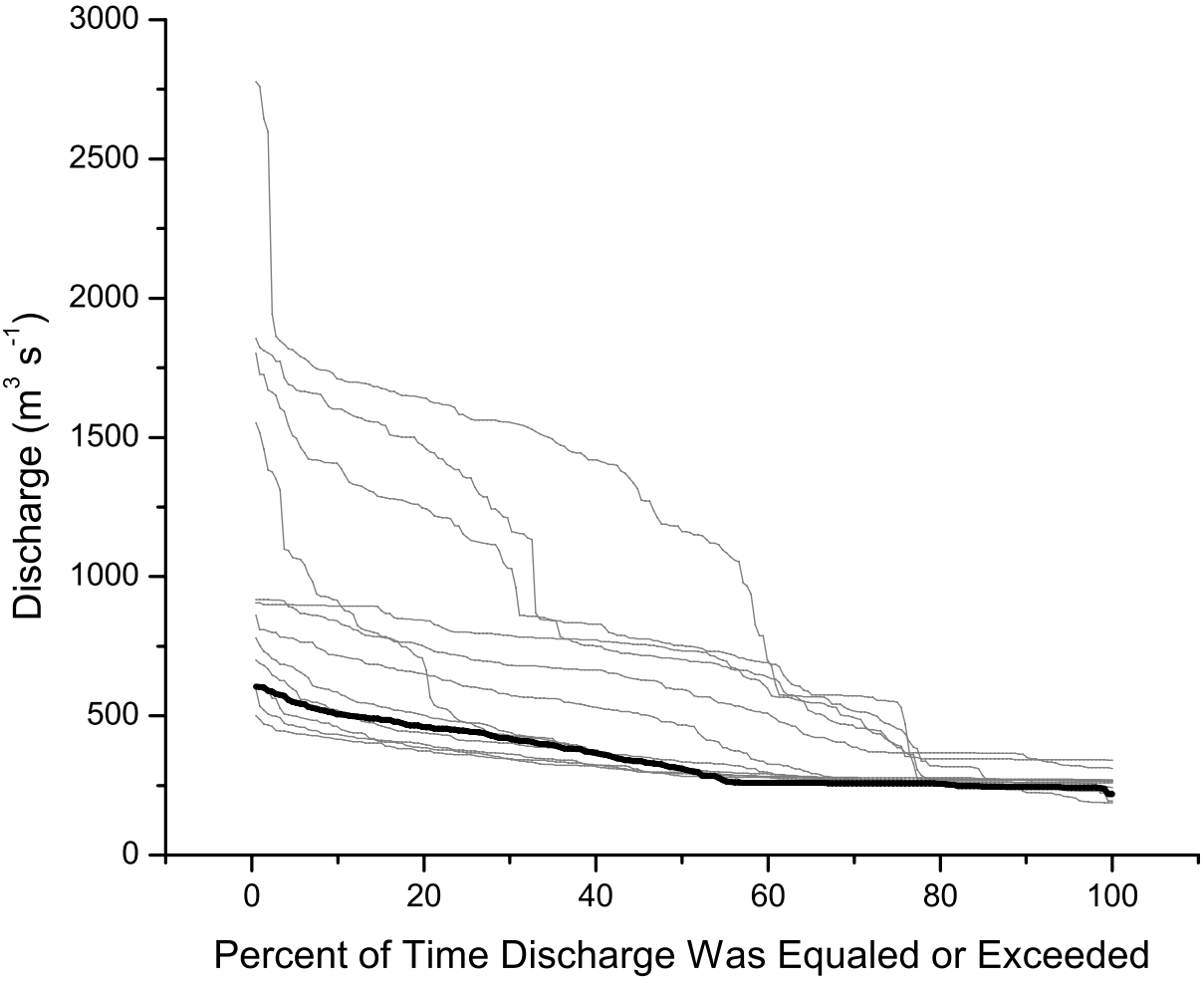

Figure 3. Complete duration series of mean daily discharge downstream from Hells Canyon Dam (USGS gage 13290450) during the period from 1 October to 1 May for the water years 1990–2003. The slope of each duration series is indicative of the variation in daily discharge during each time period, with a low slope indicating low variation. Discharge during the sampling period (2002–2003) is shown as a solid black line, while all other water years are shown in gray.

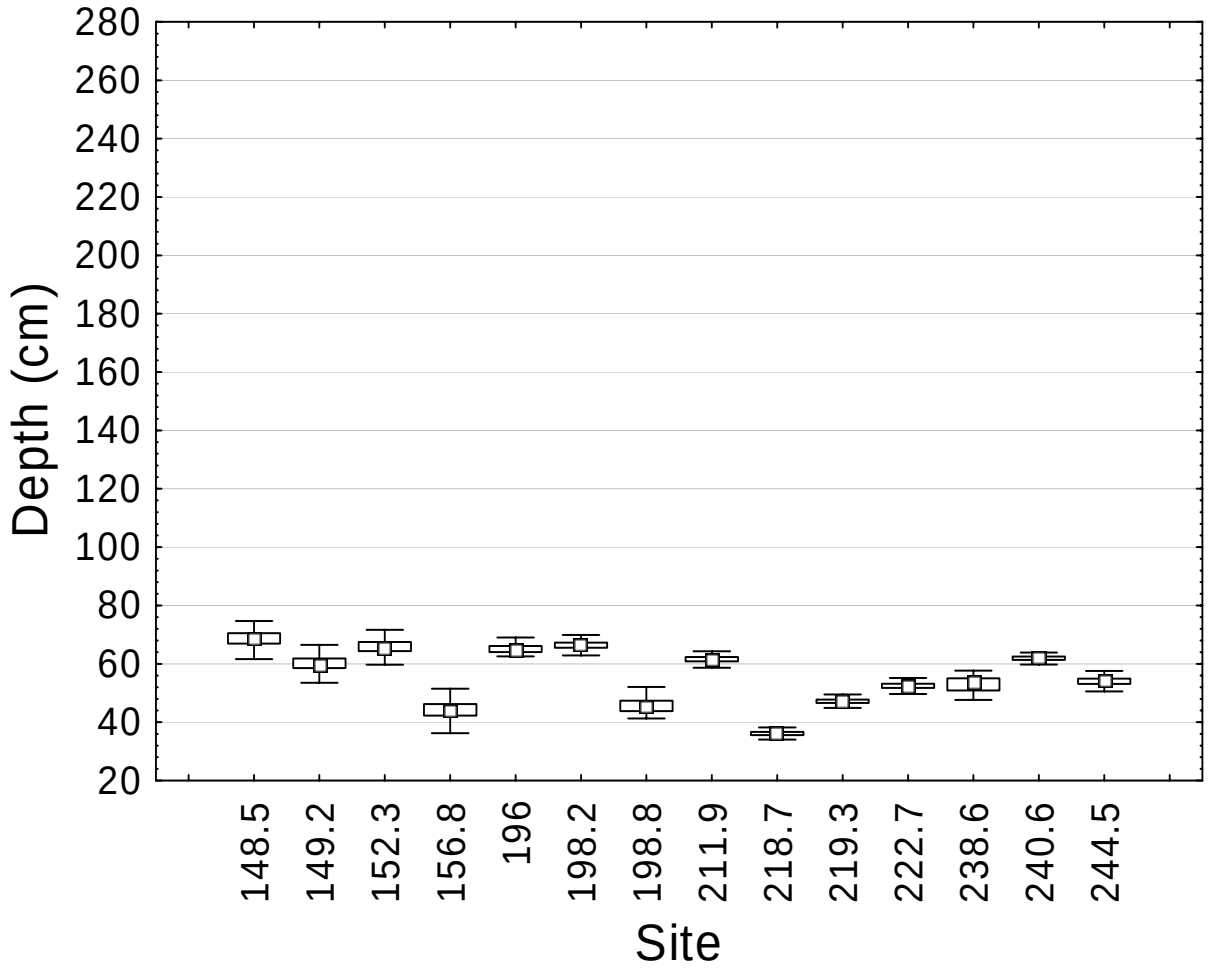

Figure 4. Water depth of the river (cm) at each site during the spawning period (20 October 2002 – 2 December 2002). Each boxplot represents a summary of hourly water depths. The point in the center of the boxplot indicates the median, the box is equal to the upper (75%) and lower (25%) quartile range, and the whiskers represent the range.

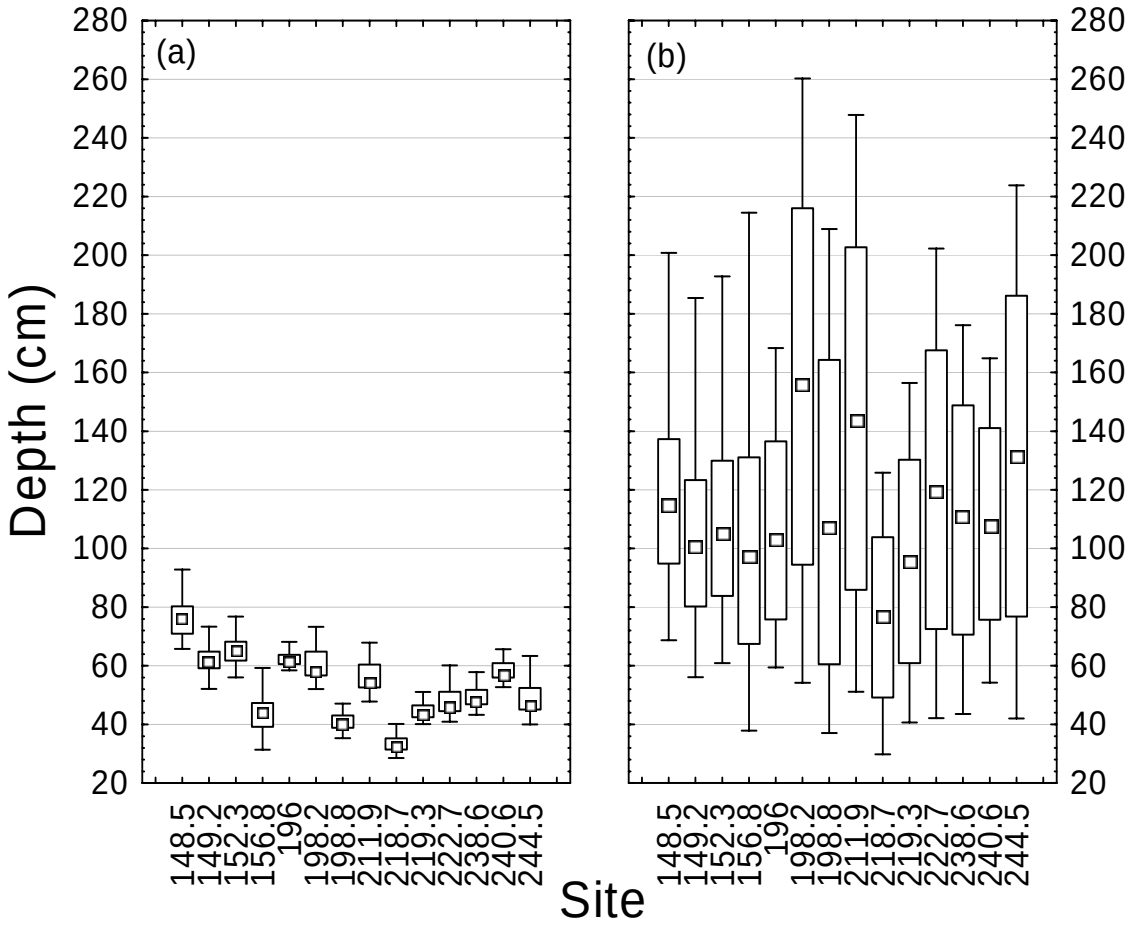

Figure 5. Water depth of the river (cm) at each site during (a) the incubation period with low, stable discharge (19 November 2002 – 7 January 2003), and (b) the incubation period with variable discharge (8 January – 2 March 2003). Each boxplot represents a summary of hourly water depths. The point in the center of the boxplot indicates the median, the box is equal to the upper (75%) and lower (25%) quartile range, and the whiskers represent the range.

Table 4. Summary of mean (± standard deviation) and range (maximum–minimum) of water depths (cm) at each site during the spawning period (20 October 2002–2 December 2002), the early incubation period with low, stable discharge (19 November 2002–7 January 2003), and the incubation period with variable discharge (8 January–2 March 2003).

		Water Depth (cm)					
		Spawning Period		Incubation Period, stable discharge		Incubation Period, variable discharge	
Segment	Site	Mean (±SD)	Range	Mean (±SD)	Range	Mean (±SD)	Range
lower	148.5	68.8 (3.7)	26.5	76.2 (6.2)	37.3	120.7 (33.6)	134.5
	149.2	59.9 (2.8)	13.5	62.0 (4.3)	33.4	106.0 (32.9)	129.3
	152.3	65.7 (2.4)	12.1	65.1 (4.2)	29.6	111.3 (34.4)	131.9
	156.8	44.0 (3.3)	16.6	43.4 (5.4)	38.1	105.2 (46.1)	176.6
middle	196.0	65.2 (1.4)	6.5	62.1 (2.2)	22.6	106.8 (34.7)	108.9
	198.2	66.4 (1.4)	10.1	60.2 (5.5)	56.2	154.9 (67.7)	206.0
	198.8	45.6 (2.0)	10.8	40.8 (3.1)	34.5	113.1 (56.4)	171.8
	211.9	61.6 (1.0)	6.4	56.0 (5.3)	54.5	144.9 (64.7)	196.7
	218.7	36.2 (0.8)	4.6	33.1 (2.8)	27.6	75.8 (30.7)	96.0
	219.3	47.2 (0.9)	6.4	44.3 (2.9)	30.0	95.5 (38.1)	115.8
	222.7	52.5 (1.1)	7.2	47.4 (4.5)	44.5	120.0 (52.6)	160.1
upper	238.6	53.2 (2.4)	21.2	49.3 (4.0)	45.2	108.7 (43.3)	132.6
	240.6	61.9 (0.8)	4.9	58.1 (3.4)	31.6	107.6 (36.5)	110.5
	244.5	54.0 (1.3)	9.0	48.4 (5.4)	52.9	130.2 (60.4)	181.8

3.2 Hydraulics

The hydraulic gradients between the river and the riverbed (shallow hyporheic zone) suggested the potential for predominantly small upwelling and downwelling vertical exchange. During the spawning and early incubation periods, 10 of the 14 sites had a mean hourly difference in head pressure (*dh* in cm; hyporheic - river) within a ±2.0 cm range. During the late incubation period, 9 of the 14 sites had a mean *dh* within a ±2.0 cm range (Figures 6 and 7). Within each site there was little change in mean *dh* between time periods. Between the spawning and early incubation periods the difference in mean *dh* was less than 1.0 cm at all sites, with an average change of 0.4 cm. Between the early and late incubation periods the difference in mean *dh* was less than 1.0 cm at 11 of the 14 sites, with an average change of 0.4 cm for those sites. Study sites 149.2, 156.8, and 198.8 exhibited a change in mean *dh* of 1.7 cm, 2.1 cm, and 1.5 cm, respectively, between the early and late incubation periods. While mean *dh* did not change much between time periods, the range in *dh* changed between the low, stable discharge period and the variable discharge period (Figure 7).

Each of the lower, middle, and upper segments of the study area included sites exhibiting both upwelling and downwelling potential. Sites within the lower segment had a mean *dh* ranging from -0.1 cm (±0.7 cm SD) to 1.6 cm (±0.4 cm SD) during the spawning period, from -0.9 cm (±0.6 cm SD) to 1.6 cm (±0.3 cm SD) during the early incubation period, and from -0.6 cm (±0.7 cm SD) to 3.2 cm (±0.9 cm SD) during the late incubation period (Figures 6 and 7). Within the middle segment, the range of mean *dh* among sites was much larger, ranging from -1.0 cm (±0.4 cm SD) to 4.7 cm (±0.5 cm SD) during the spawning period, from -1.5 cm (±0.7 cm SD) to 4.6 cm (±0.4 cm SD) during the early incubation period, and from -1.0 cm (±0.5 cm SD) to 4.7 cm (±0.8 cm SD) during the late incubation period (Figures 6 and 7). Sites within the upper segment also had a large range of mean *dh*, ranging from 0.3 cm (±0.7 cm SD) to 3.4 cm (±0.6 cm SD) during the spawning period, from 0.2 cm (±0.6 cm SD) to 3.7 cm (±0.6 cm SD) during the early incubation period, and from -0.3 cm (±1.6 cm SD) to 3.1 cm (±1.2 cm SD) during the late incubation period (Figures 6 and 7). Tests for differences in mean *dh* among all sites resulted in indications of significant differences for nearly all sites in all time periods (Tables 5 and 6). However, many of the differences in mean *dh* were less than 1.5 cm, which is approaching the pressure transducer uncertainty error of ±1.4 cm.

The vertical hydraulic gradients (VHG) between the river and shallow hyporheic zone, as well as between the river and deep hyporheic zone, showed little relationship to changes in river discharge at most sites. At the large temporal scale, most sites exhibited small effects of river discharge on VHG between the low, stable discharge periods (spawning and early incubation) and the variable discharge period (late incubation) (Figure 8). Sites 149.2, 156.8, and 198.8 indicated marked changes in shallow hyporheic zone VHG between the low, stable discharge periods and the variable discharge period. At all three sites, the upwelling potential increased. During the low, stable discharge periods, 12 of the 14 study sites indicated small upwelling potential between the river and deep hyporheic zone (Figure 8). As discharge increased and became more variable during the late incubation period, only site 156.8 showed a marked change (increase) in VHG between the river and deep hyporheic zone.

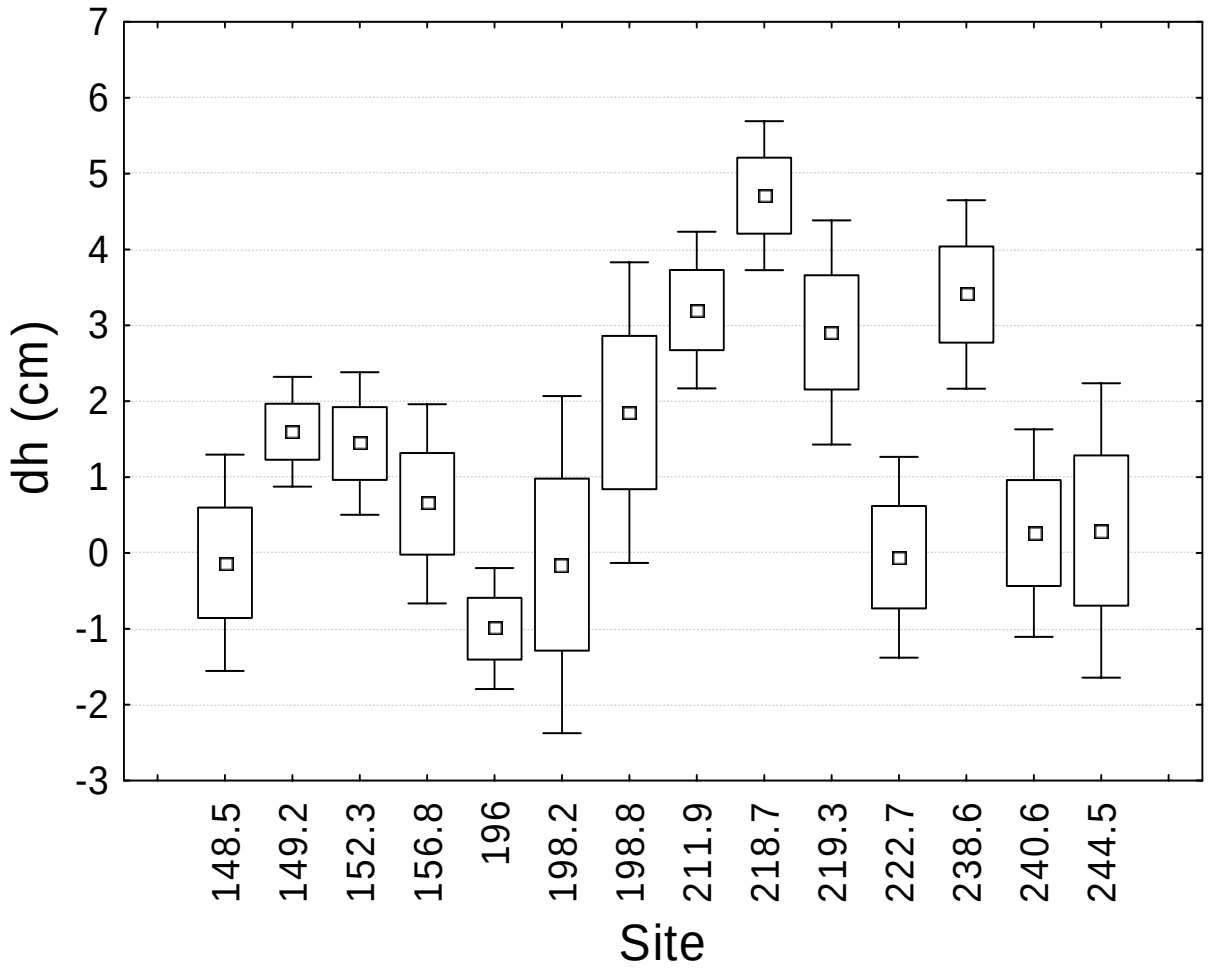

Figure 6. Difference in head pressure (*dh*; hyporheic head minus river head) at each site during the spawning period (20 October 2002 – 2 December 2002). Each boxplot represents a summary of hourly *dh* at each site. The point in the center of the boxplot indicates the mean, the box is equal to the mean ±1 standard deviation (SD), and the whiskers represent the mean ±1.96 × SD.

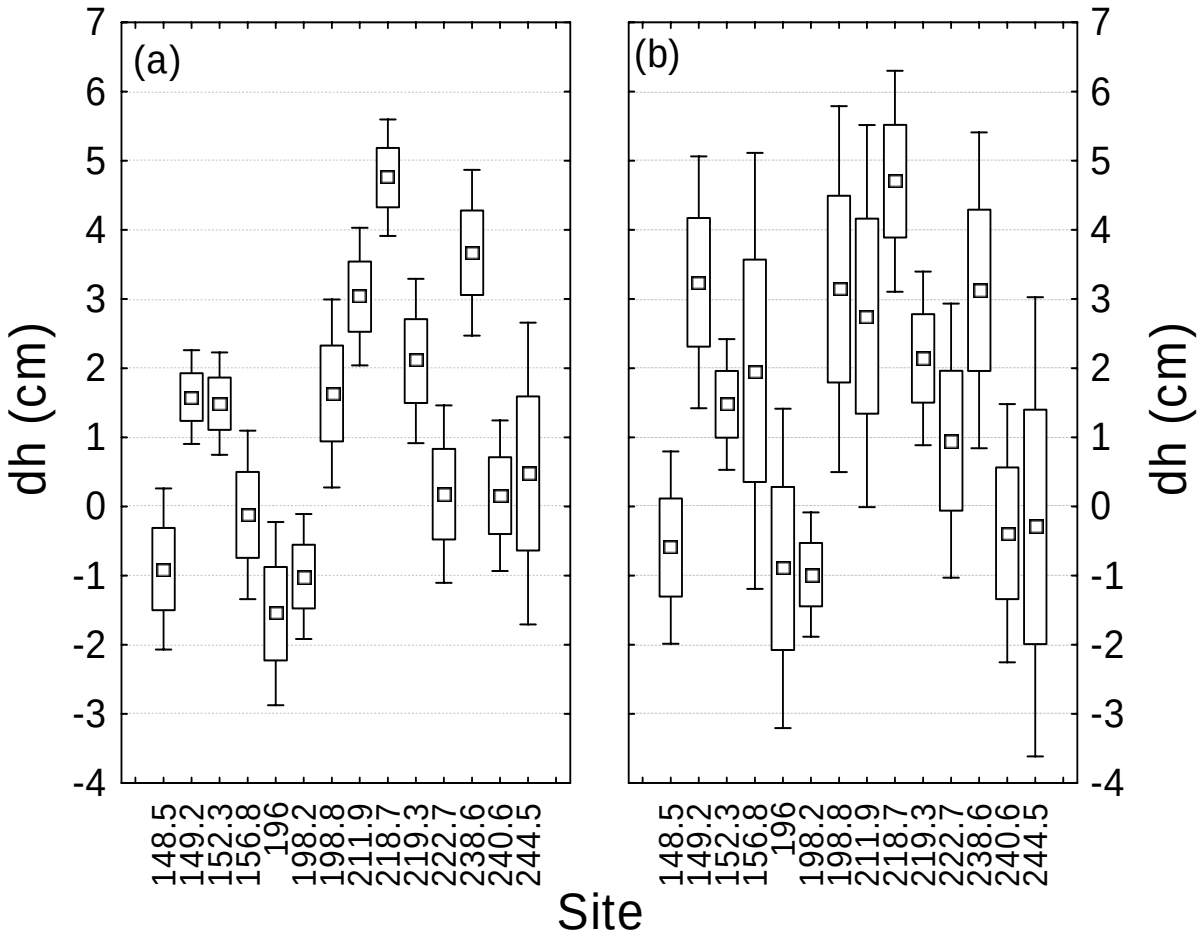

Figure 7. Difference in head pressure (*dh*; hyporheic head minus river head) at each site during (a) the incubation period with low, stable discharge (19 November 2002 – 7 January 2003), and (b) the incubation period with variable discharge (8 January – 2 March 2003). Each boxplot represents a summary of hourly *dh* at each site. The point in the center of the boxplot indicates the mean, the box is equal to the mean ±1 standard deviation (SD), and the whiskers represent the mean ±1.96 × SD.

Table 5. Results from one-way analysis of variance of mean *dh* by study site for the spawning period (20 October 2002 – 2 December 2002), the early incubation period with low, stable discharge (19 November 2002 – 7 January 2003), and the incubation period with variable discharge (8 January – 2 March 2003). Test results suggested significant differences in means among study sites for all time periods ($p << 0.05$).

Period	Source	df	SS	MS	F	p-value
spawning	site	13	38420.20	2955.40	5717.04	0.00
	error	14756	7628.05	0.51695		
early incubation	site	13	54468.19	4189.86	11044.38	0.00
	error	17122	6495.50	0.37936		
late incubation	site	13	55889.94	4299.23	3581.13	0.00
	error	17732	21287.64	1.20052		

Table 6. Results from Tukey's HSD post-hoc multiple comparison test for differences in mean *dh* by study site for the spawning period (20 October 2002 – 2 December 2002), the early incubation period with low, stable discharge (19 November 2002 – 7 January 2003), and the incubation period with variable discharge (8 January – 2 March 2003). Sites not listed in the table had significant differences in mean *dh* within each time period ($p << 0.05$).

Period	Site pair	p-value
spawning	148.5 / 198.2	1.00
	148.5 / 222.7	0.55
	198.2 / 222.7	0.10
	240.6 / 244.5	1.00
early incubation	149.2 / 198.8	0.72
	222.7 / 240.6	1.00
late incubation	149.2 / 198.8	0.56
	149.2 / 238.6	0.28
	196.0 / 198.2	0.74
	198.8 / 238.6	1.00
	240.6 / 244.5	0.68

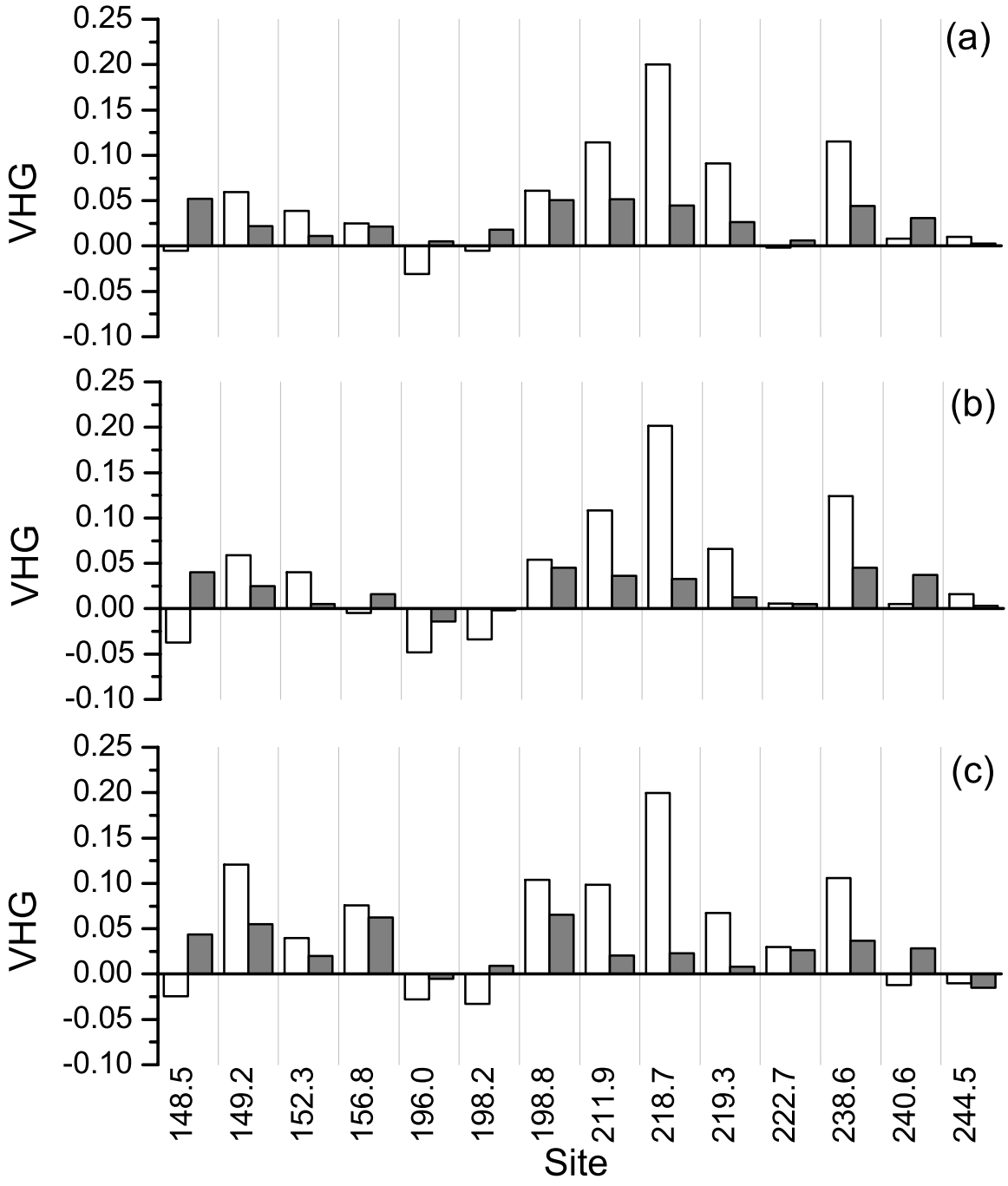

Figure 8. Mean vertical hydraulic gradient (VHG) between the river and shallow hyporheic zone (□), and between the river and deep hyporheic zone (■) during (a) the spawning period (20 October 2002 – 2 December 2002), (b) the incubation period with low, stable discharge (19 November 2002 – 7 January 2003), and (c) the incubation period with variable discharge (8 January – 2 March 2003). Positive values indicate upwelling potential while negative values indicate downwelling potential.

At a finer temporal scale (3–4 days), vertical temperature and hydraulic gradients also suggest small effects of changes in river discharge on vertical hydrologic exchange. During the low, stable discharge period sites with relatively larger upwelling potential (Figure 8) also had larger vertical temperature gradients (Appendix Figures 1–14). For example, site 149.2 had a vertical temperature gradient of nearly 1.8°C between the river and deep hyporheic zone (Figure 9), while the temperature gradient at site 196.0 was approximately 0.3°C (Figure 10). The difference in head pressure (*dh*) between the river and shallow hyporheic zone is shown to vary over a range of several centimeters even during this period of low, stable discharge (Appendix Figures 1–14). During the period of increased magnitude and variation in discharge, sites with relatively larger upwelling potential (especially from the deep hyporheic zone, Figure 8) retained larger vertical temperature gradients (Appendix Figures 15–28). For example, all of the sites in the lower segment (148.5–156.8) had an upwelling potential from the deep hyporheic zone, and maximum temperature gradients greater than 2°C during the 4 day period of fluctuating discharge (Figures 11–14). In contrast, sites with a strong downwelling potential (e.g., 196.0 and 244.5, Figure 8) have maximum temperature gradients of 0.3–0.5°C during the 4 day period of fluctuating discharge (Figures 15 and 16).

During the period of increased magnitude and variation in discharge, only 3 of the 14 sites (198.8, 211.9, and 218.7) exhibited a pronounced effect of changing river stage on hydraulic and temperature gradients (Figures 17–19). At site 198.8, as river stage increased upwelling potential increased, resulting in a slight increase in hyporheic zone temperatures (Figure 17). At site 211.9, an increase in river stage caused downwelling hydraulic gradients, resulting in a marked decrease in hyporheic zone temperatures (Figure 18). Site 218.7 exhibited a pronounced effect of changing river stage on hyporheic zone temperatures (Figure 19). As river stage increased at site 218.7, hyporheic zone temperatures decreased.

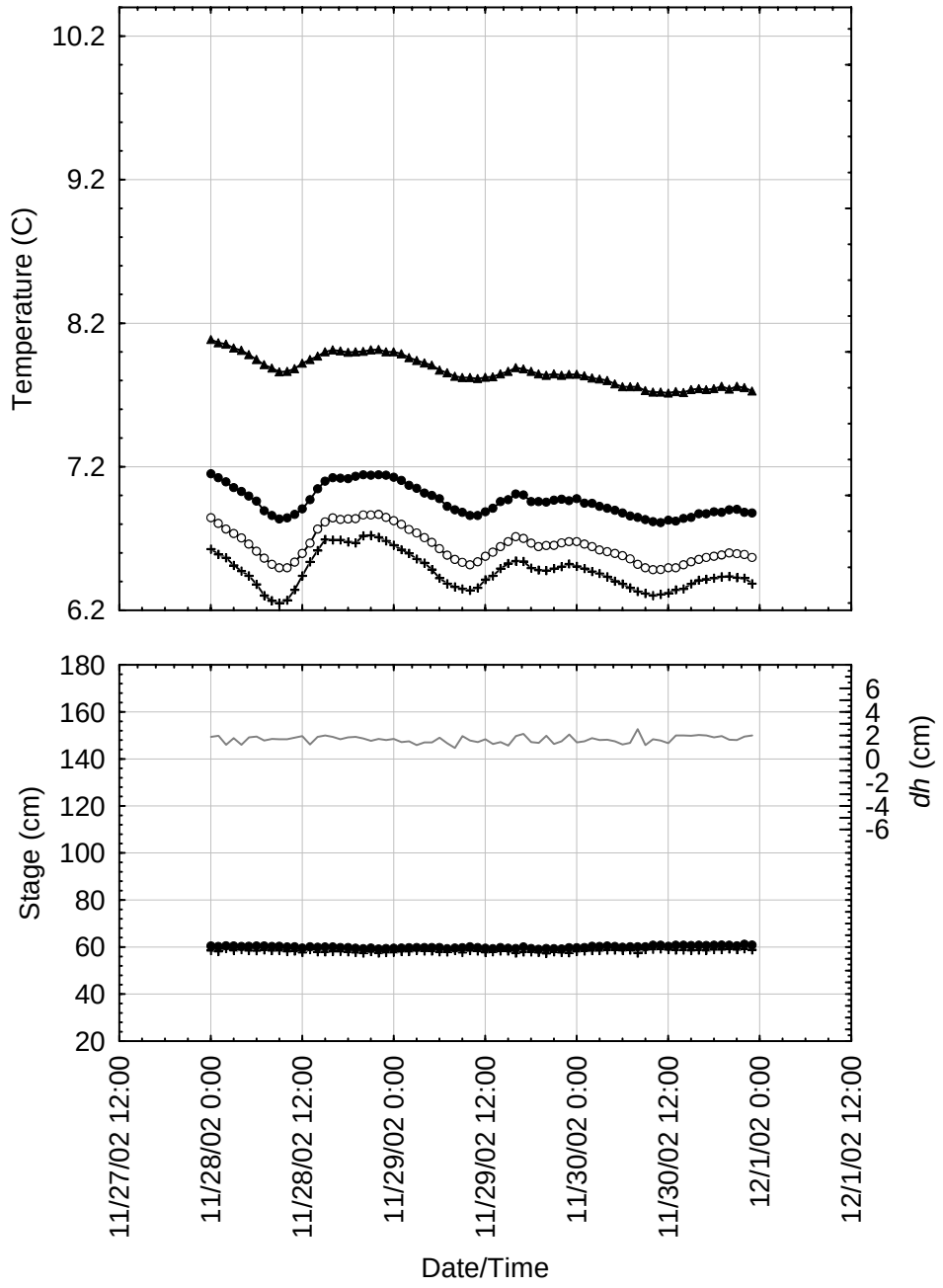

Figure 9. Time-series summary of water temperature (top panel) and river stage (bottom panel) at site 149.2 during a period of low, stable river discharge (November 28 – 30, 2002). Average hourly water temperature is shown for the river (+), egg pocket (○), shallow hyporheic (●) and deep hyporheic (▲) zones. Average hourly stage (depth) is shown for the river (+), and shallow hyporheic zone (●). The difference between these two water depths (hyporheic minus river) is plotted on the Y-right axis as *dh* (—), with positive values indicating upwelling potential.

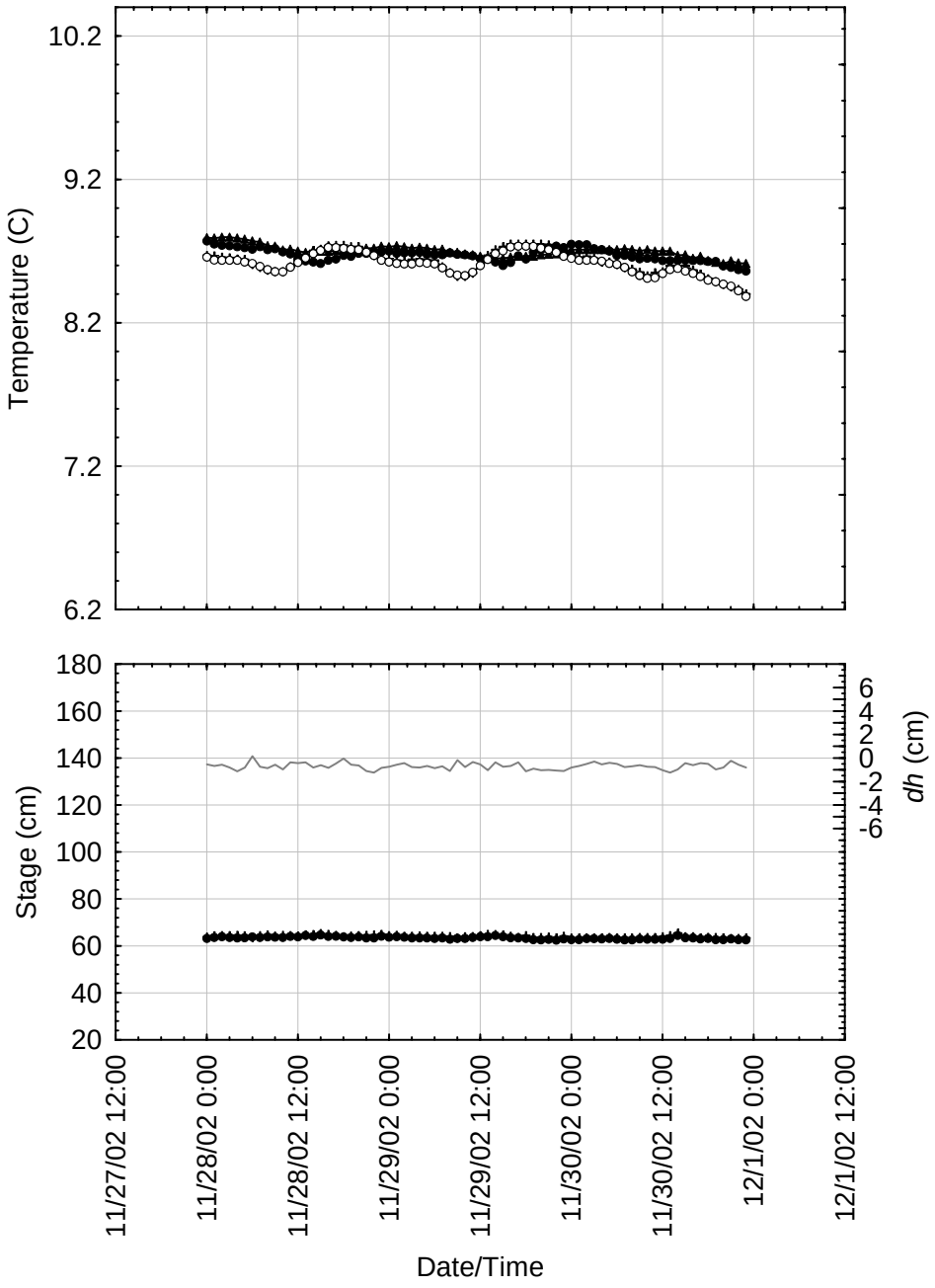

Figure 10. Time-series summary of water temperature (top panel) and river stage (bottom panel) at site 196.0 during a period of low, stable river discharge (November 28 – 30, 2002). Average hourly water temperature is shown for the river (+), egg pocket (○), shallow hyporheic (●) and deep hyporheic (▲) zones. Average hourly stage (depth) is shown for the river (+), and shallow hyporheic zone (●). The difference between these two water depths (hyporheic minus river) is plotted on the Y-right axis as *dh* (—), with positive values indicating upwelling potential.

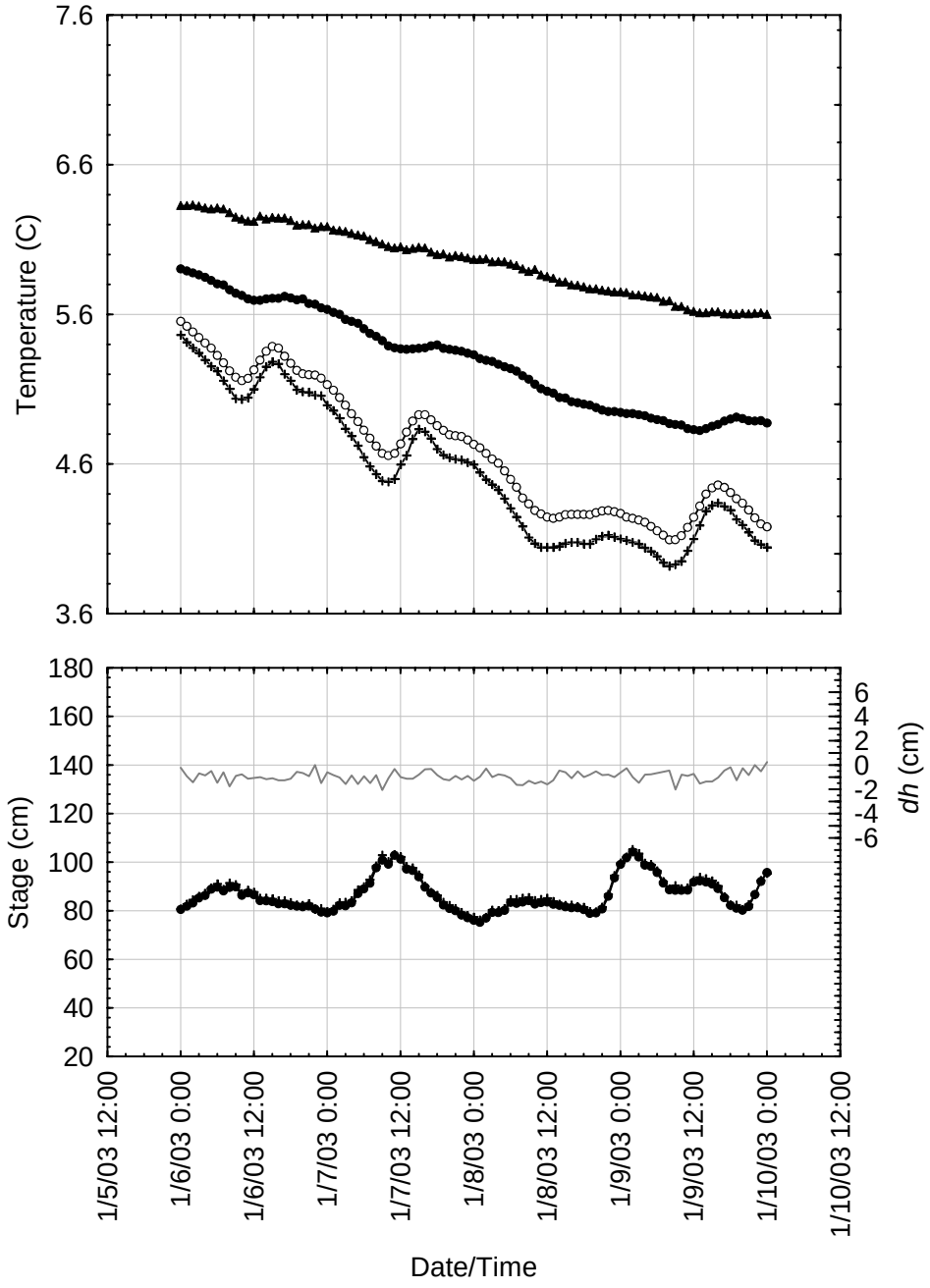

Figure 11. Time-series summary of water temperature (top panel) and river stage (bottom panel) at site 148.5 during a period of variable river discharge (January 6 – 9, 2003). Average hourly water temperature is shown for the river (+), egg pocket (○), shallow hyporheic (●) and deep hyporheic (▲) zones. Average hourly stage (depth) is shown for the river (+), and shallow hyporheic zone (●). The difference between these two water depths (hyporheic minus river) is plotted on the Y-right axis as *dh* (—), with positive values indicating upwelling potential.

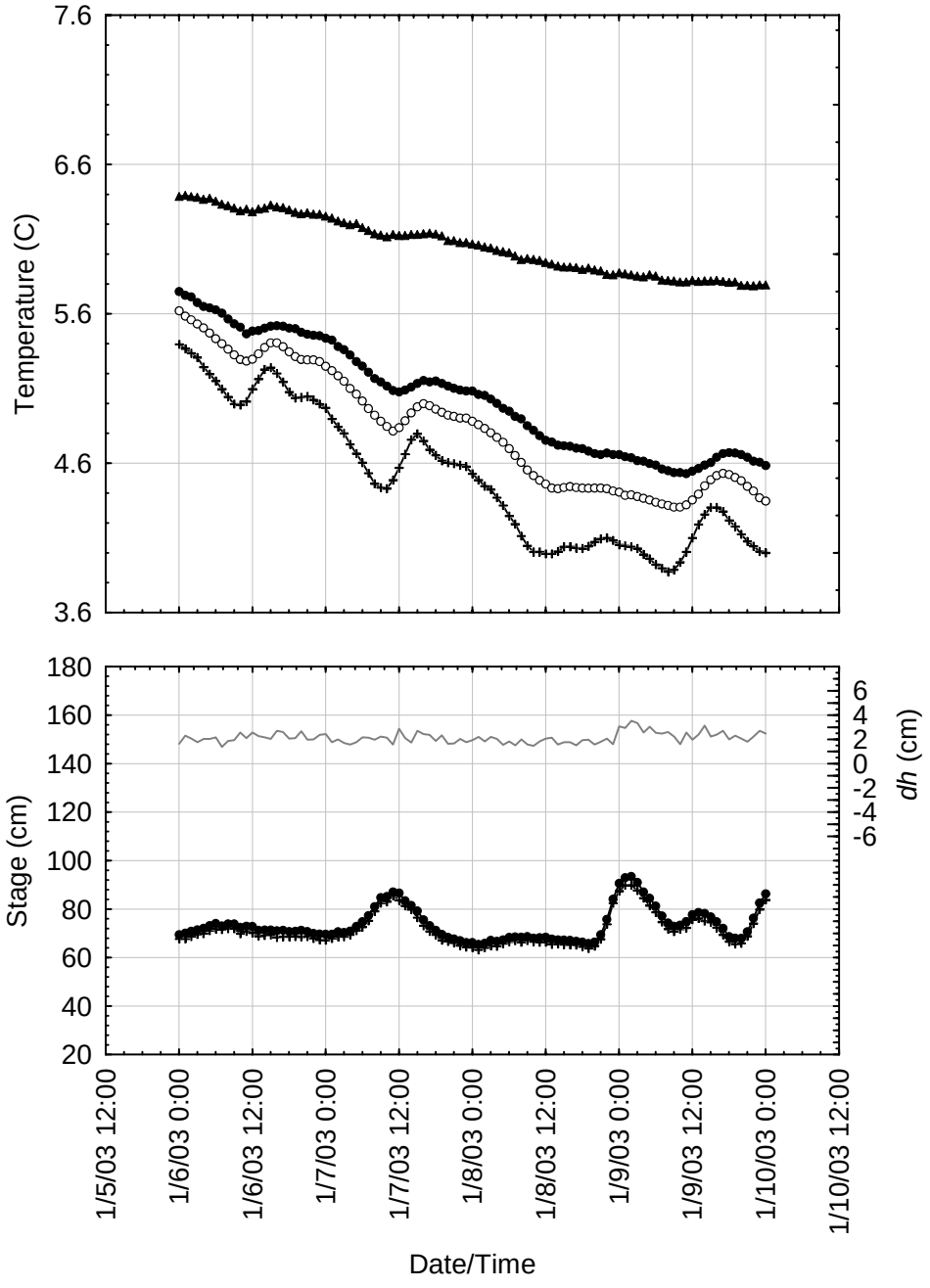

Figure 12. Time-series summary of water temperature (top panel) and river stage (bottom panel) at site 149.2 during a period of variable river discharge (January 6 – 9, 2003). Average hourly water temperature is shown for the river (+), egg pocket (○), shallow hyporheic (●) and deep hyporheic (▲) zones. Average hourly stage (depth) is shown for the river (+), and shallow hyporheic zone (●). The difference between these two water depths (hyporheic minus river) is plotted on the Y-right axis as *dh* (—), with positive values indicating upwelling potential.

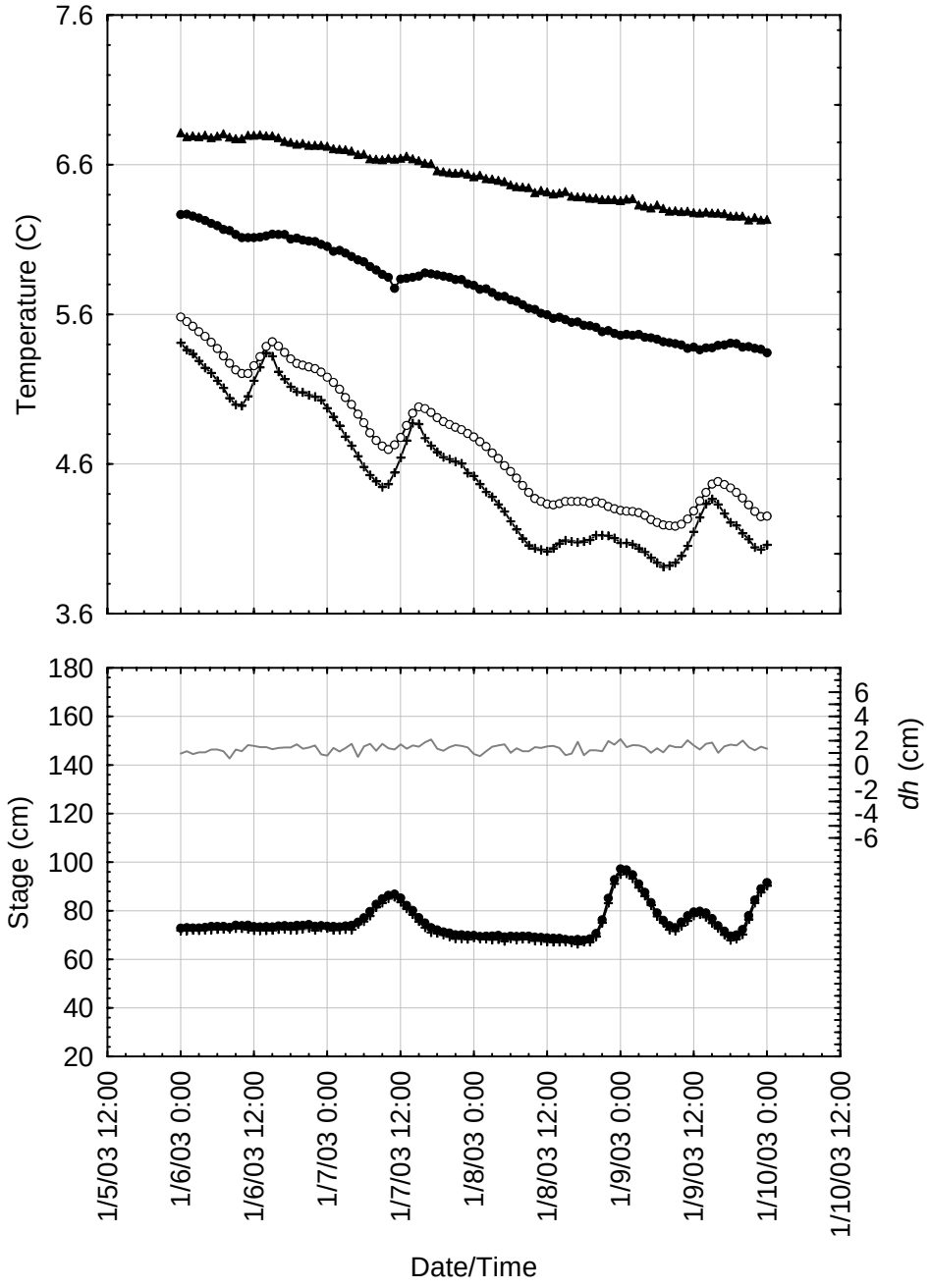

Figure 13. Time-series summary of water temperature (top panel) and river stage (bottom panel) at site 152.3 during a period of variable river discharge (January 6 – 9, 2003). Average hourly water temperature is shown for the river (+), egg pocket (○), shallow hyporheic (●) and deep hyporheic (▲) zones. Average hourly stage (depth) is shown for the river (+), and shallow hyporheic zone (●). The difference between these two water depths (hyporheic minus river) is plotted on the Y-right axis as *dh* (—), with positive values indicating upwelling potential.

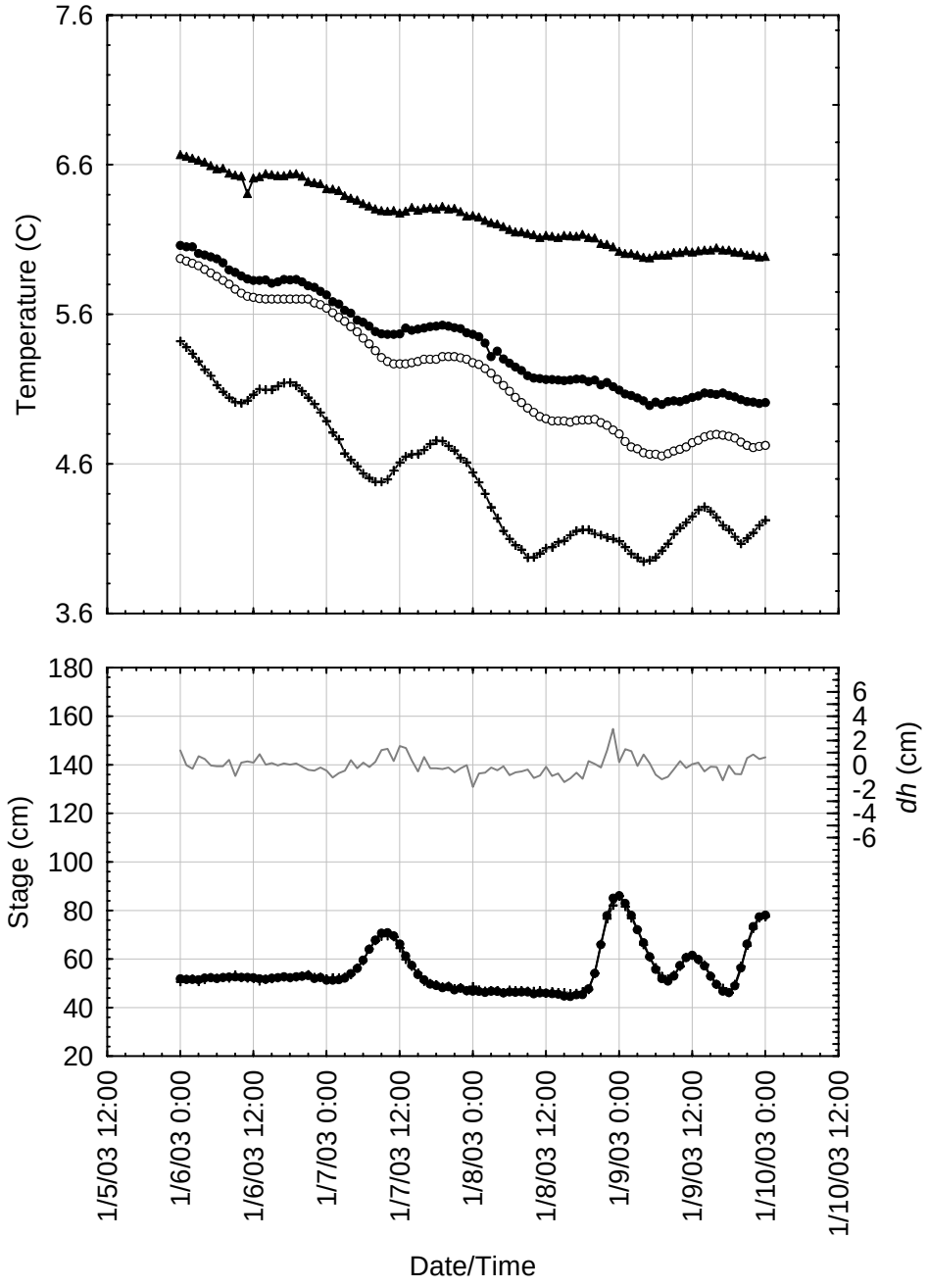

Figure 14. Time-series summary of water temperature (top panel) and river stage (bottom panel) at site 156.8 during a period of variable river discharge (January 6 – 9, 2003). Average hourly water temperature is shown for the river (+), egg pocket (○), shallow hyporheic (●) and deep hyporheic (▲) zones. Average hourly stage (depth) is shown for the river (+), and shallow hyporheic zone (●). The difference between these two water depths (hyporheic minus river) is plotted on the Y-right axis as *dh* (—), with positive values indicating upwelling potential.

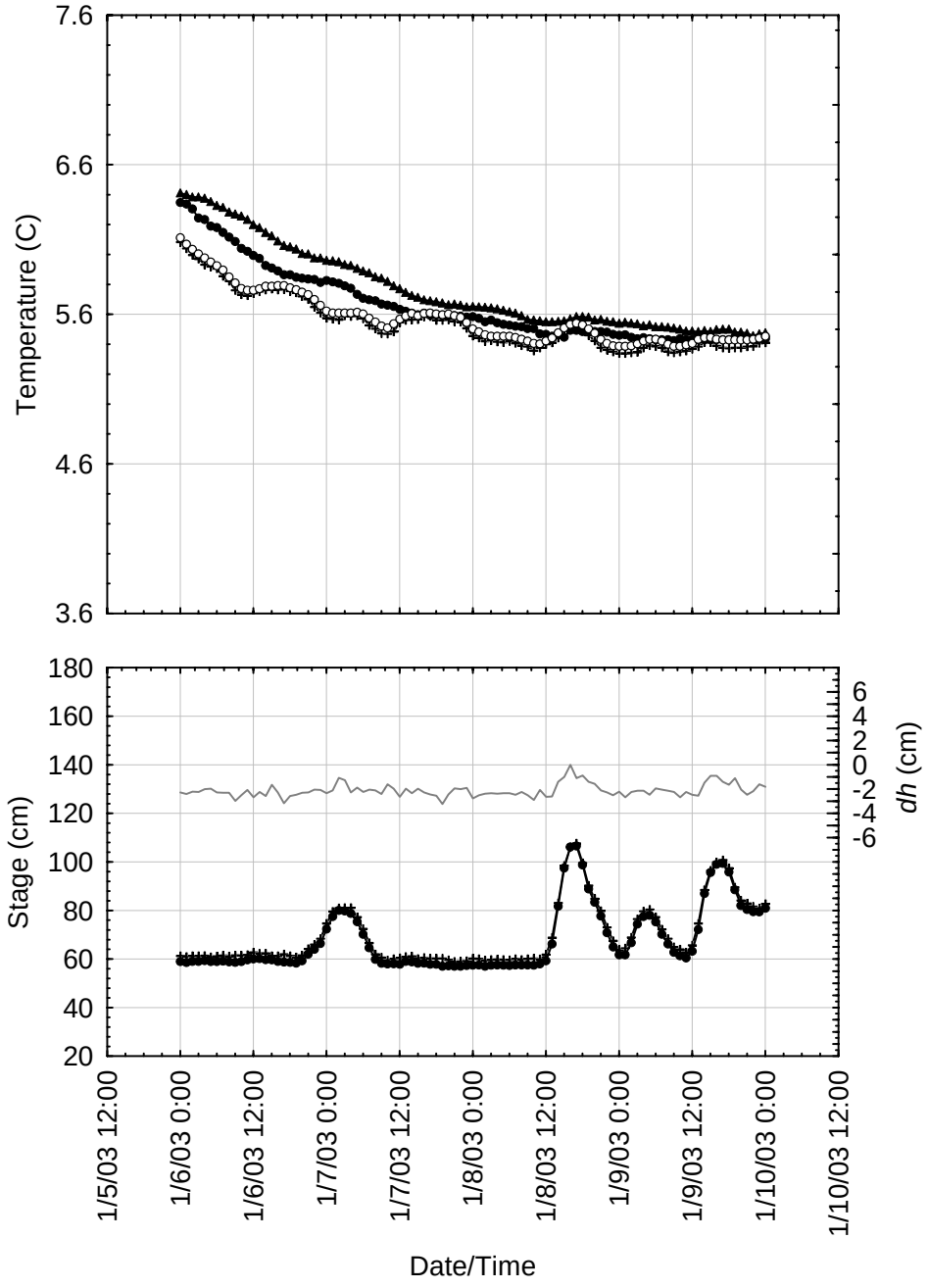

Figure 15. Time-series summary of water temperature (top panel) and river stage (bottom panel) at site 196.0 during a period of variable river discharge (January 6 – 9, 2003). Average hourly water temperature is shown for the river (+), egg pocket (○), shallow hyporheic (●) and deep hyporheic (▲) zones. Average hourly stage (depth) is shown for the river (+), and shallow hyporheic zone (●). The difference between these two water depths (hyporheic minus river) is plotted on the Y-right axis as *dh* (—), with positive values indicating upwelling potential.

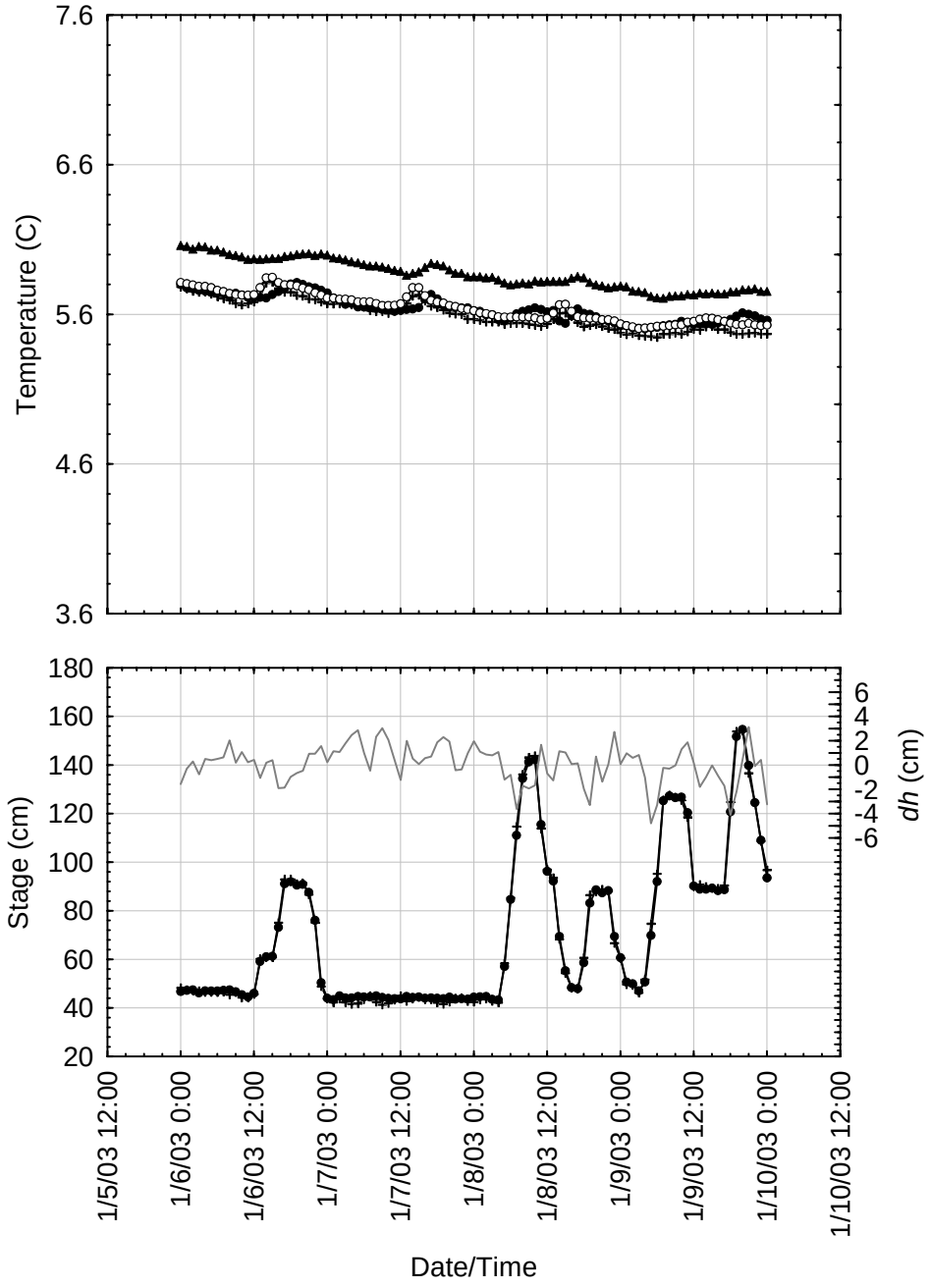

Figure 16. Time-series summary of water temperature (top panel) and river stage (bottom panel) at site 244.5 during a period of variable river discharge (January 6 – 9, 2003). Average hourly water temperature is shown for the river (+), egg pocket (○), shallow hyporheic (●) and deep hyporheic (▲) zones. Average hourly stage (depth) is shown for the river (+), and shallow hyporheic zone (●). The difference between these two water depths (hyporheic minus river) is plotted on the Y-right axis as *dh* (—), with positive values indicating upwelling potential.

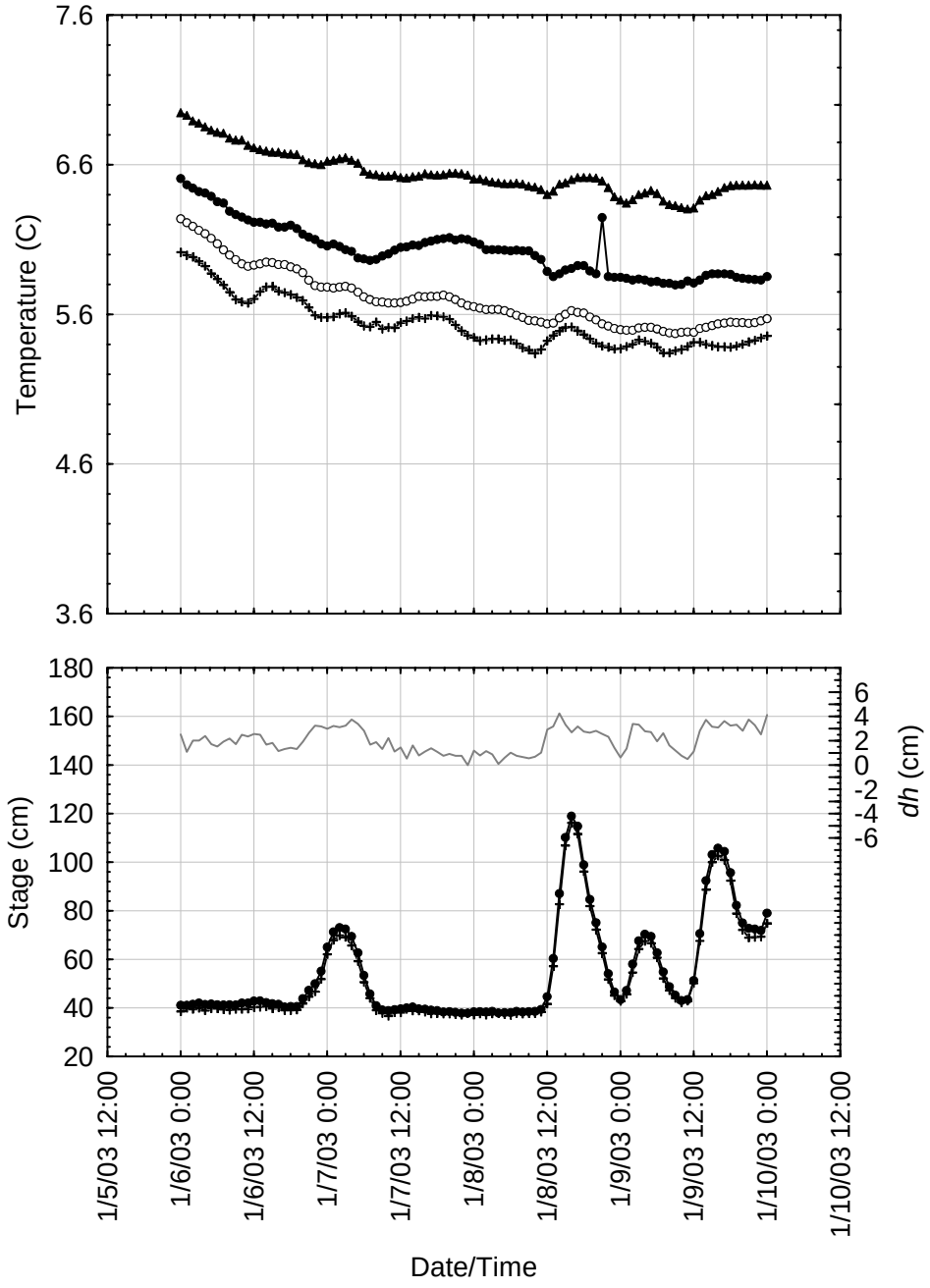

Figure 17. Time-series summary of water temperature (top panel) and river stage (bottom panel) at site 198.8 during a period of variable river discharge (January 6 – 9, 2003). Average hourly water temperature is shown for the river (+), egg pocket (○), shallow hyporheic (●) and deep hyporheic (▲) zones. Average hourly stage (depth) is shown for the river (+), and shallow hyporheic zone (●). The difference between these two water depths (hyporheic minus river) is plotted on the Y-right axis as *dh* (—), with positive values indicating upwelling potential.

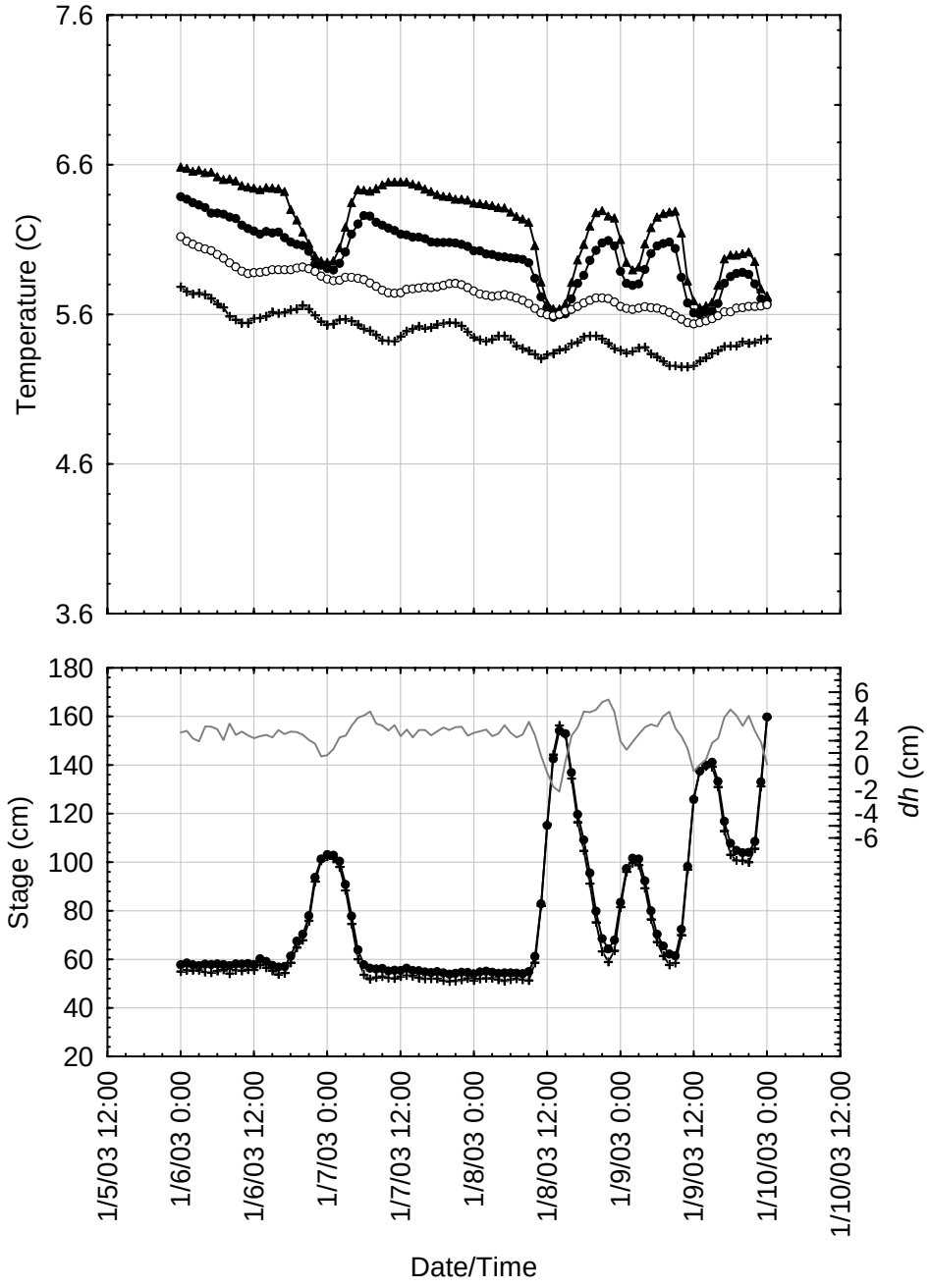

Figure 18. Time-series summary of water temperature (top panel) and river stage (bottom panel) at site 211.9 during a period of variable river discharge (January 6 – 9, 2003). Average hourly water temperature is shown for the river (+), egg pocket (○), shallow hyporheic (●) and deep hyporheic (▲) zones. Average hourly stage (depth) is shown for the river (+), and shallow hyporheic zone (●). The difference between these two water depths (hyporheic minus river) is plotted on the Y-right axis as *dh* (—), with positive values indicating upwelling potential.

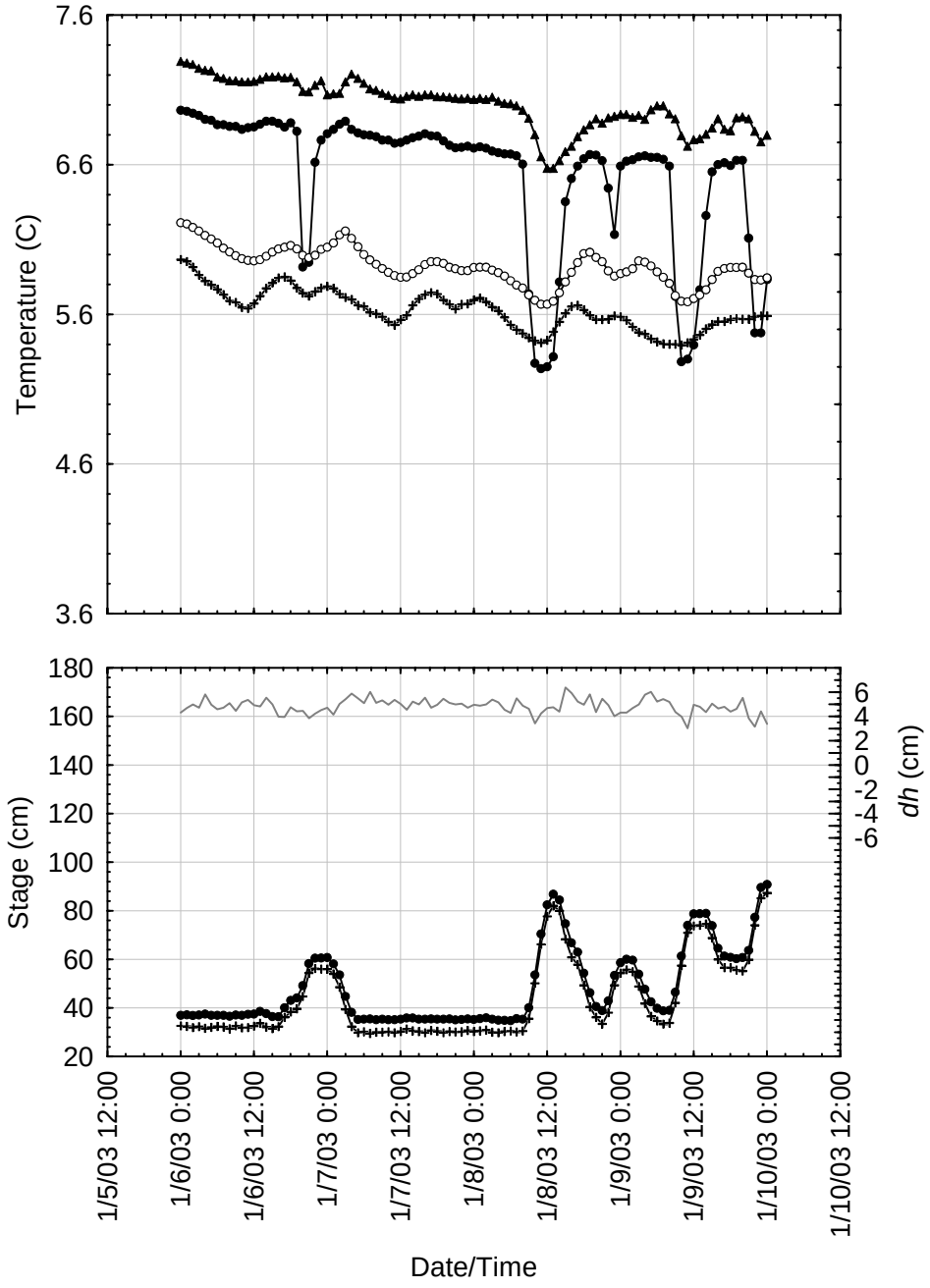

Figure 19. Time-series summary of water temperature (top panel) and river stage (bottom panel) at site 218.7 during a period of variable river discharge (January 6 – 9, 2003). Average hourly water temperature is shown for the river (+), egg pocket (○), shallow hyporheic (●) and deep hyporheic (▲) zones. Average hourly stage (depth) is shown for the river (+), and shallow hyporheic zone (●). The difference between these two water depths (hyporheic minus river) is plotted on the Y-right axis as *dh* (—), with positive values indicating upwelling potential.

3.3 Numerical Modeling

Despite the relatively small vertical hydraulic gradients at most sites, the results from the numerical modeling of apparent velocity (v_z) and hyporheic zone temperatures suggest that there was significant vertical hydrologic exchange during all time periods. During the periods of low, stable discharge (spawning and early incubation) 12 of the 14 study sites exhibited a downward flux of surface water entering the riverbed. The apparent velocity of pore water at these sites was 0.2–5.4 cm h^{-1} (Table 7). During the period of increased magnitude and variability of discharge (late incubation period), the apparent velocity at 8 of the 14 sites was a downward flux of 0.2–2.9 cm h^{-1} (Table 7). The direction of hydrologic exchange between the river and the hyporheic zone is also indicated by time-series temperature plots (Appendix Figures 29–42). A downward flux of river water is indicated where the shallow hyporheic zone temperature is close to the river temperature (e.g., site 198.2, Figure 20); an upward flux is indicated where the shallow hyporheic zone temperature is close to the deep hyporheic zone temperature (e.g., site 152.3, Figure 21).

The results from the numerical model suggest that the hydrologic interactions between the river and the riverbed at most sites was largely unaffected by changes in hydrologic regime. At the large temporal scale (i.e., weeks to months), only 3 of the 14 sites (196.0, 211.9, and 219.3) displayed a reversal in flux direction resulting from the change in hydrologic regime (i.e., when the discharge pattern changed from low and stable to high and variable) (Table 7). In mid-January, site 196.0 experienced a change in flux from strong downwelling to slight upwelling. Because the riverbed at this site is highly mobile, it is likely that the increased discharge in mid-January resulted in localized bed scour and deposition that changed the bed temperature patterns. This is reflected in the unusual temperature patterns from mid-January through the end of the study period (Figure 22). A similar change in flux direction occurred at site 222.7, also likely a result of bed mobilization and deposition that changed bed temperature patterns. Sites 211.9 and 219.3 displayed a change in flux from slight downwelling to stronger upwelling as a result of the increased magnitude and variability in discharge (Table 7, Figures 23 and 24). Site 218.7 experienced acute changes (i.e., hourly) in flux direction resulting from the change in hydrologic regime. However, at the large temporal scale the shallow hyporheic zone temperatures suggested a trend toward a constant upward flux of 0.9 cm h^{-1} (Table 7, Figure 25). An additional 2 of the 14 sites (156.8 and 198.2) displayed small changes in the magnitude of flux as a result of the change in hydrologic regime (Table 7, Figures 26 and 27). During the period of increased discharge the downward flux increased slightly at site 156.8 and decreased slightly at site 198.2. For the remaining 7 of the 14 study sites shallow hyporheic zone temperatures were accurately predicted by using a constant value of apparent velocity for the entire study period (Table 7).

The accuracy of the model predictions are evidenced by the average prediction error (taken as the mean absolute error [MAE]), which was within the accuracy of the temperature sensor (±0.15°C) for all sites and time periods, except one (Table 7). Estimates of apparent velocity from the numerical model matched well with those from the time travel model (Table 8). Time-series plots of observed and predicted temperatures also suggest that the numerical model adequately characterized the hydrologic exchange at most sites (Appendix Figures 29–42). At 12 of the 14 study sites, predicted shallow hyporheic zone temperature closely matched the observed temperature. At the remaining two sites (211.9 and 218.7), the numerical model accurately predicted the average temperature trend of the shallow

hyporheic zone, but did not account for the rapid changes in shallow hyporheic zone temperature that were clearly a result of short-term changes in river stage (Figures 23 and 25). For example, at site 211.9 the long-term temperature trend of the shallow hyporheic zone reflects a change in apparent velocity from downwelling to upwelling as the hydrologic regime changes from low and stable to high and variable. However, at the hourly time scale, acute increases in river stage clearly cause the flux direction to reverse to downwelling (Figure 18). A similar acute flux reversal from upwelling to downwelling is also evident at site 218.7 (Figure 19). The combined results of temperature monitoring and numerical modeling indicate that only two sites (211.9 and 218.7) are significantly affected by short-term (hourly to daily) large magnitude changes in discharge.

Table 7. Apparent velocity v_z of pore water derived from the numerical model of shallow hyporheic zone temperatures at each site. The v_z was held constant during the period indicated. Positive v_z indicates downward flux; negative v_z indicates upward flux. Comparison of modeled and observed shallow hyporheic zone temperatures is provided by the mean absolute error (MAE) and root mean-squared error (RMSE).

Site	Segment	Period	v_z (cm h^{-1})	MAE (°C)	RMSE (°C)
148.5	lower	20 October 2002–2 March 2003	0.2	0.09	0.13
149.2	lower	20 October 2002–2 March 2003	1.3	0.11	0.15
152.3	lower	20 October 2002–2 March 2003	-0.4	0.06	0.08
156.8	lower	20 October 2002–14 January 2003	0.2	0.13	0.17
		15 January 2003–1 February 2003	1.1	0.08	0.09
		2 February 2003–2 March 2003	1.8	0.12	0.14
196.0	middle	20 October 2002–14 January 2003	5.4	0.06	0.09
		15 January 2003–1 March 2003	-0.4	0.05	0.07
198.2	middle	20 October 2002–5 January 2003	2.2	0.11	0.17
	middle	6 January 2003–2 March 2003	1.4	0.06	0.09
198.8	middle	20 October 2002–2 March 2003	0.4	0.07	0.11
211.9	middle	20 October 2002–5 January 2003	0.4	0.12	0.14
		6 January 2003–2 March 2003	-1.8	0.13	0.16
218.7	middle	20 October 2002–5 January 2003	-0.9	0.10	0.13
		6 January 2003–2 March 2003	-0.9[†]	0.25	0.35
219.3	middle	20 October 2002–7 January 2003	0.4	0.08	0.09
		8 January 2003–2 March 2003	-1.8	0.03	0.04
222.7	middle	20 October 2002–6 November 2002	0.4	0.08	0.09
		7 November 2002–2 March 2003	-1.1	0.10	0.12
238.6	upper	20 October 2002–2 March 2003	0.7	0.09	0.11
240.6	upper	20 October 2002–2 March 2003	0.7	0.04	0.05
244.5	upper	20 October 2002–2 March 2003	2.9	0.06	0.07

[†]Temperature changes in the shallow hyporheic zone were too large during this period to model the daily change by adjusting v_z.

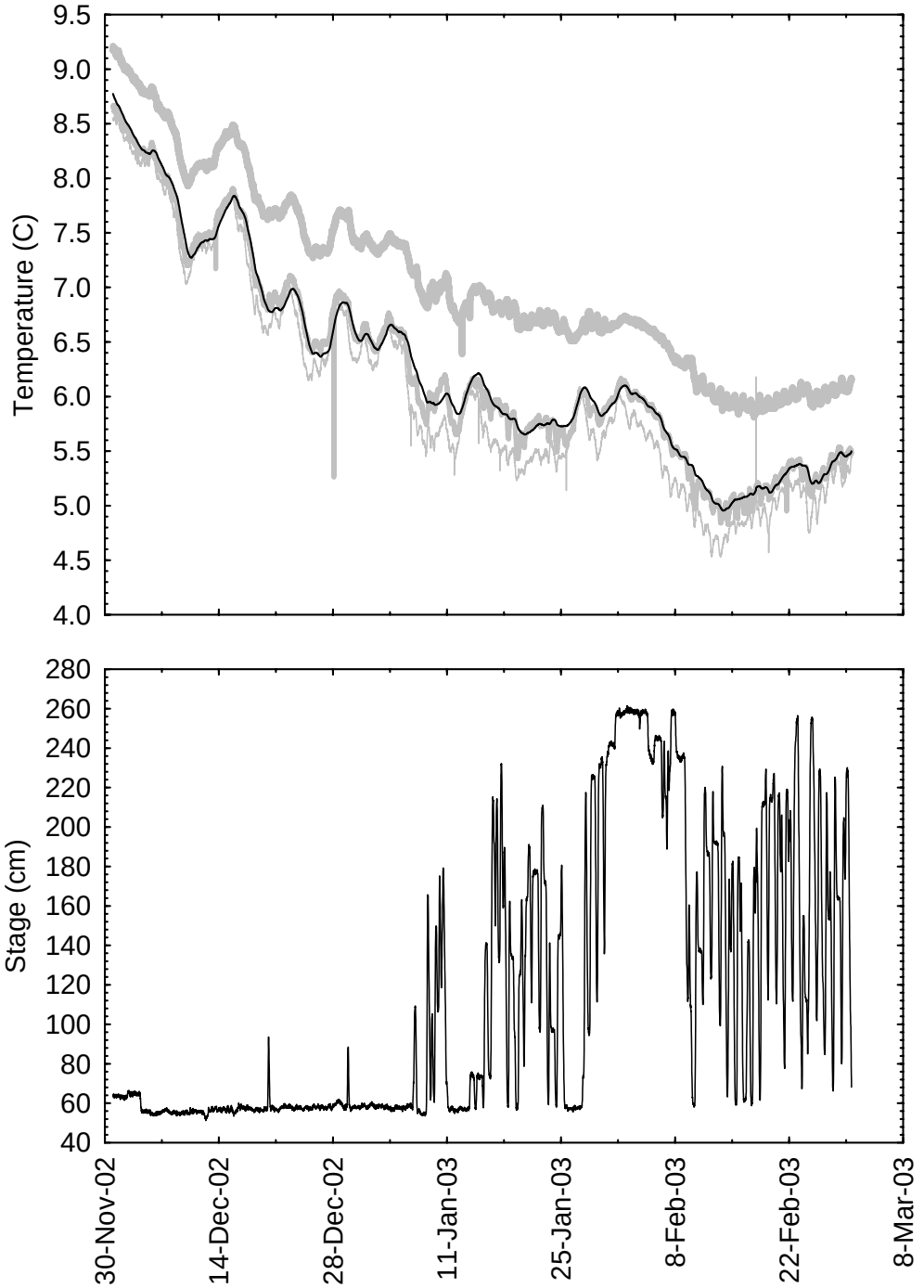

Figure 20. Time-series summary of observed and modeled water temperature (top panel) and river stage (bottom panel) at site 198.2 during the period 1 December 2002 – 2 March 2003. Water temperatures recorded at 20 min intervals in the river (——), shallow hyporheic zone (——), and deep hyporheic zone (——) are compared with modeled water temperature at 20 min intervals in the shallow hyporheic zone (——).

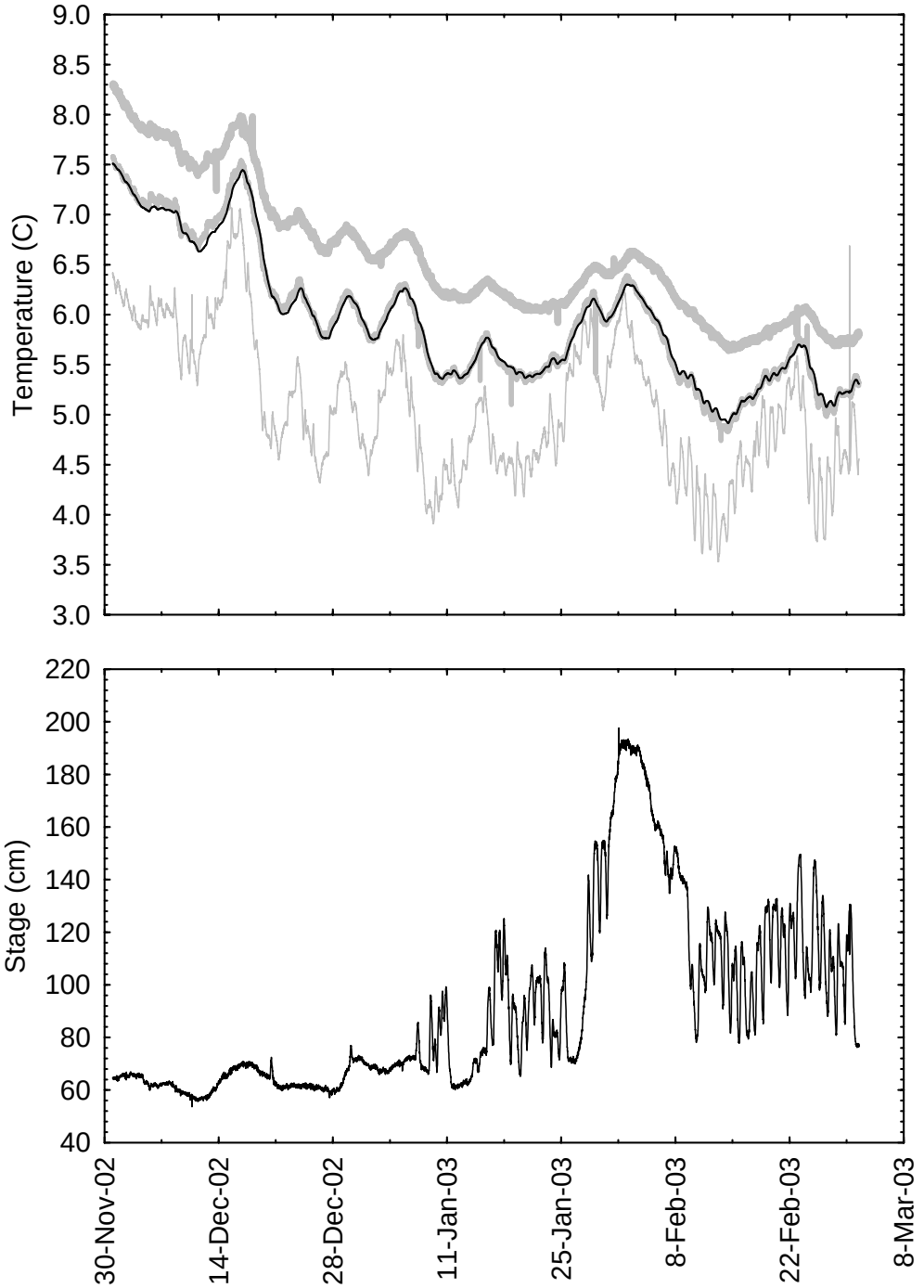

Figure 21. Time-series summary of observed and modeled water temperature (top panel) and river stage (bottom panel) at site 152.3 during the period 1 December 2002 – 2 March 2003. Water temperatures recorded at 20 min intervals in the river (——), shallow hyporheic zone (——), and deep hyporheic zone (——) are compared with modeled water temperature at 20 min intervals in the shallow hyporheic zone (——).

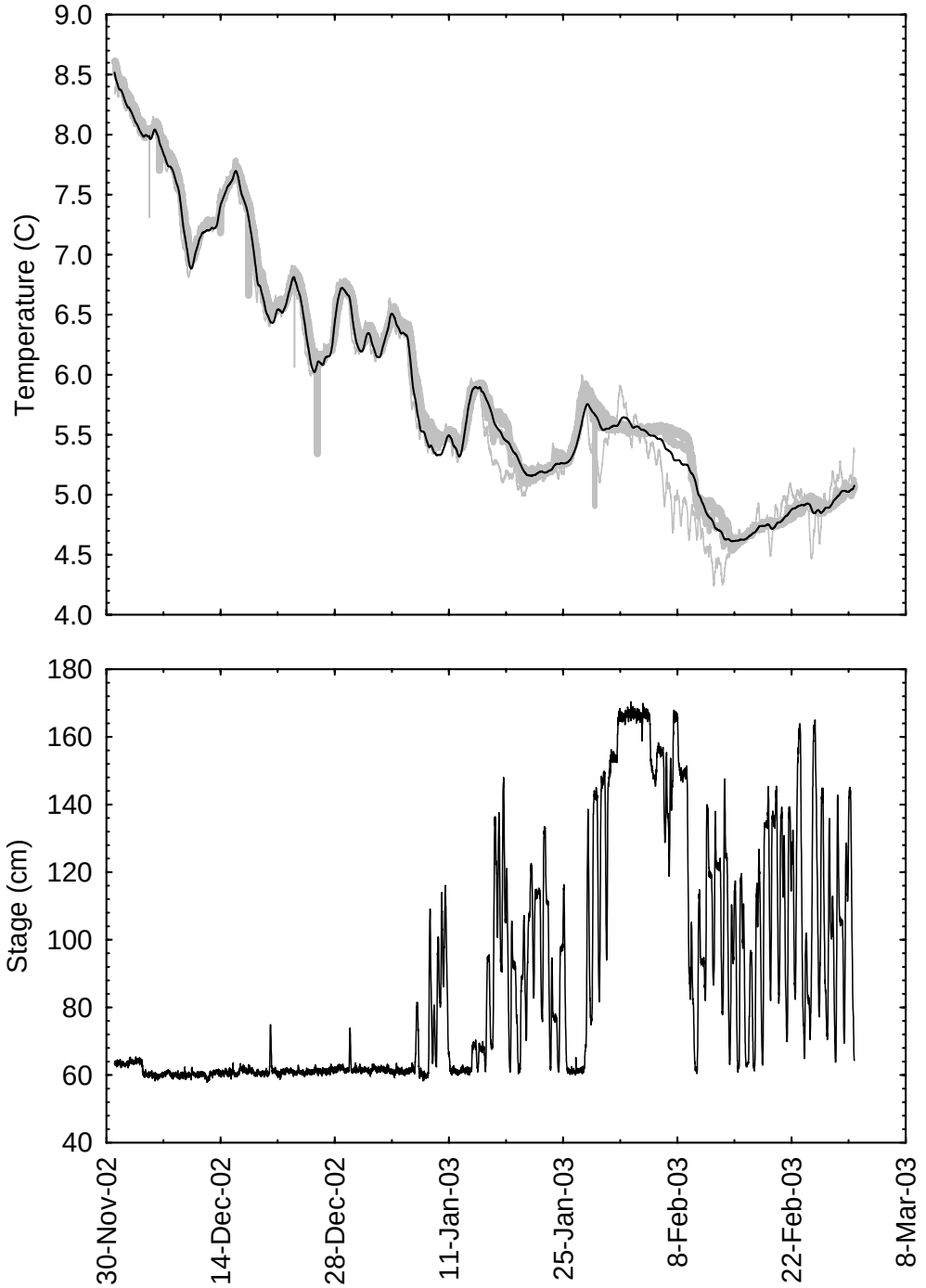

Figure 22. Time-series summary of observed and modeled water temperature (top panel) and river stage (bottom panel) at site 196.0 during the period 1 December 2002 – 2 March 2003. Water temperatures recorded at 20 min intervals in the river (——), shallow hyporheic zone (——), and deep hyporheic zone (——) are compared with modeled water temperature at 20 min intervals in the shallow hyporheic zone (——).

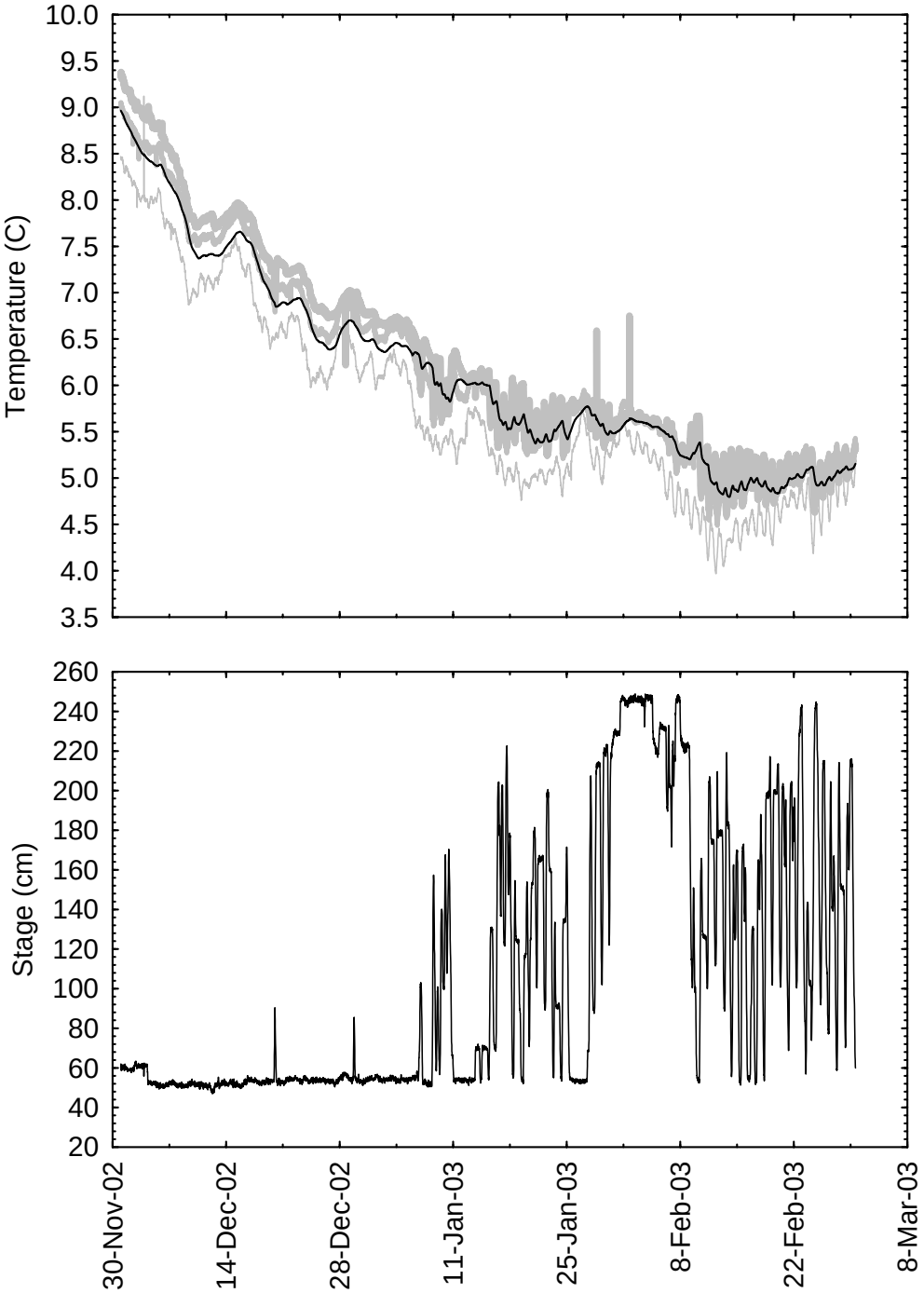

Figure 23. Time-series summary of observed and modeled water temperature (top panel) and river stage (bottom panel) at site 211.9 during the period 1 December 2002 – 2 March 2003. Water temperatures recorded at 20 min intervals in the river (——), shallow hyporheic zone (——), and deep hyporheic zone (——) are compared with modeled water temperature at 20 min intervals in the shallow hyporheic zone (——).

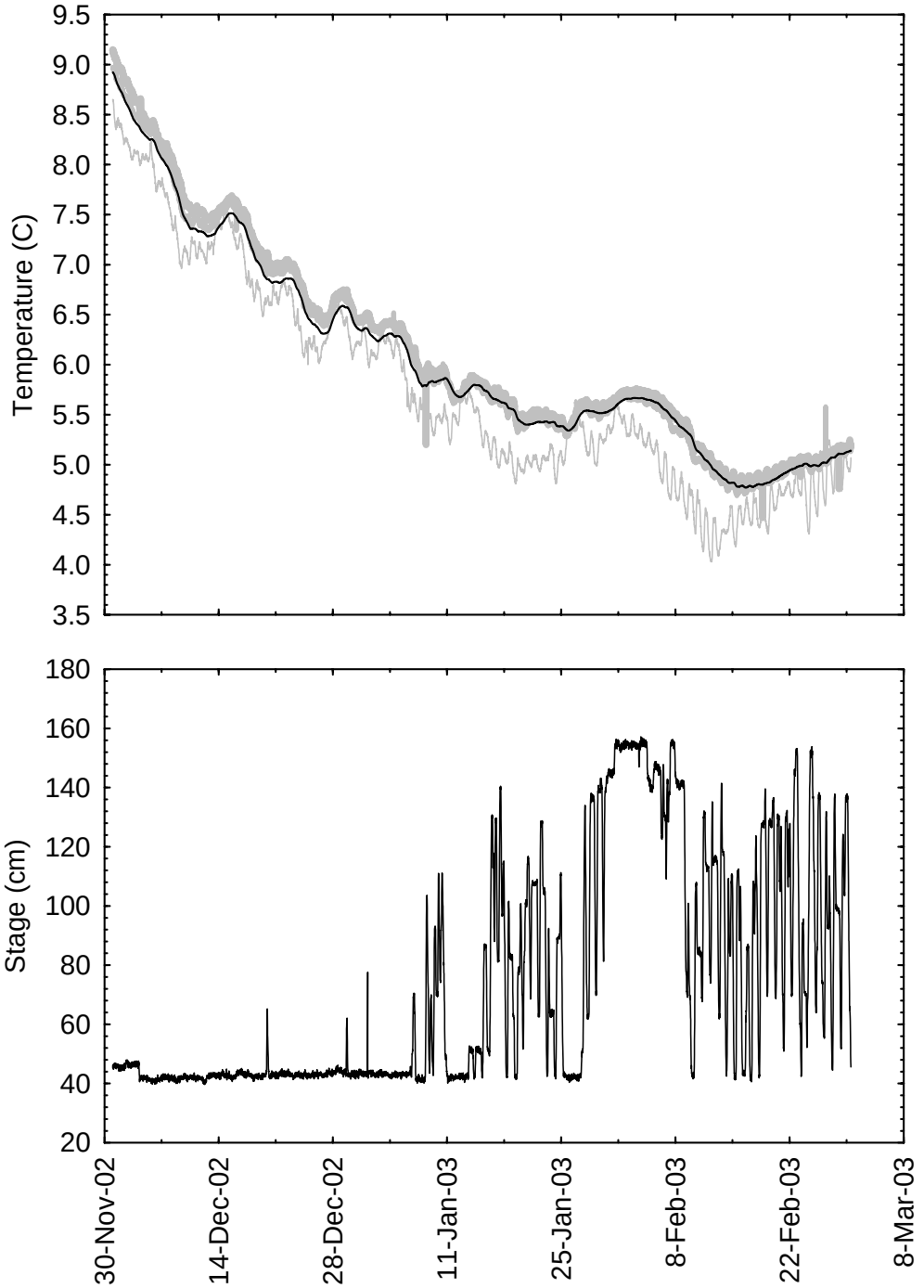

Figure 24. Time-series summary of observed and modeled water temperature (top panel) and river stage (bottom panel) at site 219.3 during the period 1 December 2002 – 2 March 2003. Water temperatures recorded at 20 min intervals in the river (——), shallow hyporheic zone (——), and deep hyporheic zone (——) are compared with modeled water temperature at 20 min intervals in the shallow hyporheic zone (——).

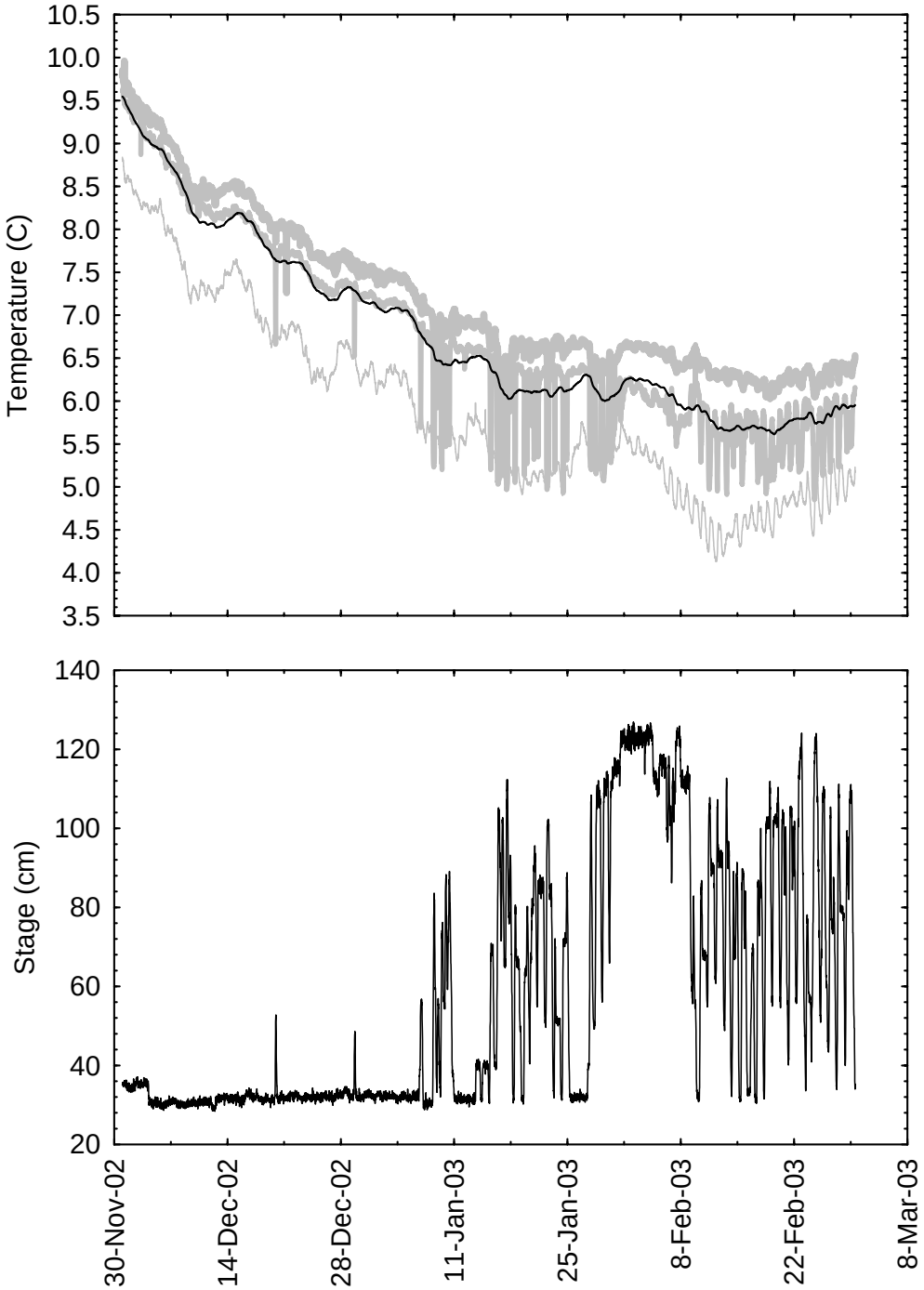

Figure 25. Time-series summary of observed and modeled water temperature (top panel) and river stage (bottom panel) at site 218.7 during the period 1 December 2002 – 2 March 2003. Water temperatures recorded at 20 min intervals in the river (——), shallow hyporheic zone (▬), and deep hyporheic zone (▬) are compared with modeled water temperature at 20 min intervals in the shallow hyporheic zone (——).

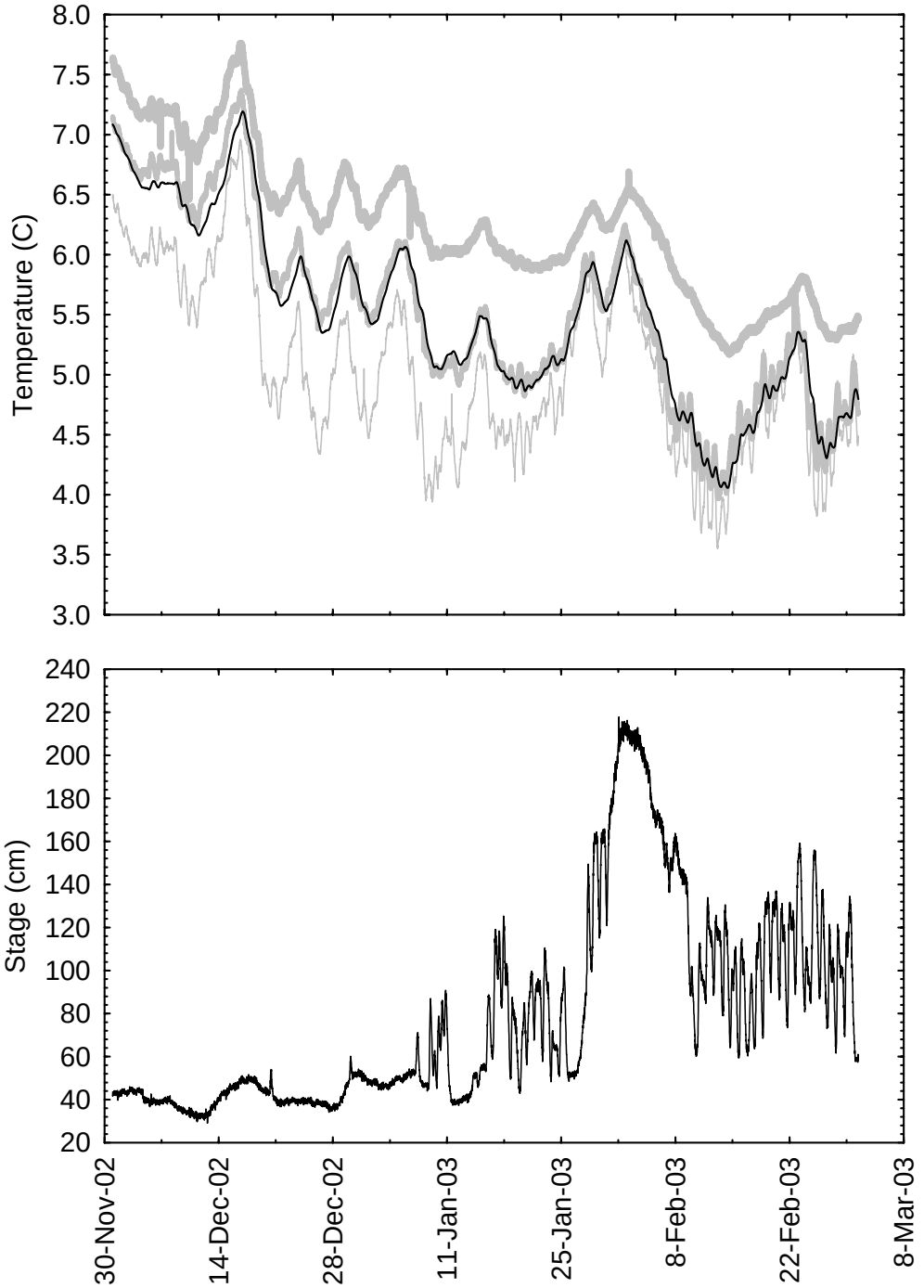

Figure 26. Time-series summary of observed and modeled water temperature (top panel) and river stage (bottom panel) at site 156.8 during the period 1 December 2002 – 2 March 2003. Water temperatures recorded at 20 min intervals in the river (——), shallow hyporheic zone (——), and deep hyporheic zone (——) are compared with modeled water temperature at 20 min intervals in the shallow hyporheic zone (——).

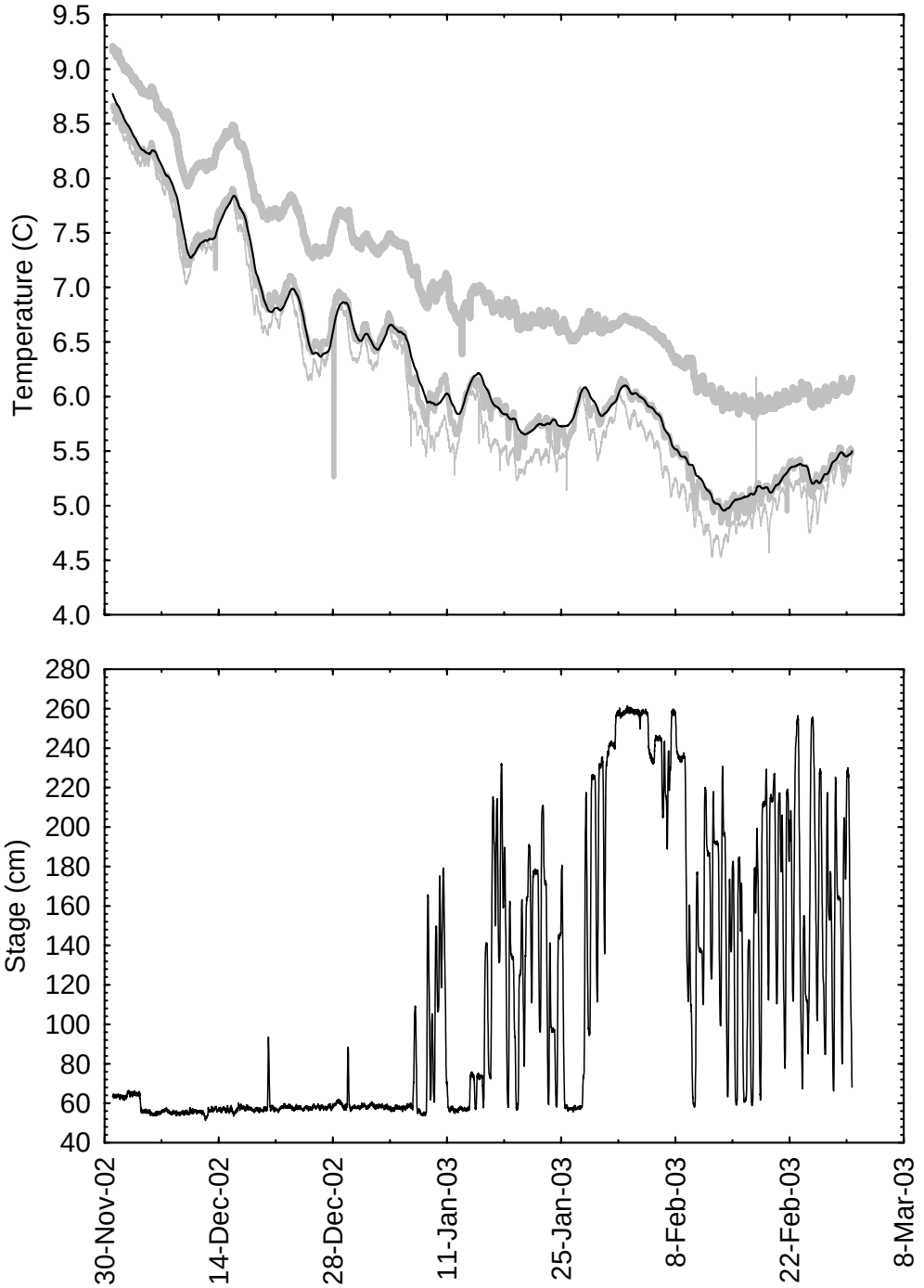

Figure 27. Time-series summary of observed and modeled water temperature (top panel) and river stage (bottom panel) at site 198.2 during the period 1 December 2002 – 2 March 2003. Water temperatures recorded at 20 min intervals in the river (——), shallow hyporheic zone (——), and deep hyporheic zone (——) are compared with modeled water temperature at 20 min intervals in the shallow hyporheic zone (——).

Table 8. Comparison of apparent velocity of pore water derived from the numerical model v_{zn} and travel time model v_{ztt}. Values of v_z represent the flux rate between the riverbed surface and the shallow hyporheic zone. Positive v_z indicates downward flux; negative v_z indicates upward flux.

Site	Segment	Period	v_{zn} (cm h^{-1})	v_{ztt} (cm h^{-1})
196.0	middle	20 October 2002–14 January 2003	5.4	5.0
		15 January 2003–1 March 2003	-0.4	2.4
198.2	middle	20 October 2002–5 January 2003	2.2	6.1
		6 January 2003–2 March 2003	1.4	4.2
244.5	upper	20 October 2002–2 March 2003	2.9	5.4
		6 January 2003–2 March 2003	2.9	2.9

3.4 Temperature

During the early spawning period (20 October 2002–18 November 2002) there was a positive temperature gradient between the river and the riverbed at all sites, with water temperatures increasing with depth into the riverbed. At sites in the lower segment the mean temperature gradient between the river and the deep hyporheic zone was 0.6–1.4°C (Table 9). This temperature gradient was smaller at sites in the middle segment (0.1–1.0°C) and upper segment (0.2–0.8°C) (Table 9). Sites exhibiting a strong downward flux of river water entering the riverbed (196.0, 198.2, 244.5–Table 7) possessed smaller temperature gradients, with shallow hyporheic zone temperatures closer to the river temperature than to the deep hyporheic zone temperature (Table 9). During this period, the temperature of the river and hyporheic zone was colder at the lower sites than at the middle and upper sites. The mean temperature of the river was 10.0°C at the lower sites, 12.6°C at the middle sites, and 12.8°C at the upper sites (Table 9). Similar temperature differences among segments existed for riverbed temperatures, with a mean shallow hyporheic zone temperature of 10.5°C at the lower sites, 12.9°C at the middle sites, and 13.0°C at the upper sites (Table 9). The mean temperature of the deep hyporheic zone was 11.0°C at the lower sites, 13.2°C at the middle sites, and 13.3°C at the upper sites (Table 9). Differences in median temperatures among segments were even larger, owing to the strong positive skewness of the temperature distributions, especially at the lower sites (Figure 28). The temperature range at each site during this period decreased with depth into the riverbed (Figure 28). At the lower sites, the average temperature range was 5.5°C in the river, 4.8°C in the shallow hyporheic zone, and 4.6°C in the deep hyporheic zone. A similar pattern existed for the middle sites, where the average temperature range was 5.0°C in the river, 4.7°C in the shallow hyporheic zone, and 4.6°C in the deep hyporheic zone. At the upper sites, the average temperature range was 4.8°C in the river, 4.5°C in the shallow hyporheic zone, and 4.4°C in the deep hyporheic zone (Figure 28).

The positive temperature gradient between the river and the riverbed at all sites remained during the late spawning and early incubation period (19 November – 2 December 2002), with water temperatures increasing with depth into the riverbed. At 11 of the 14 study sites, the average egg pocket temperature at

each site was within 0.2°C of the river temperature (Table 9), indicating rapid advection of river water into the egg pockets. At the deeper locations within the riverbed, temperature gradients were similar in magnitude as during the early spawning period. At sites in the lower segment, the mean temperature gradient between the river and the deep hyporheic zone was 0.8–1.4°C (Table 9). This temperature gradient was smaller at sites in the middle segment (0.1–0.9°C) and upper segment (0.2–1.0°C) (Table 9). The three sites exhibiting a strong downward flux of river water entering the riverbed (196.0, 198.2, 244.5–Table 7) continued to have smaller temperature gradients, with shallow hyporheic zone temperatures closer to the river temperature than to the deep hyporheic zone temperature (Table 9). As was the case during the early spawning period, the temperature of the river and riverbed during the late spawning period was colder at the lower sites than at the middle and upper sites. The mean temperature of the river was 7.8°C at the lower sites, and 9.6°C at the middle and upper sites (Table 9). A similar pattern existed for mean egg pocket temperatures, which were 7.9°C at the lower sites, 9.5°C at the middle sites and 9.4°C at the upper sites. Temperature differences of similar magnitude existed for riverbed temperatures, with a mean shallow hyporheic zone temperature of 8.4°C at the lower sites, 10.0°C at the middle sites, and 9.9°C at the upper sites (Table 9). The mean temperature of the deep hyporheic zone was 8.9°C at the lower sites, and 10.2°C at the middle and upper sites (Table 9). The temperature range at each site during this period decreased with depth into the riverbed (Figure 29). At the lower sites, the average temperature range was 3.4°C in the river, 3.1°C at egg pocket depth, 2.8°C in the shallow hyporheic zone, and 2.5°C in the deep hyporheic zone. A similar pattern existed for the middle sites, where the average temperature range was 2.8°C in the river, 2.6°C at egg pocket depth, 2.5°C in the shallow hyporheic zone, and 2.4°C in the deep hyporheic zone. At the upper sites, the average temperature range was 2.6°C in the river, 2.4°C at egg pocket depth, 2.4°C in the shallow hyporheic zone, and 2.3°C in the deep hyporheic zone (Figure 29).

During the incubation period with low, stable discharge (19 November 2002 – 7 January 2003), temperature gradient patterns between the river and the riverbed were similar to other time periods. At 13 of the 14 study sites, the average egg pocket temperature at each site was within 0.2°C of the river temperature (Table 9). At the deeper locations within the riverbed, temperature gradients were similar in magnitude as during the earlier time periods. At sites in the lower segment, the mean temperature gradient between the river and the deep hyporheic zone was 1.0–1.6°C (Table 9). This temperature gradient was smaller at sites in the middle segment (0.1–1.1°C) and upper segment (0.3–1.2°C) (Table 9). The three sites exhibiting a strong downward flux of river water entering the riverbed (196.0, 198.2, 244.5–Table 7) continued to have smaller temperature gradients, with shallow hyporheic zone temperatures closer to the river temperature than to the deep hyporheic zone temperature (Table 9). Differences in temperatures among segments were reduced during this time period. The mean temperature of the river was 6.1°C at the lower sites, and 7.6°C at the middle and upper sites (Table 9). A similar pattern existed for mean egg pocket temperatures, which were 6.3°C at the lower sites, 7.6°C at the middle sites and 7.5°C at the upper sites. Temperature differences of similar magnitude existed for riverbed temperatures, with a mean shallow hyporheic zone temperature of 6.8°C at the lower sites, 8.1°C at the middle sites, and 7.9°C at the upper sites (Table 9). The mean temperature of the deep hyporheic zone was 7.4°C at the lower sites, and 8.3°C at the middle and upper sites (Table 9). The pattern of decreased temperature range with depth into the riverbed remained during this time period (Figure 30). At the lower sites, the average temperature range was 5.1°C in the river, 4.7°C at egg pocket depth, 4.3°C in the shallow hyporheic zone, and 3.8°C in the deep hyporheic zone. A similar pattern existed for the middle

sites, where the average temperature range was 5.5°C in the river, 5.2°C at egg pocket depth, 5.3°C in the shallow hyporheic zone, and 4.9°C in the deep hyporheic zone. At the upper sites, the average temperature range was 5.4°C in the river, 5.0°C at egg pocket depth, 5.1°C in the shallow hyporheic zone, and 5.0°C in the deep hyporheic zone (Figure 30).

During the late incubation period with variable discharge (8 January 2003 – 2 March 2003), the temperature gradient patterns within each site remained similar to other time periods, while temperature differences between sites were smaller than during previous time periods. At 11 of the 14 study sites, the average egg pocket temperature at each site was within 0.2°C of the river temperature (Table 9). At the deeper locations within the riverbed, temperature gradients were similar in magnitude as during the earlier time periods. At sites in the lower segment, the mean temperature gradient between the river and the deep hyporheic zone was 0.9–1.4°C (Table 9). This temperature gradient was smaller and more variable among sites in the middle segment (0.1–1.4°C) and upper segment (0.2–1.3°C) (Table 9). The three sites exhibiting a strong downward flux of river water entering the riverbed (196.0, 198.2, 244.5–Table 7) continued to have smaller temperature gradients, with shallow hyporheic zone temperatures closer to the river temperature than to the deep hyporheic zone temperature (Table 9). The two sites (211.9 and 218.7) exhibiting acute flux reversals resulting from short-term (hourly to daily) large magnitude changes in discharge maintained large temperature gradients when averaged over the entire late incubation period. The mean temperature gradient between the river and shallow hyporheic zone was 0.5°C and 0.9°C at site 211.9 and 218.7, respectively (Table 9). Differences in temperatures among segments during this time period were significantly reduced from previous time periods. The mean temperature of the river was 4.8°C at the lower sites, 5.1°C at the middle sites, and 5.0°C at the upper sites (Table 9). A similar pattern existed for mean egg pocket temperatures, which were 4.9°C at the lower sites, 5.3°C at the middle sites and 5.1°C at the upper sites. Temperature differences of similar magnitude existed for riverbed temperatures, with a mean shallow hyporheic zone temperature of 5.2°C at the lower sites, 5.6°C at the middle sites, and 5.3°C at the upper sites (Table 9). The mean temperature of the deep hyporheic zone was 5.8°C at the lower sites, 6.0°C at the middle sites, and 5.7°C at the upper sites (Table 9). The temperature range at each site was smaller than during previous periods. The pattern of decreased temperature range with depth into the riverbed remained for the lower and middle sites, but not for the upper sites (Figure 31). At the lower sites, the average temperature range was 2.7°C in the river, 2.2°C at egg pocket depth, 1.9°C in the shallow hyporheic zone, and 1.2°C in the deep hyporheic zone. A similar pattern existed for the middle sites, where the average temperature range was 1.7°C in the river, 1.4°C at egg pocket depth, 1.5°C in the shallow hyporheic zone, and 1.3°C in the deep hyporheic zone. At the upper sites, the average temperature range was 1.5°C in the river, 1.4°C at egg pocket depth, 1.4°C in the shallow hyporheic zone, and 1.5°C in the deep hyporheic zone (Figure 31).

Table 9. Summary of mean (± standard deviation) water temperature (°C) in the river (R), egg pocket (EP), shallow hyporheic zone (SH), and deep hyporheic zone (DH) at each site during the early spawning period (20 October 2002–18 November 2002), the mid-to-late spawning period and early incubation period (19 November–2 December 2002), the early incubation period with low, stable discharge (19 November 2002–7 January 2003), and the incubation period with variable discharge (8 January–2 March 2003). The overlapping time periods are provided for the separate analyses of fall Chinook salmon life stages (i.e., spawning and incubation).

	Mean (±SD) water temperature (°C)															
	Early spawning period			Late spawning period				Incubation period -- stable discharge				Incubation period -- variable discharge				
Site	R	SH	DH	R	EP	SH	DH	R	EP	SH	DH	R	EP	SH	DH	
L[†]																
148.5	10.0 (1.7)	10.3 (1.6)	10.6 (1.5)	7.8 (1.2)	7.8 (1.2)	8.2 (1.0)	8.6 (1.0)	6.1 (1.3)	6.1 (1.2)	6.6 (1.2)	7.1 (1.1)	4.7 (0.5)	4.9 (0.4)	5.1 (0.4)	5.6 (0.3)	
149.2	9.9 (1.7)	10.2 (1.6)	10.9 (1.5)	7.7 (1.2)	7.8 (1.1)	8.1 (1.1)	8.8 (0.9)	6.0 (1.3)	6.2 (1.2)	6.5 (1.2)	7.2 (1.1)	4.7 (0.5)	4.9 (0.4)	4.9 (0.4)	5.6 (0.3)	
152.3	10.0 (1.7)	10.9 (1.5)	11.4 (1.5)	7.8 (1.2)	7.8 (1.2)	8.7 (0.9)	9.2 (0.8)	6.1 (1.3)	6.2 (1.2)	7.1 (1.2)	7.7 (1.1)	4.7 (0.5)	4.8 (0.5)	5.5 (0.3)	6.1 (0.2)	
156.8	10.1 (1.7)	10.4 (1.6)	10.8 (1.5)	7.8 (1.1)	8.2 (0.9)	8.3 (1.0)	8.7 (0.9)	6.1 (1.3)	6.6 (1.1)	6.8 (1.1)	7.3 (1.0)	4.7 (0.5)	4.9 (0.4)	5.0 (0.4)	5.8 (0.3)	
M[†]																
196.0	12.5 (1.6)	12.5 (1.5)	12.6 (1.6)	9.5 (1.0)	9.4 (0.9)	9.6 (1.0)	9.6 (0.9)	7.5 (1.4)	7.6 (1.2)	7.6 (1.4)	7.6 (1.4)	5.1 (0.3)	5.3 (0.3)	5.2 (0.3)	5.2 (0.3)	
198.2	12.6 (1.5)	12.6 (1.5)	13.0 (1.5)	9.6 (0.9)	9.4 (0.9)	9.7 (0.9)	10.1 (0.8)	7.7 (1.4)	7.6 (1.2)	7.8 (1.3)	8.5 (1.2)	5.3 (0.3)	5.3 (0.3)	5.5 (0.3)	6.4 (0.3)	
198.8	12.5 (1.5)	12.7 (1.5)	12.9 (1.4)	9.5 (1.0)	9.4 (0.9)	9.8 (0.9)	10.1 (0.9)	7.5 (1.4)	7.5 (1.2)	8.0 (1.4)	8.3 (1.3)	5.1 (0.3)	5.3 (0.3)	5.6 (0.2)	6.2 (0.2)	
211.9	12.5 (1.6)	13.0 (1.6)	13.5 (1.6)	9.4 (0.9)	9.5 (0.8)	9.9 (0.8)	10.2 (0.8)	7.5 (1.4)	7.6 (1.3)	7.9 (1.4)	8.2 (1.4)	4.9 (0.3)	5.2 (0.3)	5.4 (0.3)	5.4 (0.4)	
218.7	12.7 (1.6)	13.2 (1.4)	13.4 (1.4)	9.6 (0.8)	9.6 (0.7)	10.4 (0.7)	10.5 (0.7)	7.6 (1.4)	7.7 (1.2)	8.5 (1.3)	8.7 (1.2)	5.0 (0.3)	5.4 (0.2)	5.9 (0.4)	6.5 (0.2)	
219.3	12.6 (1.6)	13.0 (1.6)	13.0 (1.6)	9.5 (0.9)	9.3 (0.8)	9.8 (0.8)	10.0 (0.8)	7.5 (1.4)	7.5 (1.2)	7.8 (1.4)	7.9 (1.4)	4.9 (0.3)	5.1 (0.3)	5.3 (0.3)	5.4 (0.3)	
222.7	12.8 (1.6)	13.3 (1.4)	13.4 (1.4)	9.7 (0.8)	9.4 (0.6)	10.6 (0.7)	10.6 (0.7)	7.7 (1.4)	7.6 (1.2)	8.7 (1.4)	8.9 (1.2)	5.0 (0.3)	5.3 (0.3)	6.0 (0.4)	6.4 (0.4)	
U[†]																
238.6	12.8 (1.6)	13.1 (1.4)	13.6 (1.3)	9.7 (0.7)	9.3 (0.6)	10.2 (0.6)	10.7 (0.6)	7.7 (1.4)	7.5 (1.2)	8.2 (1.3)	8.9 (1.2)	4.9 (0.3)	5.1 (0.3)	5.5 (0.3)	6.2 (0.3)	
240.6	12.8 (1.6)	13.1 (1.6)	13.3 (1.6)	9.5 (0.8)	9.4 (0.6)	9.8 (0.7)	10.2 (0.7)	7.5 (1.4)	7.5 (1.2)	7.8 (1.4)	8.1 (1.4)	4.8 (0.3)	5.0 (0.3)	5.0 (0.3)	5.3 (0.3)	
244.5	12.8 (1.6)	12.8 (1.6)	13.0 (1.6)	9.5 (0.7)	9.3 (0.6)	9.6 (0.7)	9.7 (0.7)	7.5 (1.4)	7.4 (1.2)	7.5 (1.4)	7.8 (1.4)	4.8 (0.3)	4.9 (0.3)	4.9 (0.3)	5.0 (0.3)	

[†] L, M, and U denote the sites grouped by lower, middle, and upper segments of the study area, respectively.

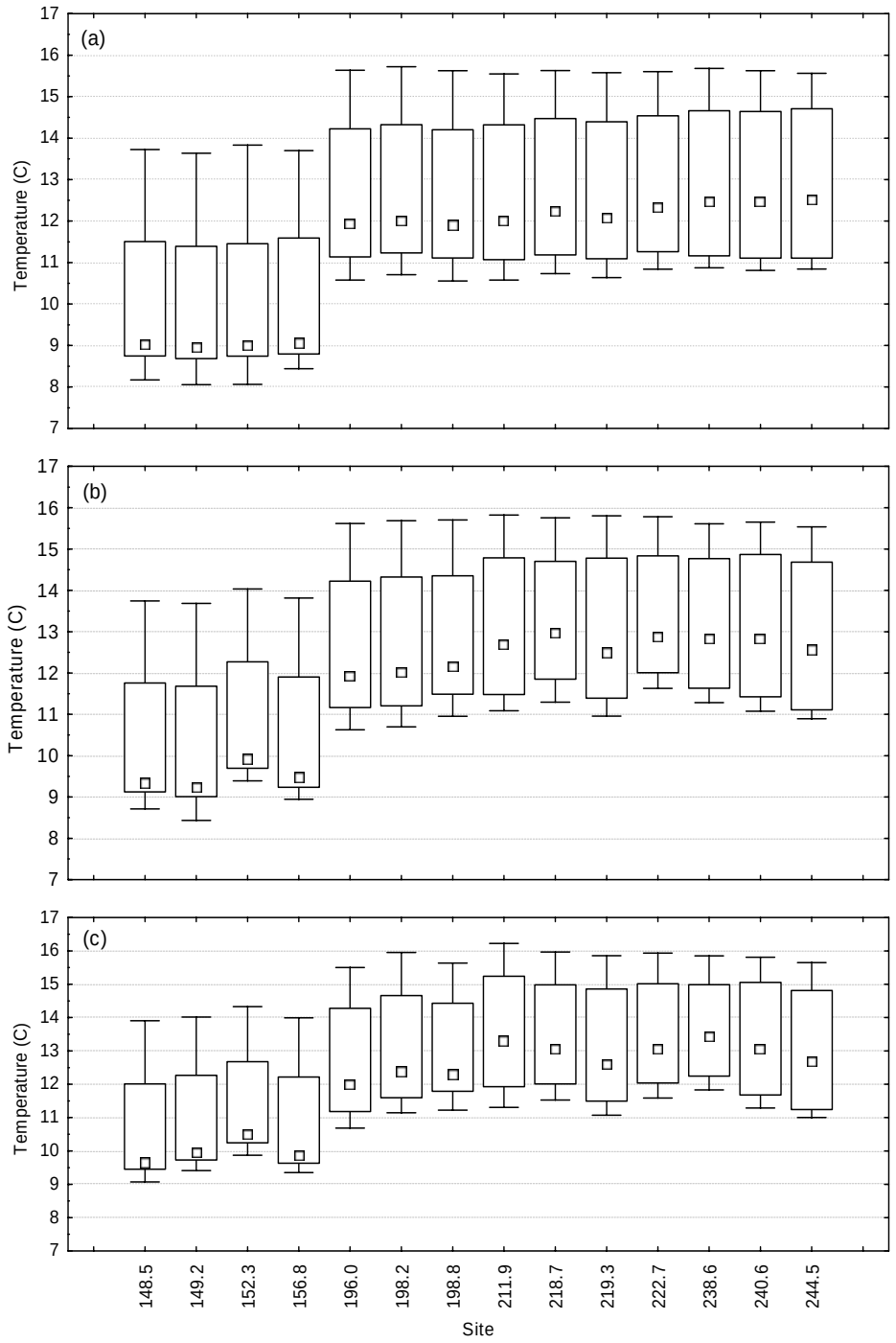

Figure 28. Study sites comparison of water temperature in (a) the river, (b) the shallow hyporheic zone, and (c) the deep hyporheic zone during the early spawning period (20 October – 18 November 2002). Each boxplot represents a summary of hourly water temperature. The point in the center of the boxplot indicates the median, the box is equal to the upper (75%) and lower (25%) quartile range, and the whiskers represent the range.

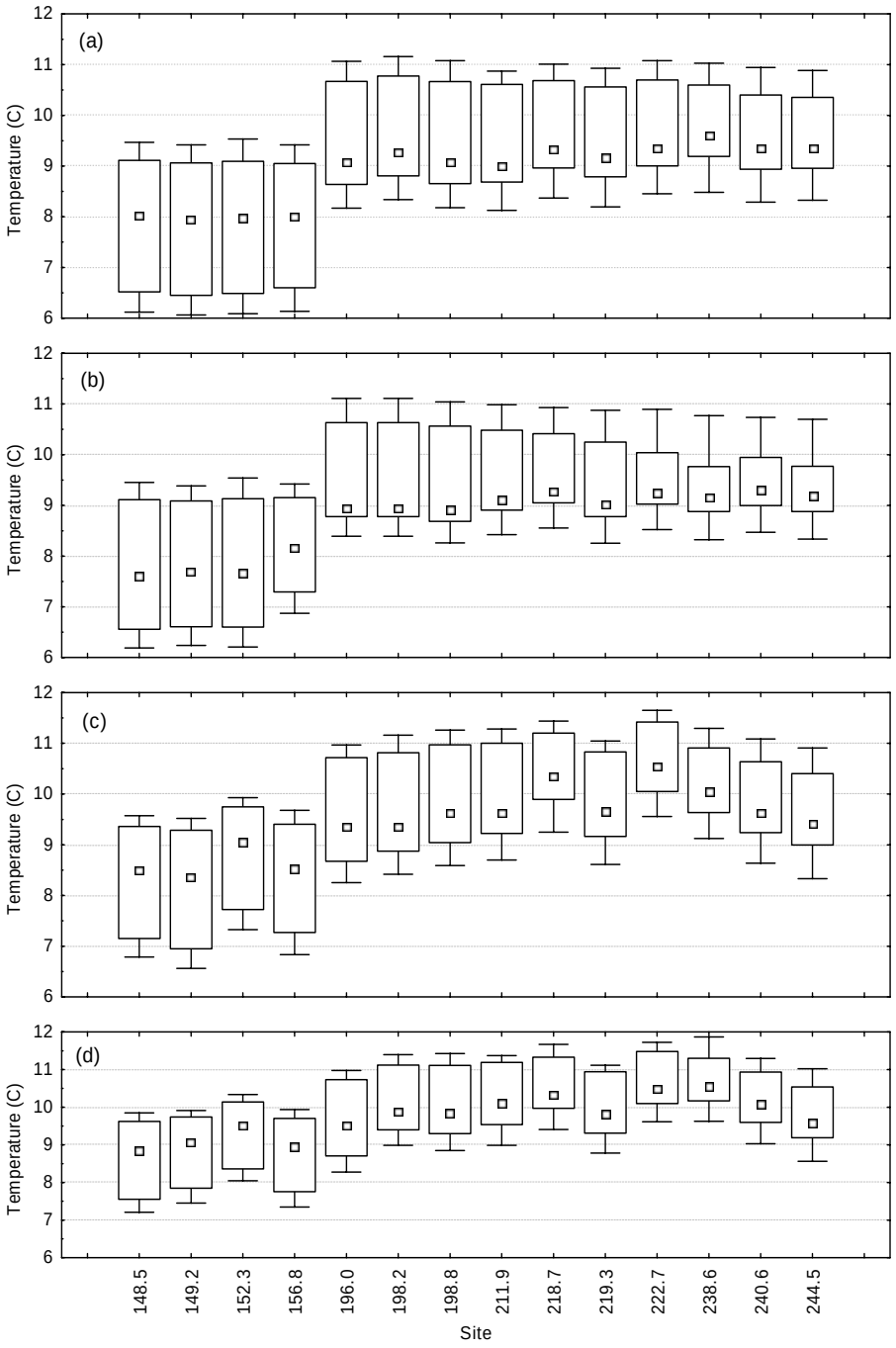

Figure 29. Study sites comparison of water temperature in (a) the river, (b) egg pocket depth, (c) the shallow hyporheic zone, and (d) the deep hyporheic zone during the mid-to-late spawning period and early incubation period (19 November – 2 December 2002). Each boxplot represents a summary of hourly water temperature. The point in the center of the boxplot indicates the median, the box is equal to the upper (75%) and lower (25%) quartile range, and the whiskers represent the range.

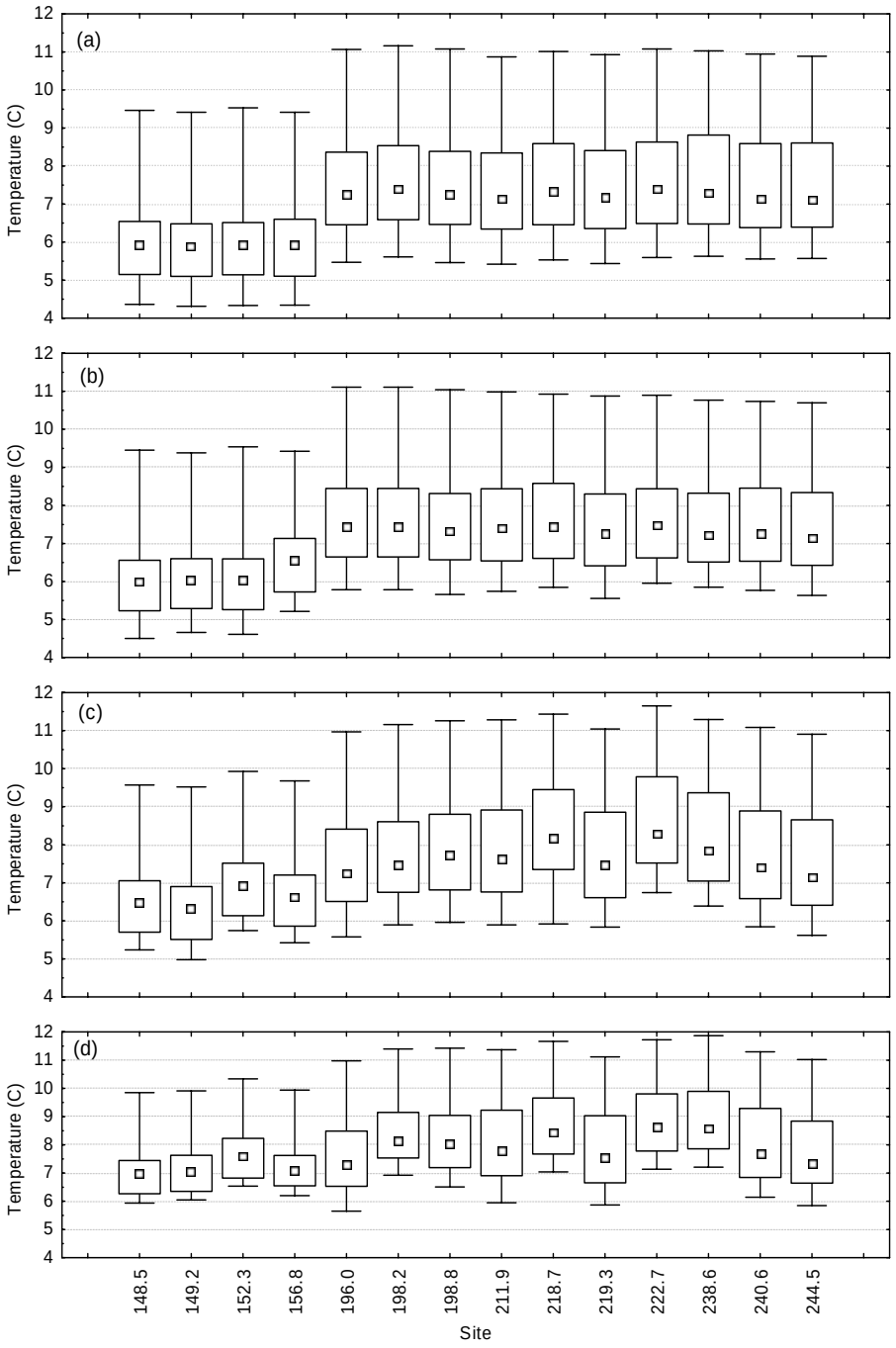

Figure 30. Study sites comparison of water temperature in (a) the river, (b) egg pocket depth, (c) the shallow hyporheic zone, and (d) the deep hyporheic zone during the incubation period with low, stable river discharge (19 November 2002 – 7 January 2003). Each boxplot represents a summary of hourly water temperature. The point in the center of the boxplot indicates the median, the box is equal to the upper (75%) and lower (25%) quartile range, and the whiskers represent the range.

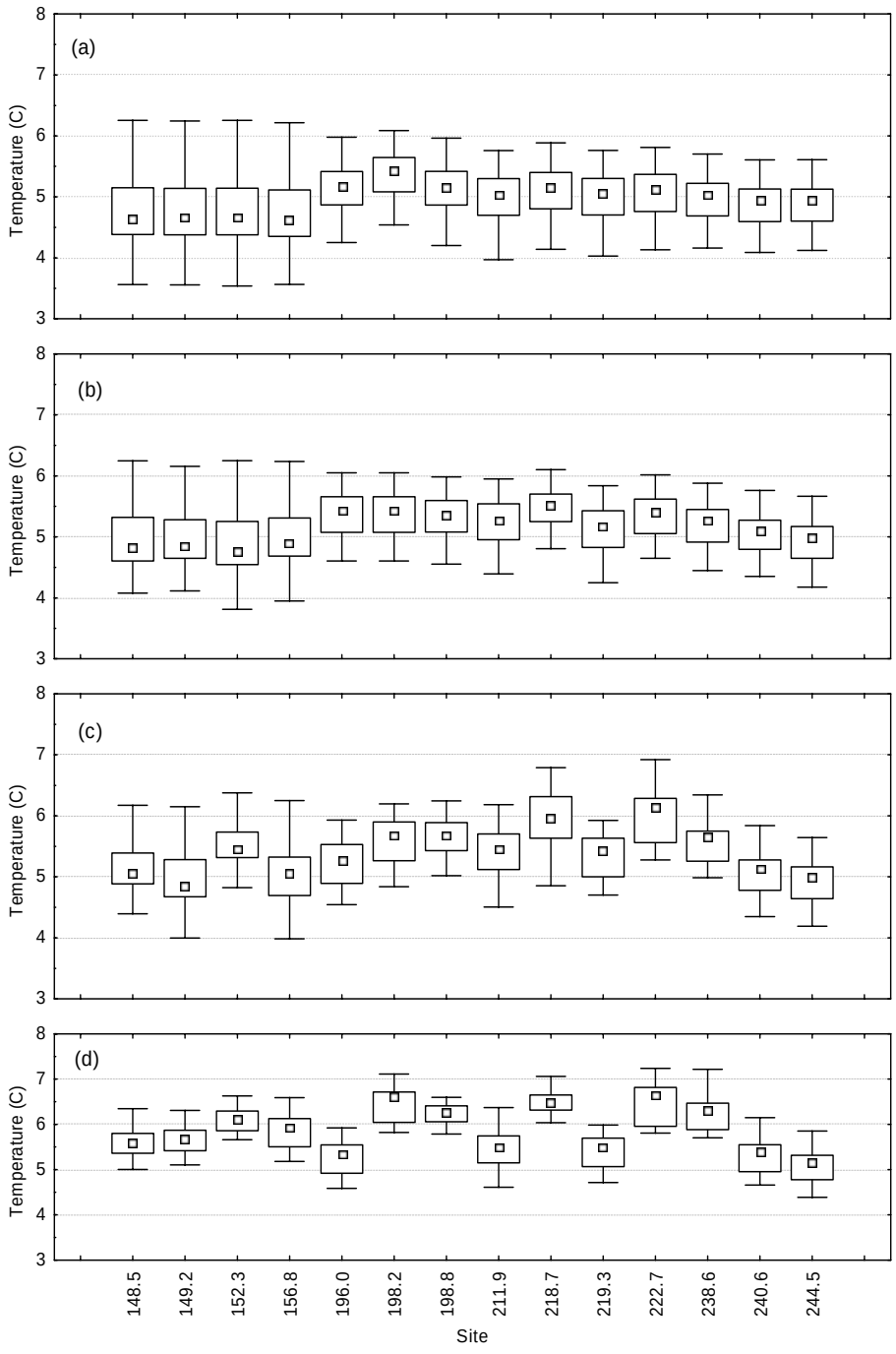

Figure 31. Study sites comparison of water temperature in (a) the river, (b) egg pocket depth, (c) the shallow hyporheic zone, and (d) the deep hyporheic zone during the incubation period with variable river discharge (8 January – 2 March 2003). Each boxplot represents a summary of hourly water temperature. The point in the center of the boxplot indicates the median, the box is equal to the upper (75%) and lower (25%) quartile range, and the whiskers represent the range.

All of the study sites exhibited a daily positive vertical temperature gradient with depth into the riverbed for the entire study period (Appendix Figures 43–56). All sites displayed positive temperature gradients for daily maxima and daily minima, however the magnitude of the temperature gradient varied among sites. At nearly all sites, the temperature gradient increased as water temperature decreased through the study period, indicating a stronger retention of heat within the riverbed at these sites. At site 211.9, the temperature gradient decreased through time (Figure 32), while the temperature gradient at site 244.5 was unchanged (Figure 33). Sites exhibiting a strong downward flux of river water entering the riverbed (196.0, 198.2, 244.5–Table 7) possessed smaller temperature gradients, with shallow hyporheic zone temperatures closer to the river temperature than to the deep hyporheic zone temperature (Figures 34, 35, and 33, respectively). The two sites (211.9 and 218.7) exhibiting acute flux reversals resulting from short-term (hourly to daily) large magnitude changes in discharge possessed different patterns of daily temperature gradient. Site 211.9 displayed a comparatively smaller temperature gradient that decreased throughout the study period (Figure 32), while site 218.7 exhibited a larger temperature gradient that increased through time (Figure 36).

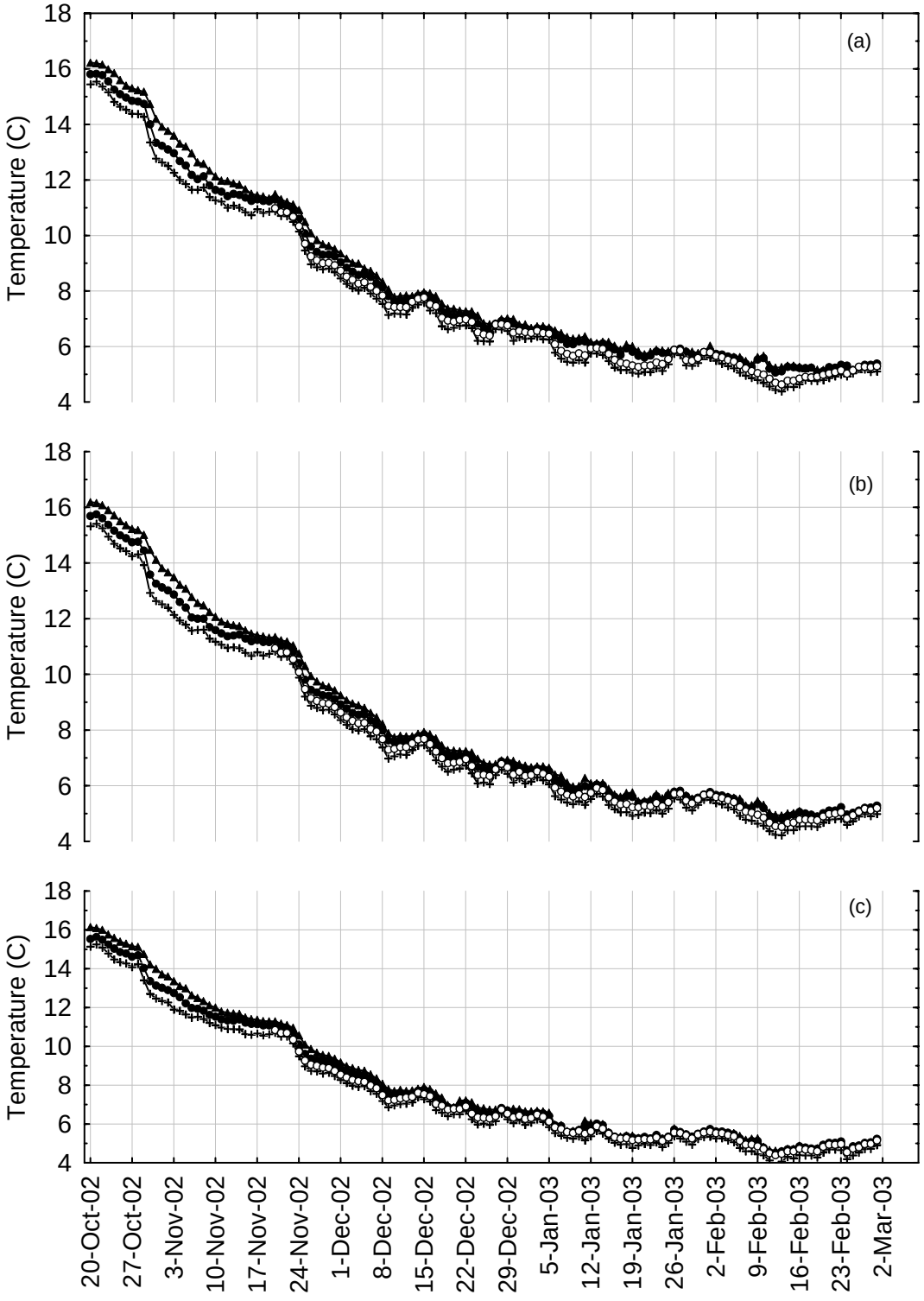

Figure 32. Daily maximum (a), average (b), and minimum (c) temperature of the river (+), egg pocket (○), shallow hyporheic (●) and deep hyporheic (▲) zones at site 211.9.

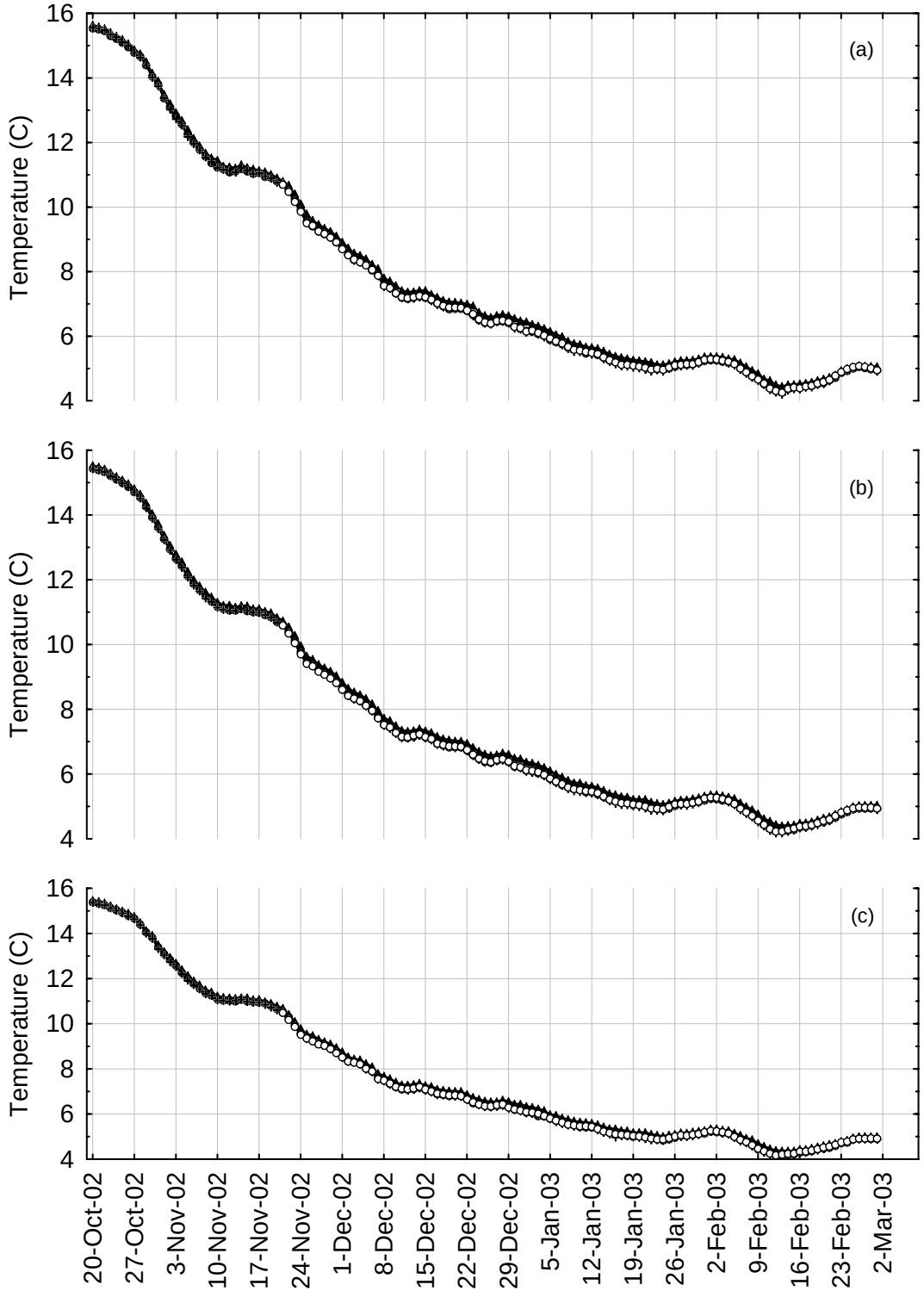

Figure 33. Daily maximum (a), average (b), and minimum (c) temperature of the river (+), egg pocket (○), shallow hyporheic (●) and deep hyporheic (▲) zones at site 244.5.

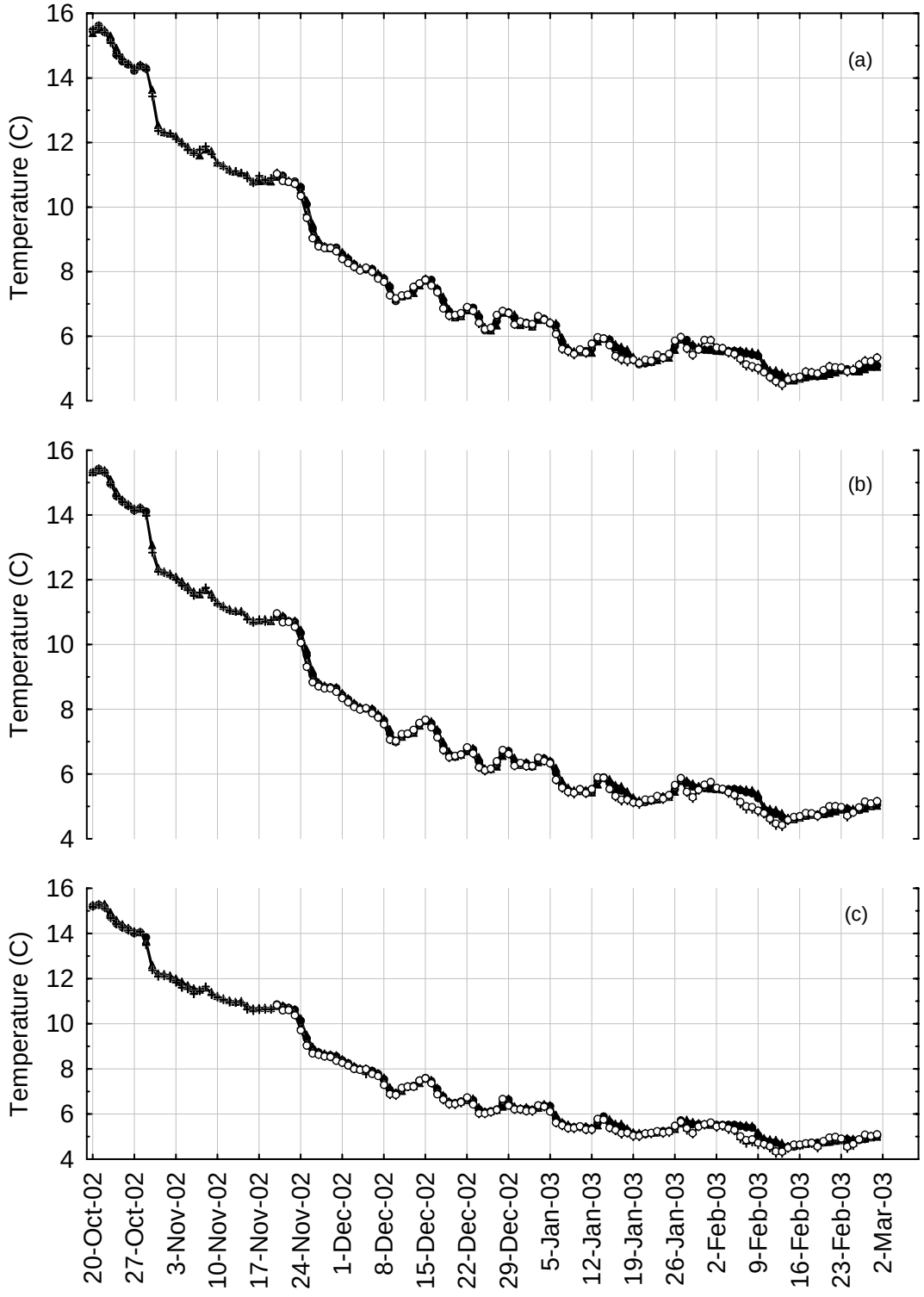

Figure 34. Daily maximum (a), average (b), and minimum (c) temperature of the river (+), egg pocket (○), shallow hyporheic (●) and deep hyporheic (▲) zones at site 196.0.

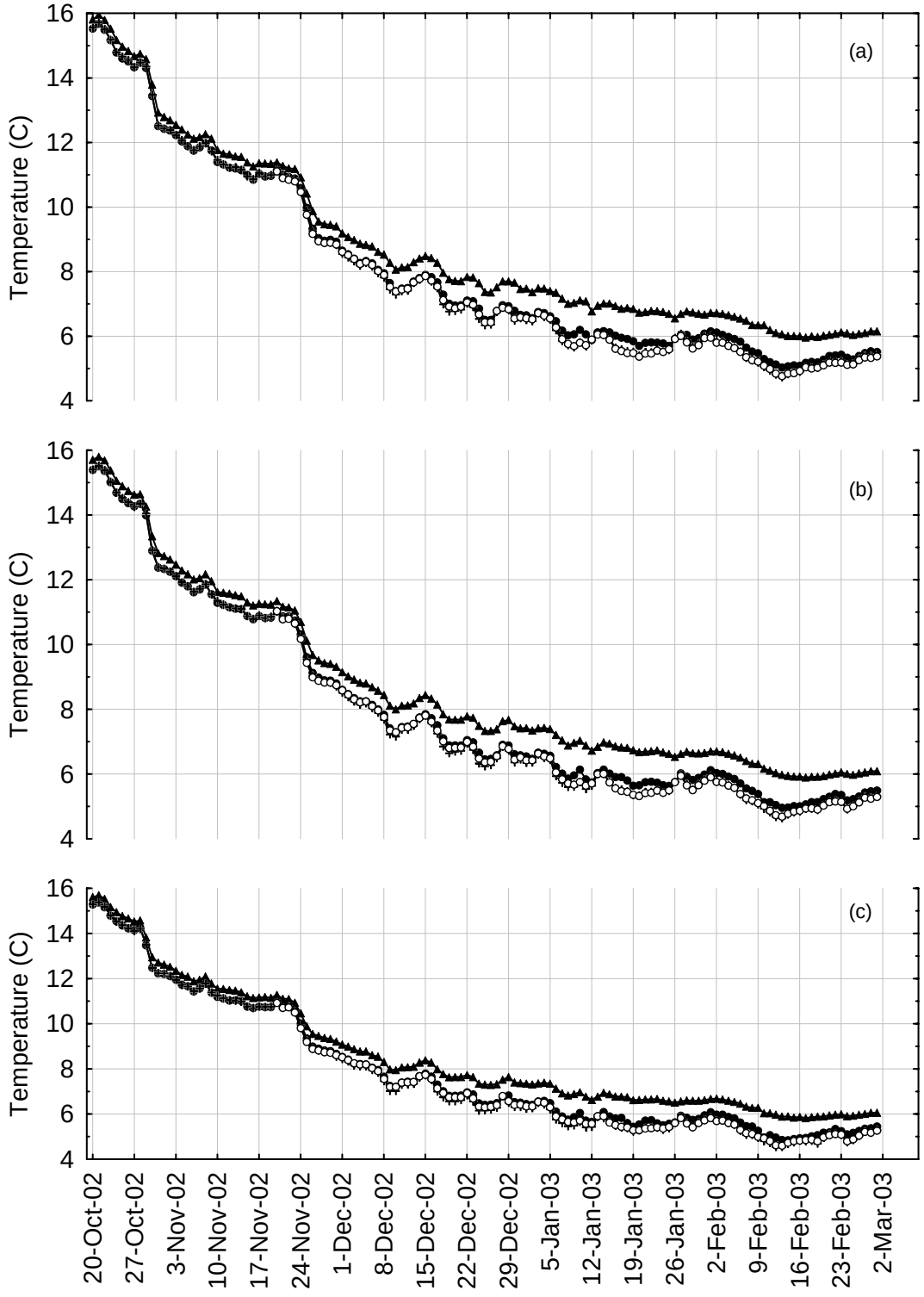

Figure 35. Daily maximum (a), average (b), and minimum (c) temperature of the river (+), egg pocket (○), shallow hyporheic (●) and deep hyporheic (▲) zones at site 198.2.

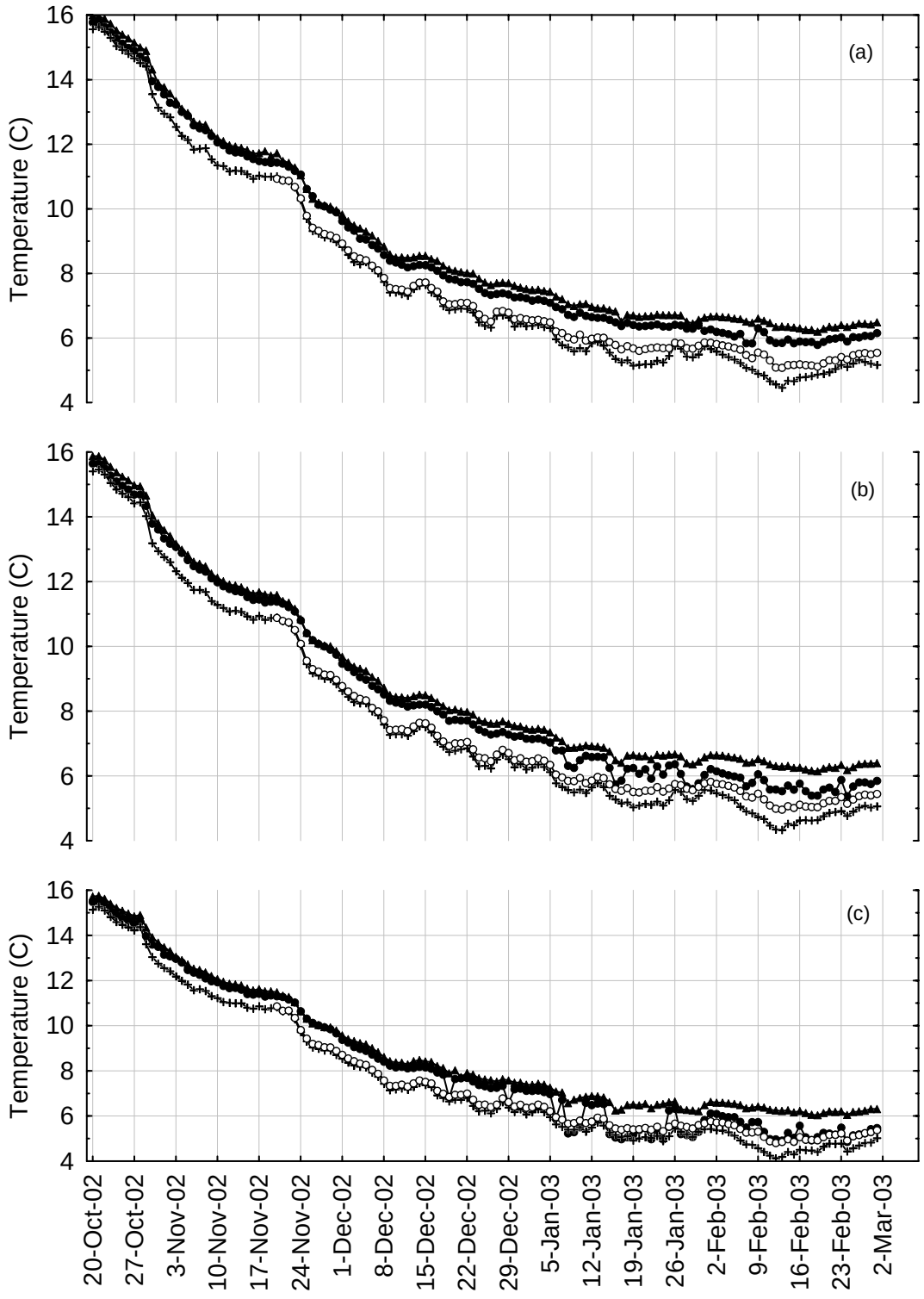

Figure 36. Daily maximum (a), average (b), and minimum (c) temperature of the river (+), egg pocket (○), shallow hyporheic (●) and deep hyporheic (▲) zones at site 218.7.

3.5 Laboratory Egg/Alevin Growth Rates

Eggs ranged in weight from 229 to 370 mg and in diameter from 7.4 to 8.8 mm (Table 10). Egg diameters and weights were fairly consistent within females, but differed significantly (ANOVA, df =5 and 299, P <<0.0001) between females. The largest variation was observed between females 1 and 3, but all fish differed. Largest eggs were observed in female 1, and smallest eggs were observed in female 3.

Maximum alevin wet weight (MAWW) did not differ between the Swan Falls group (Females 1–3) and the Hells Canyon group (Females 4-6) (t-test = -0.764, df =4, P=0.487) with averages from individual females ranging from 333.2 to 501.6 mg (Table 11). The maximum tissue weight (MTW) and maximum fork length (MFL) also did not differ between the two groups (t-test = -0.634, df=4, P = 0.56 for MTW and t-test = -1.46, df = 4, P = 0.22 for MFL) with individual values for MTW and MFL ranging from 48.6 to 78.4 mg and 36.5 to 39.9 mm, respectively (Table 11). Although there were no differences in the maximum growth metrics between temperature regimes, the time to achieve these growth metrics was faster in the embryos raised in the Swan Falls temperature regime as compared to the Hells Canyon temperature regime. For example, the time post-fertilization to achieve MAWW for fish in the Swan Falls temperature regime was 145.3 days (standard error (SE) = 1.5 d) as compared to 152.7 days (SE = 1.5 d) in the Hells Canyon group. Similar differences were noted for MTW and MFL, with Swan Falls fish reaching MTW and MFL in 154 and 150 days, respectively, as compared to 162 and 160 days in Hells Canyon fish. Growth rates from hatch to achievement of MAWW, however, did not differ between the two groups (t-test = 0.606, df = 4, P = 0.5773), averaging 0.644 mg/d (SE = 0.09 mg/d) in the Swan Falls group compared to 0.569 mg/d (SE = 0.09 mg/d) in the Hells Canyon group (Table 12).

There was no difference between the two groups in the ATUs at MAWW, MTW, MFL, and minimum k_d values (Table 13). For example, at the time of MAWW, Swan Falls fish had accumulated an average of 987 ATUs (range 954 to 1015) as compared to 997 ATUs in the Hells Canyon group (range 982 to 1019) (Figure 37). These values were not different (t-test 0.468, df = 4, P = 0.66). The critical ATU values for MTW, MFL, and k_d tended to be higher than those determined for MAWW (Table 13).

Table 10. Egg Mass and Diameter. 50 eggs from each female were sampled for mass and diameter. Values represent the mean with the 95% confidence interval in parentheses.

Female	Initial egg mass (mg)	Egg diameter (mm)
1	371	8.8
	(368–373)	(8.8–8.9)
2	274	7.8
	(271–276)	(7.8–7.9)
3	229	7.4
	(227–231)	(7.3–7.4)
4	299	8.0
	(297–301)	(8.0–8.1)
5	308	8.1
	(306–310)	(8.0–8.1)
6	333	8.3
	(330–335)	(8.2–8.4)

Table 11. Female-specific differences in the wet weight, length, k_d, and tissue-yolk composition of fall Chinook salmon at three stages: maximum alevin wet weight; maximum tissue weight, and maximum fork length. n=5, df=days post fertilization.

Female	Time (day pf)	Wet weight (mg)	Fork length (mm)	k_d	Composition	
					Tissue dry weight (mg)	Yolk dry weight (mg)
Maximum Alevin Wet Weight						
1	146	501.6	39.5	2.01	72.8	23.3
2	148	382.3	37.3	1.95	53.2	18.4
3	142	333.2	36.2	1.92	44.5	12.9
4	155	430.3	38.8	1.95	63.0	11.2
5	151	427.0	39.2	1.92	62.1	13.1
6	152	481.3	39.6	1.99	68.0	18.5
Maximum Tissue Weight						
1	154	514.0	40.6	1.96	78.4	10.6
2	160	400.8	38.9	1.88	58.2	4.9
3	148	335.0	36.8	1.89	48.6	7.7
4	163	443.0	39.6	1.92	64.9	3.1
5	160	437.9	40.1	1.89	65.7	3.8
6	162	495.9	40.6	1.94	71.8	7.0
Maximum Alevin Length						
1	152	510.7	39.9	1.97	78.0	13.7
2	151	387.8	37.2	1.93	55.1	15.1
3	147	334.2	36.5	1.89	46.8	8.6
4	165	445.4	39.1	1.91	68.4	1.2
5	159	436.9	39.5	1.89	66.6	4.9
6	157	489.8	39.6	1.96	71.0	12.7

Table 12. Growth Rates and Gross Yolk Conversion Efficiency

Female	Growth rate (mg/d) (SE)	Yolk conversion efficiency (%)
1	0.87 (0.08)	67.8
2	0.62 (0.04)	66.6
3	0.44 (0.05)	74.1
4	0.54 (0.04)	80.5
5	0.56 (0.04)	79.9
6	0.60 (0.04)	74.3

Table 13. Critical ATU Values. MAWW = maximum alevin wet weight, MTW = maximum tissue weight, MFL = maximum fork length.

Female	MAWW	MTW	MFL	Min k_d
1	995	1091	1067	1095
2	1015	1164	1055	1059
3	954	1026	1014	1071
4	1019	1087	1105	1165
5	982	1065	1052	1113
6	991	1082	1038	1054

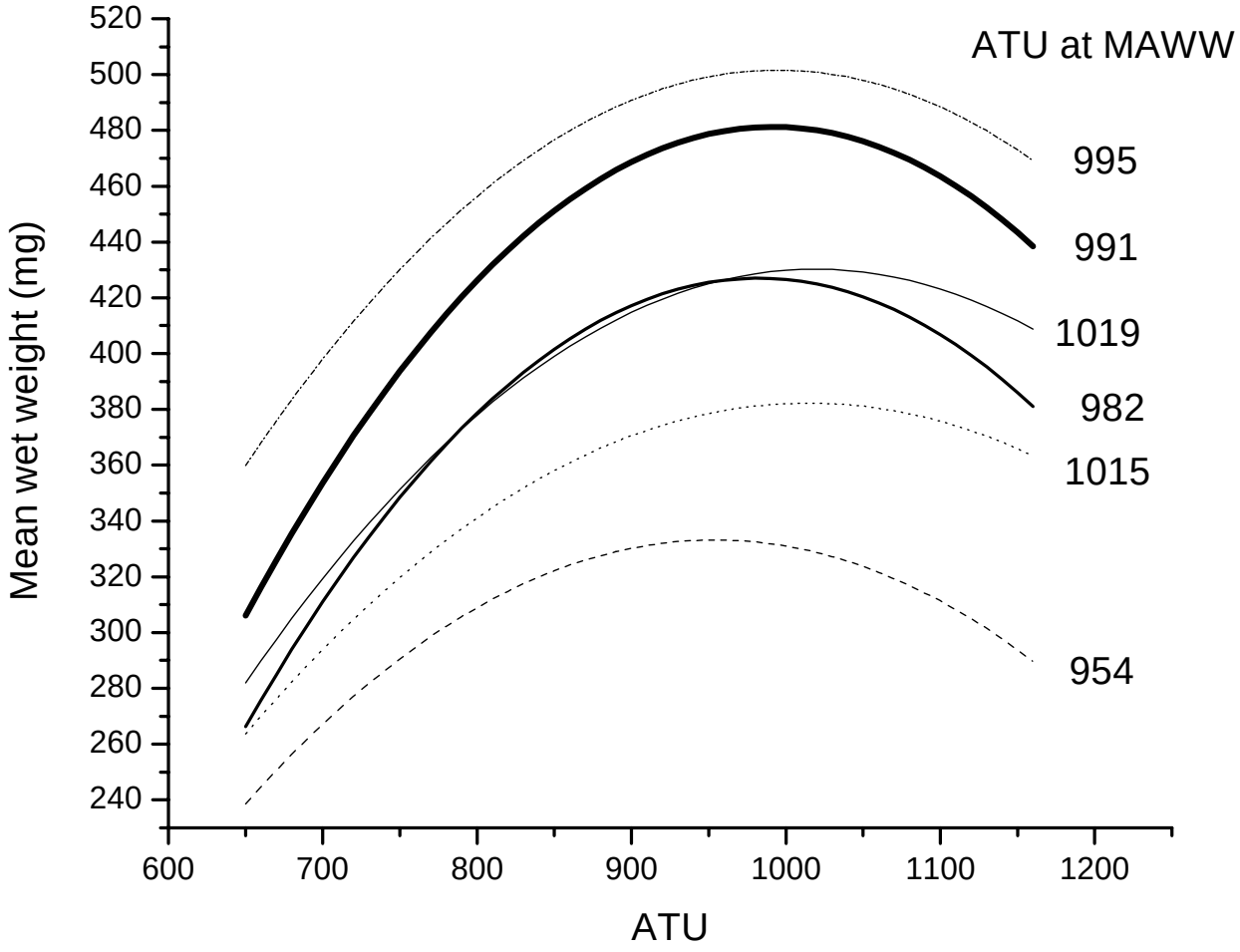

Figure 37. Growth curves for alevin offspring from six different females. At maximum alevin wet weight (MAWW), alevins from female group 1 (_ . _ .), 2 (.....), 3 (- - - - -), 4 (____), 5 (____), and 6 (▬▬), had 995, 1015, 954, 1019, 982, and 991 accumulated temperature units (ATU), respectively.

3.6 Emergence Timing

At nearly all of the 14 study sites, the artificial egg pockets accumulated temperature units at approximately the same rate as the surface water, owing to the small temperature gradient between the river and artificial egg pocket depth. The egg pockets at all of the study sites reached 1000 ATU (the time period when emergence is often considered to occur) within seven days of the surface water reaching 1000 ATU (Appendix Figures 57–70). At 10 of the 14 study sites, the egg pockets and surface water reached 1000 ATU within 4 days or less. Within each site, the number of days post-fertilization required to reach 1000 ATU was highly variable among the different depths within the riverbed. The within-site difference between egg pocket depth and the shallow hyporheic zone in the number of days post-fertilization required to reach 1000 ATU ranged from 0 days at site 244.5 to 14 days at site 222.7 (Figure 38). This difference was smallest at sites exhibiting a strong downward flux of surface water (196.0 and 244.5), and largest at sites characterized by a strong upward flux (152.3 and 222.7) (Table 7, Figure 38). Among all the study sites, the number of days post-fertilization required to reach 1000 ATU was also highly variable. At sites in the lower segment, the number of days required to reach 1000 ATU was 144–148 in the artificial egg pockets, 136–145 in the shallow hyporheic zone, and 125–135 in the deep hyporheic zone (Figure 38). A much larger range occurred among the middle sites, where the number of days required to reach 1000 ATU was 134–138 in the artificial egg pockets, 121–136 in the shallow hyporheic zone, and 116–135 in the deep hyporheic zone (Figure 38). At the upper sites, the number of days required to reach 1000 ATU was 139–142 in the artificial egg pockets, 129–142 in the shallow hyporheic zone, and 117–139 in the deep hyporheic zone (Figure 38).

Results from the laboratory rearing of eggs and alevins indicated a large range in ATU at MAWW (the index of emergence timing) among the six different female groups. Offspring from female 3 reached MAWW at 954 ATU, while offspring from female 4 reached MAWW at 1019 ATU (Figure 37). Based on the average egg pocket temperature within each site, the number of days post-fertilization required to reach the range of ATU at MAWW from the six female groups differed over a range of 9 to 13 days (Figure 39). This range of days post-fertilization to ATU at MAWW based on female-specific differences is as large as or larger than the range based on site-specific differences of depth within the riverbed (0–14 days, Figure 38). Among the study sites and female groups, the number of days post-fertilization required to reach the range of ATU at MAWW differed over a range of 0 to 27 days (Figure 39).

Although two sites (211.9 and 218.7) exhibited acute flux reversals between river water and hyporheic water resulting from short-term (hourly to daily) large magnitude changes in discharge, these flux reversals had minimal effect on emergence timing estimates based on ATU. At both sites, the average temperature gradient between the river and artificial egg pocket depth was 0.1°C (Table 9), and thus short-term changes in discharge did not affect artificial egg pocket temperatures (Figures 32 and 36). As such, the rate of ATU at egg pocket depth was unaffected by short-term changes in discharge (Figures 40 and 41). Similarly, emergence timing estimates based on ATU in the shallow hyporheic zone were largely unaffected by short-term changes in discharge. When the numerical model was used to estimate the shallow hyporheic zone temperatures that would have occurred in the absence of large discharge fluctuations, the emergence timing estimates based on ATU changed by 1 day or less

(Figure 42). At site 211.9, the estimated emergence timing was 1 day later than the observed, while at site 218.7 there was no difference between the estimated and observed emergence timing based on ATU (Figure 42).

The results of growth rates and emergence timing estimates for eggs placed within the egg tubes located in the artificial egg pockets were confounded by low rates of survival to emergence. Live alevins were collected from 11 of the 14 study sites. Among all sites, 20 of the 42 egg tubes contained live alevins. The overall survival rate for all egg tubes was 34%. Post-retrieval field tests of the egg tubes suggested that the low survival rates were likely a function of egg tube design (clogging of the perforated screen), rather than site-specific characteristics.

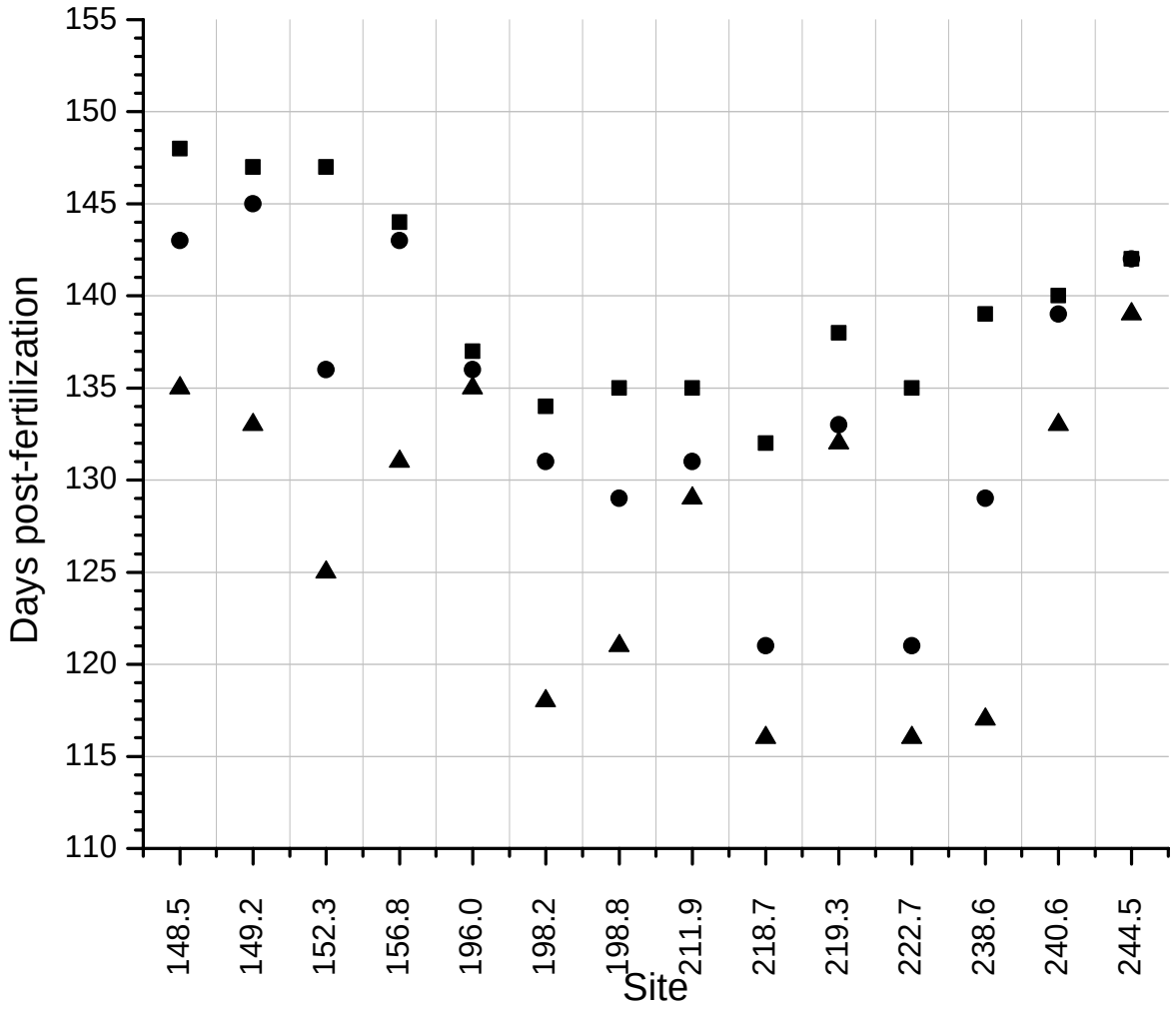

Figure 38. Summary of the number of days post-fertilization required to reach 1000 accumulated temperature units (ATU) in the artificial egg pockets (■), shallow hyporheic zone (●), and deep hyporheic zone (▲) at each site. The daily average temperature at each depth within the riverbed is the basis for the ATU.

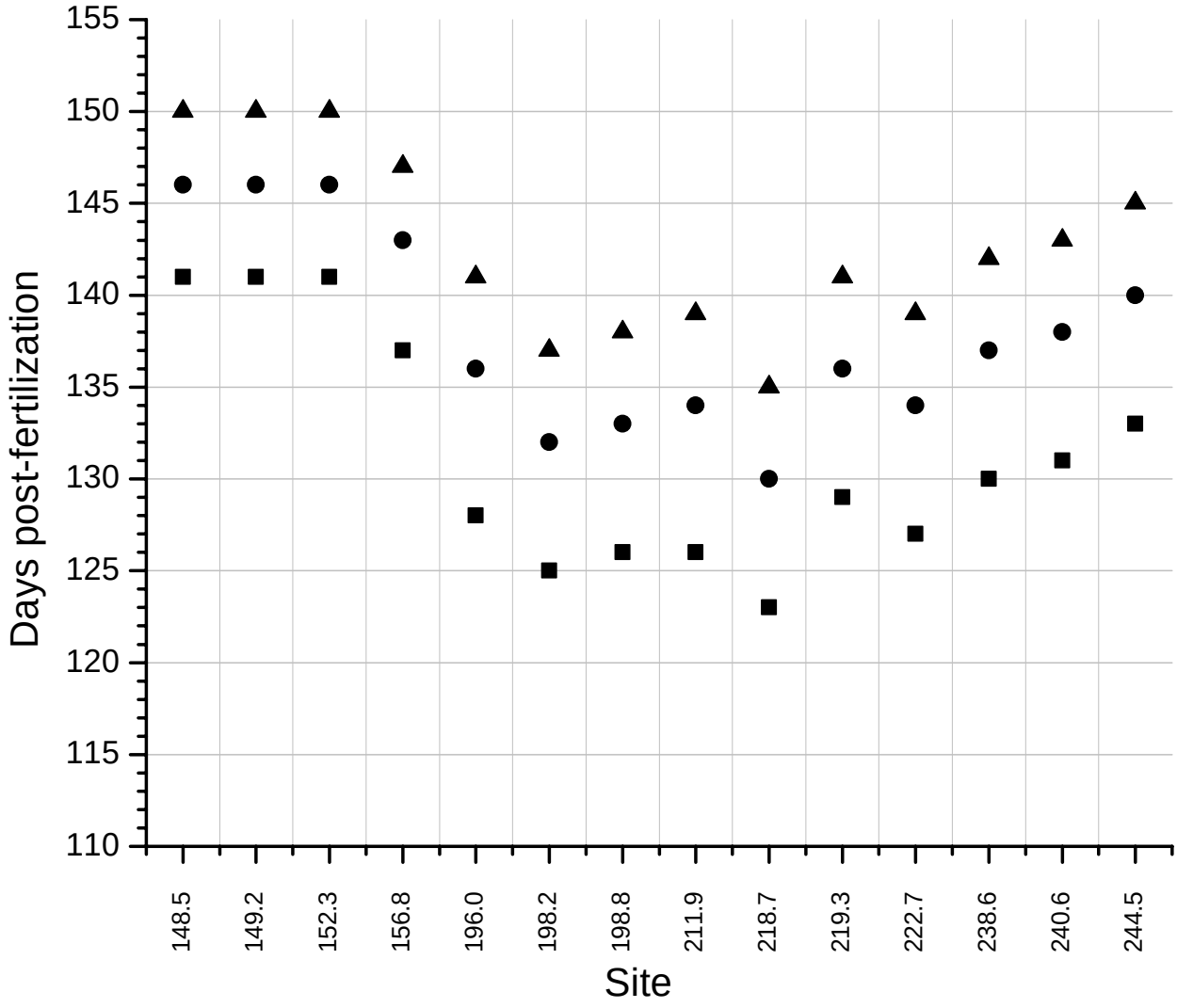

Figure 39. Summary of the number of days post-fertilization for the artificial egg pockets at each site to reach 954 (■), 991 (●), and 1019 (▲) accumulated temperature units (ATU). The daily average temperature of three egg pockets at each site is the basis for the ATU. The three different ATU values (954, 991, and 1019) correspond to the low, middle, and high maximum alevin wet weight (MAWW) for three different alevin groups reared in the laboratory. MAWW is often used as an index of emergence timing.

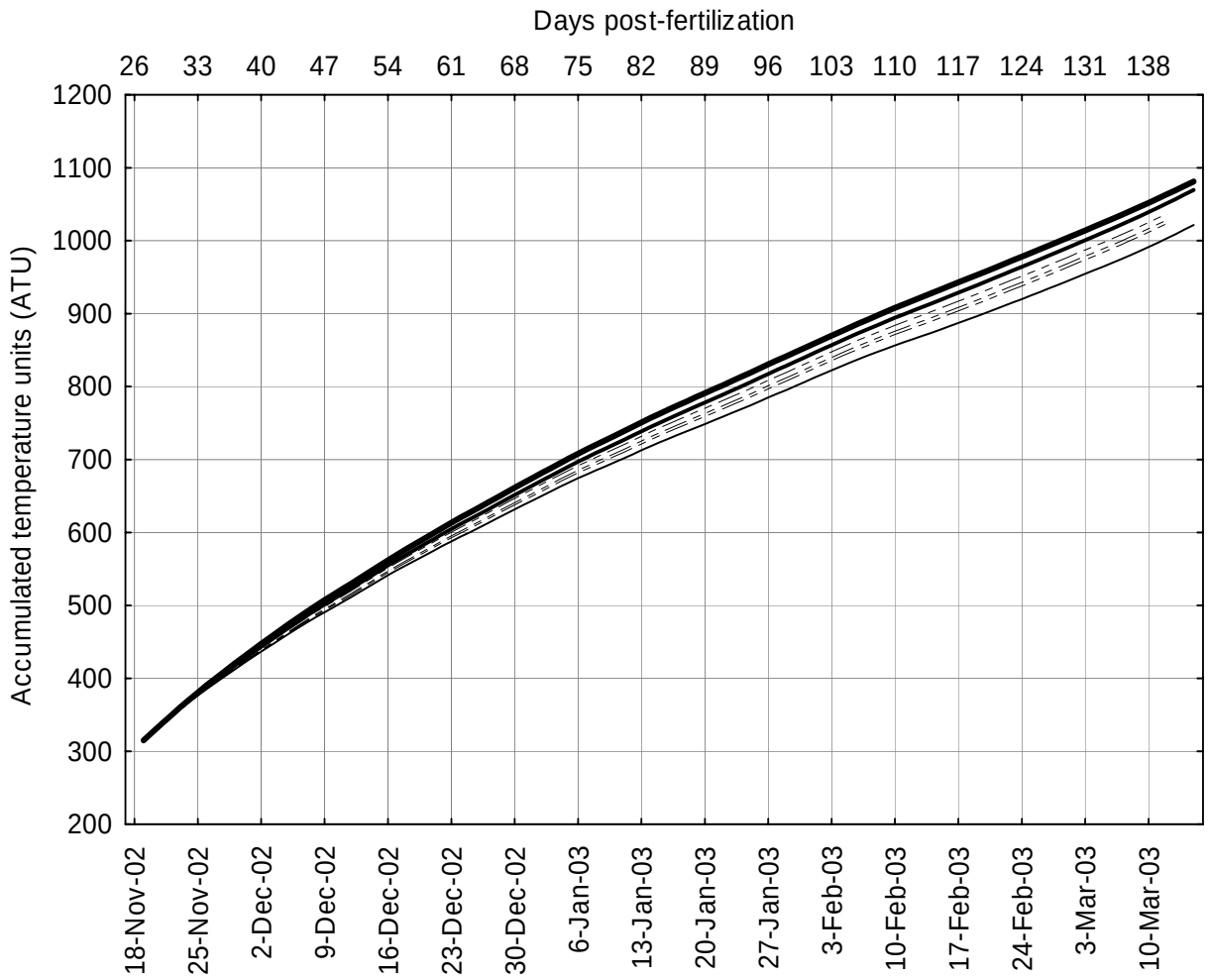

Figure 40. Accumulated temperature units (ATU) at site 211.9 based on temperatures from the river (——), egg pockets (– – –), shallow hyporheic (——), and deep hyporheic (▬▬) zones.

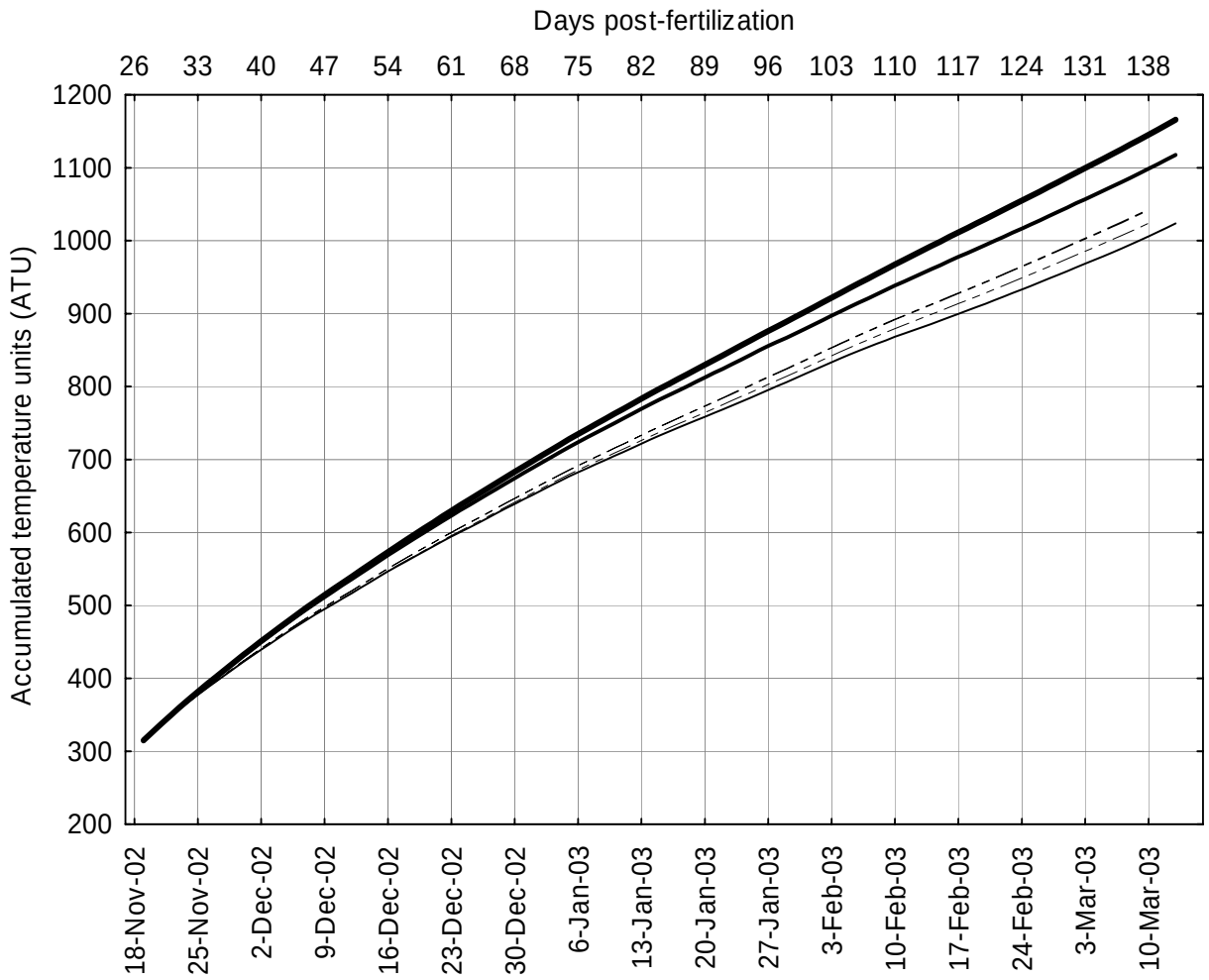

Figure 41. Accumulated temperature units (ATU) at site 218.7 based on temperatures from the river (——), egg pockets (– – –), shallow hyporheic (——), and deep hyporheic (▬▬) zones.

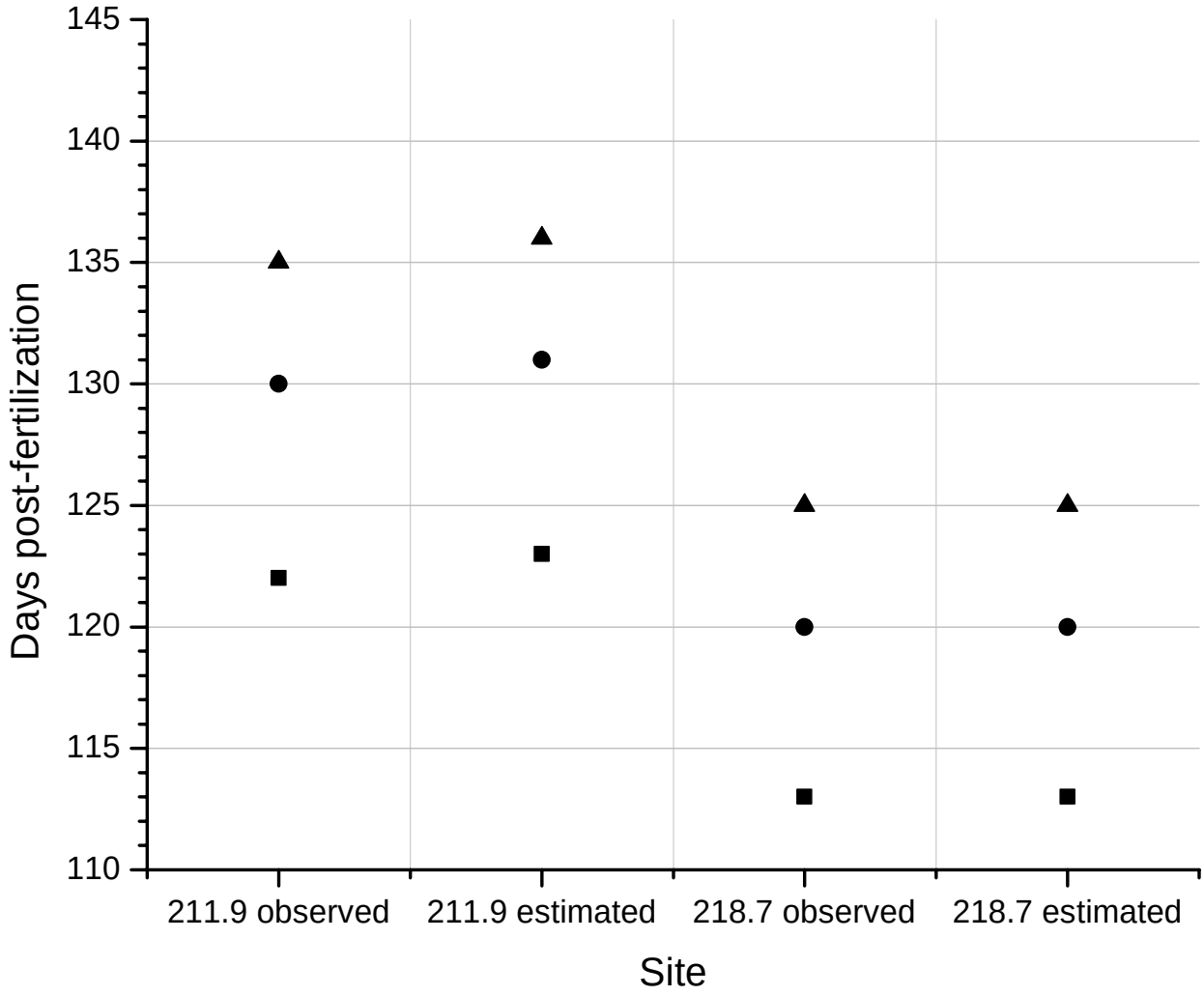

Figure 42. Comparison of the number of days post-fertilization for the shallow hyporheic zone at sites 211.9 and 218.7 to reach 954 (■), 991 (●), and 1019 (▲) accumulated temperature units (ATU). The daily average temperature of the shallow hyporheic zone is the basis for the observed ATU. The estimated ATU values are based on daily average shallow hyporheic zone temperatures derived from numerical modeling. The model removed the short-term (i.e., sub-hourly) changes in shallow hyporheic zone temperature that were a result of acute changes in river stage. The three different ATU values (954, 991, and 1019) correspond to the low, middle, and high maximum alevin wet weight (MAWW) for three different alevin groups reared in the laboratory. MAWW is often used as an index of emergence timing.

4.0 Discussion

Although the local vertical hydraulic gradients were rather small, the estimates of apparent velocity in the hyporheic zone indicated significant interactions between surface and subsurface water. This finding suggests that local differences in hydrostatic pressure (i.e., as measured by small-scale piezometric head differences) play a minor role in the hydrologic exchange between the river and riverbed. The processes controlling this hydrologic exchange are likely to be bedform-induced advective pumping, turbulence at the riverbed surface, and large-scale piezometric gradients along the longitudinal profile of the riverbed. The mobile riverbed at all of the study sites allows the development of local undulations of the riverbed surface, including those caused by spawning Chinook salmon (i.e., redd pits and tailspills) as well as by local bed scour and deposition. These bedforms promote advective pumping exchange between the river and riverbed, whereby the acceleration of flow over the bedform and flow separation at the crest create localized pressure variations that induce flow into and out of the bed (Savant et al. 1987; Elliott and Brooks 1997a). Even in the absence of bedforms, exchange between surface water and flat gravel riverbeds has been observed (Nagaoka and Ohgaki 1990; Shimizu et al. 1990). The mechanism of this exchange has been described as turbulent momentum transfer across the river–riverbed interface (Zhou and Mendoza 1993; Packman et al. 2004). Packman et al. (2004) also observed advective transport on flat gravel beds, which was induced by bed surface irregularities as small as one grain diameter. The magnitude of exchange with bedforms and flat beds scales with the Reynolds number based on sediment grain diameter (Packman et al. 2004). Because all of the study sites have coarse bed surfaces (d_g of 24–80 mm) and high surface water velocities (0.4–1.4 m s^{-1}), it is likely that advective pumping and turbulent diffusion are major processes controlling hydrologic exchange between the river and riverbed. These processes are likely complemented by the hydrologic exchange occurring at the larger scale of the pool–rapid/riffle sequences. Because of the high longitudinal bed slope at the upper and middle sites, and the confined nature of the river corridor (i.e., lack of floodplain), the upstream–downstream piezometric gradients likely contribute significantly to the surface–subsurface exchange (Castro and Hornberger 1991; Larkin and Sharp 1992; Harvey and Bencala 1993). These larger-scale piezometric gradients likely become the dominant exchange process with increasing depth into the riverbed, where the horizontal flow component can be more significant than vertical flow (Saenger 2002).

Our results indicate that hyporheic water at the study sites has the potential to simultaneously flow in multiple directions from the same location within the hyporheic zone. These seemingly contradictory results may be caused by the difficulty in measuring small hydraulic gradients. It is more likely that the observations reflect the complex nature of the hydraulic interactions between the river and riverbed. Hyporheic flow in the vertical (both upward and downward) and horizontal direction at the same location has been modeled (Elliott and Brooks 1997b; Worman et al. 2002) and observed in the laboratory (Thibodeaux and Boyle 1987; Elliott and Brooks 1997b; Packman et al. 2004), but has not been widely observed in riverbeds. Using tracer injections and piezometric potential measurements in multilevel probes placed in the riverbed, Saenger (2002) was able to divide the apparent velocity vector into its vertical and horizontal components. She found that vertical flow dominated in the upper 20 cm of the riverbed, while horizontal flow dominated in the sediments deeper than 20 cm. Our findings seem to correlate well with those of Saenger (2002), and with the model and laboratory observations cited above. For example, at 13 of the 14 study sites the average VHG between the shallow hyporheic zone and the

river was greater than the VHG between the deep hyporheic zone and the river. This finding implies that at some area of the riverbed near the shallow hyporheic zone, pore water had the potential for both upwelling and downwelling. Results from the numerical model and temperature monitoring support this finding. For example, at site 198.8 the positive VHG potential (upwelling) from the shallow hyporheic zone was larger than the positive VHG potential (upwelling) from the deep hyporheic zone, resulting in a small downwelling potential from the shallow to the deep hyporheic zone. Results from the numerical model suggested an average downward flux of 0.4 cm h^{-1} from the river to the riverbed. The temperature monitoring indicated that this advective infiltration from the river must be tempered by horizontal and/or vertical flux (advective or diffusive) from deeper within the riverbed, as in the absence of these secondary processes the temperature gradient between the river and the hyporheic zone would be much smaller than observed. This finding of three-dimensional flow at the same point within a riverbed matches very well with recent laboratory observations. Packman et al. (2004) injected dye at 3 cm below a gravel bed surface in a flume, and observed the dye moving upward, downward and horizontally from the same injection point.

The results from this study suggest that at most of the study sites there is a negligible effect of river discharge on vertical hydrologic exchange. During the periods of low, stable discharge and high, variable discharge, the measured shallow hyporheic zone temperatures at most sites could be accurately modeled with a constant estimate of apparent velocity. At most sites, acute changes in river discharge had a small effect on measured VHG. In many cases, the measured head differences approached the measurement error of the equipment (approximately ±1.6 cm). At most of the sites with a measurable relationship (positive or negative) between river stage and VHG, the resulting effect was a very small or nonexistent change in bed temperature. Similar observations of the negligible effect of river stage on exchange flux have resulted from modeling (Storey et al. 2003) and field studies (Lenk and Saenger 2000).

The combined results of temperature monitoring and numerical modeling indicated that at only two sites (211.9 and 218.7) was the vertical hydrologic exchange significantly affected by short-term (hourly to daily) large magnitude changes in discharge. At both of these sites, a large increase in river stage caused the exchange flux to reverse from upwelling to downwelling. Similar observations have been made within fall Chinook salmon spawning areas in the Columbia River (Geist 2000). The exact mechanism for this flux reversal has not been fully explored, although it may result from the proximity of piezometers located in highly permeable substrate adjacent to riverbanks with significant storage capacity (Geist 2000). The physical characteristics of sites 211.9 and 218.7 are similar enough to the other upper and middle sites that the hydrologic exchange between the riverbed and banks should be quite similar. Thus, it is not likely that bank storage alone explains the observed flux reversals. Another possible reason for the flux reversals may be that sites 211.9 and 218.7 contain shallow riverbed layers of relatively low hydraulic conductivity (K), such that advected surface water is not easily entrained into the riverbed. However, permeability alone does not explain the flux reversals observed at sites 211.9 and 218.7 that were not observed at the other sites. The average K at 218.7 was estimated from slug tests to be 0.16 cm s^{-1}, which is an order of magnitude higher than the K estimate of 0.05 cm s^{-1} at site 196.0 (TP Hanrahan, unpublished data), a site where rapid advection of surface water into the riverbed resulted in near isothermal conditions between the river and riverbed. The K estimate of 0.01 cm s^{-1} at site 211.9 is within the same order of magnitude as the K estimate at most of the upper and middle sites, and an order of magnitude larger than the K estimate at the lower sites. Application of the temperature travel

time model to estimate the flux rate at sites 211.9 and 218.7 (just during the periods of acute stage changes and rapid downwelling) resulted in apparent velocity estimates of 3.0 cm h^{-1} and 5.7 cm h^{-1}, respectively, which is near the upper end of the range among all sites. Based on the temperature monitoring and numerical modeling at sites 211.9 and 218.7, it appears that at low river discharge the riverbed at these sites is dominated by horizontal/longitudinal flow that has a relatively long residence time in the bed, thus being considerably warmer than the river; when the stage increases, the local hydraulics (e.g., water surface slope) change such that advective processes dominate the exchange, even to a depth of 60 cm below the riverbed surface. This explanation is qualitatively supported by the model results from Storey et al. (2003).

The numerical model used to estimate the vertical apparent velocity (v_z) in the hyporheic zone has some limitations, but the results indicate that the model performed well. Application of the model assumes that 1) v_z is constant over time and depth within the riverbed and 2) flux occurs only in the vertical direction. These assumptions are likely violated, as hyporheic flow is often observed to be unsteady and three-dimensional (Worman et al. 2002; Storey et al. 2003). Estimates of v_z from the numerical model match well with those based on other methods. At four of the study sites (152.3, 198.8, 222.7, and 240.6), previous investigations estimated v_z as the product of vertical hydraulic gradients (VHG) measured in standpipes and hydraulic conductivity (K) estimated with slug tests (Arntzen et al. 2001). At sites 152.3 and 222.7, the v_z estimate from the numerical model was within the same order of magnitude as the average v_z from the empirical data. At sites 198.8 and 240.6, v_z estimates from the numerical model and empirical data differed by two orders of magnitude. It is likely that the differences are due to methodological issues and small-scale variability in hyporheic zone characteristics, as both VHG and K varied by one to three orders of magnitude within the same site (Arntzen et al. 2001). At other contemporary and historic fall Chinook salmon spawning locations in the Columbia and Snake rivers, application of similar empirical methods resulted in v_z estimates of comparable magnitude to our numerical estimates of v_z (Geist 2000; Hanrahan et al. in press). Estimates of v_z from the numerical model also match well with v_z estimates based on similar numerical models from other gravel-bed rivers (Silliman et al. 1995; Constantz and Thomas 1996; Lenk and Saenger 2000; Saenger 2002). Our evaluation of model performance by comparing modeled and measured bed temperatures indicated that the model was fairly robust over long time periods. While the numerical model does not predict total flux rates (owing to the one-dimensional solution), it is a tool that provides a good means of comparing the relative apparent velocity in the hyporheic zones among different locations.

Our findings regarding the hydraulic interactions between the river and riverbed illustrate both the difficulty of measuring surface–subsurface exchange and the complexity of that exchange. Elliott and Brooks (1997a) noted that the spatial and temporal complexity of the hyporheic zone makes modeling (or observing) the fluid mechanics a formidable task. Indeed, it is in the different treatment of the basic fluid mechanics of the system under investigation that contributes to the difficulty in discerning the dominant hydraulic process of the system. When considering the advection and turbulent diffusion of surface water into the riverbed, the interface zone is treated similar to open channel problems, wherein the energy due to the velocity head is explicitly considered. These processes are most important over small temporal and spatial scales (Elliott and Brooks 1997b), especially where the hydraulic conductivity of the shallow subsurface is much higher than deeper within the riverbed. When considering piezometric head differences between surface and subsurface water, the interface zone is treated as a groundwater system

wherein the kinetic energy (i.e., the velocity head) is excluded from the solution. These processes are most important over larger temporal and spatial scales (Elliott and Brooks 1997b). It is likely that we observed advective and diffusive processes over small and large temporal and spatial scales, all of which are important to the riverbed incubation environment of Chinook salmon.

Temperature monitoring results indicated that all of the study sites possessed a positive vertical temperature gradient with depth into the riverbed for the entire study period. However, the magnitude of the temperature gradient varied among sites, depending largely on the magnitude of the downward flux of river water entering the riverbed. Sites with a large downward flux exhibited smaller temperature gradients. At all sites, the temperature gradient between the riverbed surface and the artificial egg pocket depth was very small, indicating that river water rapidly advected into the artificial egg pockets. This was likely a combined function of the shallow burial depth of the temperature sensor within the egg pocket, and very high hydraulic conductivity in the egg pocket resulting from egg pocket construction. At most of the sites the amplitude of daily temperature fluctuations decreased with depth into the riverbed, a finding not uncommon among studies of riverbed temperatures (Crisp 1990; Malcolm et al. 2002; Malcolm et al. 2004). However, during the period of variable discharge, the amplitude of daily temperature fluctuations within the hyporheic zone at sites 211.9 and 218.7 was as large as or larger than surface water temperature fluctuations. Despite the large, short-term (hourly) fluctuations in temperature resulting from acute changes in river stage, these two sites maintained large temperature gradients when averaged over the entire late incubation period.

The positive vertical temperature gradient with depth into the riverbed resulted in a concomitant increased rate of accumulated temperature units (ATU) with depth into the riverbed. The artificial egg pockets at all of the study sites reached 1000 ATU (the time period when emergence is often considered to occur) within seven days of the surface water reaching 1000 ATU. The within-site difference between egg pocket depth and the shallow hyporheic zone in the number of days post-fertilization required to reach 1000 ATU ranged from 0 days at site 244.5 to 14 days at site 222.7. The temperature sensors in the artificial egg pockets and shallow hyporheic zone piezometers were located at depths below the riverbed surface that were well within the range (19–37 cm) of observed fall Chinook salmon egg pocket depths in the Columbia River (Chapman 1988). However, because the shallow hyporheic zone temperature was measured in the undisturbed riverbed, a reduced hydraulic conductivity at this location may have contributed to the large temperate gradient between artificial egg pocket depth and the shallow hyporheic zone observed at some sites. The differences in riverbed temperature characteristics among the study sites resulted in a similar range in the number of days required to reach 1000 ATU. For example, the difference among sites in the number of days required to reach 1000 ATU in the artificial egg pockets ranged from 0 to 16 days, while that same difference for the shallow hyporheic zone ranged from 0 to 24 days. The rate of ATU at all sites was largely unaffected by the changes in river stage resulting from hydropower operations at the Hells Canyon Complex. Even the two sites (211.9 and 218.7) exhibiting acute flux reversals resulting from hydropower operations displayed a minimal effect of flux reversals on emergence timing estimates based on ATU. When the numerical model was used to estimate the shallow hyporheic zone temperatures that would have occurred in the absence of large discharge fluctuations, the emergence timing estimates based on ATU changed by 1 day or less. This minimal effect of hydropower operations on ATU is attributed to 1) acute river stage changes due to power-peaking operations were

short in duration and 2) by the time power-peaking operations began in early-January, the riverbed at sites 211.9 and 218.7 had already accumulated over 700 temperature units.

Our results indicate that the range of emergence timing estimates due to differences among the eggs from different females can be as large as or larger than the emergence timing estimates due to site differences (i.e., bed temperatures within and among sites). Based on ATU at maximum alevin wet weight (MAWW) as an index of emergence timing, female differences within a site resulted in emergence timing differences ranging over 9 to 13 days. Among all the female groups and among sites, the emergence timing differences ranged over 0 to 27 days. Similar large ranges in the emergence timing of Chinook salmon fry has been observed through laboratory and modeling studies. Much of the range in emergence timing is often attributed to egg size. Egg size is highly variable in Chinook salmon and it is not uncommon to find more than a three-fold difference in the initial egg weights from the same population (Rombough 1985). Eggs from coastal spawning stocks of British Columbia Chinook salmon averaged 8.85 mm (SE = 0.03 mm) and 356.1 mg (SE = 4.3 mg); eggs from another Chinook stock spawning in a coastal river (Bella Coola) were 9.14 mm in diameter (SE = 0.04 mm) and 396.0 mg (SE = 4.8 mg) in weight; eggs from an interior spawning Chinook population from the Quesnel River stock were 8.47 mm (SE = 0.02 mm) in diameter and 317.4 mg (SE = 1.5 mg) in weight (all data reported in Beacham and Murray 1989). When incubated in the laboratory over a range of controlled temperatures, the ATU at emergence timing for these stocks ranged from 844 to 1016 (Beacham and Murray 1989). Two stocks of Methow Basin Chinook salmon which spawn in August (spring Chinook) and in October (summer Chinook salmon) had average egg masses of 218 mg and 284 mg, respectively (Beer and Anderson 2001). Initial mean weight of fall-run Chinook salmon eggs from the Campbell River was 490 mg (95% confidence limits 485-495 mg) (Heming 1982). The sizes of eggs from fall Chinook salmon in our study, although variable, were similar to other stocks of Chinook salmon.

The voluntary emergence of Chinook alevins from gravel is closely correlated with the attainment of MAWW (Heming et al. 1982; Heming 1982). Initial egg weight has a significant effect on the time it takes Chinook salmon alevins to reach MAWW and emergence (Rombough 1985; Beacham and Murray 1985; Becham et al. 1985). This was true in our study as well, with initial egg mass able to explain approximately 97% of the variance in MAWW. Some researchers have determined a relationship between egg mass and time to MAWW. Beacham and Murray (1985) found egg size had a considerable effect on the time to emergence in chum salmon. Heming (1982) found smaller Chinook salmon eggs hatched earlier in development because there was less yolk to absorb, concluding that the duration of yolk absorption is longer for alevins from larger eggs than for alevins from small eggs. Although the smallest eggs in the Swan Falls group (female 3) reached MAWW the fastest, this was not true in the Hells Canyon group where the smallest eggs (female 4) took longest to reach MAWW. In fact, there did not appear to be any relationship between days post-fertilization to MAWW and initial egg mass. This differs from Rombough's (1985) results which showed the smallest Chinook eggs reached MAWW the fastest. In fact, at 5°C his results suggested 500-mg eggs would take approximately 31 days longer to reach MAWW than alevins from 200-mg eggs (a 16% increase in total incubation period).

Our findings indicate that during the 2002–2003 fall Chinook salmon incubation period, hydropower operations of the Hells Canyon Complex had an insignificant effect on fry emergence timing at the study sites. It appears that short-term (i.e., hourly to daily) manipulations of discharge from the Hells Canyon

Complex during the incubation period would not substantially alter egg pocket incubation temperatures, and thus would not affect fry emergence timing at the study sites. However, the use of hydropower operational manipulations at the Hells Canyon Complex to accelerate egg incubation and fry emergence should not be ruled out on the basis of only one water year's worth of study. Further investigation of the incubation environment of Snake River fall Chinook salmon is warranted based on the complexity of hyporheic zone characteristics and the variability of surface–subsurface interactions among dry, normal, and wet water years.

5.0 Literature Cited

Arntzen EV, DR Geist, and TP Hanrahan. 2001. *Substrate quality of fall Chinook salmon spawning habitat, Hells Canyon Reach, Snake River, Idaho*. Final report to Idaho Power Company, PNWD-3114. Battelle Pacific Northwest Division, Richland, Washington.

Bams RA. 1970. "Evaluation of a revised hatchery method tested on pink and chum salmon fry." *Journal of the Fisheries Research Board of Canada* 27(8):1429-1452.

Beacham TD and CB Murray. 1985. "Effect of female size, egg size, and water temperature on developmental biology of chum salmon (*Oncorhynchus keta*) from the Nitinat River, British Columbia." *Canadian Journal of Fisheries and Aquatic Sciences* 42:1755-1765.

Beacham TD and CB Murray. 1989. "Variation in developmental biology of sockeye salmon (*Oncorhynchus nerka*) and Chinook salmon (*O. tshawytscha*) in British Columbia." *Canadian Journal of Zoology* 67:2081-2089.

Beacham TD, FC Withler, and RB Morley. 1985. "Effect of egg size on incubation time and alevin and fry size in chum salmon (*Oncorhynchus keta*) and coho salmon (*O. kisutch*)." *Canadian Journal of Zoology* 63:847-850.

Beer NW and JJ Anderson. 2001. "Effect of spawning day and temperature on salmon emergence: interpretations of a growth model for Methow River Chinook." *Canadian Journal of Fisheries and Aquatic Sciences* 58:943-949.

Berggren TJ and MJ Filardo. 1993. "An analysis of variables influencing the migration of juvenile salmonids in the Columbia River Basin." *North American Journal of Fisheries Management* 13(1):48-63.

Castro NM and GM Hornberger. 1991. "Surface-subsurface water interactions in an alluviated mountain stream channel." *Water Resources Research* 27(7):1613-1621.

Chapman DW. 1988. "Critical review of variables used to define effects of fines in redds of large salmonids." *Transactions of the American Fisheries Society* 117(1):1-21.

Connor WP, HL Burge, and DH Bennett. 1998. "Detection of PIT-tagged subyearling Chinook salmon at a Snake River dam: Implications for summer flow augmentation." *North American Journal of Fisheries Management* 18(3):530-536.

Connor WP. 1999. "Subyearling Chinook salmon early life history timing and survival in the Snake River, 1995 to 1998." In: *Post-release attributes and survival of hatchery and natural fall Chinook salmon in the Snake River, Annual Report 1998*, KF Tiffan, DW Rondorf, WP Connor, and HL Burge (eds.), Bonneville Power Administration, Portland, Oregon.

Connor WP, HL Burge, R. Waitt, AP Garcia, and TC Bjornn. 2001. "Snake River fall Chinook salmon early life history and growth as affected by dams." In: *Post-release attributes and survival of hatchery and natural fall Chinook salmon in the Snake River, Annual Report 1999*, KF Tiffan, DW Rondorf, WP Connor, and HL Burge (eds.), Bonneville Power Administration, Portland, Oregon.

Constantz J and CL Thomas. 1996. "The use of streambed temperature profiles to estimate the depth, duration, and rate of percolation beneath arroyos." *Water Resources Research* 32(12):3597-3602.

Crisp DT. 1990. "Water temperature in a stream gravel bed and implications for salmonid incubation." *Freshwater Biology* 23:601-612.

Dauble DD, TP Hanrahan, DR Geist, and MJ Parsley. 2003. "Impacts of the Columbia River hydroelectric system on main-stem habitats of fall Chinook salmon." *North American Journal of Fisheries Management* 23:641-659.

Dreher KJ. 2000. *Review of survival, flow, temperature, and migration data for hatchery-raised subyearling fall Chinook salmon above Lower Granite Dam, 1995-1998*. Idaho Department of Water Resources, Idaho Department of Fish and Game, Boise, Idaho.

Elliott AH and NH Brooks. 1997a. "Transfer of nonsorbing solutes to a streambed with bed forms: Theory." *Water Resources Research* 33(1):123-136.

Elliott AH and NH Brooks. 1997b. :Transfer of nonsorbing solutes to a streambed with bed forms: laboratory experiments." *Water Resources Research* 33(1):137-151.

Fetter CW. 1994. *Applied hydrogeology*. 3rd. Merrill Publishing Company, Upper Saddle River, New Jersey, 458 pp.

Geist DR, TP Hanrahan, EA Arntzen, and ZK Bevens. 1999. *Assessment of hyporheic discharge within fall Chinook salmon spawning habitat in the Hells Canyon Reach of the Snake River*. Final Report Prepared for Idaho Power Company, Boise, Idaho.

Geist D. 2000. "Hyporheic discharge of river water into fall Chinook salmon (*Oncorhynchus tshawytscha*) spawning areas in the Hanford Reach, Columbia River." *Canadian Journal of Fisheries and Aquatic Sciences* 57(8):1647-1656.

Giorgi AE, TW Hillman, JR Stevenson, SG Hayes, and CM Pevan. 1997. "Factors that influence the downstream migration rates of juvenile salmon and steelhead through the hydroelectric system in the mid-Columbia River Basin." *North American Journal of Fisheries Management* 17(2):268-282.

Hanrahan TP, DR Geist, and EV Arntzen. In press. "Habitat quality of historic Snake River fall Chinook salmon spawning locations and implications for incubation survival: Part 1, substrate quality." *River Research and Applications*, accepted for publication 24 May 2004.

Harvey JW and KE Bencala. 1993. "The effect of streambed topography on surface-subsurface water exchange in mountain catchments." *Water Resources Research* 29(1): 89-98.

Heming TA. 1982. "Effects of temperature on utilization of yolk by Chinook salmon (*Oncorhynchus tshawytscha*) eggs and alevins." *Canadian Journal of Fisheries and Aquatic Sciences* 39:184-190.

Heming TA, JE McInerney, and DF Alderdice. 1982. "Effects of temperature on initial feeding in alevins of Chinook salmon (*Oncorhynchus tshawytscha*)." *Canadian Journal of Fisheries and Aquatic Sciences* 39:1554-1562.

Lapham WW. 1989. *Use of temperature profiles beneath streams to determine rates of vertical ground-water flow and vertical hydraulic conductivity*. Water-Supply Paper 2337, U.S. Geological Survey, Denver, Colorado.

Larkin RG and JM Sharp. 1992. "On the relationship between river-basin geomorphology, aquifer hydraulics, and ground-water flow direction in alluvial aquifers." *Geological Society of America Bulletin* 104:1608-1620.

Lenk M and N Saenger. 2000. "Exchange processes in the river bed and their influence on temperature variations." *Verh. Internat. Verein. Limnol.* 27:427-430.

Lunardini VJ. 1981. *Heat transfer in cold climates*. Van Nostrand Reinhold Company, New York, 731 pp.

Malcolm IA, C Soulsby, and AF Youngson. 2002. "Thermal regime in the hyporheic zone of two contrasting salmonid spawning streams: ecological and hydrological implications." *Fisheries Management and Ecology* 9:1-10.

Malcolm IA, C Soulsby, AF Youngson, DM Hannah, IS McLaren, and A Thorne. 2004. "Hydrological influences on hyporheic water quality: implications for salmon egg survival." *Hydrologic Processes* 18(9):1543-1560.

Nagaoka H and AJ Ohgaki. 1990. "Mass transfer mechanism in a porous riverbed." *Water Research* 24(4):417-425.

National Marine Fisheries Service (NMFS). 2000a. *Endangered Species Act – Section 7 Consultation Biological Opinion*, *Reinitiation of Consultation on Operation of the Federal Columbia River Power System, Including the Juvenile Fish Transportation Program, and 19 Bureau of Reclamation Projects in the Columbia Basin*. National Marine Fisheries Service, Seattle, Washington.

National Marine Fisheries Service (NMFS). 2000b. *Biological opinion on operation of the Federal Columbia River Power System*. National Marine Fisheries Service, Seattle, Washington.

National Marine Fisheries Service (NMFS). 1992. *Threatened status for Snake River spring/summer Chinook salmon, threatened status for Snake River fall Chinook salmon*. 14653-14663, Federal Register.

O'Connor JE. 1993. *Hydrology, hydraulics, and geomorphology of the Bonneville Flood*. Special Paper 274. Geological Society of America, Boulder, Colorado.

Packman AI, M Salehin, and M Zaramella. 2004. "Hyporheic exchange with gravel beds: Basic hydrodynamic interactions and bedform-induced advective flows." *Journal of Hydraulic Engineering* 130(7):647-656.

Rombough PJ. 1985. "Initial egg weight, time to maximum alevin wet weight, and optimal ponding times for Chinook salmon (*Oncorhynchus tshawytscha*)." *Canadian Journal of Fisheries and Aquatic Sciences* 42:287-291.

Saenger N. 2002. "Estimation of flow velocities within the hyporheic zone." *Verh. Internat. Verein. Limnol.* 28:1790-1795.

Savant SA, DD Reible, and LJ Thibodeaux. 1987. "Convective transport within stable river sediments." *Water Resources Research* 23(9):1763-1768.

Schalchli U. 1995. "Basic equations for siltation of riverbeds." *Journal of Hydraulic Engineering* 121(3):274-287.

Shimizu Y, T Tsujimoto, and H. Nakagawa. 1990. "Experiment and macroscopic modelling of flow in highly permeable porous medium under free-surface flow." *Journal of Hydroscience and Hydraulic Engineering* 8(1):69-78.

Silliman SE, J Ramirez, and RL McCabe. 1995. "Quantifying downflow through creek sediments using temperature time series: one-dimensional solution incorporating measured surface temperature." *Journal of Hydrology* 167:99-119.

Stallman RW. 1965. "Steady one-dimensional fluid flow in a semi-infinite porous medium with sinusoidal surface temperature." *Journal of Geophysical Research* 70(12):2821-2827.

Storey RG, KWF Howard, and DD Williams. 2003. "Factors controlling riffle-scale hyporheic exchange flows and their seasonal changes in a gaining stream: A three-dimensional groundwater flow model." *Water Resources Research* 39(2):1034, DOI:10.1029/2002WR001367.

Thibodeaux LJ and JD Boyle. 1987. "Bedform-generated convective transport in bottom sediment." *Nature* 325:341-343.

Weatherly AH and HS Gill. 1995. "Growth." In: *Physiological ecology of Pacific Salmon*, C Groot, L Margolis, and WC Clarke (eds.), University of British Columbia Press, Vancouver, BC, Canada.

Worman A, AI Packman, H Johansson, and K Jonsson. 2002. "Effect of flow-induced exchange in hyporheic zones on longitudinal transport of solutes in streams and rivers." *Water Resources Research* 38(1):1001, DOI:10.1029/2001WR000769.

Zhou D and C Mendoza. 1993. "Flow through porous bed of turbulent stream." *Journal of Engineering Mechanics* 119(2):365-383.

Appendix Figures

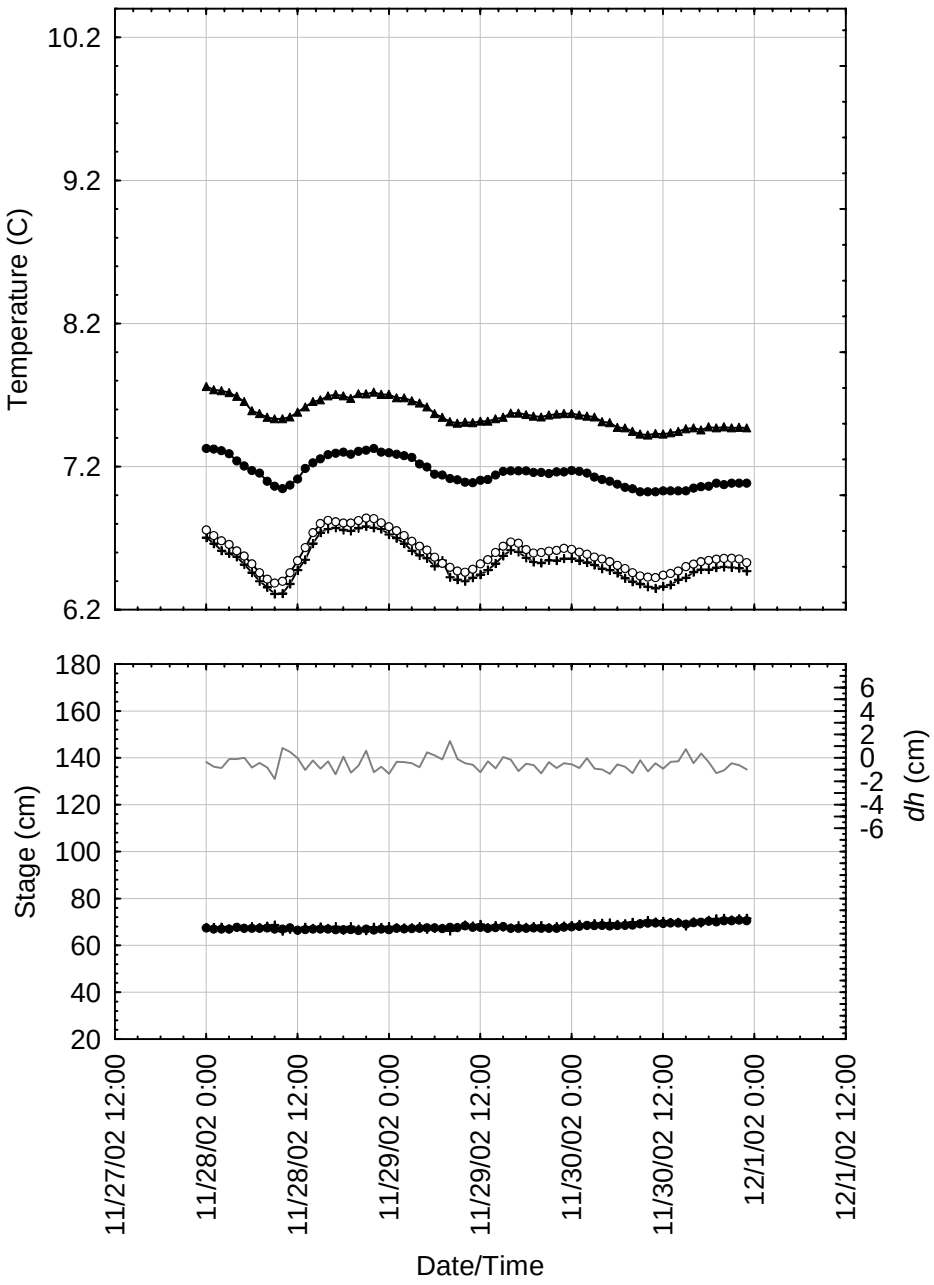

Appendix Figure 1. Time-series summary of water temperature (top panel) and river stage (bottom panel) at site 148.5 during a period of low, stable river discharge (November 28 – 30, 2002). Average hourly water temperature is shown for the river (+), egg pocket (○), shallow hyporheic (●) and deep hyporheic (▲) zones. Average hourly stage (depth) is shown for the river (+), and shallow hyporheic zone (●). The difference between these two water depths (hyporheic minus river) is plotted on the Y-right axis as *dh* (—), with positive values indicating upwelling potential.

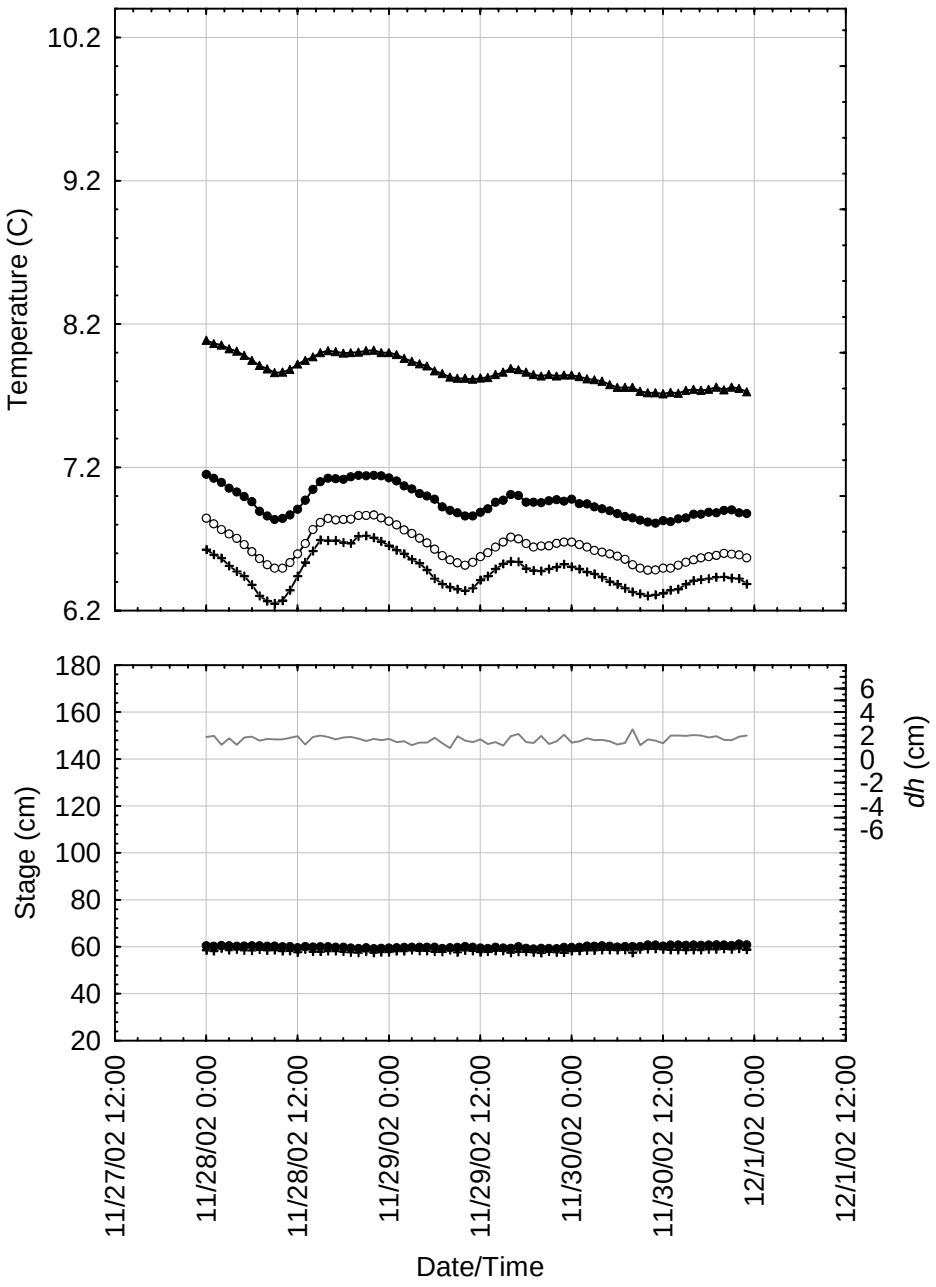

Appendix Figure 2. Time-series summary of water temperature (top panel) and river stage (bottom panel) at site 149.2 during a period of low, stable river discharge (November 28 – 30, 2002). Average hourly water temperature is shown for the river (+), egg pocket (○), shallow hyporheic (●) and deep hyporheic (▲) zones. Average hourly stage (depth) is shown for the river (+), and shallow hyporheic zone (●). The difference between these two water depths (hyporheic minus river) is plotted on the Y-right axis as *dh* (—), with positive values indicating upwelling potential.

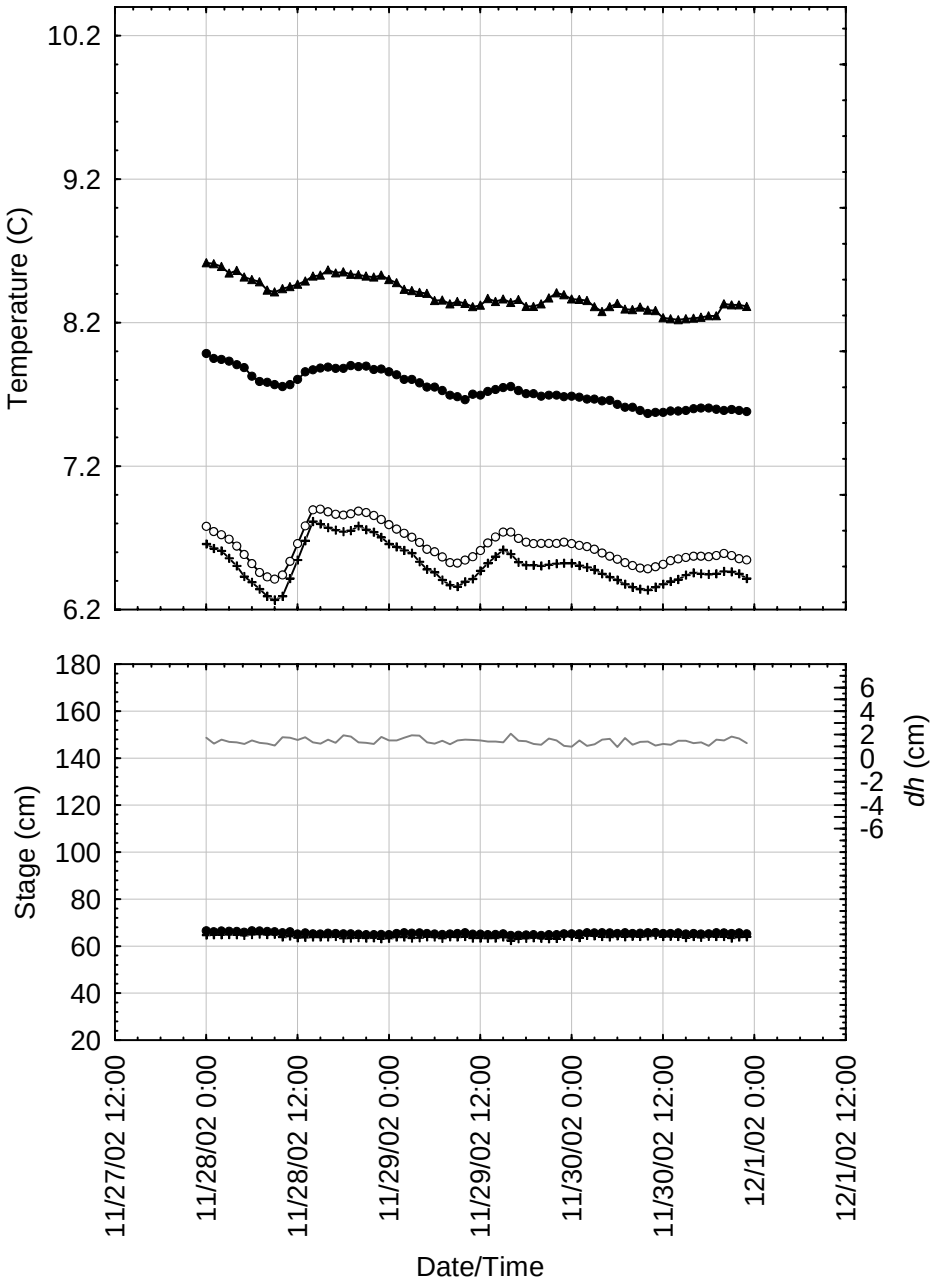

Appendix Figure 3. Time-series summary of water temperature (top panel) and river stage (bottom panel) at site 152.3 during a period of low, stable river discharge (November 28 – 30, 2002). Average hourly water temperature is shown for the river (+), egg pocket (○), shallow hyporheic (●) and deep hyporheic (▲) zones. Average hourly stage (depth) is shown for the river (+), and shallow hyporheic zone (●). The difference between these two water depths (hyporheic minus river) is plotted on the Y-right axis as *dh* (—), with positive values indicating upwelling potential.

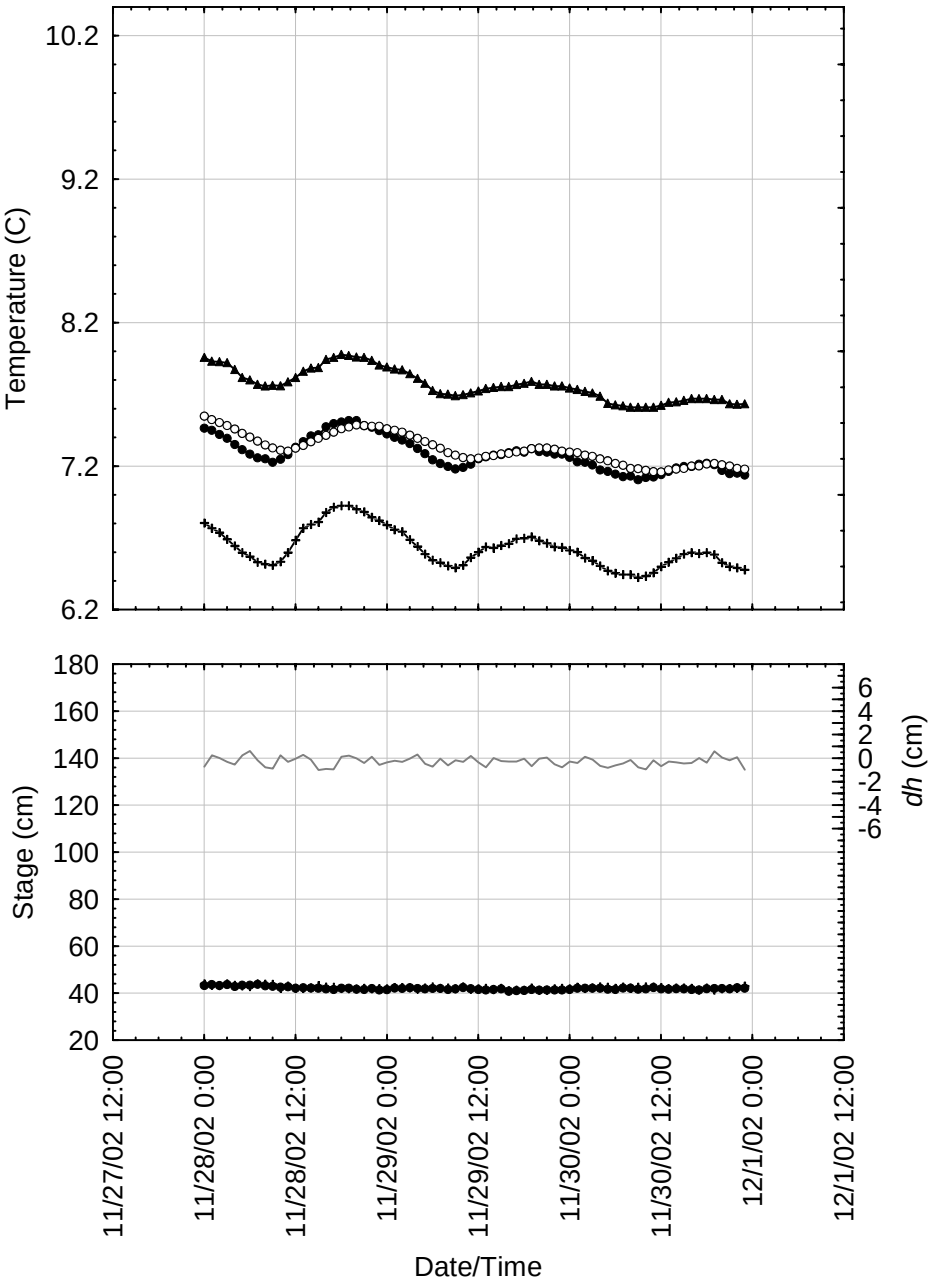

Appendix Figure 4. Time-series summary of water temperature (top panel) and river stage (bottom panel) at site 156.8 during a period of low, stable river discharge (November 28 – 30, 2002). Average hourly water temperature is shown for the river (+), egg pocket (○), shallow hyporheic (●) and deep hyporheic (▲) zones. Average hourly stage (depth) is shown for the river (+), and shallow hyporheic zone (●). The difference between these two water depths (hyporheic minus river) is plotted on the Y-right axis as *dh* (—), with positive values indicating upwelling potential.

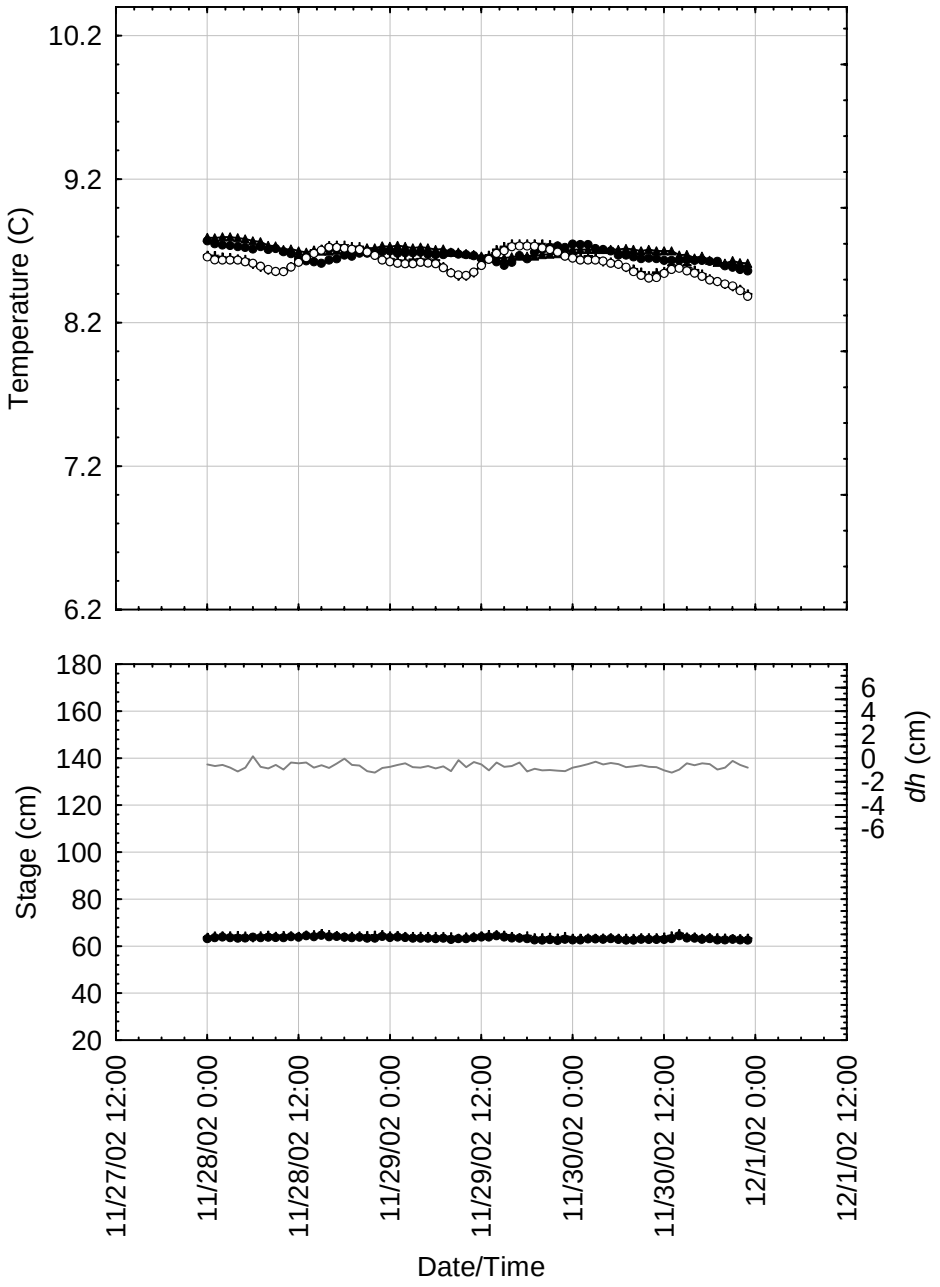

Appendix Figure 5. Time-series summary of water temperature (top panel) and river stage (bottom panel) at site 196.0 during a period of low, stable river discharge (November 28 – 30, 2002). Average hourly water temperature is shown for the river (+), egg pocket (○), shallow hyporheic (●) and deep hyporheic (▲) zones. Average hourly stage (depth) is shown for the river (+), and shallow hyporheic zone (●). The difference between these two water depths (hyporheic minus river) is plotted on the Y-right axis as *dh* (—), with positive values indicating upwelling potential.

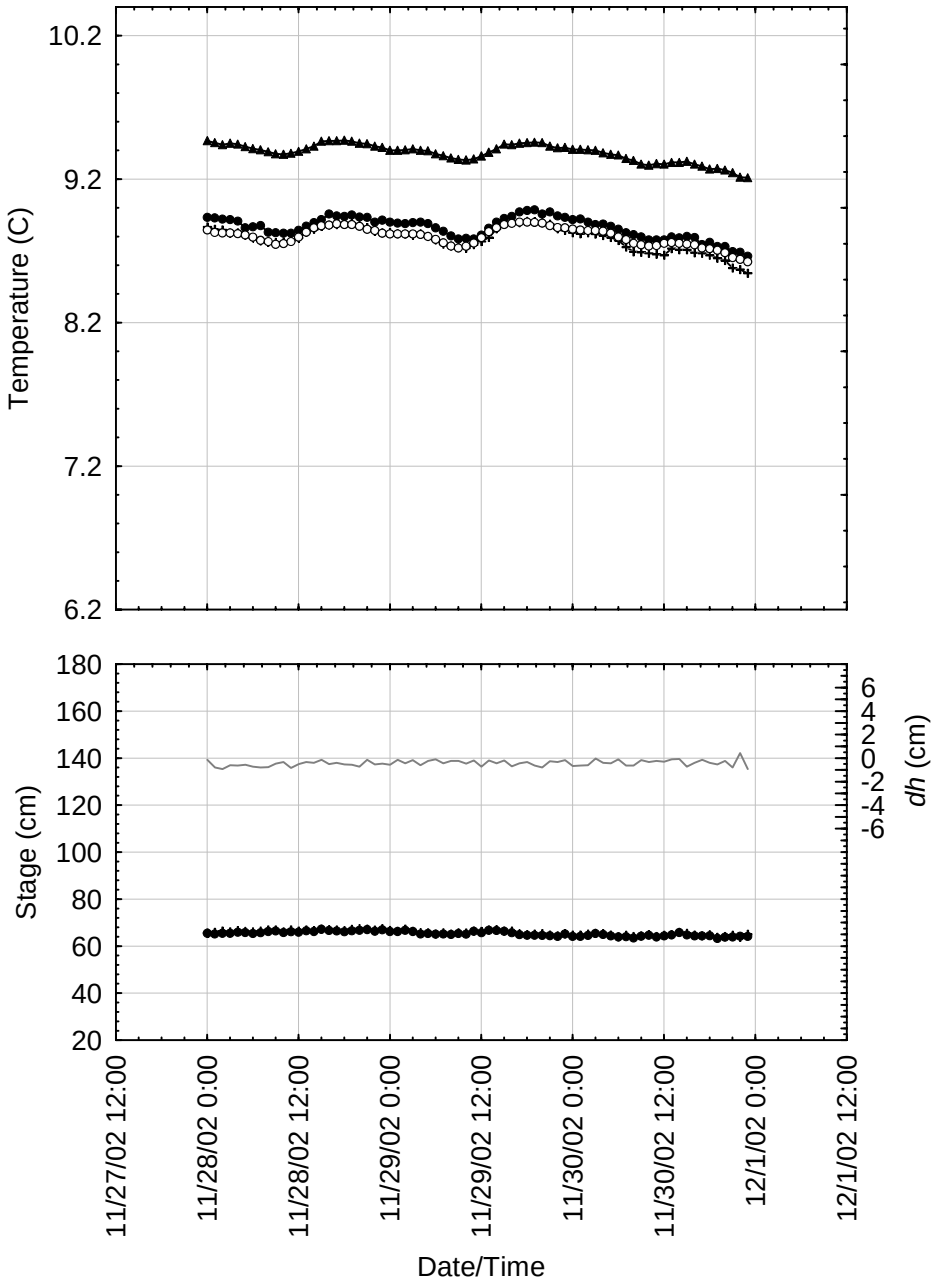

Appendix Figure 6. Time-series summary of water temperature (top panel) and river stage (bottom panel) at site 198.2 during a period of low, stable river discharge (November 28 – 30, 2002). Average hourly water temperature is shown for the river (+), egg pocket (○), shallow hyporheic (●) and deep hyporheic (▲) zones. Average hourly stage (depth) is shown for the river (+), and shallow hyporheic zone (●). The difference between these two water depths (hyporheic minus river) is plotted on the Y-right axis as *dh* (—), with positive values indicating upwelling potential.

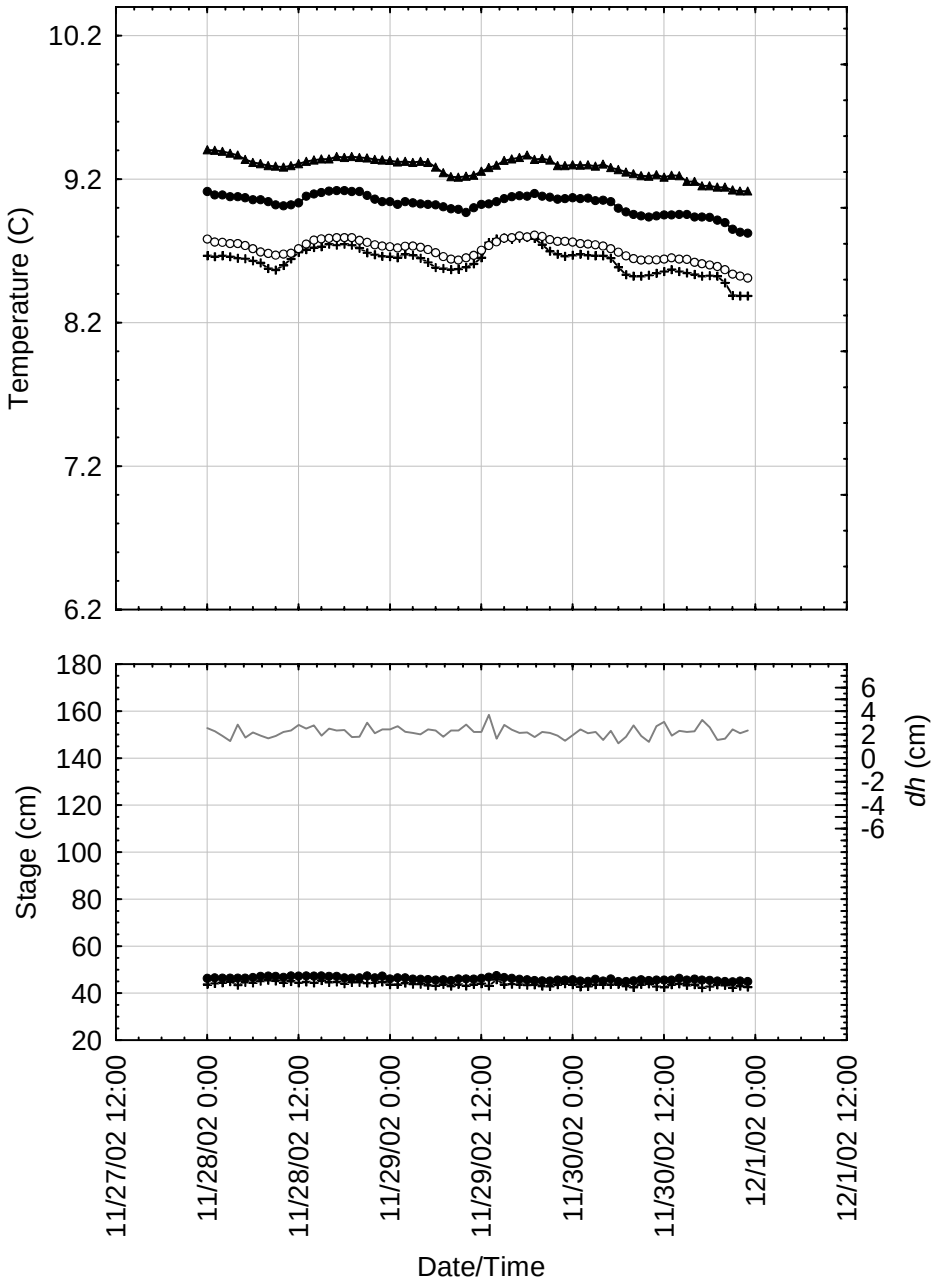

Appendix Figure 7. Time-series summary of water temperature (top panel) and river stage (bottom panel) at site 198.8 during a period of low, stable river discharge (November 28 – 30, 2002). Average hourly water temperature is shown for the river (+), egg pocket (○), shallow hyporheic (●) and deep hyporheic (▲) zones. Average hourly stage (depth) is shown for the river (+), and shallow hyporheic zone (●). The difference between these two water depths (hyporheic minus river) is plotted on the Y-right axis as *dh* (—), with positive values indicating upwelling potential.

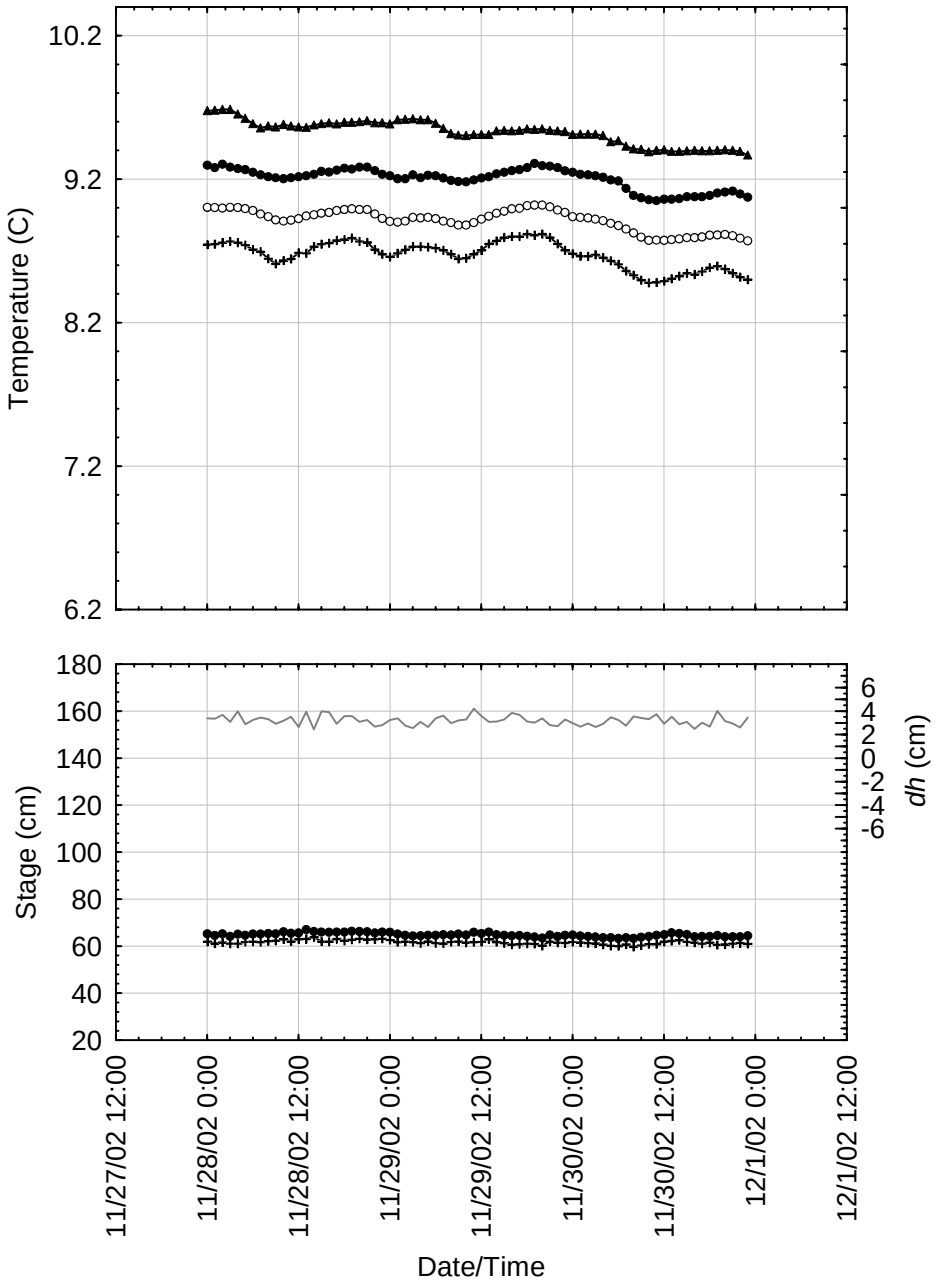

Appendix Figure 8. Time-series summary of water temperature (top panel) and river stage (bottom panel) at site 211.9 during a period of low, stable river discharge (November 28 – 30, 2002). Average hourly water temperature is shown for the river (+), egg pocket (○), shallow hyporheic (●) and deep hyporheic (▲) zones. Average hourly stage (depth) is shown for the river (+), and shallow hyporheic zone (●). The difference between these two water depths (hyporheic minus river) is plotted on the Y-right axis as *dh* (—), with positive values indicating upwelling potential.

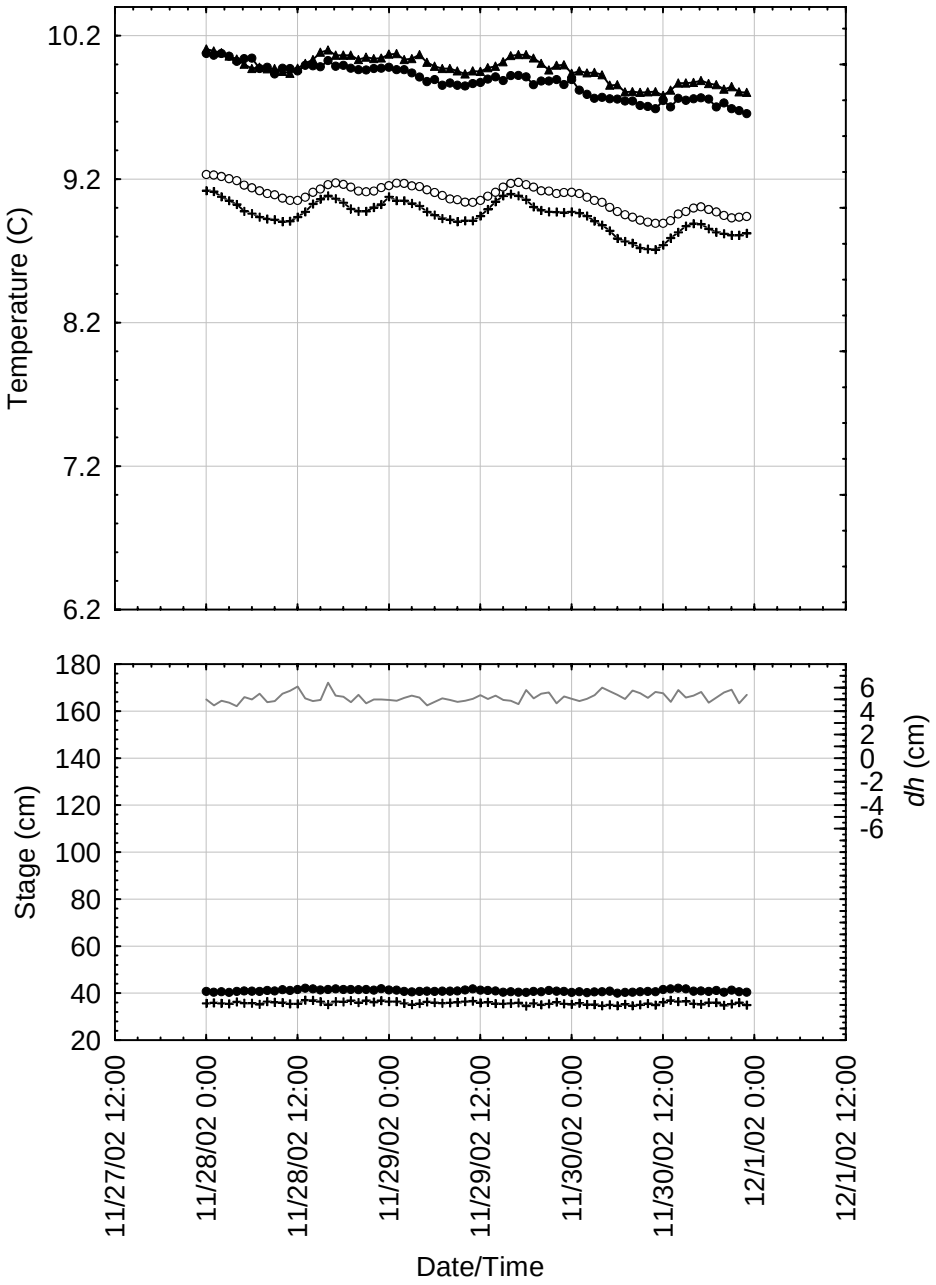

Appendix Figure 9. Time-series summary of water temperature (top panel) and river stage (bottom panel) at site 218.7 during a period of low, stable river discharge (November 28 – 30, 2002). Average hourly water temperature is shown for the river (+), egg pocket (○), shallow hyporheic (●) and deep hyporheic (▲) zones. Average hourly stage (depth) is shown for the river (+), and shallow hyporheic zone (●). The difference between these two water depths (hyporheic minus river) is plotted on the Y-right axis as *dh* (—), with positive values indicating upwelling potential.

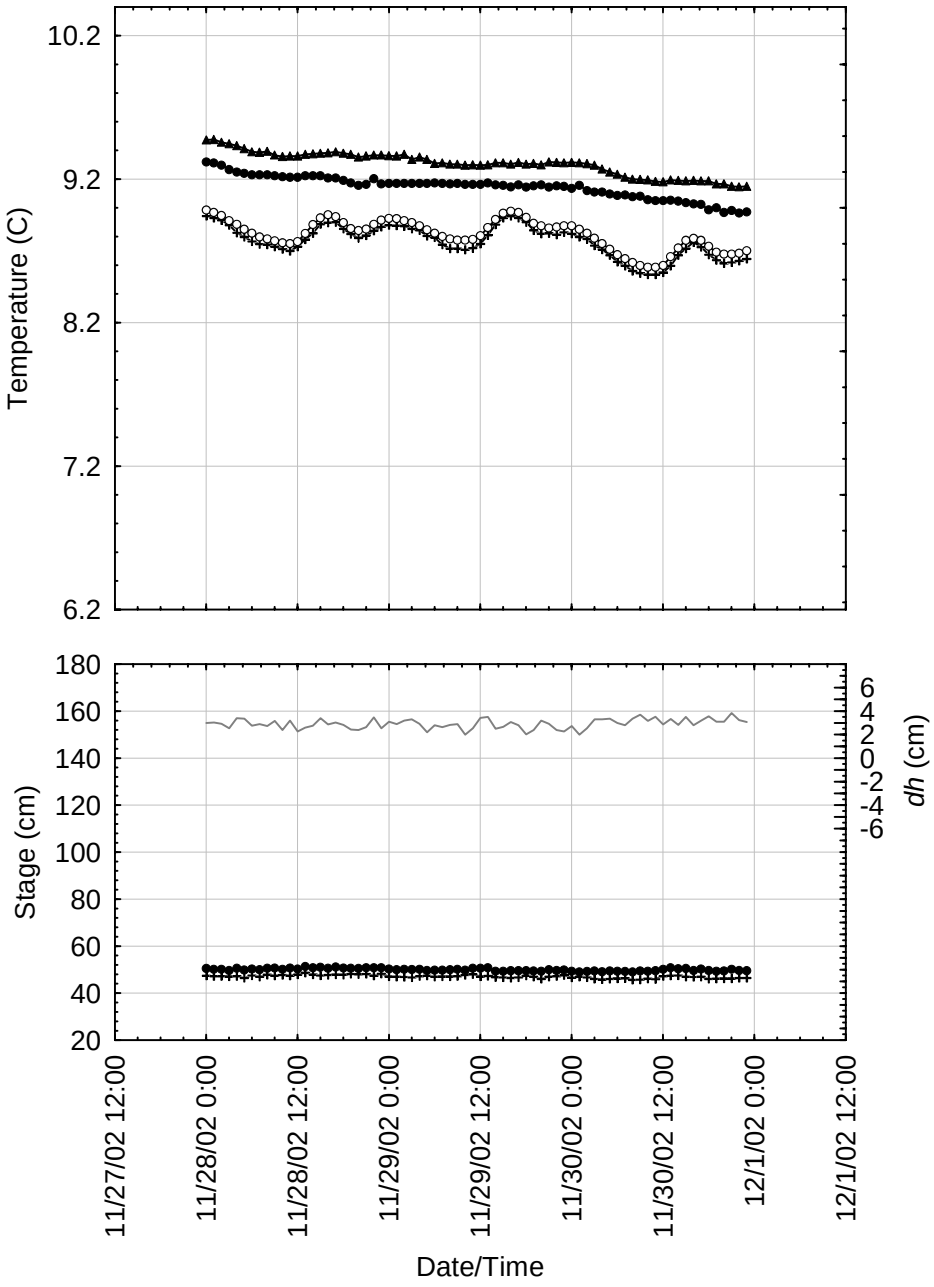

Appendix Figure 10. Time-series summary of water temperature (top panel) and river stage (bottom panel) at site 219.3 during a period of low, stable river discharge (November 28 – 30, 2002). Average hourly water temperature is shown for the river (+), egg pocket (○), shallow hyporheic (●) and deep hyporheic (▲) zones. Average hourly stage (depth) is shown for the river (+), and shallow hyporheic zone (●). The difference between these two water depths (hyporheic minus river) is plotted on the Y-right axis as *dh* (—), with positive values indicating upwelling potential.

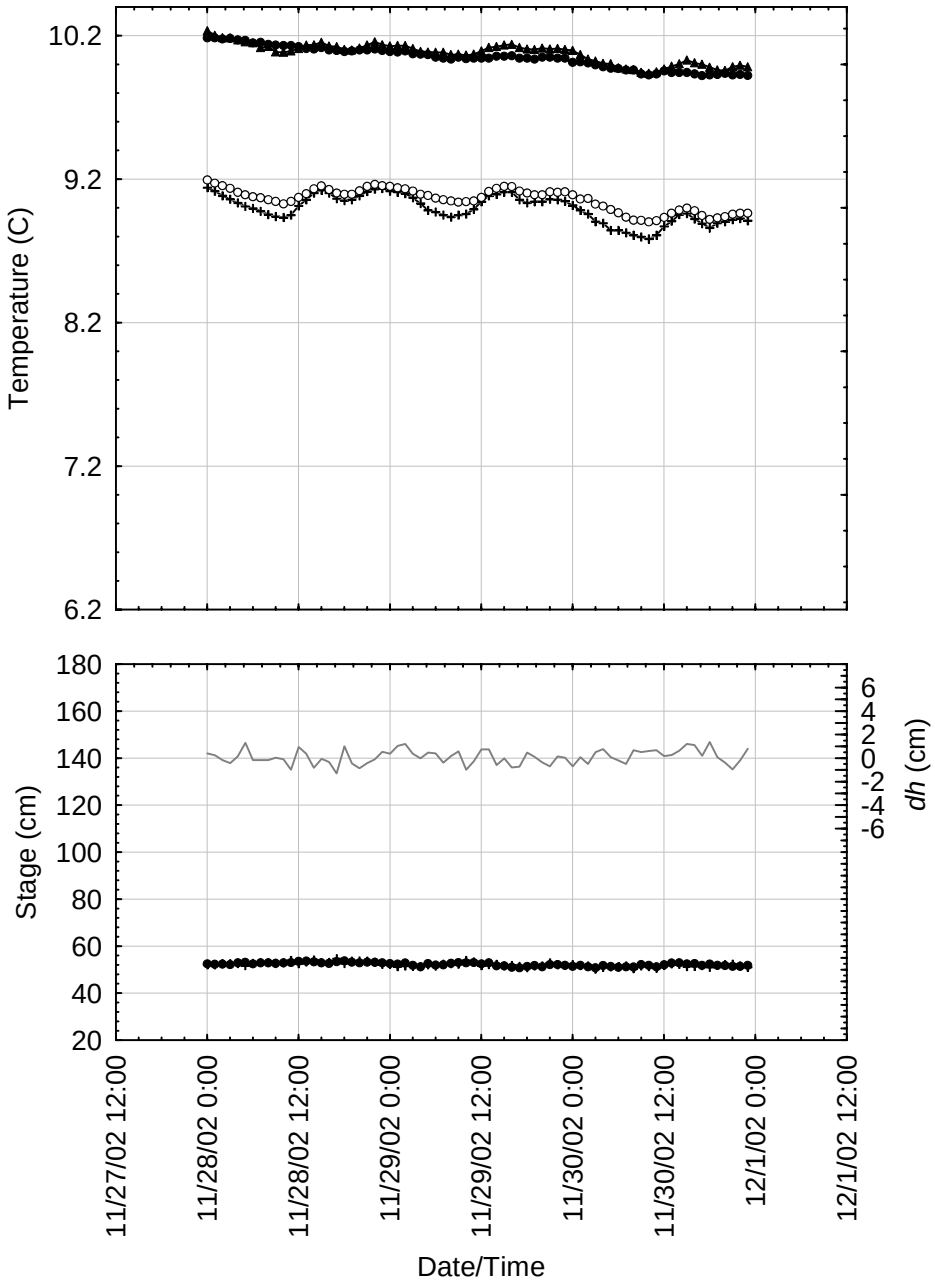

Appendix Figure 11. Time-series summary of water temperature (top panel) and river stage (bottom panel) at site 222.7 during a period of low, stable river discharge (November 28 – 30, 2002). Average hourly water temperature is shown for the river (+), egg pocket (○), shallow hyporheic (●) and deep hyporheic (▲) zones. Average hourly stage (depth) is shown for the river (+), and shallow hyporheic zone (●). The difference between these two water depths (hyporheic minus river) is plotted on the Y-right axis as *dh* (—), with positive values indicating upwelling potential.

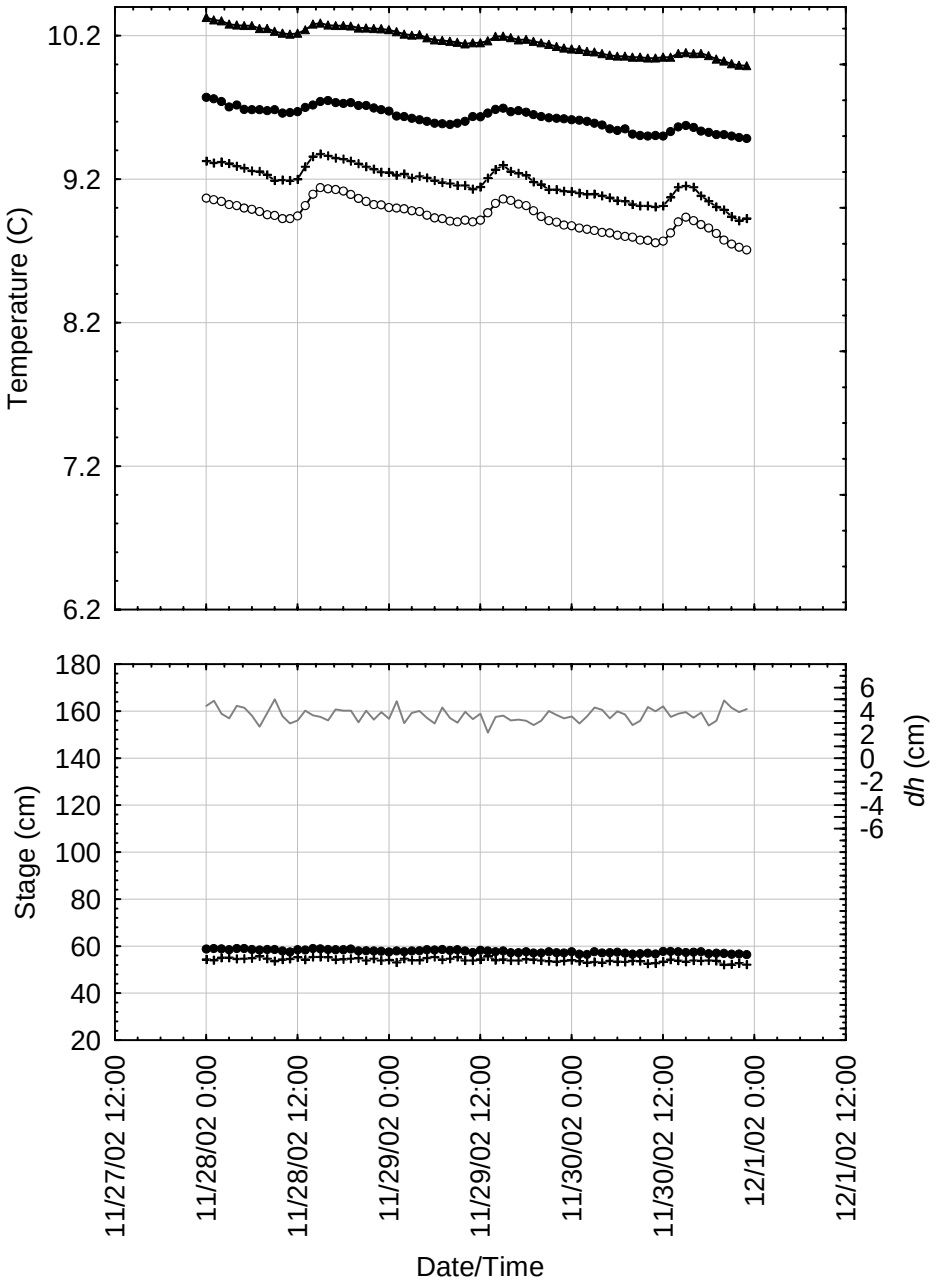

Appendix Figure 12. Time-series summary of water temperature (top panel) and river stage (bottom panel) at site 238.6 during a period of low, stable river discharge (November 28 – 30, 2002). Average hourly water temperature is shown for the river (+), egg pocket (○), shallow hyporheic (●) and deep hyporheic (▲) zones. Average hourly stage (depth) is shown for the river (+), and shallow hyporheic zone (●). The difference between these two water depths (hyporheic minus river) is plotted on the Y-right axis as *dh* (—), with positive values indicating upwelling potential.

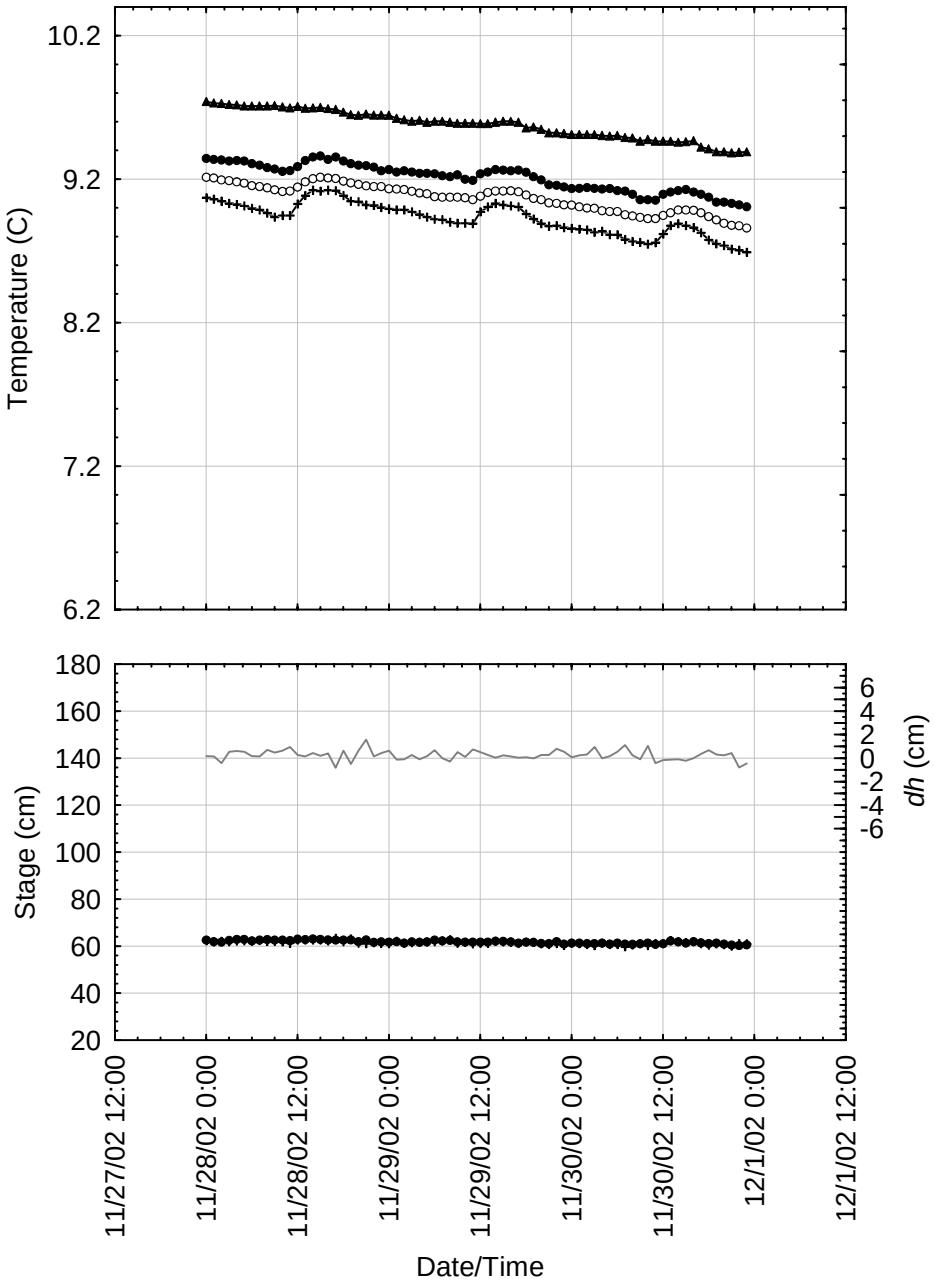

Appendix Figure 13. Time-series summary of water temperature (top panel) and river stage (bottom panel) at site 240.6 during a period of low, stable river discharge (November 28 – 30, 2002). Average hourly water temperature is shown for the river (+), egg pocket (○), shallow hyporheic (●) and deep hyporheic (▲) zones. Average hourly stage (depth) is shown for the river (+), and shallow hyporheic zone (●). The difference between these two water depths (hyporheic minus river) is plotted on the Y-right axis as *dh* (—), with positive values indicating upwelling potential.

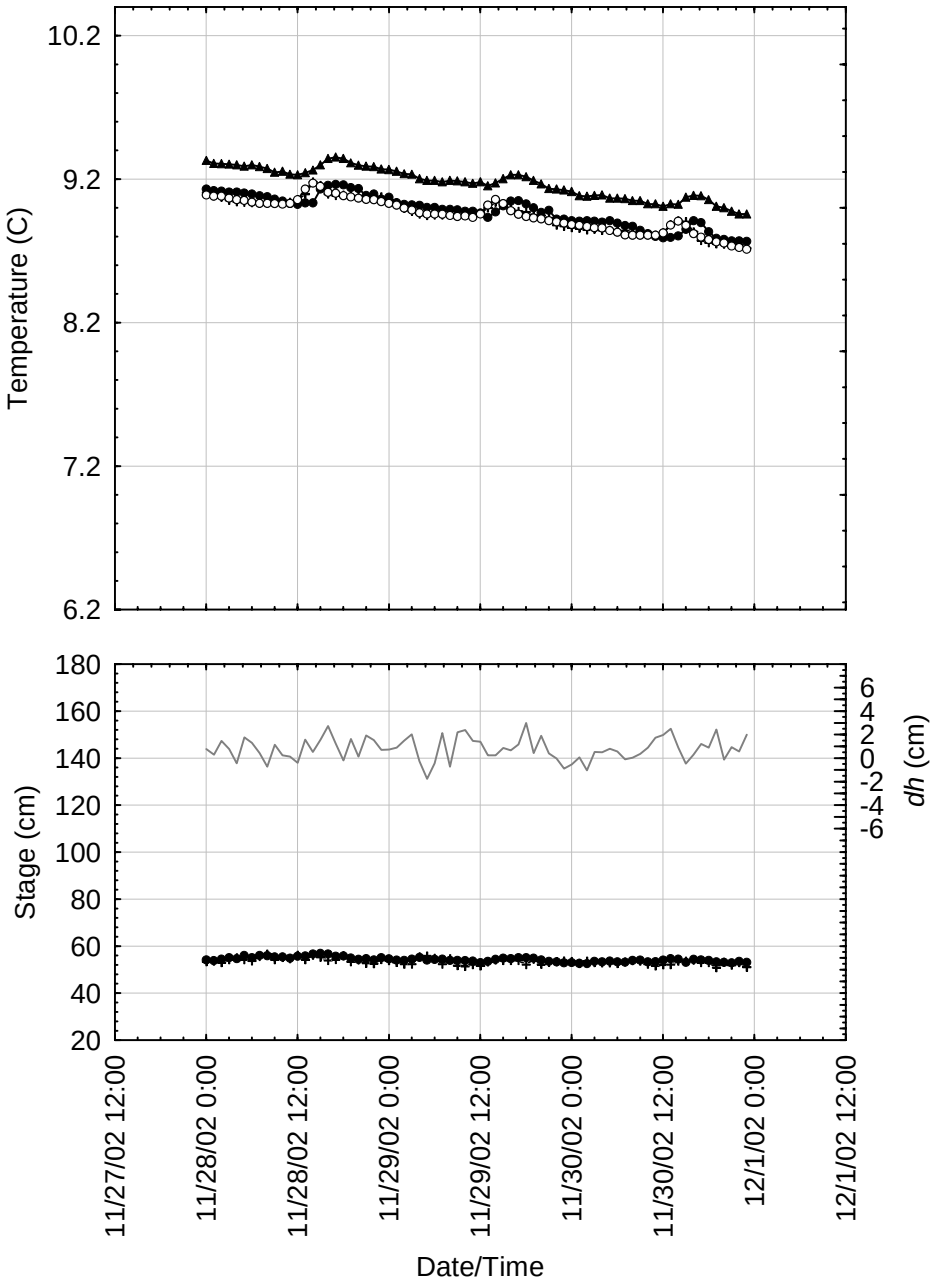

Appendix Figure 14. Time-series summary of water temperature (top panel) and river stage (bottom panel) at site 244.5 during a period of low, stable river discharge (November 28 – 30, 2002). Average hourly water temperature is shown for the river (+), egg pocket (○), shallow hyporheic (●) and deep hyporheic (▲) zones. Average hourly stage (depth) is shown for the river (+), and shallow hyporheic zone (●). The difference between these two water depths (hyporheic minus river) is plotted on the Y-right axis as *dh* (—), with positive values indicating upwelling potential.

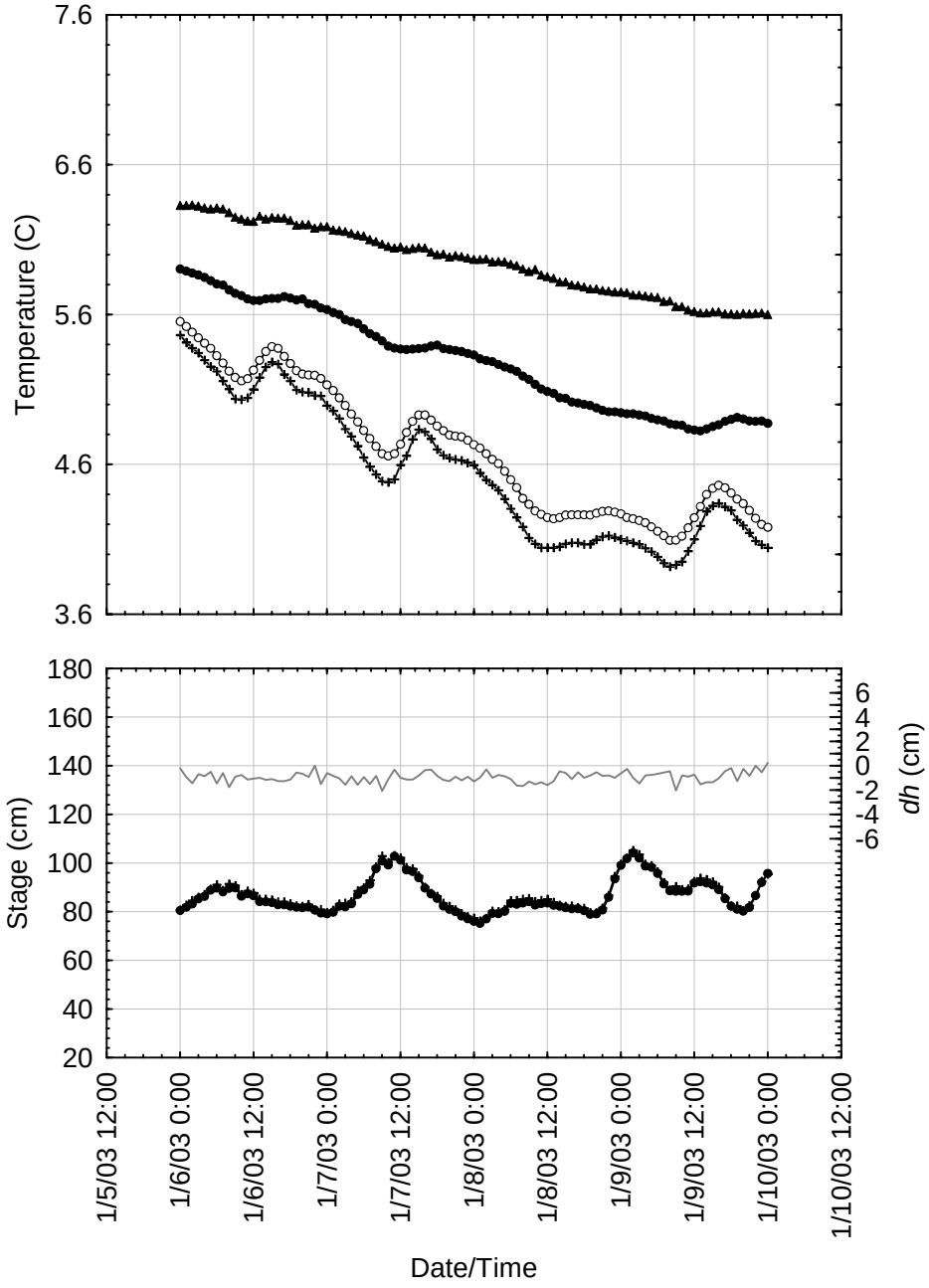

Appendix Figure 15. Time-series summary of water temperature (top panel) and river stage (bottom panel) at site 148.5 during a period of variable river discharge (January 6 – 9, 2003). Average hourly water temperature is shown for the river (+), egg pocket (○), shallow hyporheic (●) and deep hyporheic (▲) zones. Average hourly stage (depth) is shown for the river (+), and shallow hyporheic zone (●). The difference between these two water depths (hyporheic minus river) is plotted on the Y-right axis as *dh* (—), with positive values indicating upwelling potential.

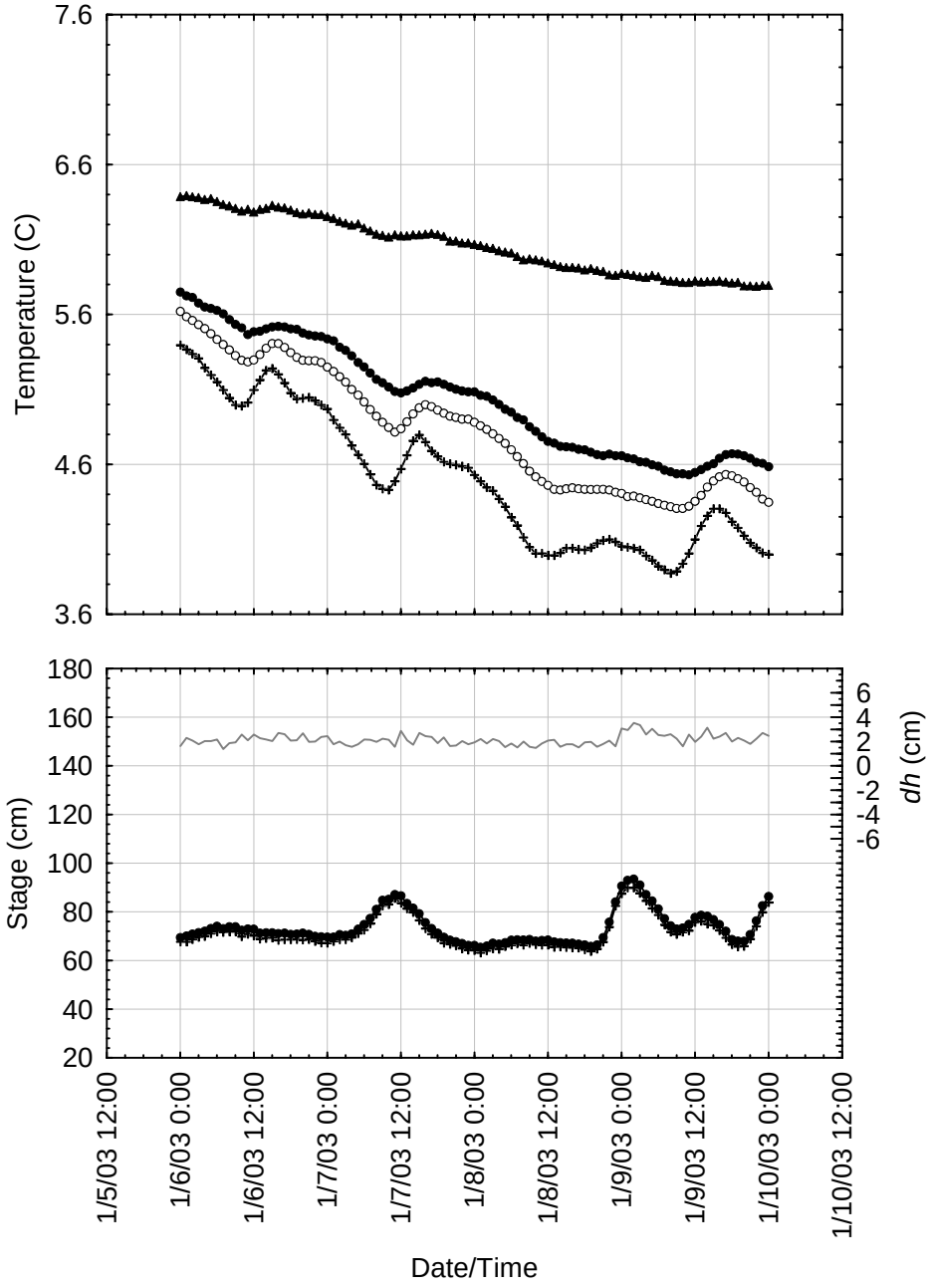

Appendix Figure 16. Time-series summary of water temperature (top panel) and river stage (bottom panel) at site 149.2 during a period of variable river discharge (January 6 – 9, 2003). Average hourly water temperature is shown for the river (+), egg pocket (○), shallow hyporheic (●) and deep hyporheic (▲) zones. Average hourly stage (depth) is shown for the river (+), and shallow hyporheic zone (●). The difference between these two water depths (hyporheic minus river) is plotted on the Y-right axis as *dh* (—), with positive values indicating upwelling potential.

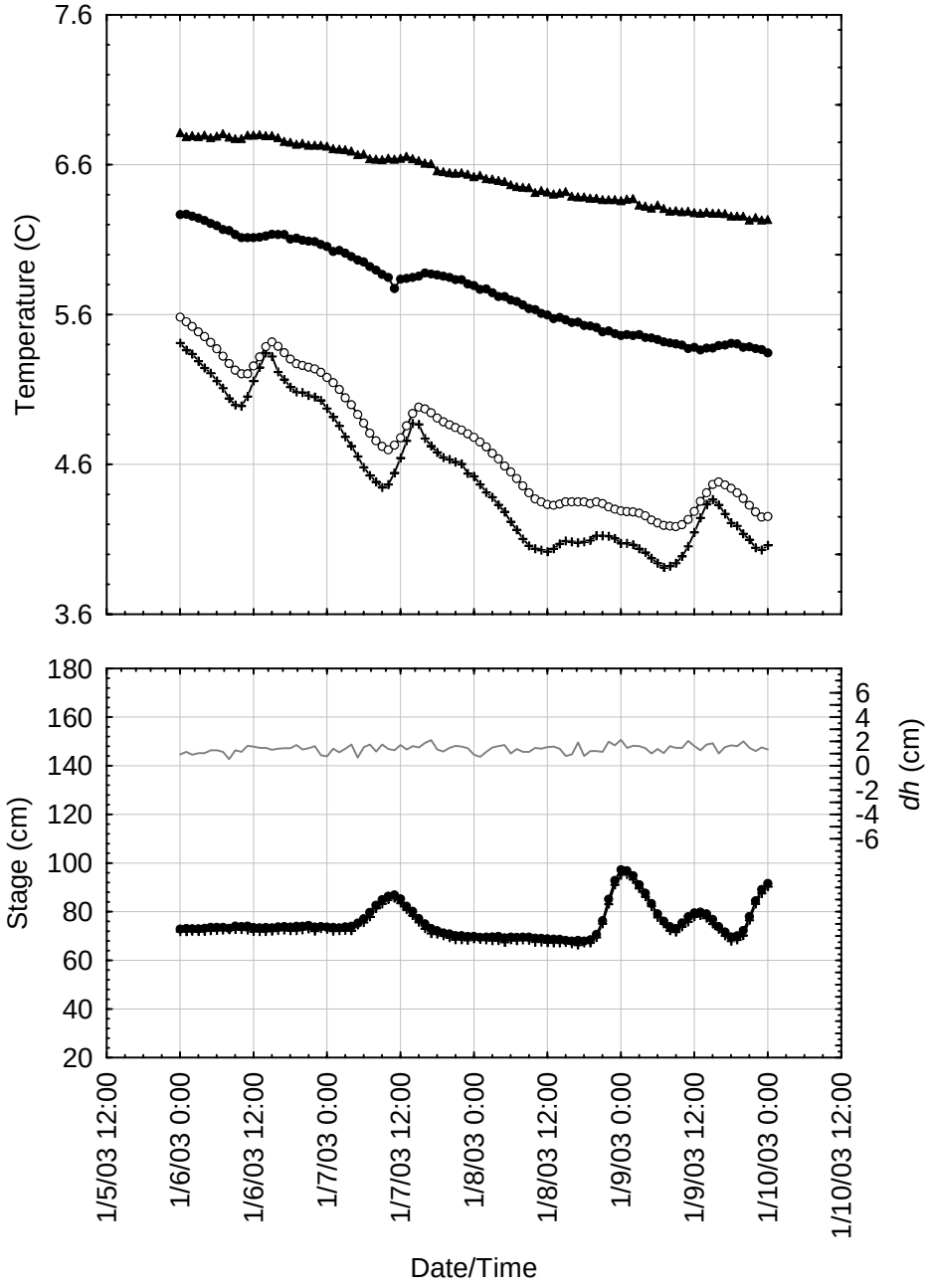

Appendix Figure 17. Time-series summary of water temperature (top panel) and river stage (bottom panel) at site 152.3 during a period of variable river discharge (January 6 – 9, 2003). Average hourly water temperature is shown for the river (+), egg pocket (○), shallow hyporheic (●) and deep hyporheic (▲) zones. Average hourly stage (depth) is shown for the river (+), and shallow hyporheic zone (●). The difference between these two water depths (hyporheic minus river) is plotted on the Y-right axis as *dh* (—), with positive values indicating upwelling potential.

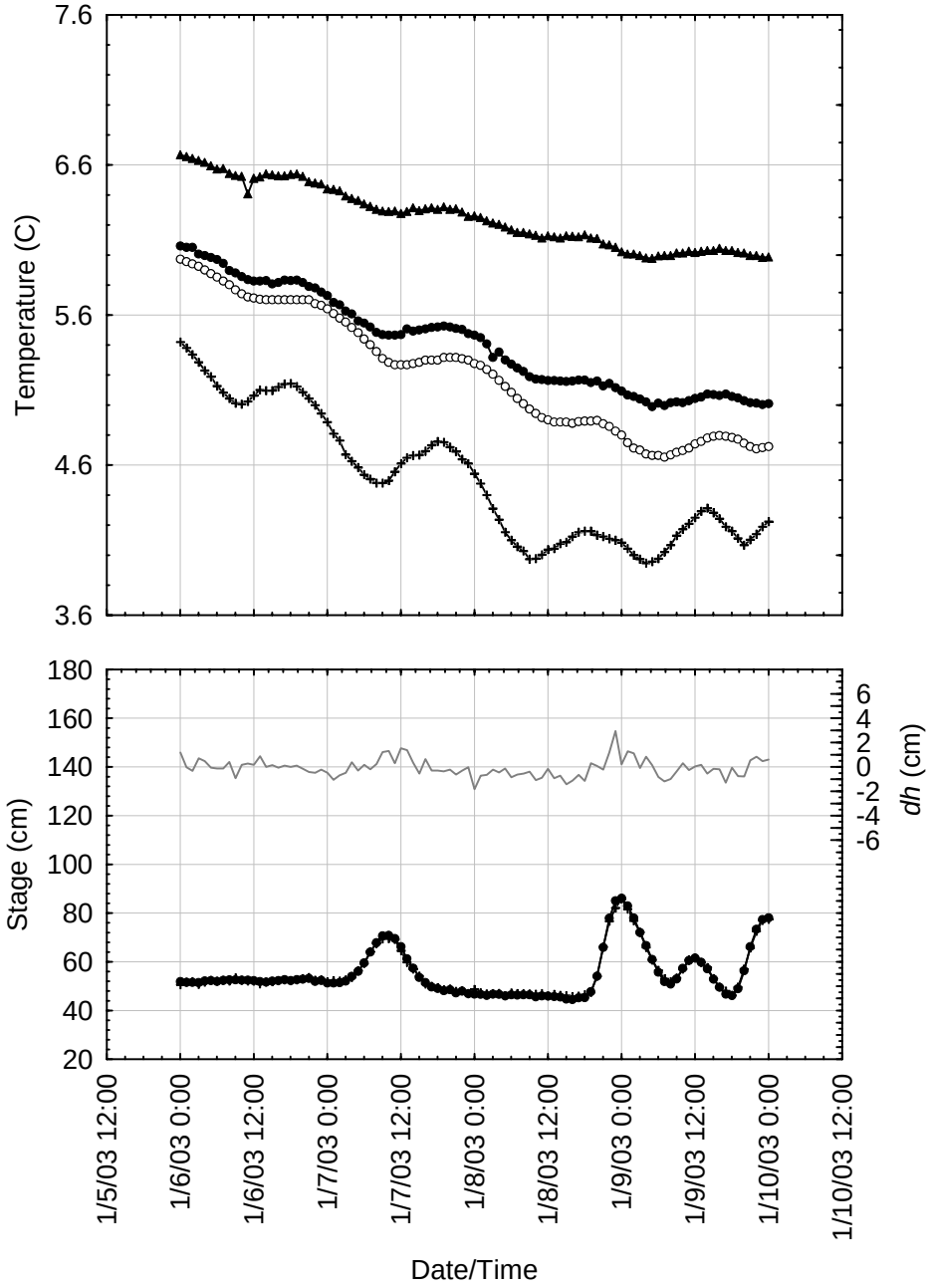

Appendix Figure 18. Time-series summary of water temperature (top panel) and river stage (bottom panel) at site 156.8 during a period of variable river discharge (January 6 – 9, 2003). Average hourly water temperature is shown for the river (+), egg pocket (○), shallow hyporheic (●) and deep hyporheic (▲) zones. Average hourly stage (depth) is shown for the river (+), and shallow hyporheic zone (●). The difference between these two water depths (hyporheic minus river) is plotted on the Y-right axis as *dh* (—), with positive values indicating upwelling potential.

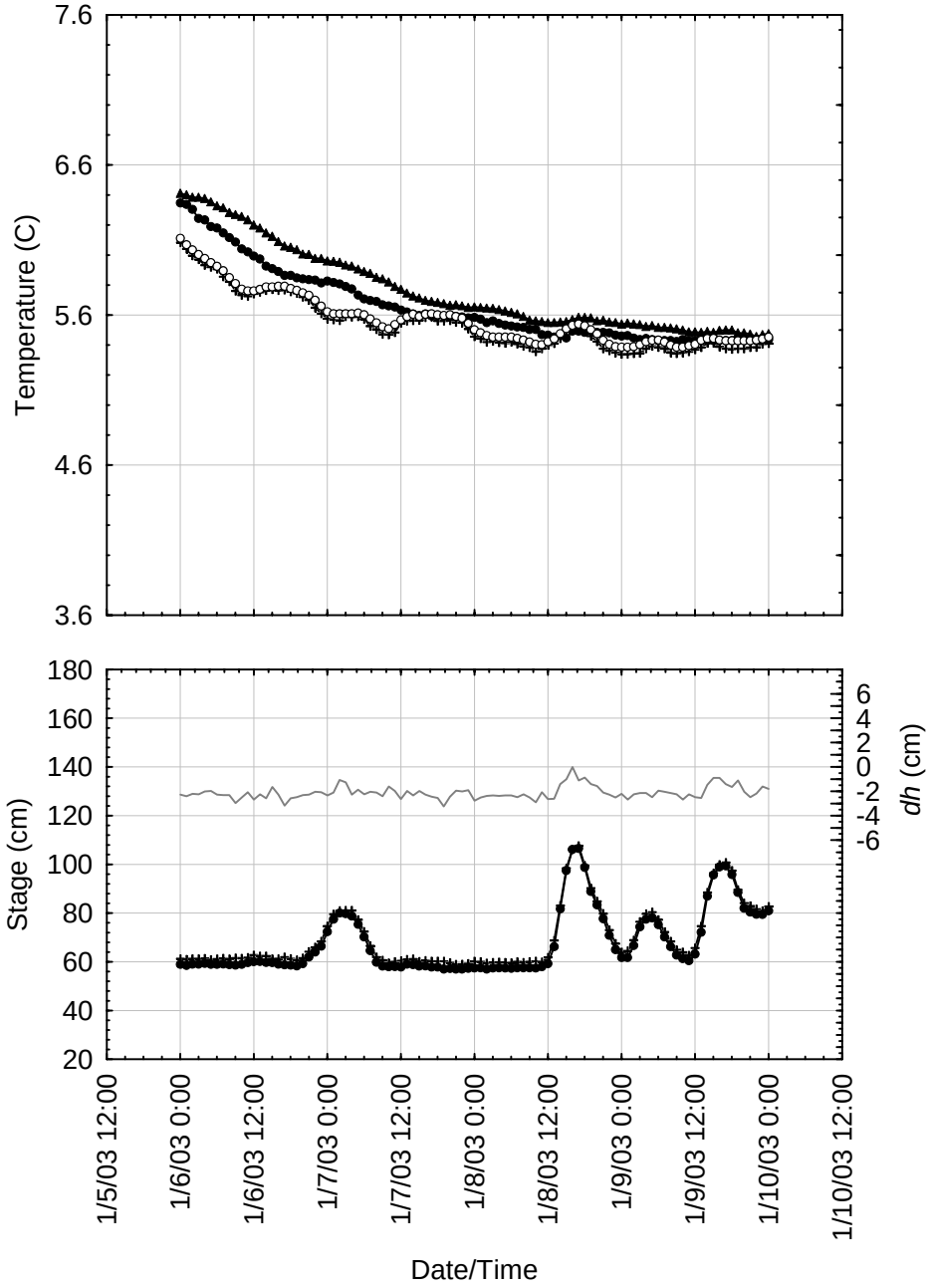

Appendix Figure 19. Time-series summary of water temperature (top panel) and river stage (bottom panel) at site 196.0 during a period of variable river discharge (January 6 – 9, 2003). Average hourly water temperature is shown for the river (+), egg pocket (○), shallow hyporheic (●) and deep hyporheic (▲) zones. Average hourly stage (depth) is shown for the river (+), and shallow hyporheic zone (●). The difference between these two water depths (hyporheic minus river) is plotted on the Y-right axis as *dh* (—), with positive values indicating upwelling potential.

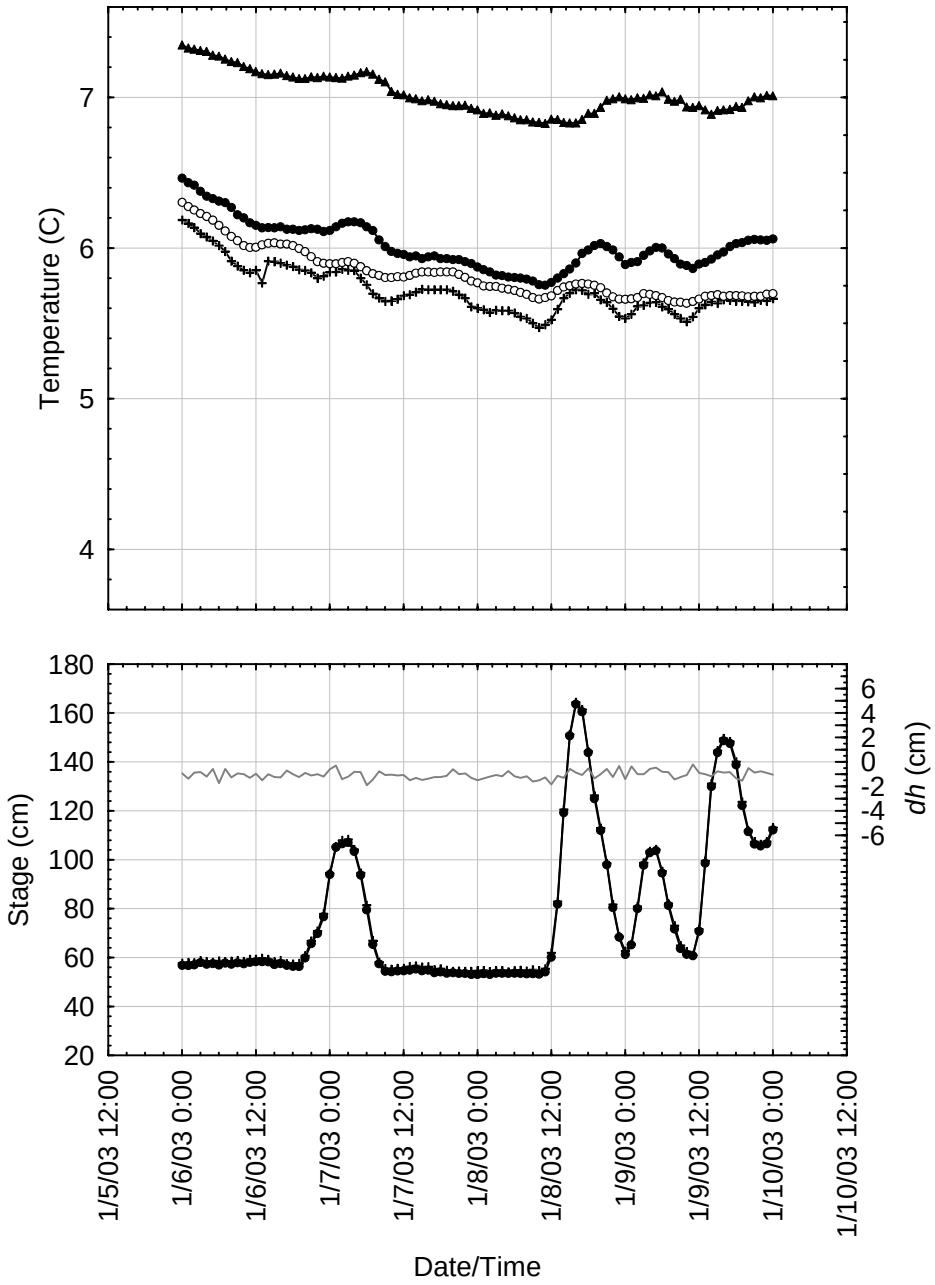

Appendix Figure 20. Time-series summary of water temperature (top panel) and river stage (bottom panel) at site 198.2 during a period of variable river discharge (January 6 – 9, 2003). Average hourly water temperature is shown for the river (+), egg pocket (○), shallow hyporheic (●) and deep hyporheic (▲) zones. Average hourly stage (depth) is shown for the river (+), and shallow hyporheic zone (●). The difference between these two water depths (hyporheic minus river) is plotted on the Y-right axis as *dh* (—), with positive values indicating upwelling potential.

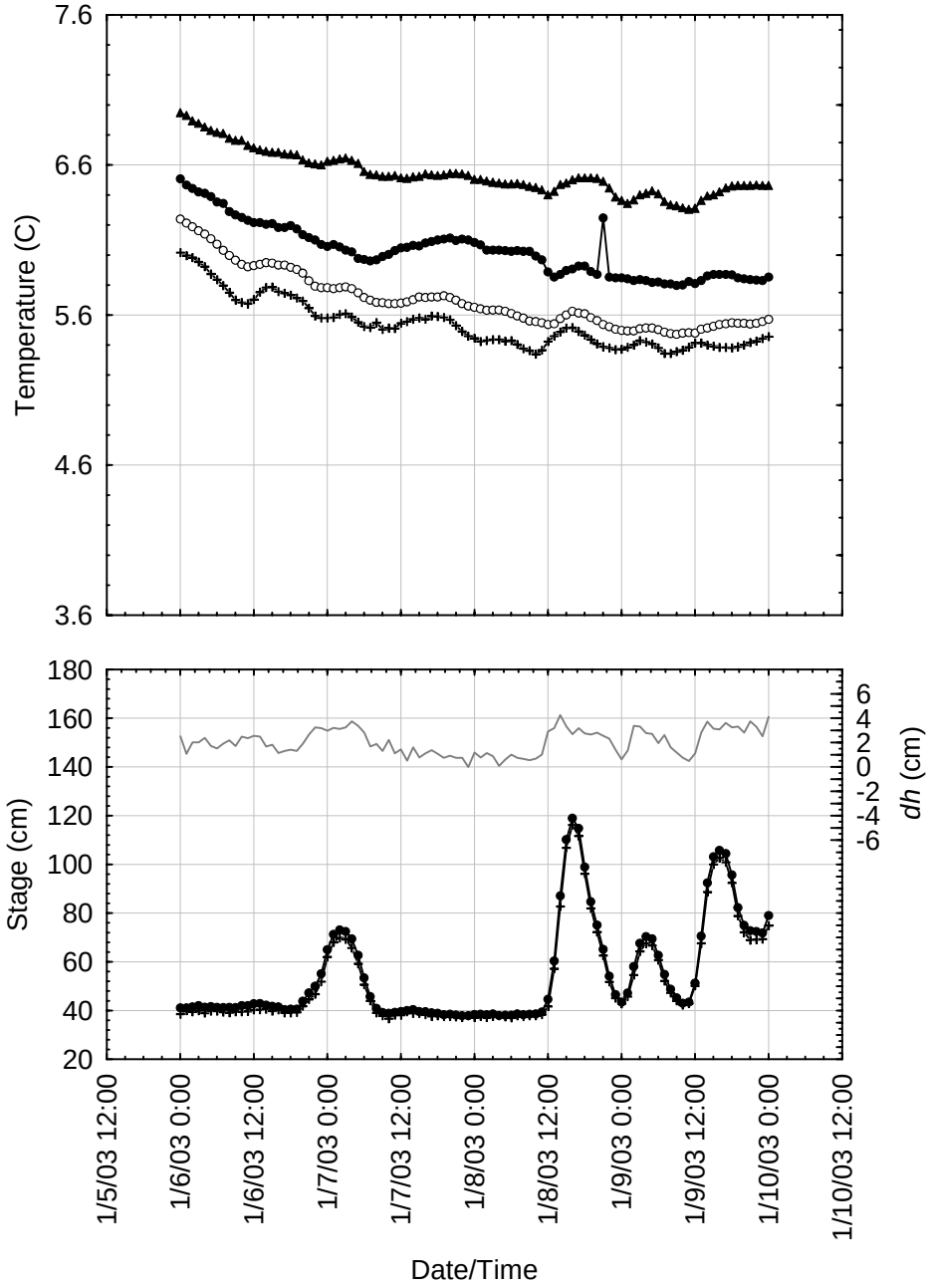

Appendix Figure 21. Time-series summary of water temperature (top panel) and river stage (bottom panel) at site 198.8 during a period of variable river discharge (January 6 – 9, 2003). Average hourly water temperature is shown for the river (+), egg pocket (○), shallow hyporheic (●) and deep hyporheic (▲) zones. Average hourly stage (depth) is shown for the river (+), and shallow hyporheic zone (●). The difference between these two water depths (hyporheic minus river) is plotted on the Y-right axis as *dh* (—), with positive values indicating upwelling potential.

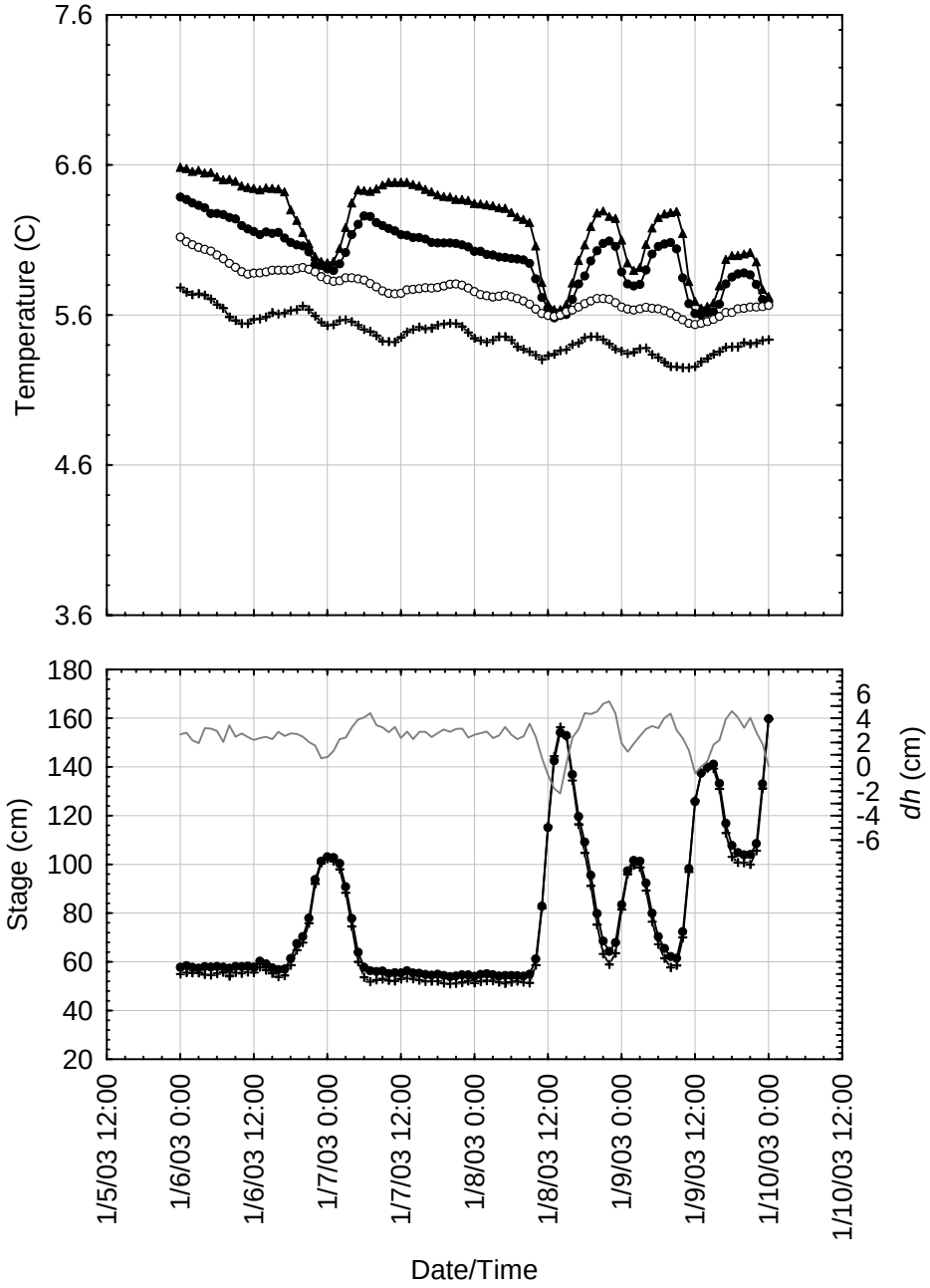

Appendix Figure 22. Time-series summary of water temperature (top panel) and river stage (bottom panel) at site 211.9 during a period of variable river discharge (January 6 – 9, 2003). Average hourly water temperature is shown for the river (+), egg pocket (○), shallow hyporheic (●) and deep hyporheic (▲) zones. Average hourly stage (depth) is shown for the river (+), and shallow hyporheic zone (●). The difference between these two water depths (hyporheic minus river) is plotted on the Y-right axis as *dh* (—), with positive values indicating upwelling potential.

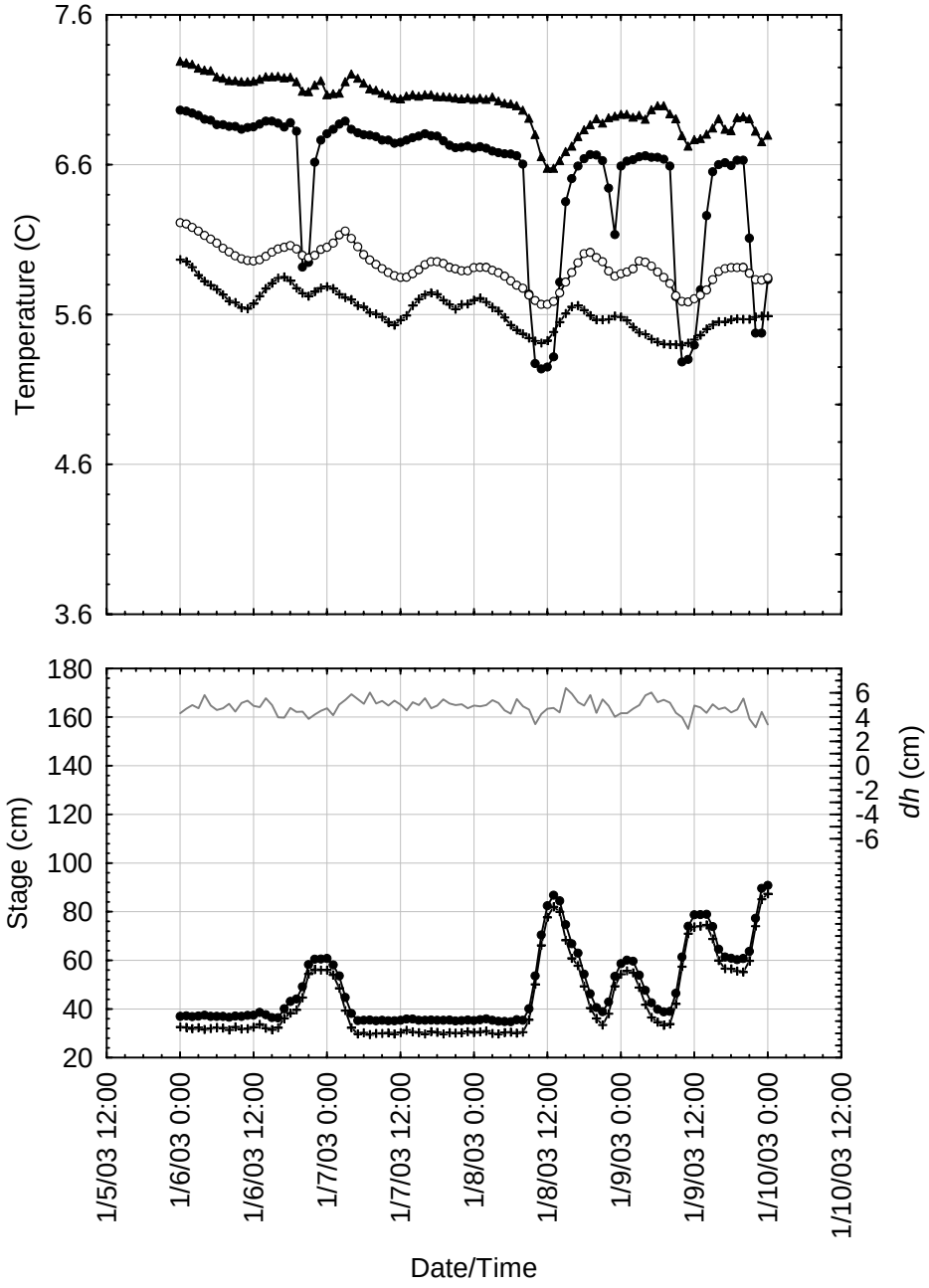

Appendix Figure 23. Time-series summary of water temperature (top panel) and river stage (bottom panel) at site 218.7 during a period of variable river discharge (January 6 – 9, 2003). Average hourly water temperature is shown for the river (+), egg pocket (○), shallow hyporheic (●) and deep hyporheic (▲) zones. Average hourly stage (depth) is shown for the river (+), and shallow hyporheic zone (●). The difference between these two water depths (hyporheic minus river) is plotted on the Y-right axis as *dh* (—), with positive values indicating upwelling potential.

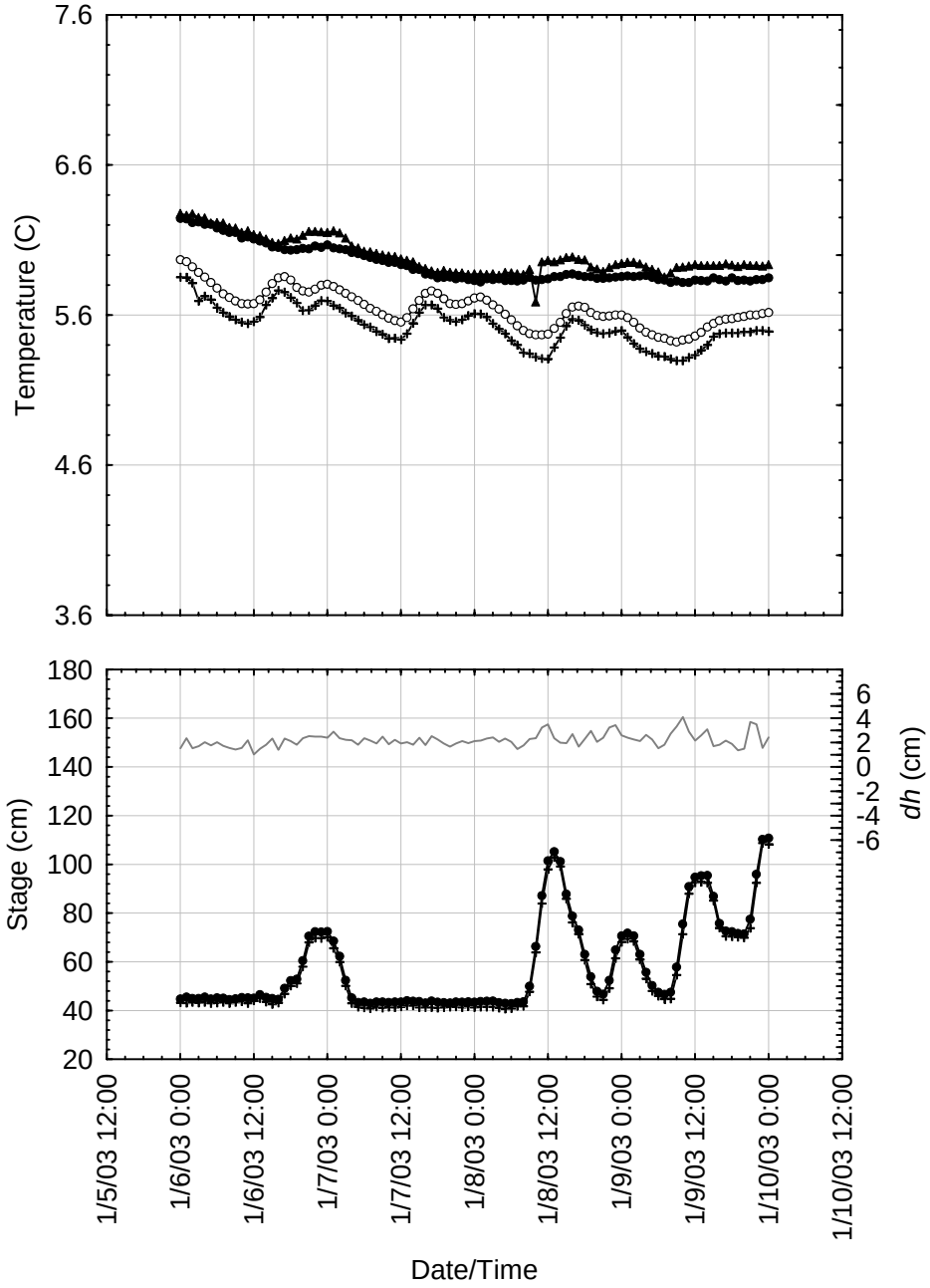

Appendix Figure 24. Time-series summary of water temperature (top panel) and river stage (bottom panel) at site 219.3 during a period of variable river discharge (January 6 – 9, 2003). Average hourly water temperature is shown for the river (+), egg pocket (○), shallow hyporheic (●) and deep hyporheic (▲) zones. Average hourly stage (depth) is shown for the river (+), and shallow hyporheic zone (●). The difference between these two water depths (hyporheic minus river) is plotted on the Y-right axis as *dh* (—), with positive values indicating upwelling potential.

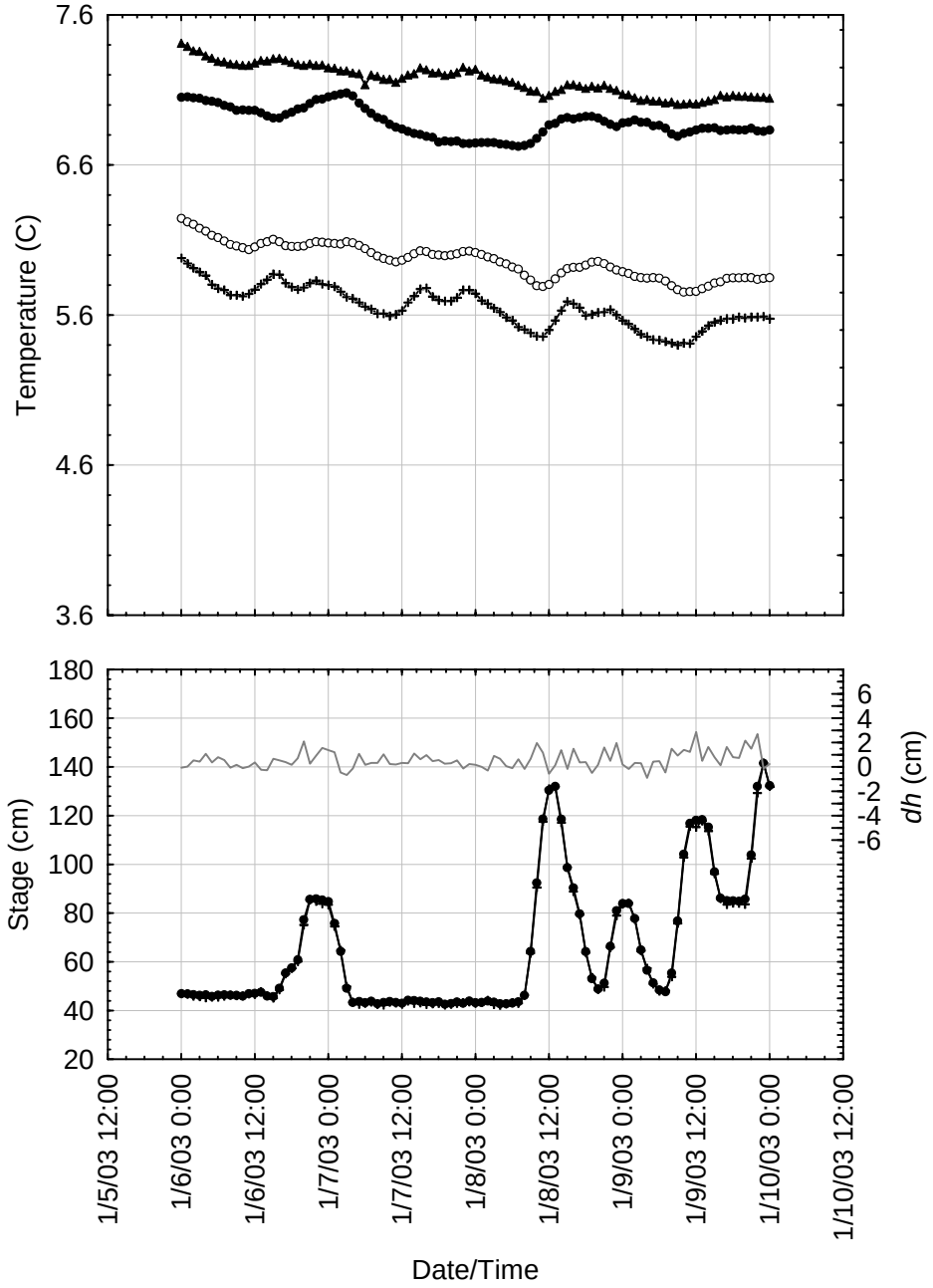

Appendix Figure 25. Time-series summary of water temperature (top panel) and river stage (bottom panel) at site 222.7 during a period of variable river discharge (January 6 – 9, 2003). Average hourly water temperature is shown for the river (+), egg pocket (○), shallow hyporheic (●) and deep hyporheic (▲) zones. Average hourly stage (depth) is shown for the river (+), and shallow hyporheic zone (●). The difference between these two water depths (hyporheic minus river) is plotted on the Y-right axis as *dh* (—), with positive values indicating upwelling potential.

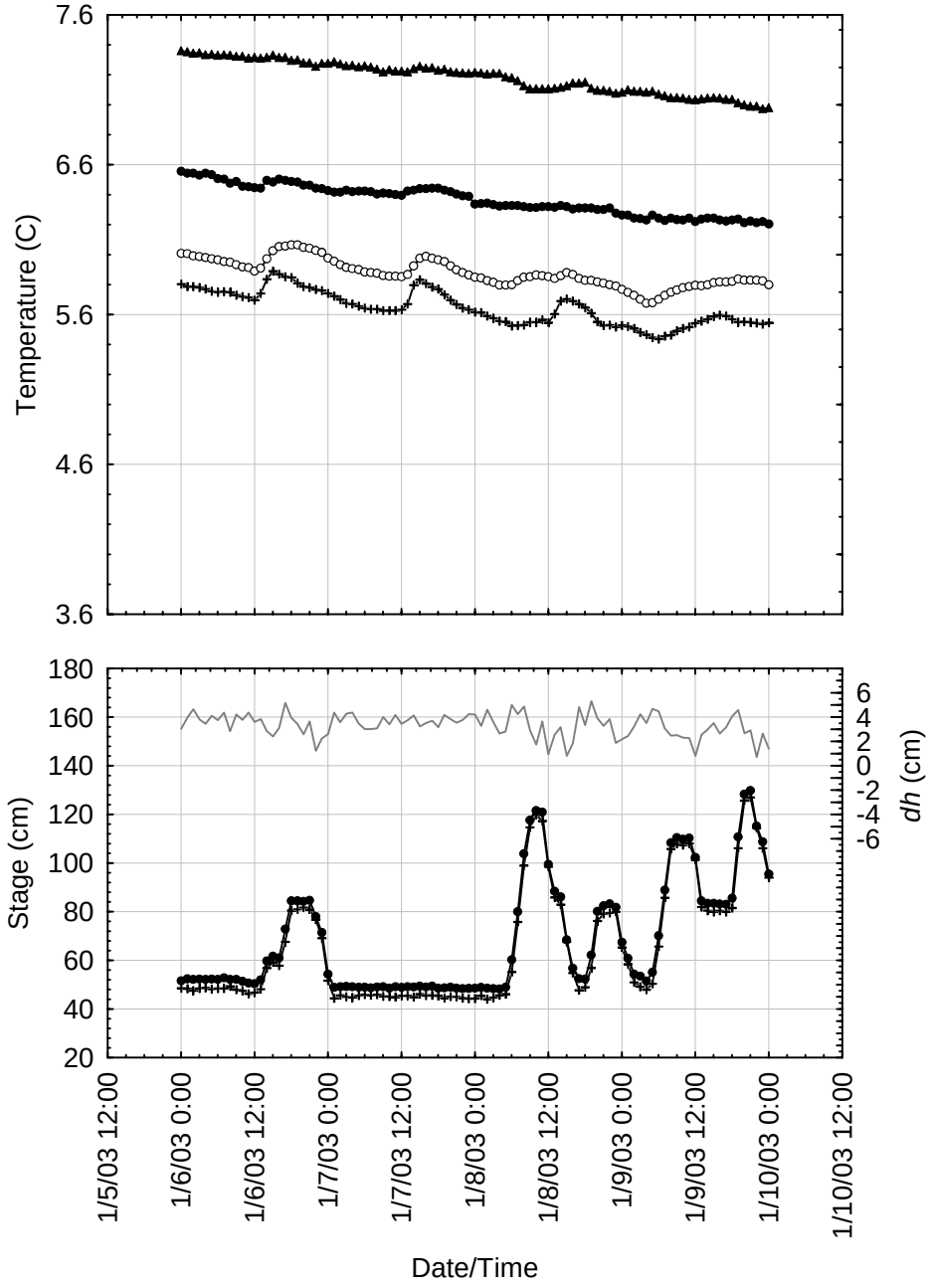

Appendix Figure 26. Time-series summary of water temperature (top panel) and river stage (bottom panel) at site 238.6 during a period of variable river discharge (January 6 – 9, 2003). Average hourly water temperature is shown for the river (+), egg pocket (○), shallow hyporheic (●) and deep hyporheic (▲) zones. Average hourly stage (depth) is shown for the river (+), and shallow hyporheic zone (●). The difference between these two water depths (hyporheic minus river) is plotted on the Y-right axis as *dh* (—), with positive values indicating upwelling potential.

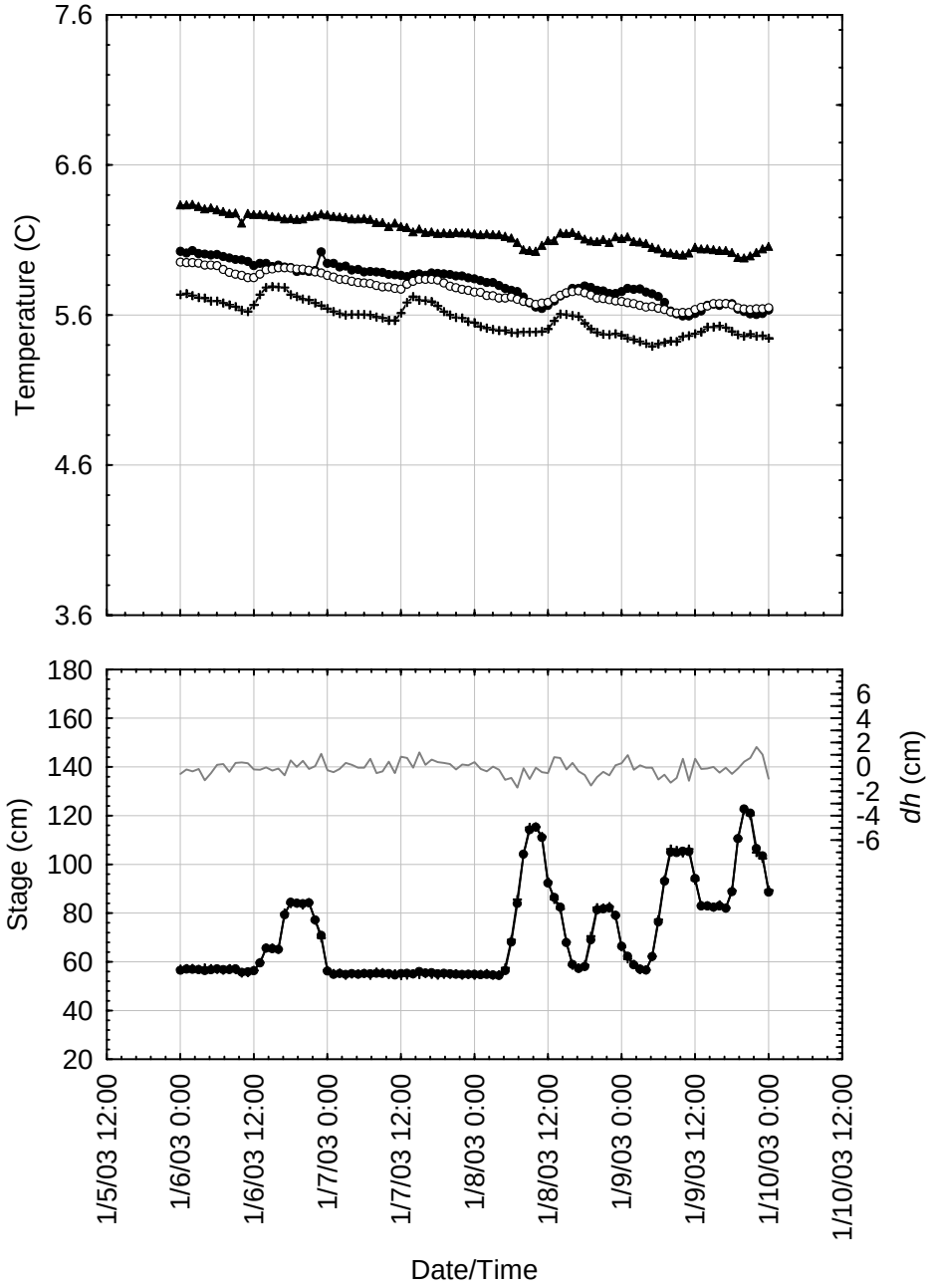

Appendix Figure 27. Time-series summary of water temperature (top panel) and river stage (bottom panel) at site 240.6 during a period of variable river discharge (January 6 – 9, 2003). Average hourly water temperature is shown for the river (+), egg pocket (○), shallow hyporheic (●) and deep hyporheic (▲) zones. Average hourly stage (depth) is shown for the river (+), and shallow hyporheic zone (●). The difference between these two water depths (hyporheic minus river) is plotted on the Y-right axis as *dh* (—), with positive values indicating upwelling potential.

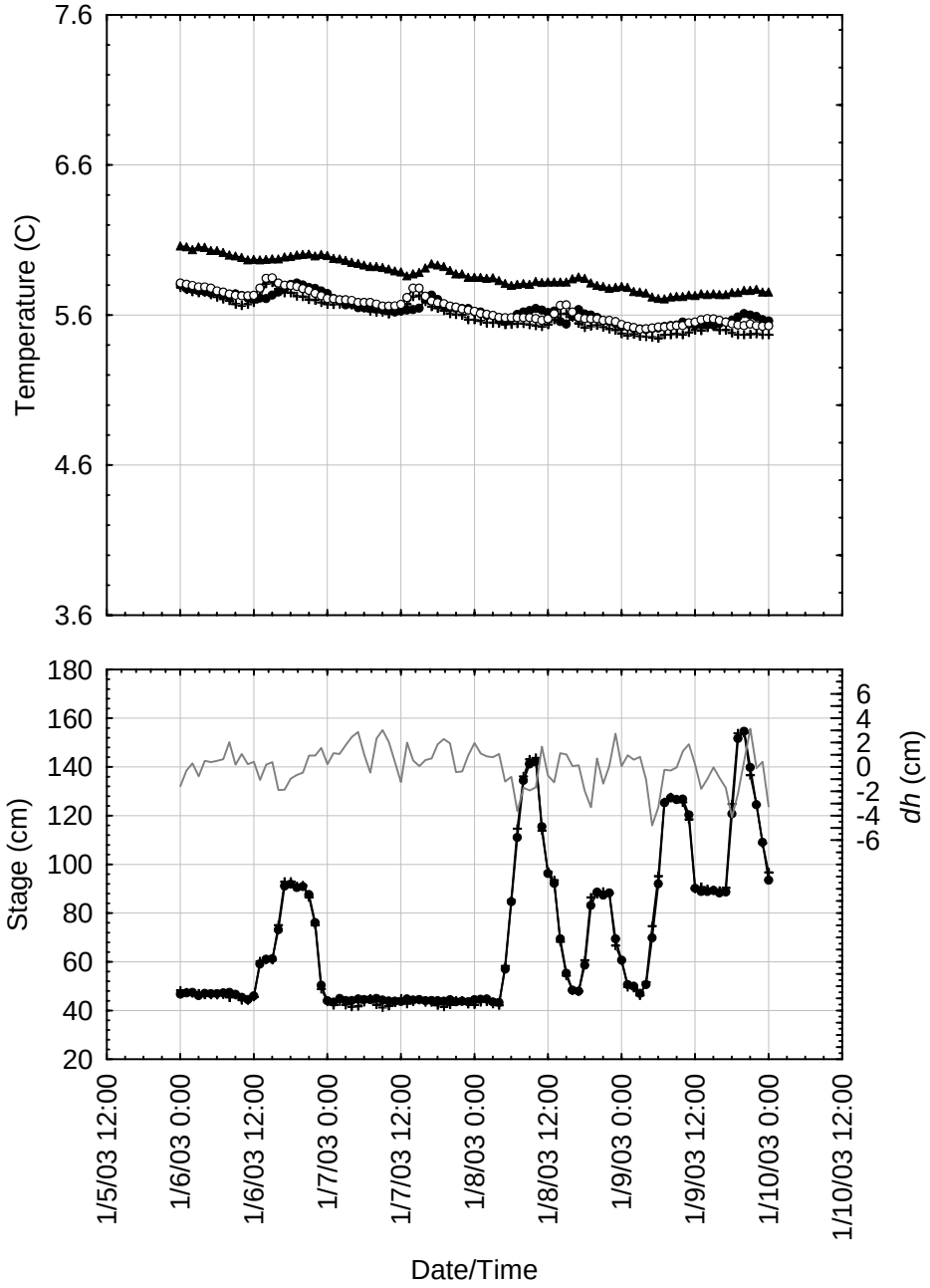

Appendix Figure 28. Time-series summary of water temperature (top panel) and river stage (bottom panel) at site 244.5 during a period of variable river discharge (January 6 – 9, 2003). Average hourly water temperature is shown for the river (+), egg pocket (○), shallow hyporheic (●) and deep hyporheic (▲) zones. Average hourly stage (depth) is shown for the river (+), and shallow hyporheic zone (●). The difference between these two water depths (hyporheic minus river) is plotted on the Y-right axis as *dh* (—), with positive values indicating upwelling potential.

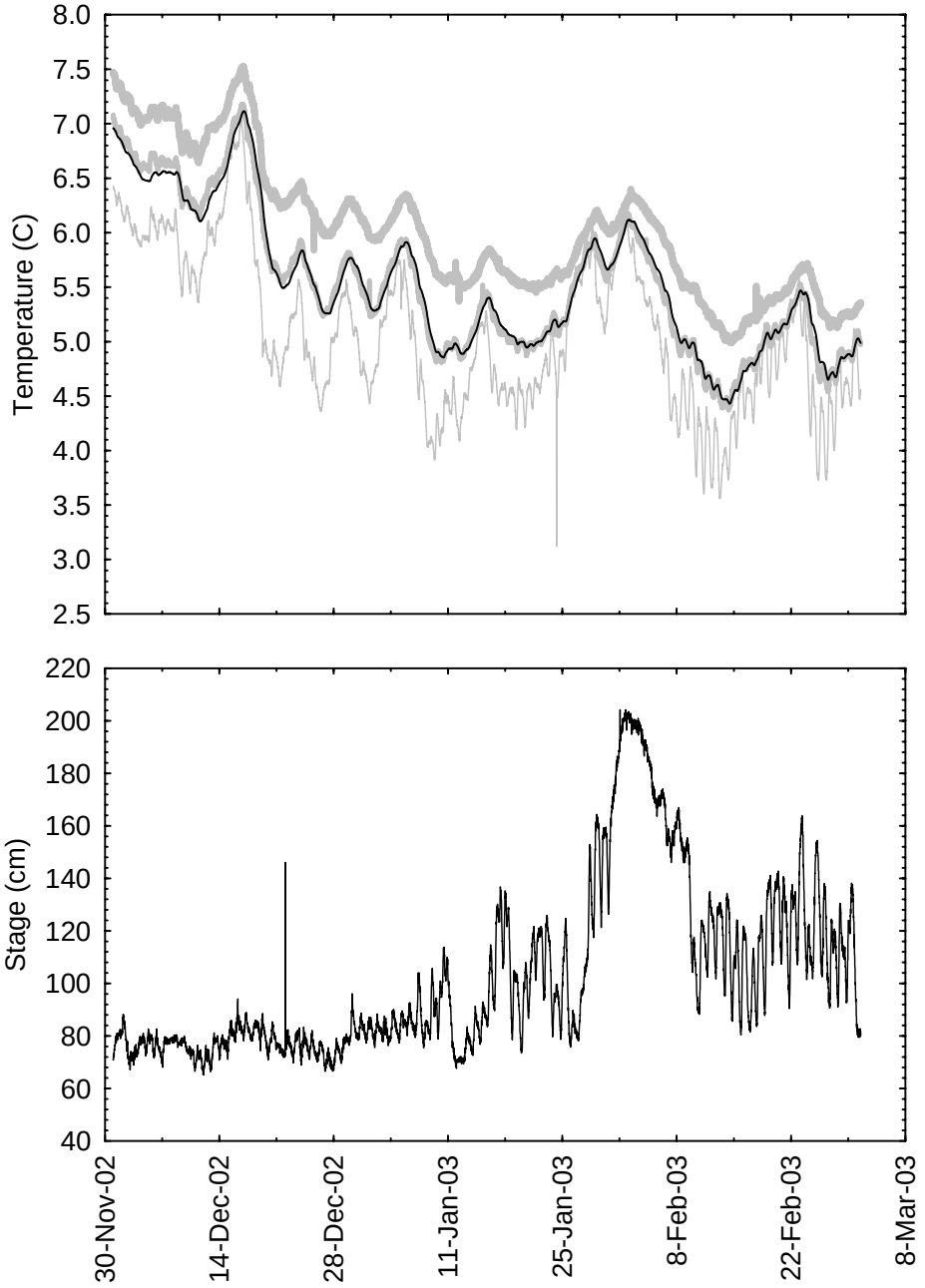

Appendix Figure 29. Time-series summary of observed and modeled water temperature (top panel) and river stage (bottom panel) at site 148.5 during the period 1 December 2002 – 2 March 2003. Water temperatures recorded at 20 min intervals in the river (——), shallow hyporheic zone (——), and deep hyporheic zone (——) are compared with modeled water temperature at 20 min intervals in the shallow hyporheic zone (——).

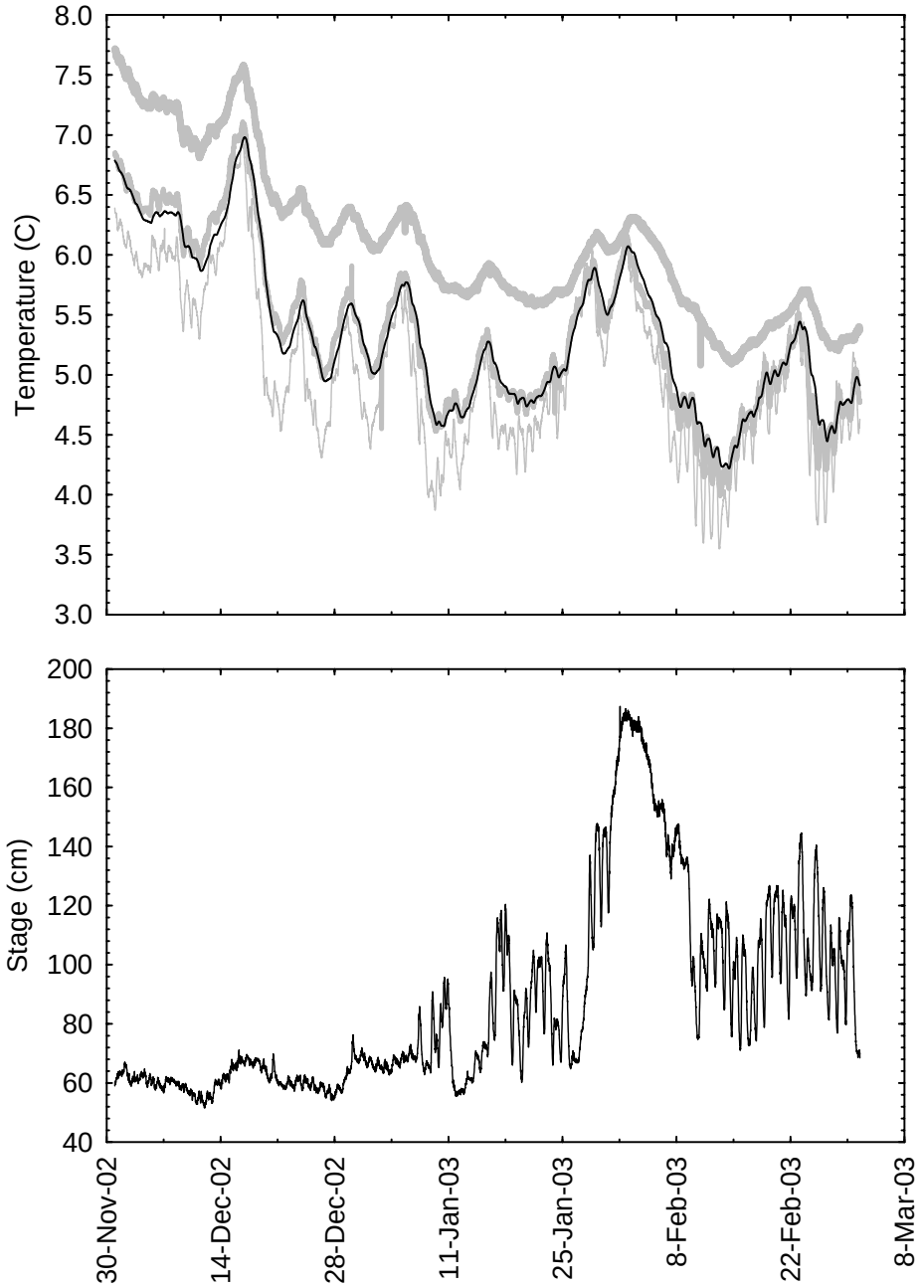

Appendix Figure 30. Time-series summary of observed and modeled water temperature (top panel) and river stage (bottom panel) at site 149.2 during the period 1 December 2002 – 2 March 2003. Water temperatures recorded at 20 min intervals in the river (——), shallow hyporheic zone (——), and deep hyporheic zone (——) are compared with modeled water temperature at 20 min intervals in the shallow hyporheic zone (——).

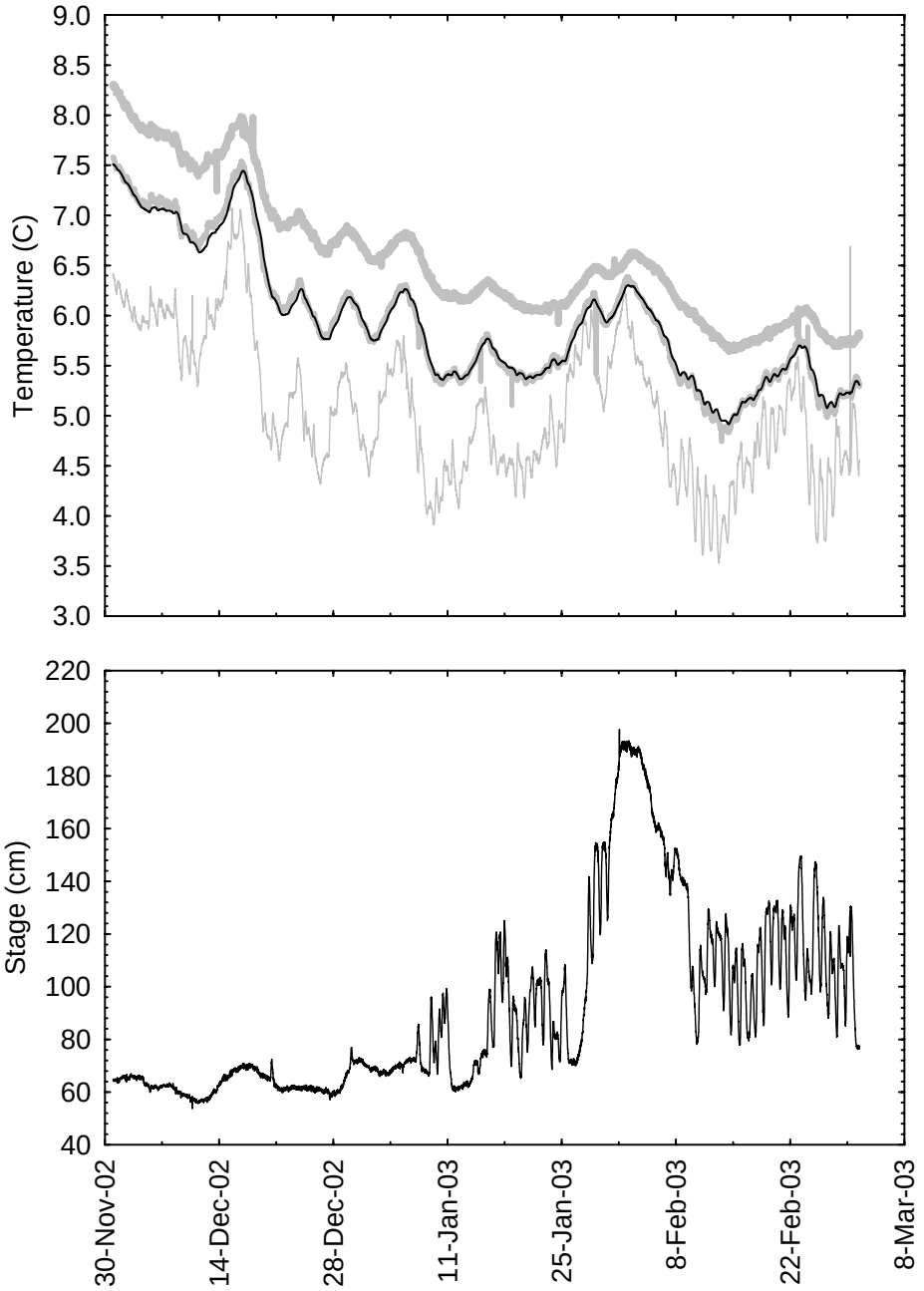

Appendix Figure 31. Time-series summary of observed and modeled water temperature (top panel) and river stage (bottom panel) at site 152.3 during the period 1 December 2002 – 2 March 2003. Water temperatures recorded at 20 min intervals in the river (——), shallow hyporheic zone (——), and deep hyporheic zone (——) are compared with modeled water temperature at 20 min intervals in the shallow hyporheic zone (——).

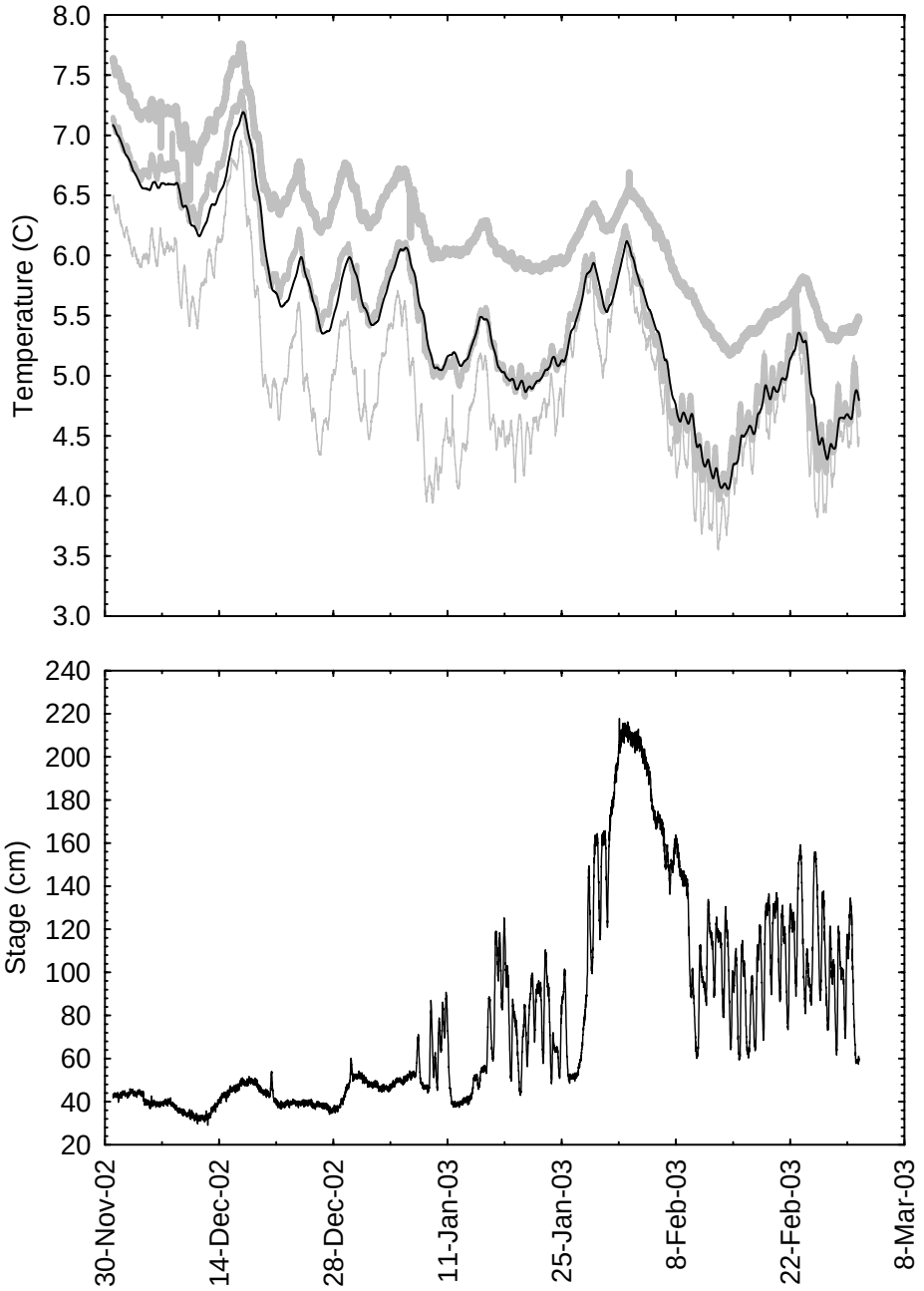

Appendix Figure 32. Time-series summary of observed and modeled water temperature (top panel) and river stage (bottom panel) at site 156.8 during the period 1 December 2002 – 2 March 2003. Water temperatures recorded at 20 min intervals in the river (——), shallow hyporheic zone (——), and deep hyporheic zone (——) are compared with modeled water temperature at 20 min intervals in the shallow hyporheic zone (——).

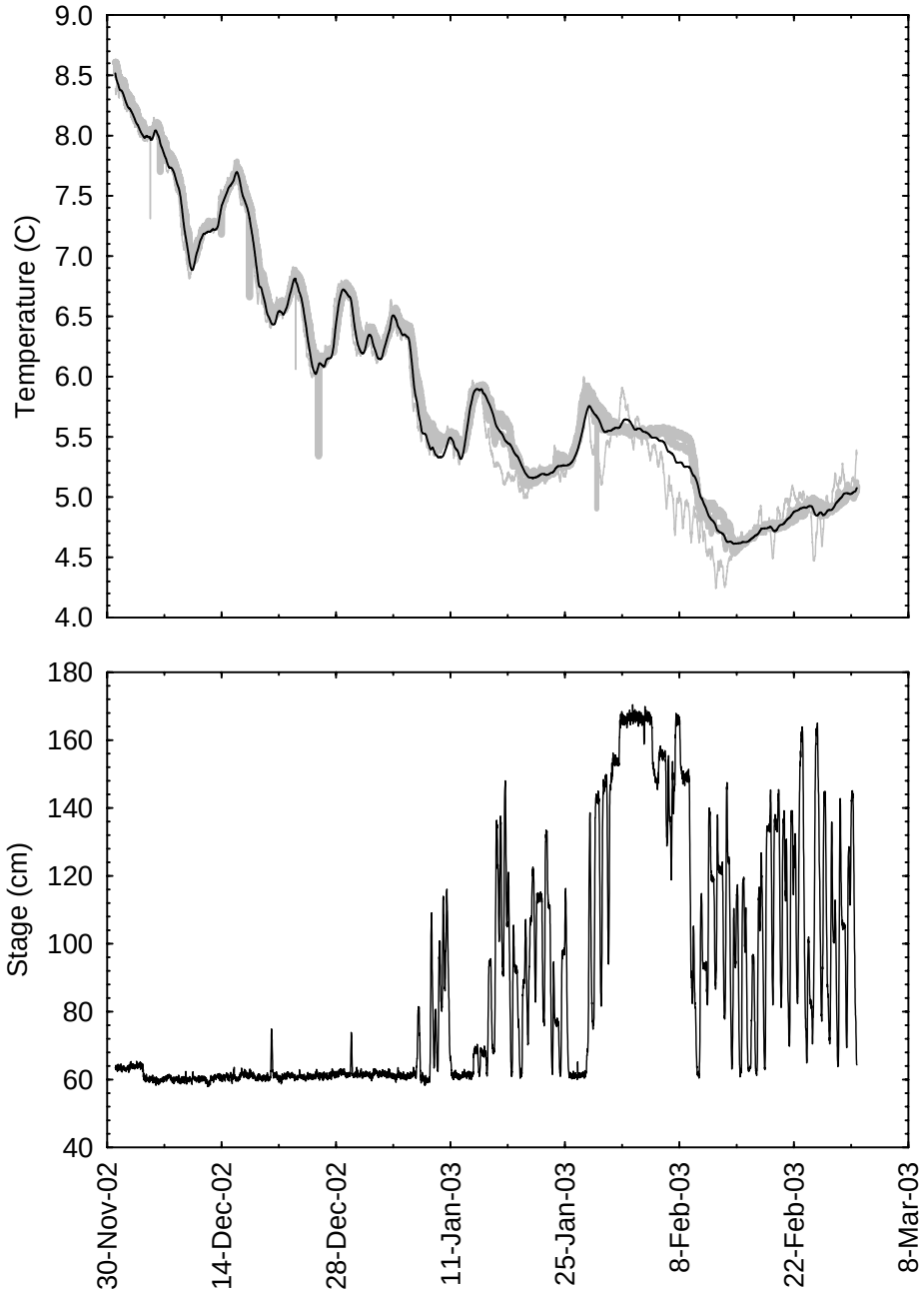

Appendix Figure 33. Time-series summary of observed and modeled water temperature (top panel) and river stage (bottom panel) at site 196.0 during the period 1 December 2002 – 2 March 2003. Water temperatures recorded at 20 min intervals in the river (——), shallow hyporheic zone (——), and deep hyporheic zone (——) are compared with modeled water temperature at 20 min intervals in the shallow hyporheic zone (——).

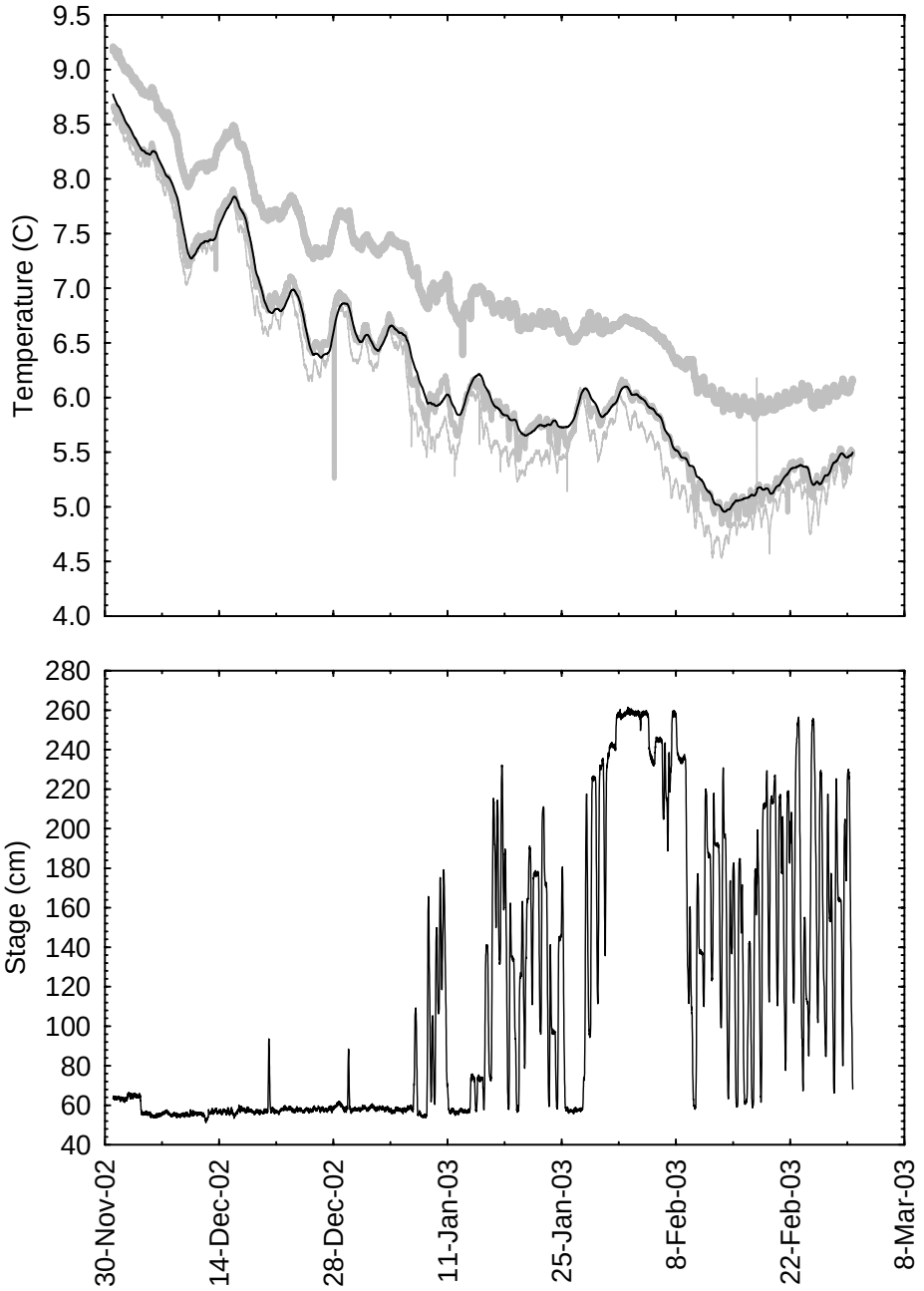

Appendix Figure 34. Time-series summary of observed and modeled water temperature (top panel) and river stage (bottom panel) at site 198.2 during the period 1 December 2002 – 2 March 2003. Water temperatures recorded at 20 min intervals in the river (——), shallow hyporheic zone (——), and deep hyporheic zone (——) are compared with modeled water temperature at 20 min intervals in the shallow hyporheic zone (——).

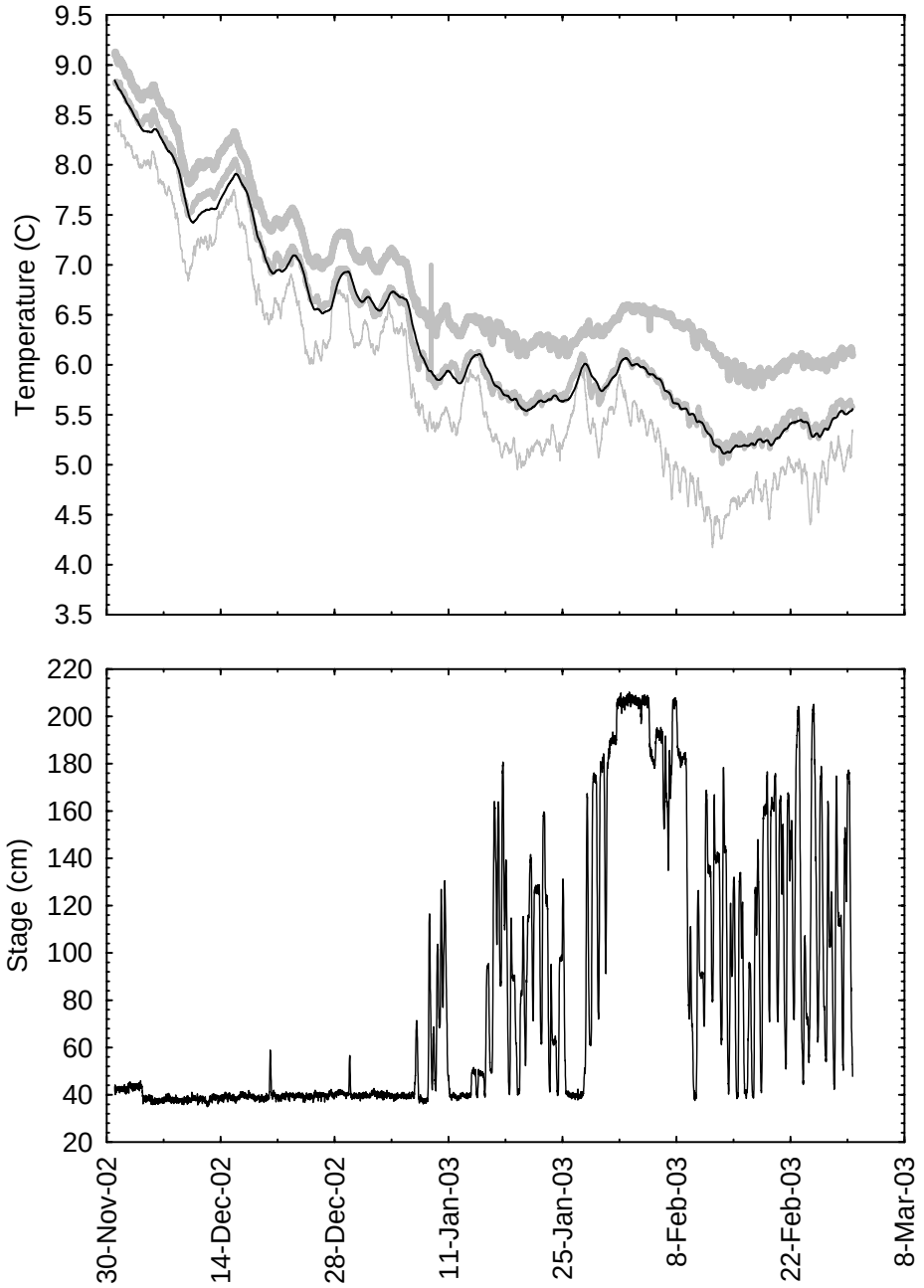

Appendix Figure 35. Time-series summary of observed and modeled water temperature (top panel) and river stage (bottom panel) at site 198.8 during the period 1 December 2002 – 2 March 2003. Water temperatures recorded at 20 min intervals in the river (——), shallow hyporheic zone (——), and deep hyporheic zone (——) are compared with modeled water temperature at 20 min intervals in the shallow hyporheic zone (——).

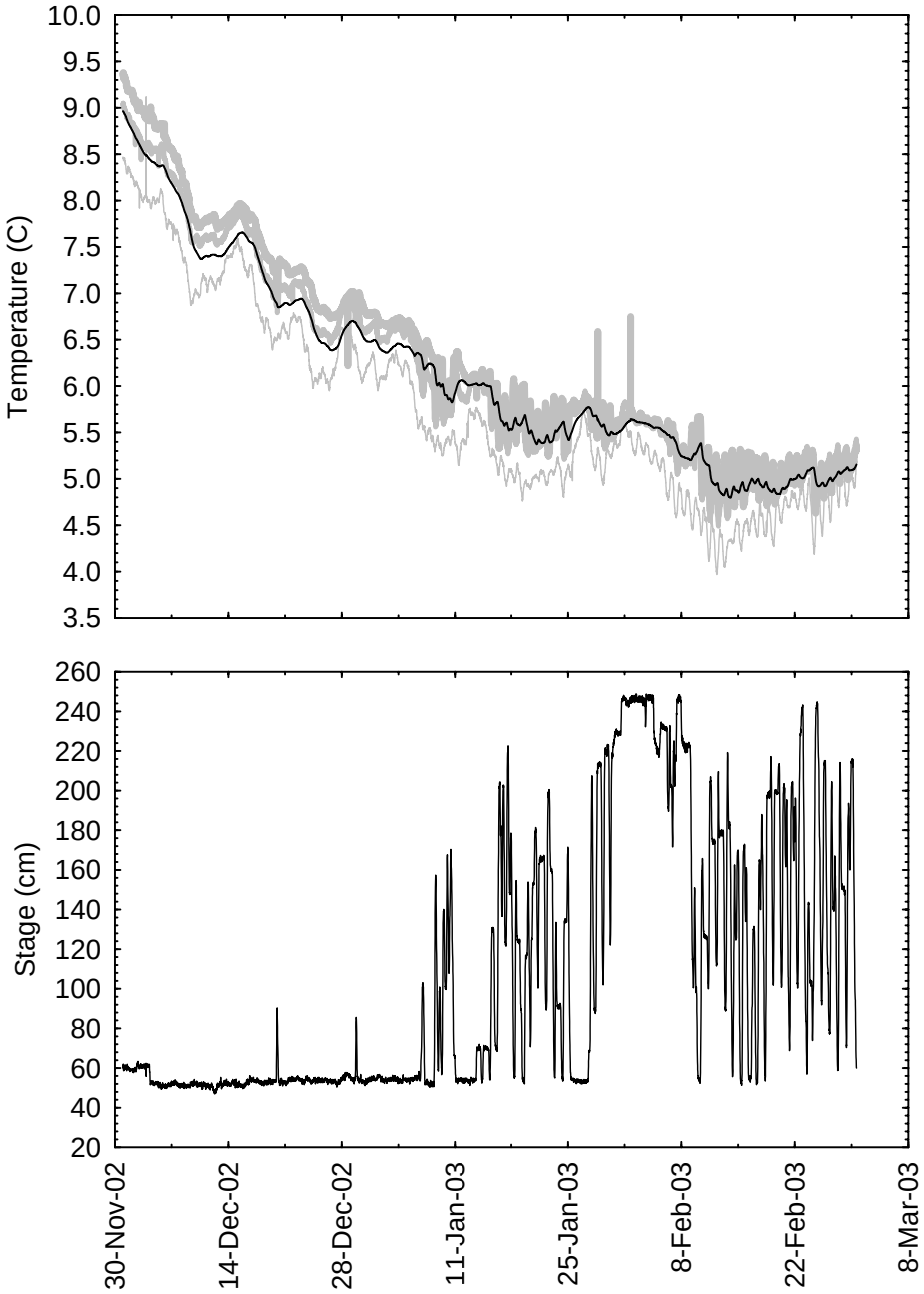

Appendix Figure 36. Time-series summary of observed and modeled water temperature (top panel) and river stage (bottom panel) at site 211.9 during the period 1 December 2002 – 2 March 2003. Water temperatures recorded at 20 min intervals in the river (——), shallow hyporheic zone (——), and deep hyporheic zone (——) are compared with modeled water temperature at 20 min intervals in the shallow hyporheic zone (——).

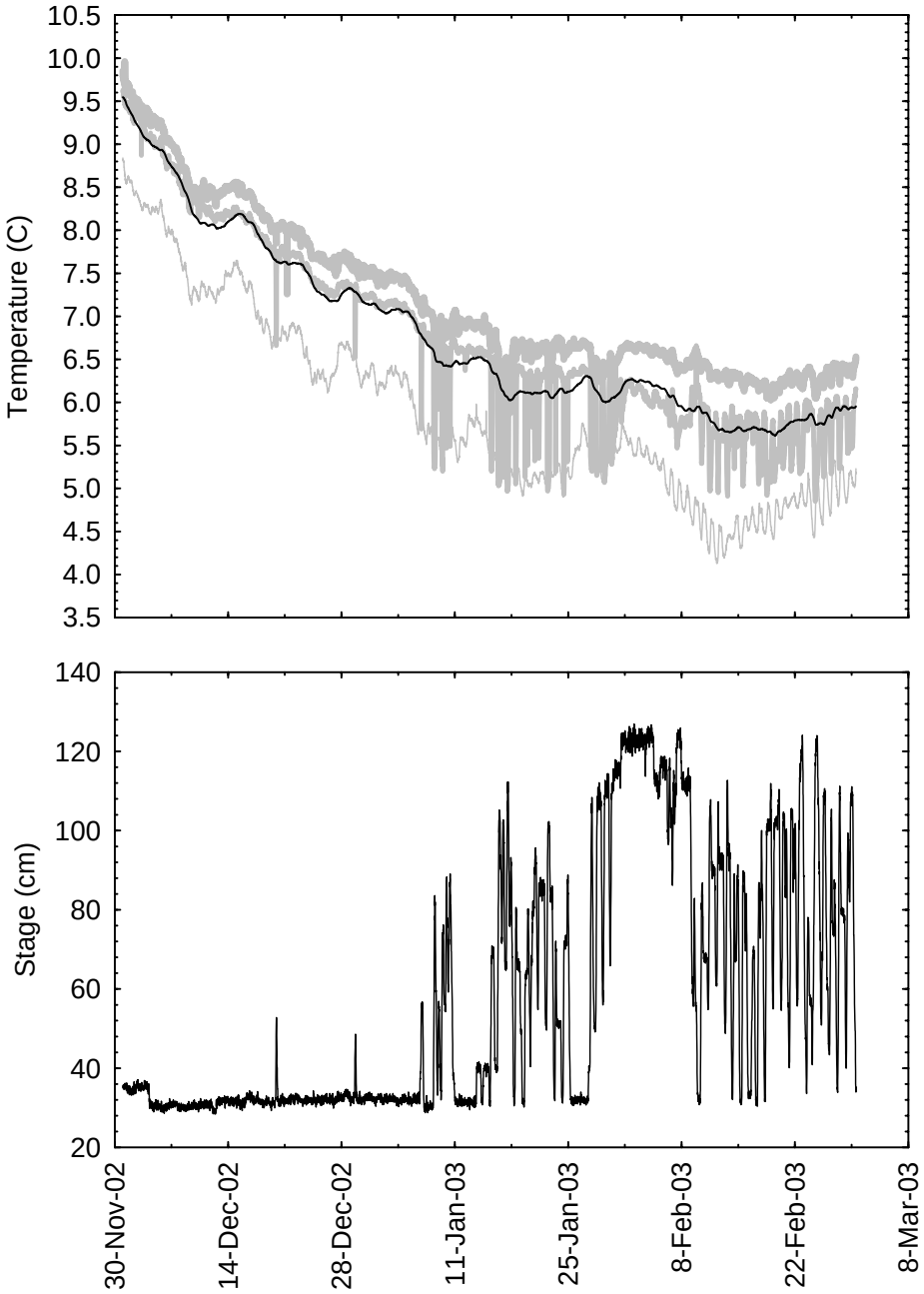

Appendix Figure 37. Time-series summary of observed and modeled water temperature (top panel) and river stage (bottom panel) at site 218.7 during the period 1 December 2002 – 2 March 2003. Water temperatures recorded at 20 min intervals in the river (——), shallow hyporheic zone (——), and deep hyporheic zone (——) are compared with modeled water temperature at 20 min intervals in the shallow hyporheic zone (——).

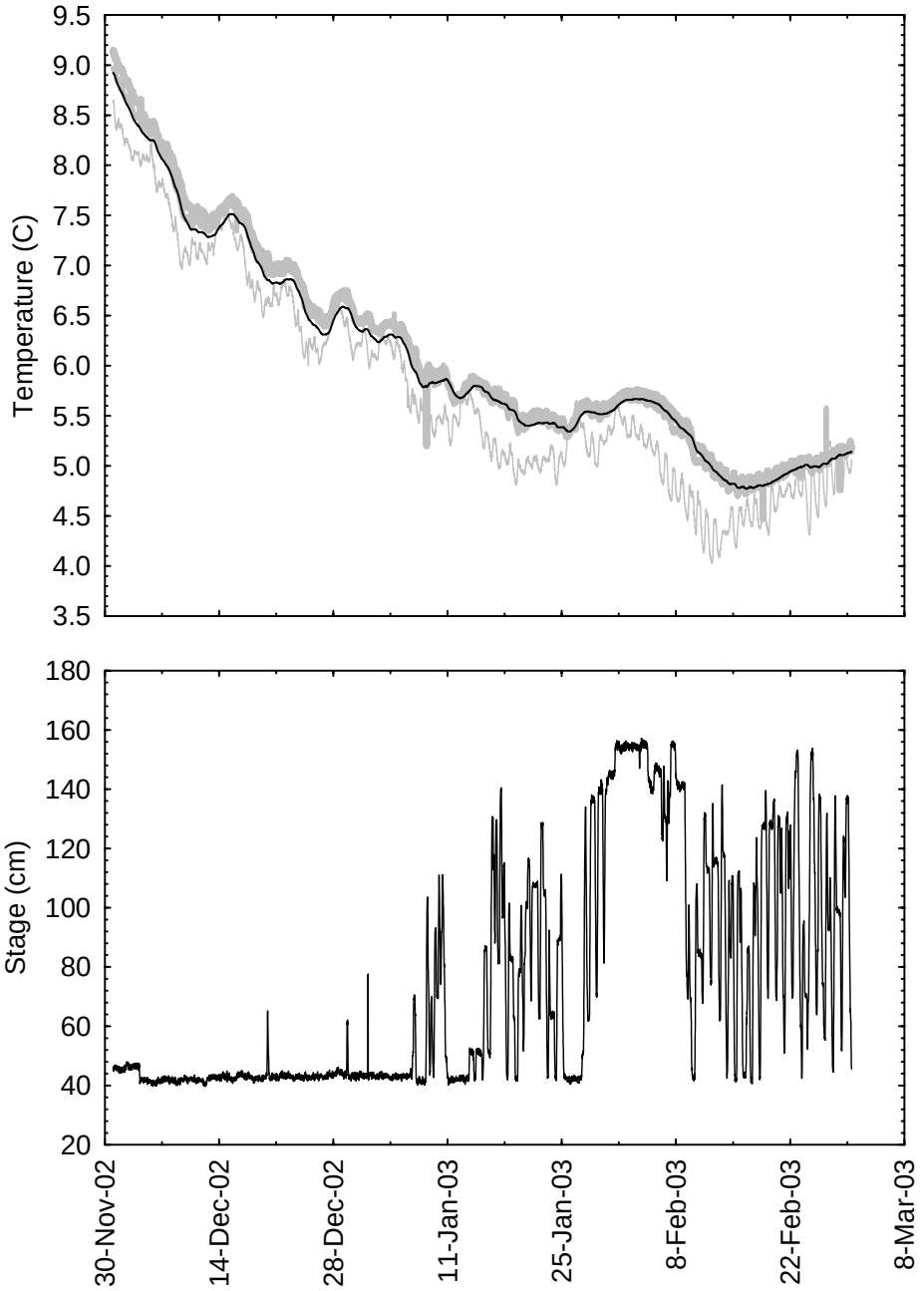

Appendix Figure 38. Time-series summary of observed and modeled water temperature (top panel) and river stage (bottom panel) at site 219.3 during the period 1 December 2002 – 2 March 2003. Water temperatures recorded at 20 min intervals in the river (——), shallow hyporheic zone (▬), and deep hyporheic zone (▬) are compared with modeled water temperature at 20 min intervals in the shallow hyporheic zone (——).

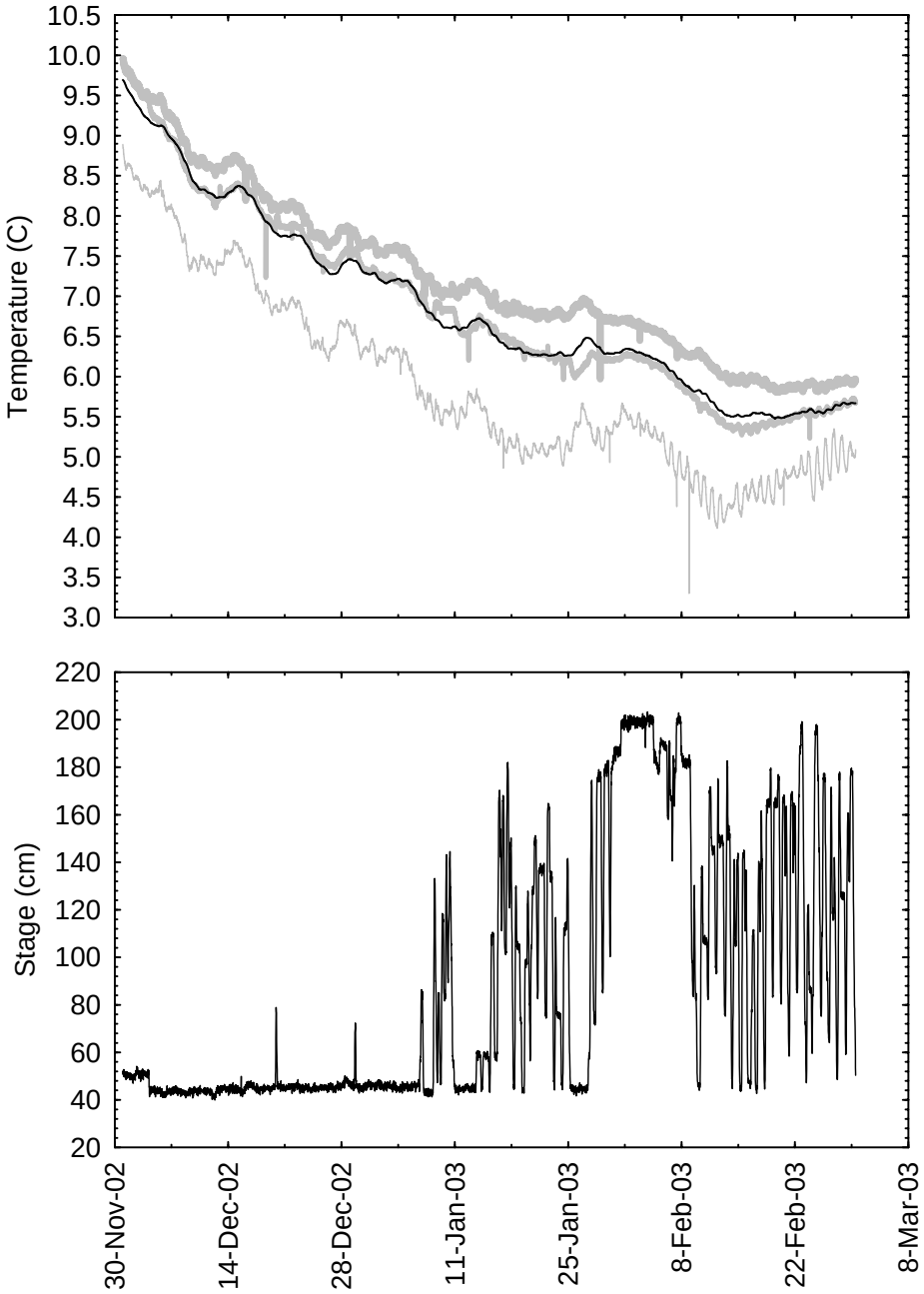

Appendix Figure 39. Time-series summary of observed and modeled water temperature (top panel) and river stage (bottom panel) at site 222.7 during the period 1 December 2002 – 2 March 2003. Water temperatures recorded at 20 min intervals in the river (——), shallow hyporheic zone (——), and deep hyporheic zone (——) are compared with modeled water temperature at 20 min intervals in the shallow hyporheic zone (——).

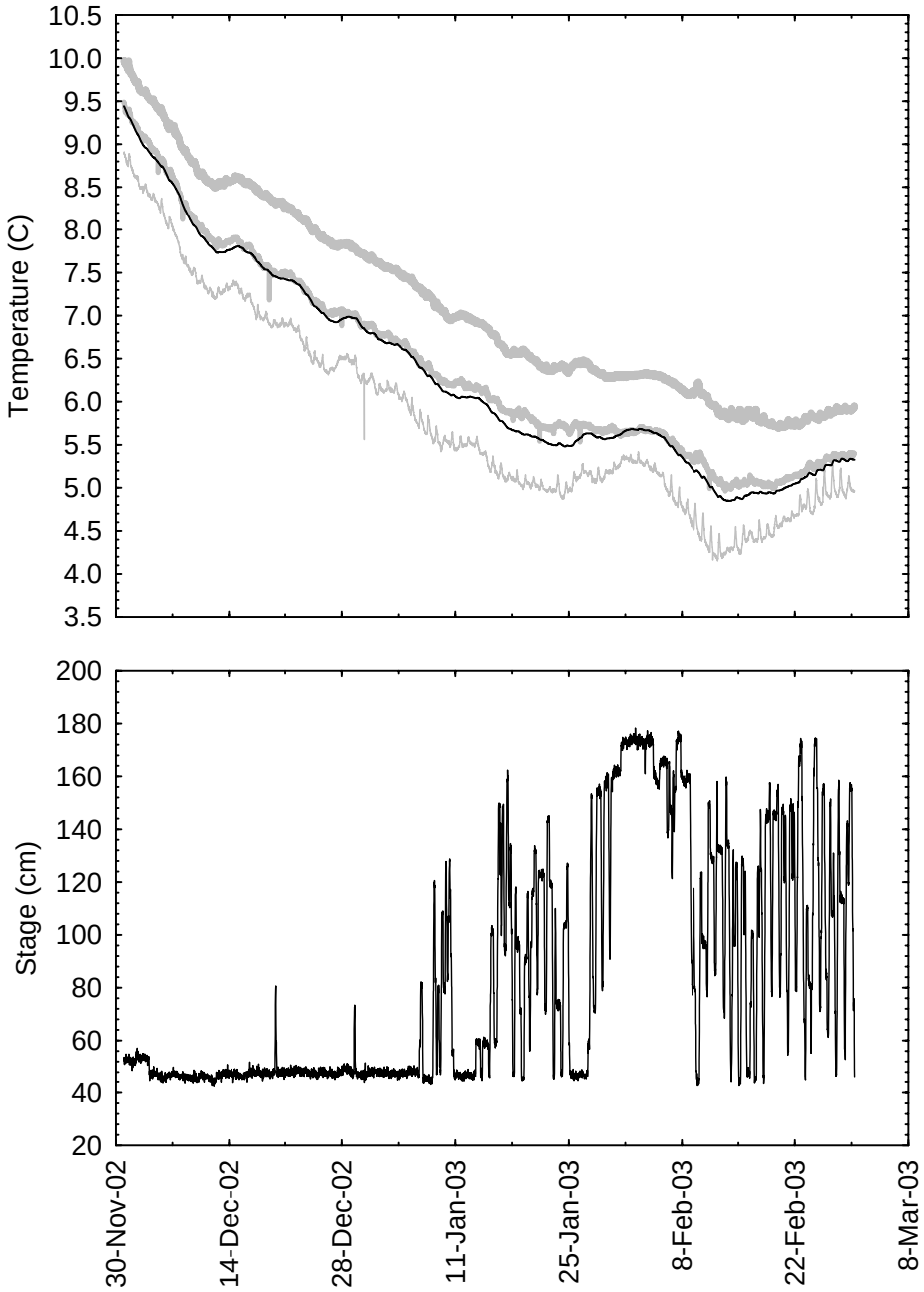

Appendix Figure 40. Time-series summary of observed and modeled water temperature (top panel) and river stage (bottom panel) at site 238.6 during the period 1 December 2002 – 2 March 2003. Water temperatures recorded at 20 min intervals in the river (——), shallow hyporheic zone (——), and deep hyporheic zone (——) are compared with modeled water temperature at 20 min intervals in the shallow hyporheic zone (——).

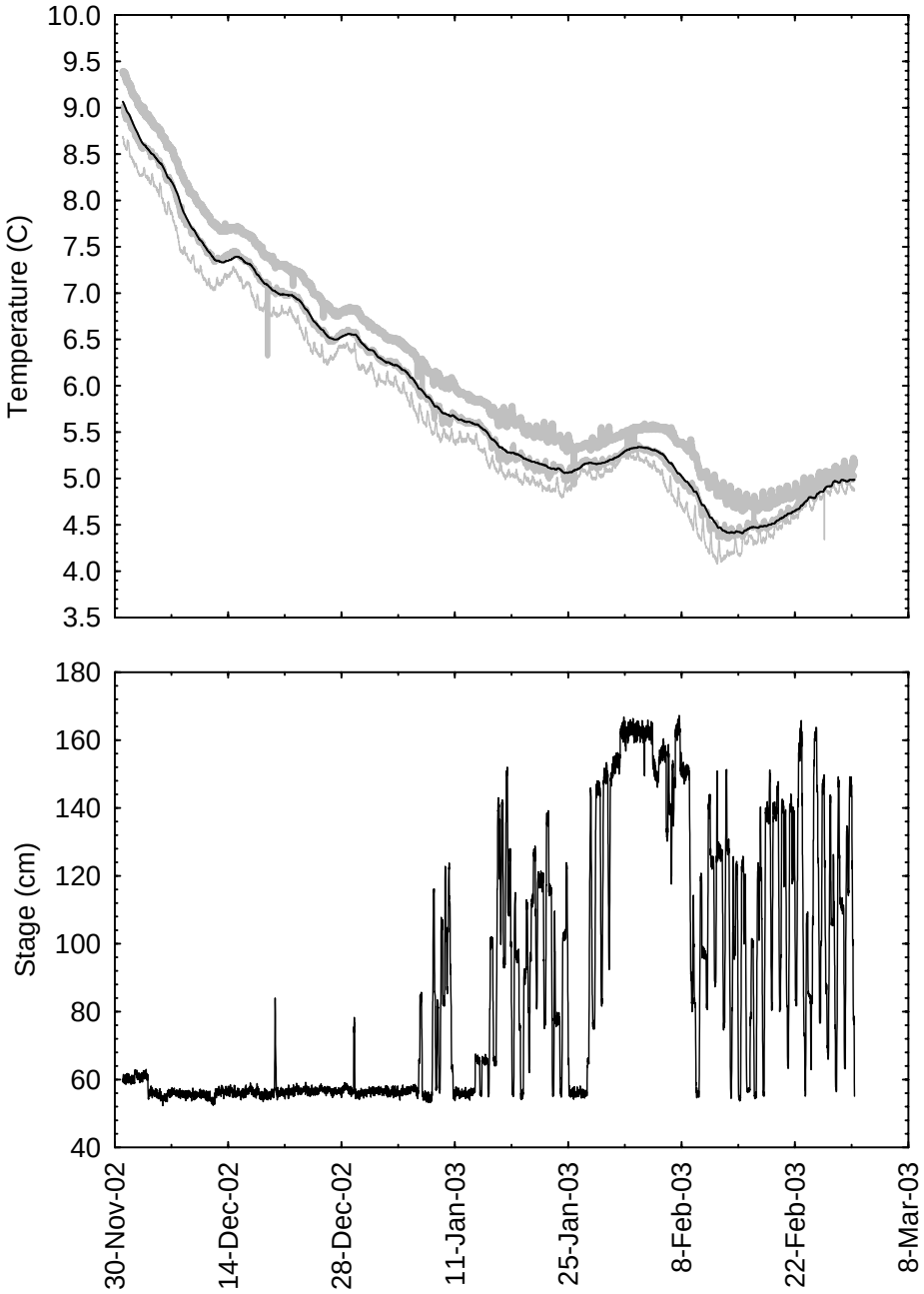

Appendix Figure 41. Time-series summary of observed and modeled water temperature (top panel) and river stage (bottom panel) at site 240.6 during the period 1 December 2002 – 2 March 2003. Water temperatures recorded at 20 min intervals in the river (——), shallow hyporheic zone (——), and deep hyporheic zone (——) are compared with modeled water temperature at 20 min intervals in the shallow hyporheic zone (——).

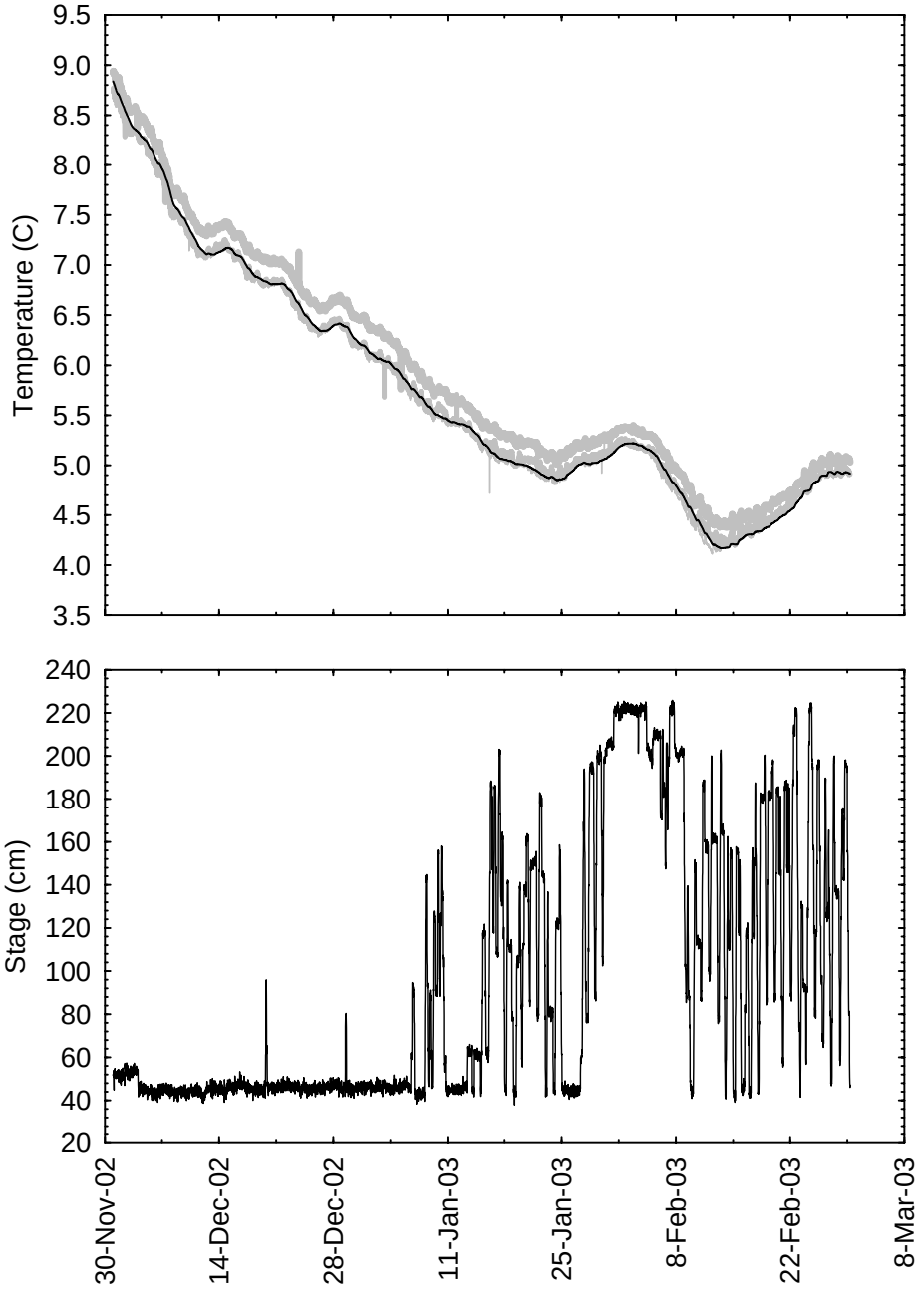

Appendix Figure 42. Time-series summary of observed and modeled water temperature (top panel) and river stage (bottom panel) at site 244.5 during the period 1 December 2002 – 2 March 2003. Water temperatures recorded at 20 min intervals in the river (____), shallow hyporheic zone (▬), and deep hyporheic zone (▬) are compared with modeled water temperature at 20 min intervals in the shallow hyporheic zone (____).

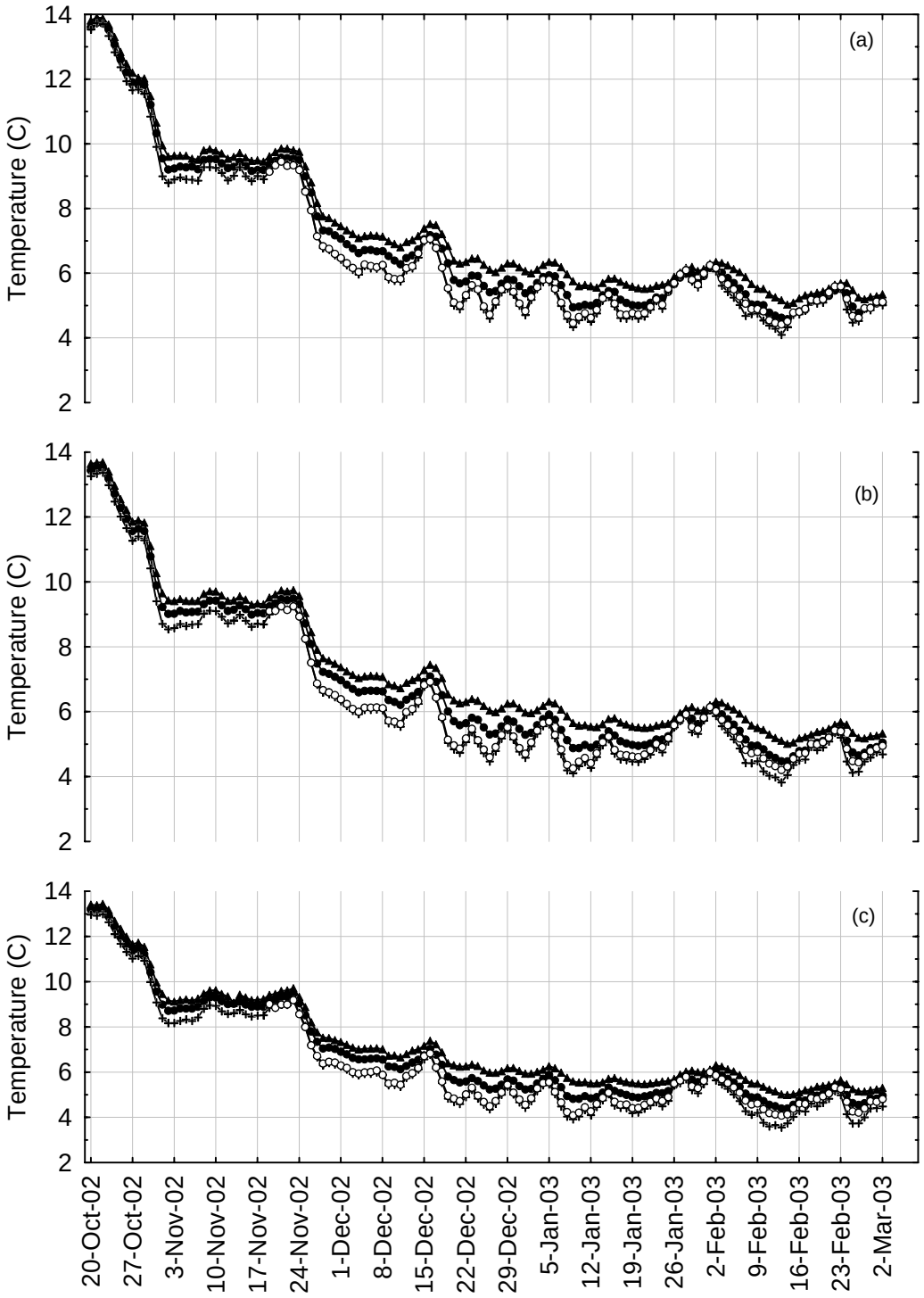

Appendix Figure 43. Daily maximum (a), average (b), and minimum (c) temperature of the river (+), egg pocket (○), shallow hyporheic (●) and deep hyporheic (▲) zones at site 148.5.

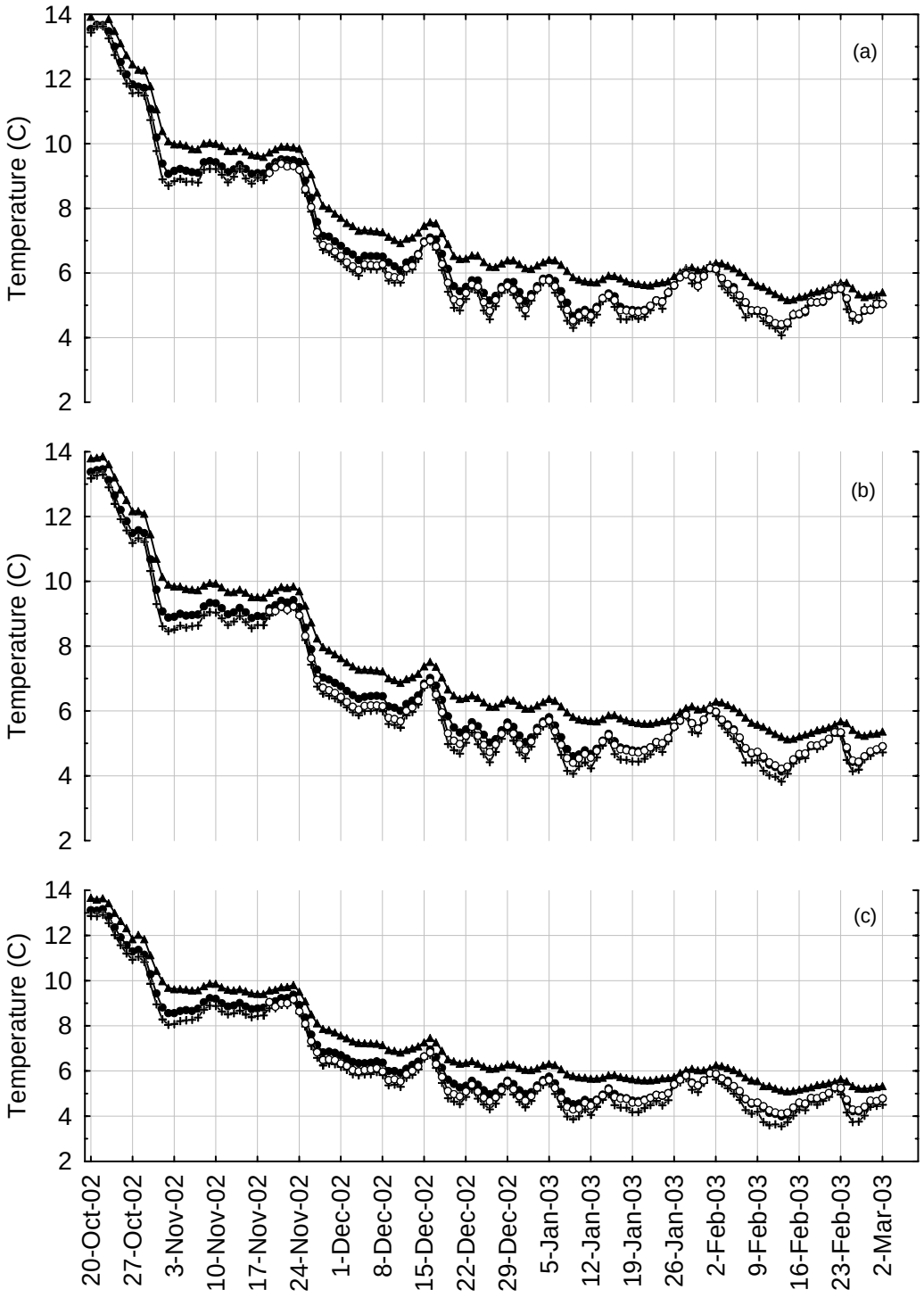

Appendix Figure 44. Daily maximum (a), average (b), and minimum (c) temperature of the river (+), egg pocket (○), shallow hyporheic (●) and deep hyporheic (▲) zones at site 149.2.

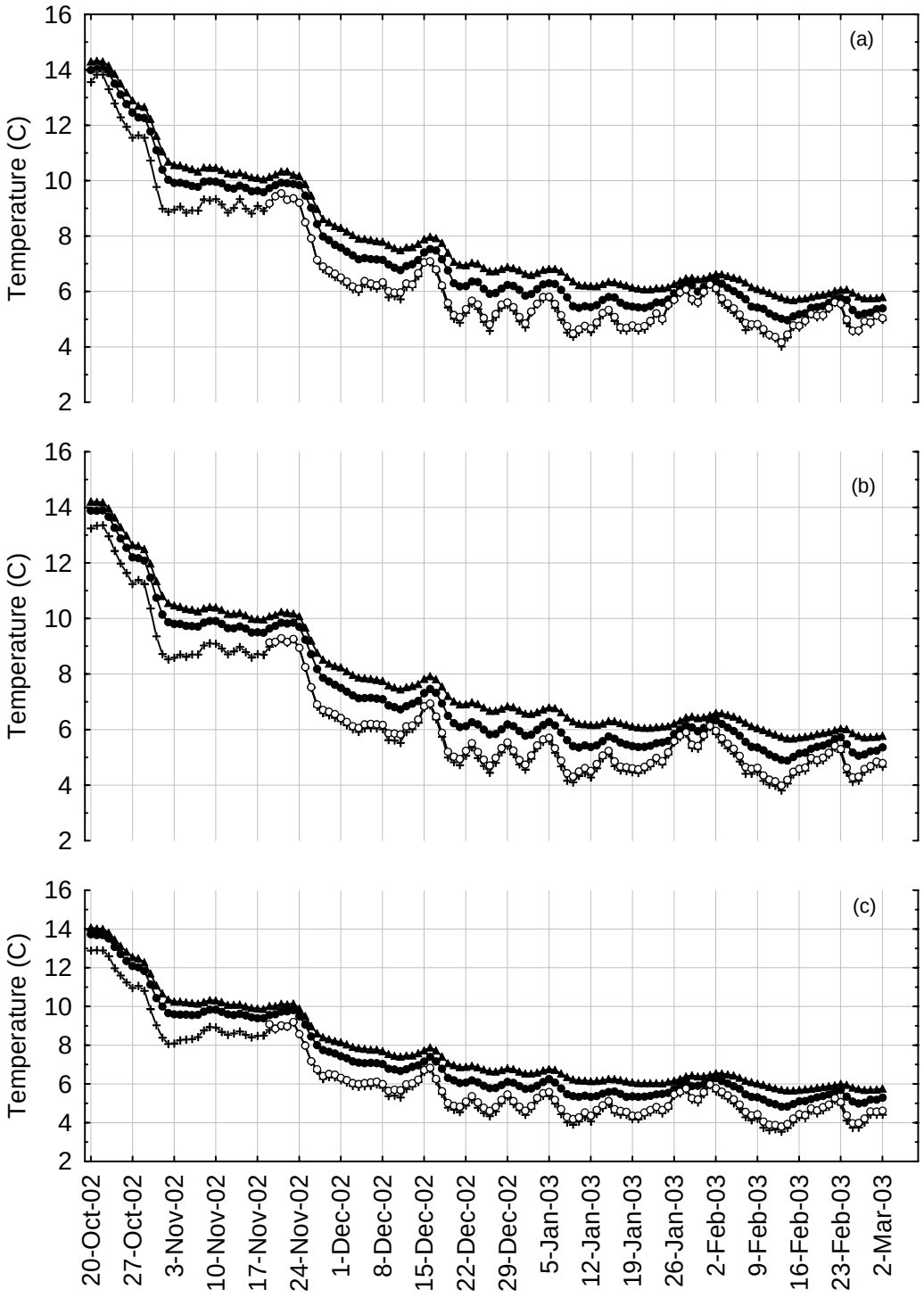

Appendix Figure 45. Daily maximum (a), average (b), and minimum (c) temperature of the river (+), egg pocket (○), shallow hyporheic (●) and deep hyporheic (▲) zones at site 152.3

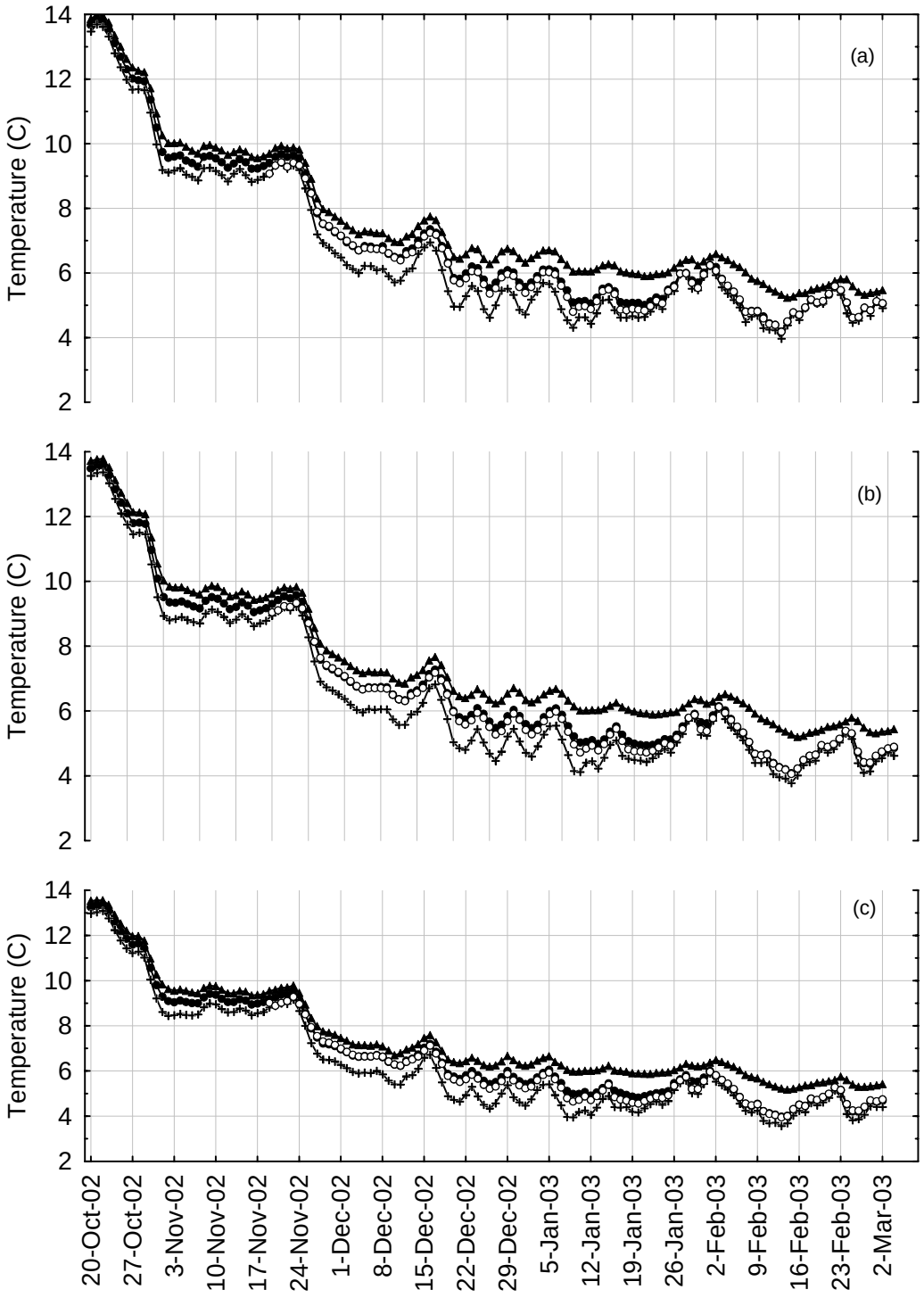

Appendix Figure 46. Daily maximum (a), average (b), and minimum (c) temperature of the river (+), egg pocket (○), shallow hyporheic (●) and deep hyporheic (▲) zones at site 156.8.

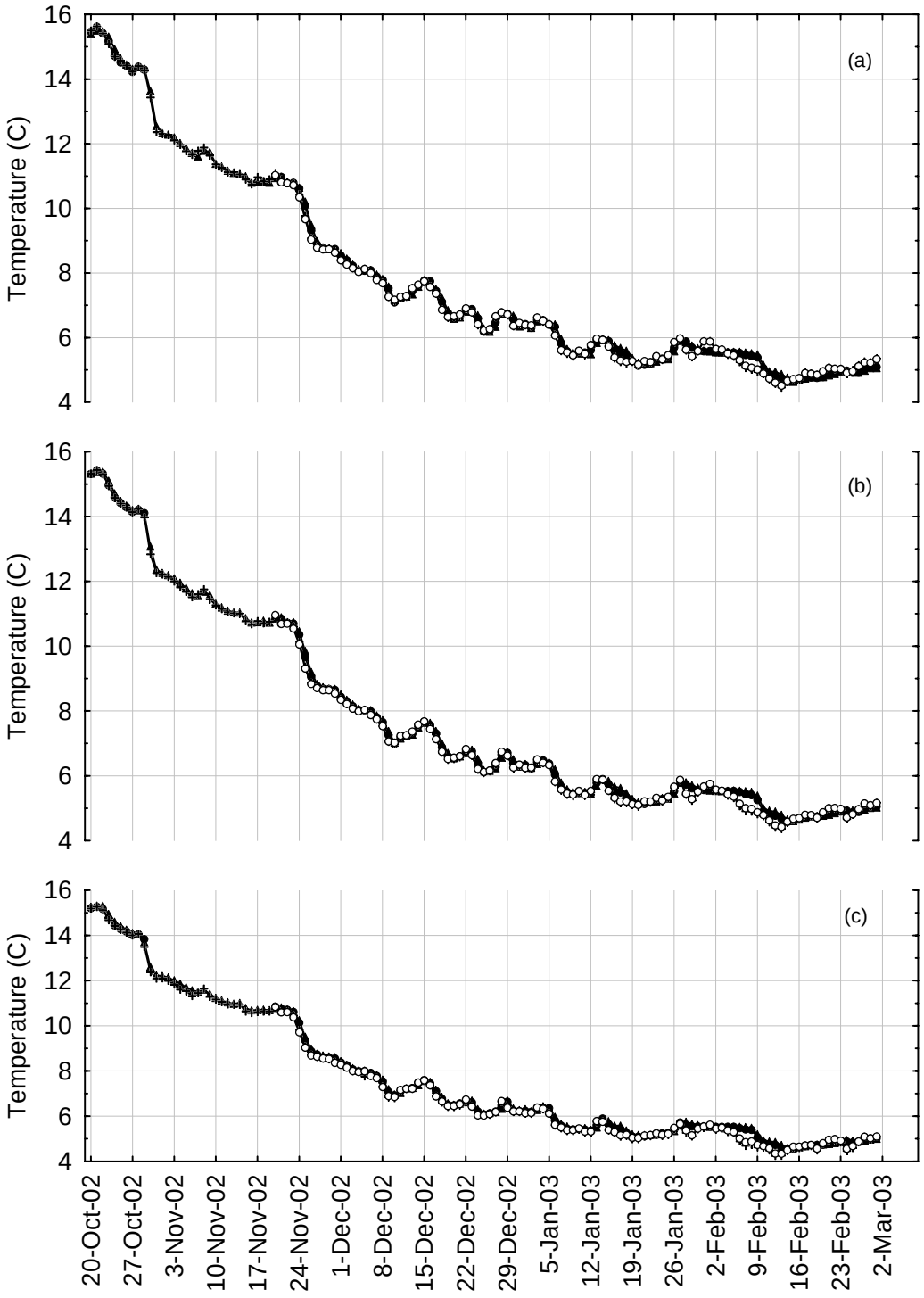

Appendix Figure 47. Daily maximum (a), average (b), and minimum (c) temperature of the river (+), egg pocket (○), shallow hyporheic (●) and deep hyporheic (▲) zones at site 196.0.

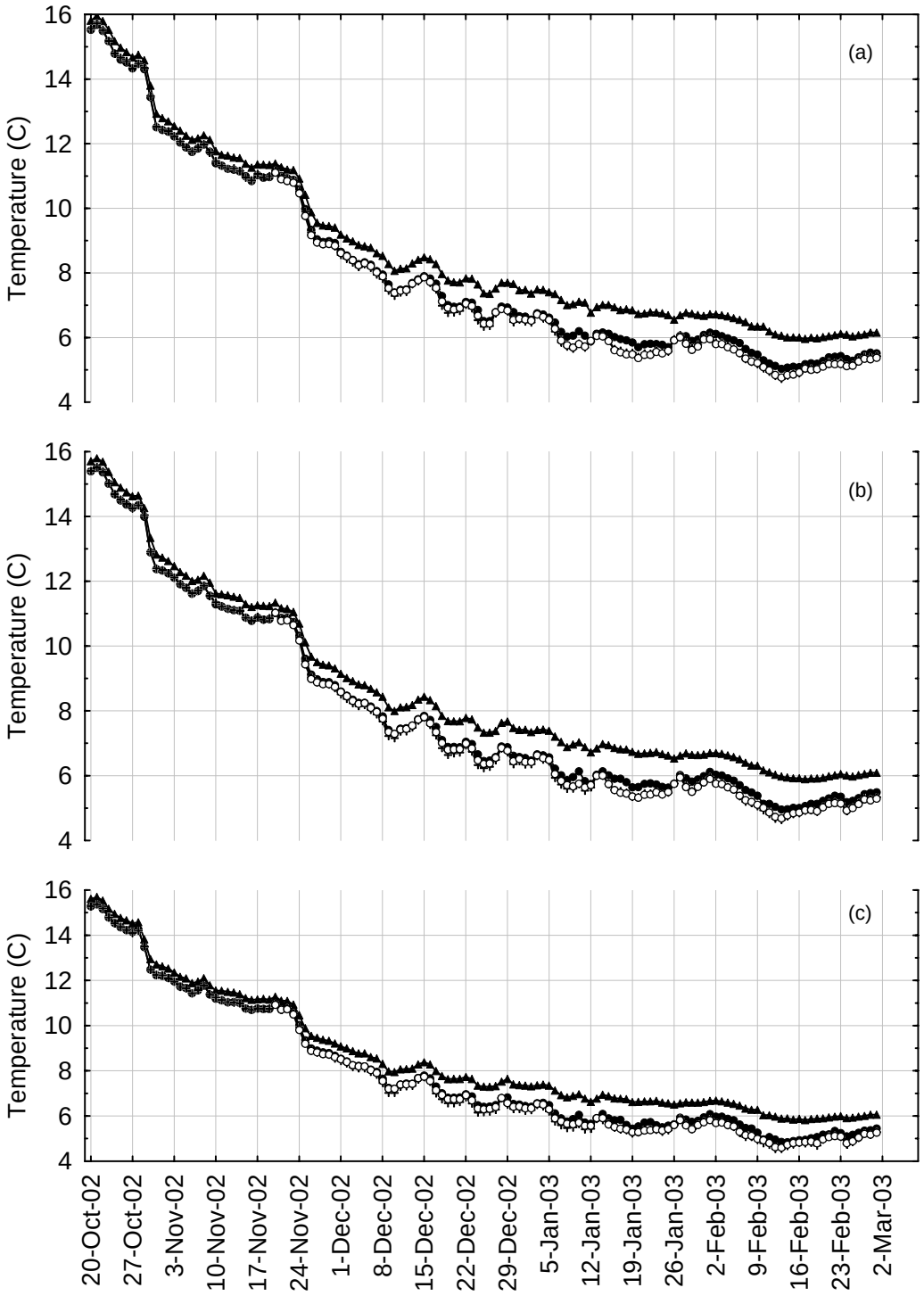

Appendix Figure 48. Daily maximum (a), average (b), and minimum (c) temperature of the river (+), egg pocket (○), shallow hyporheic (●) and deep hyporheic (▲) zones at site 198.2.

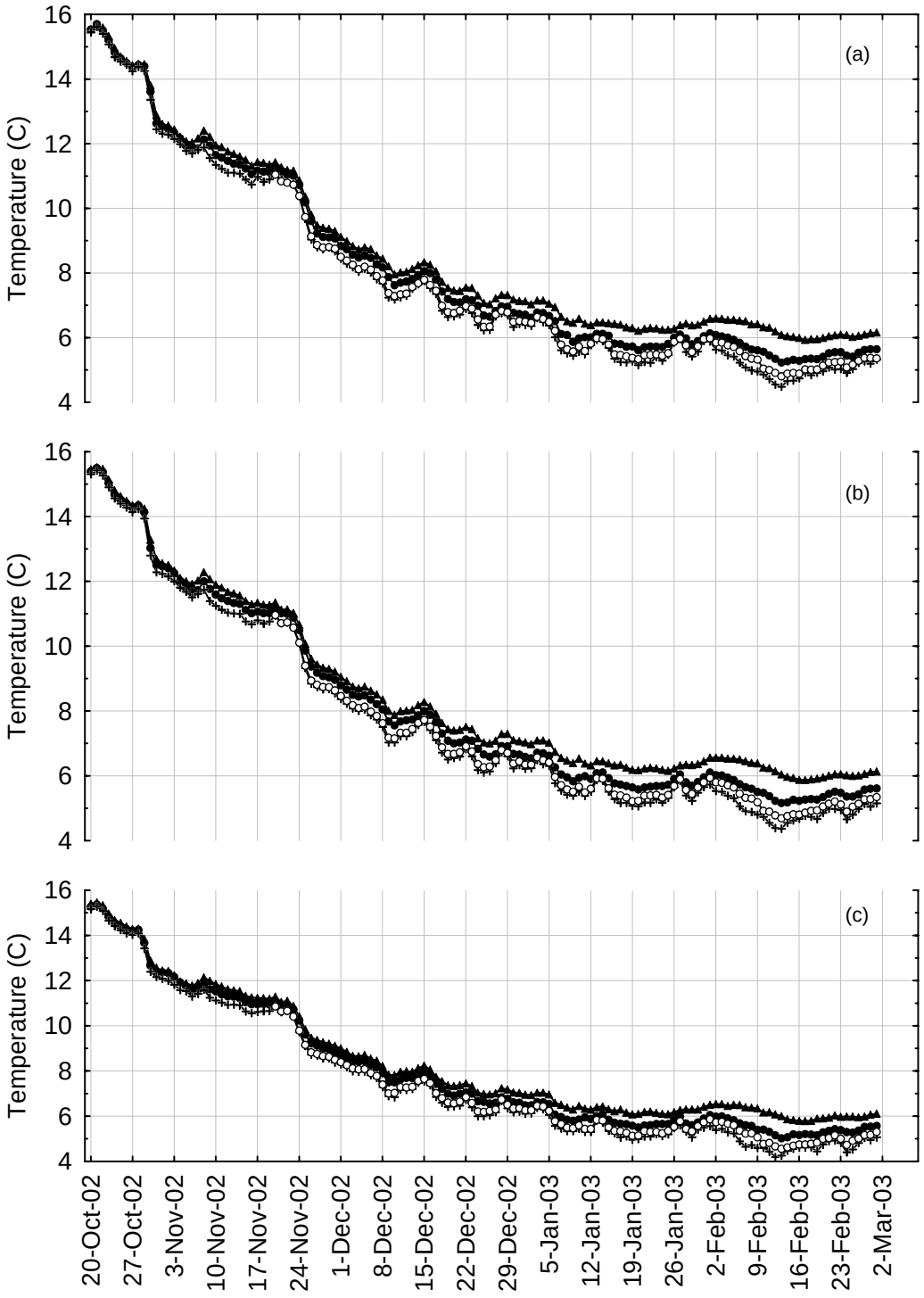

Appendix Figure 49. Daily maximum (a), average (b), and minimum (c) temperature of the river (+), egg pocket (○), shallow hyporheic (●) and deep hyporheic (▲) zones at site 198.8.

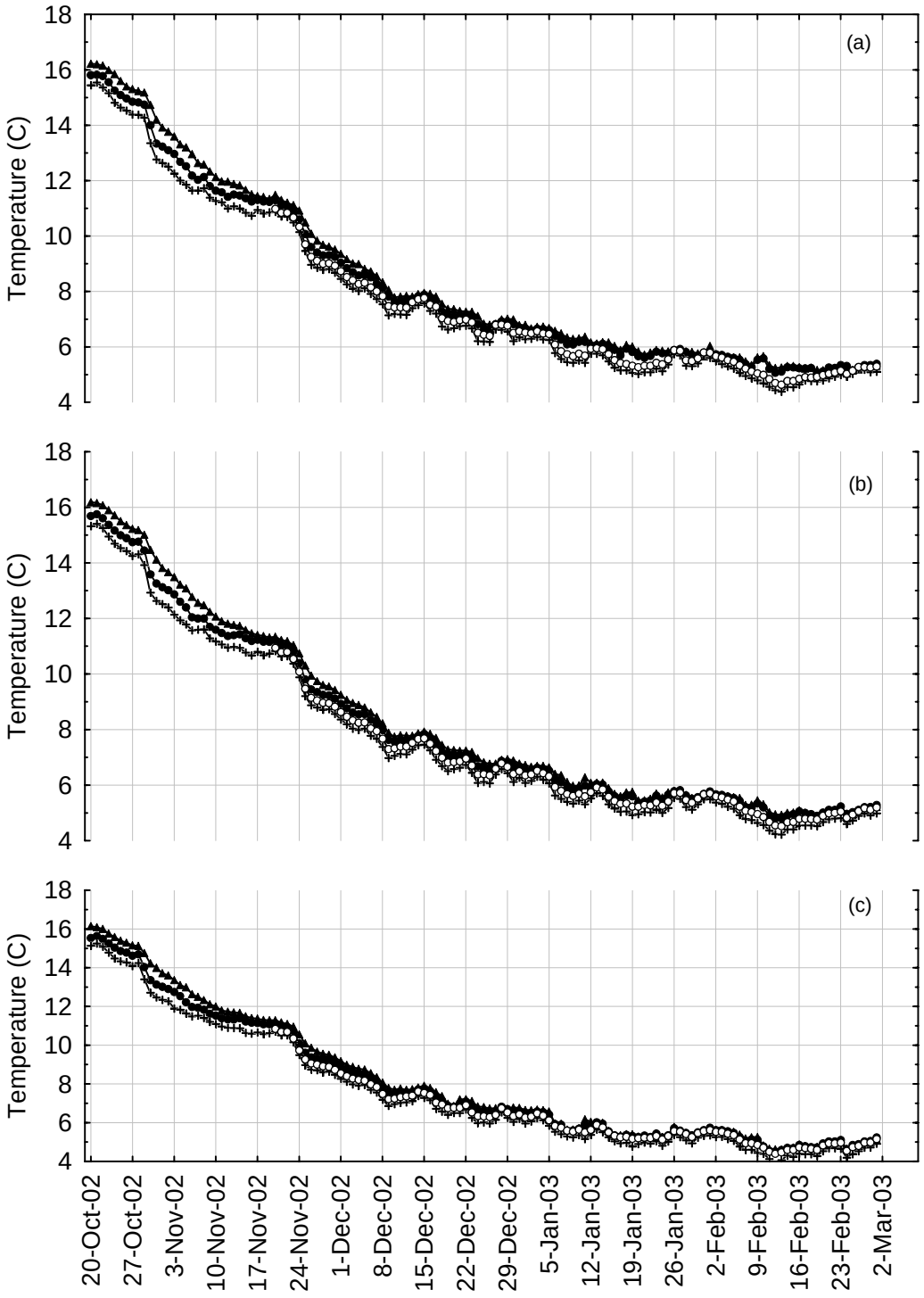

Appendix Figure 50. Daily maximum (a), average (b), and minimum (c) temperature of the river (+), egg pocket (○), shallow hyporheic (●) and deep hyporheic (▲) zones at site 211.9.

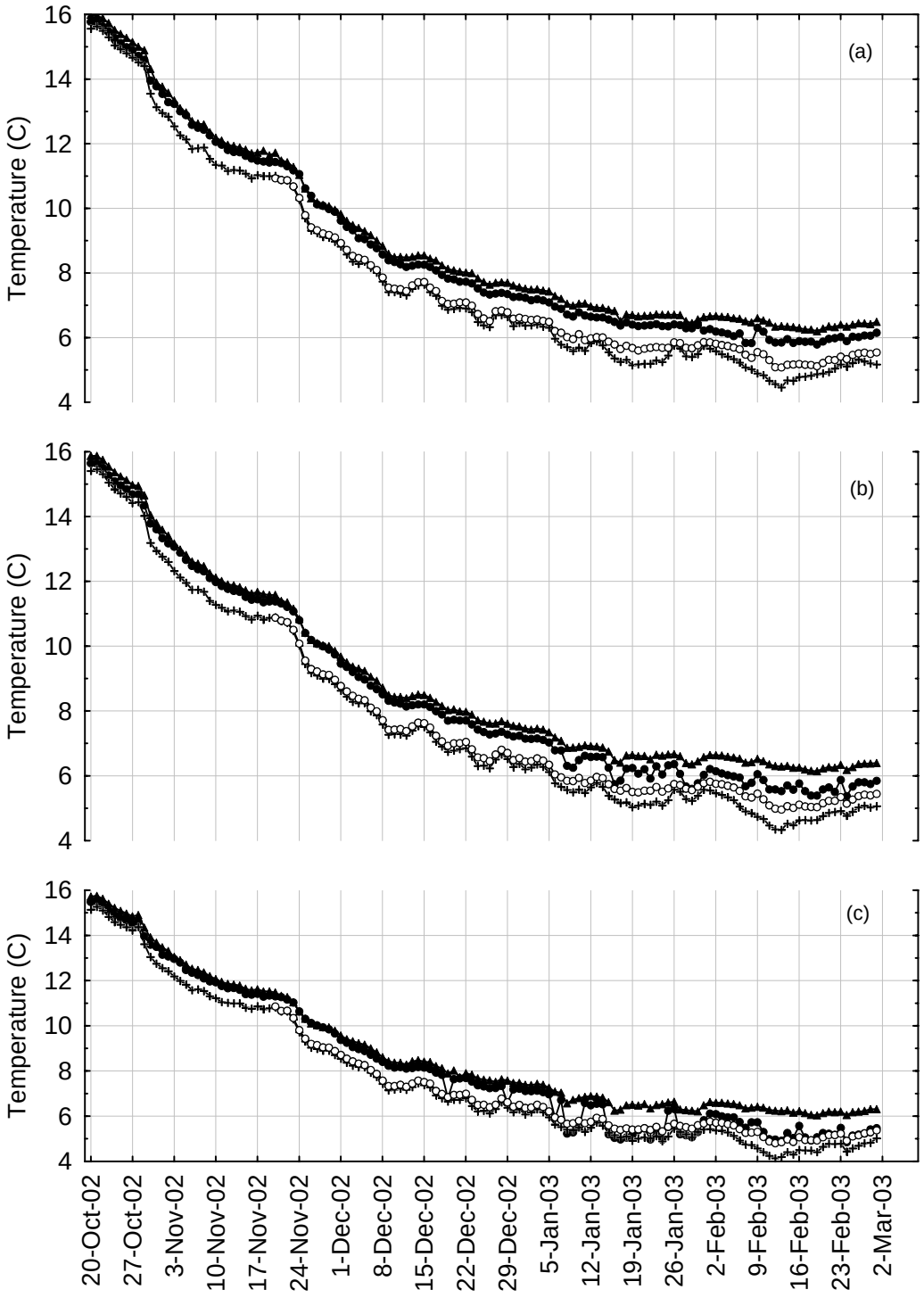

Appendix Figure 51. Daily maximum (a), average (b), and minimum (c) temperature of the river (+), egg pocket (○), shallow hyporheic (●) and deep hyporheic (▲) zones at site 218.7.

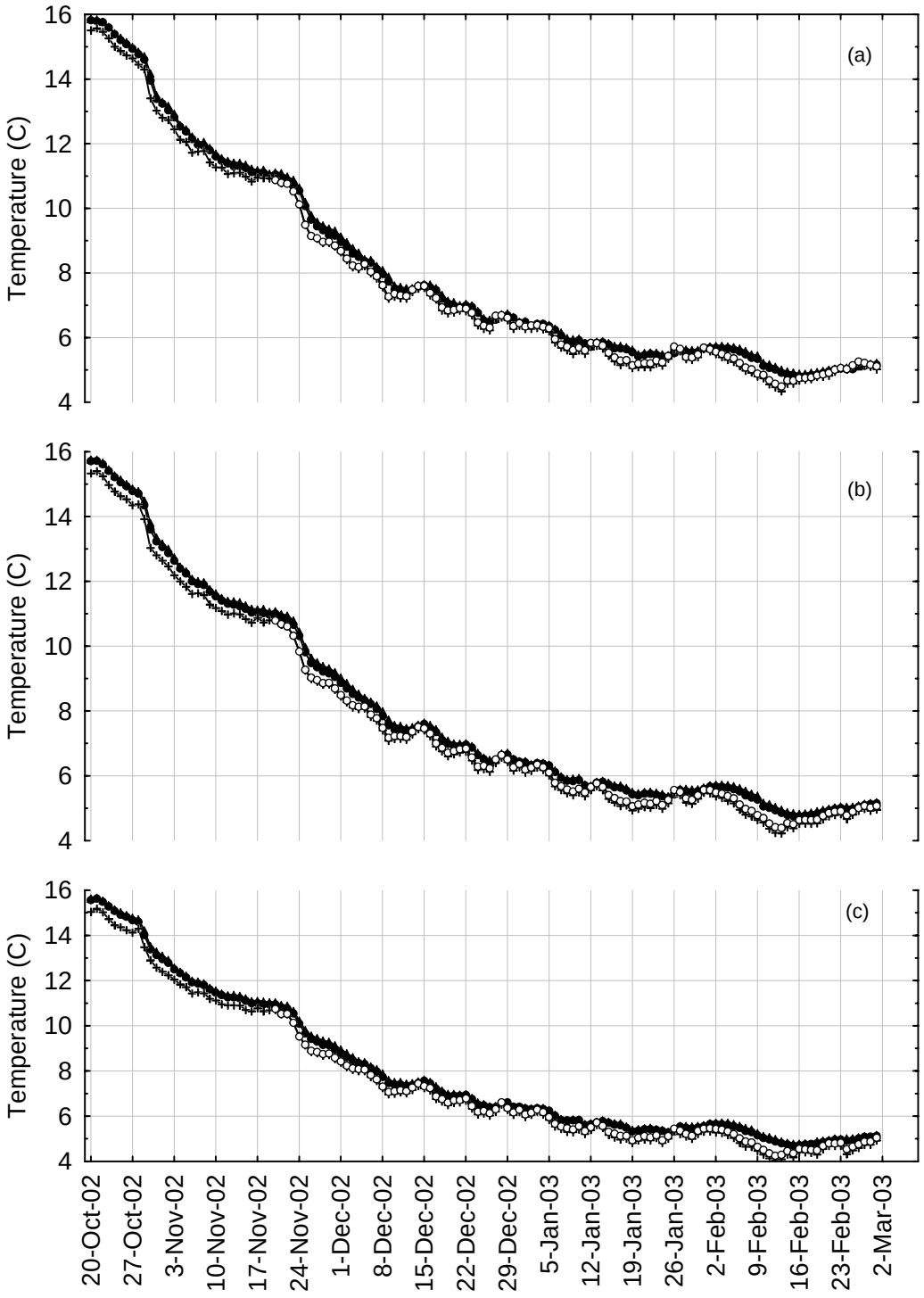

Appendix Figure 52. Daily maximum (a), average (b), and minimum (c) temperature of the river (+), egg pocket (○), shallow hyporheic (●) and deep hyporheic (▲) zones at site 219.3.

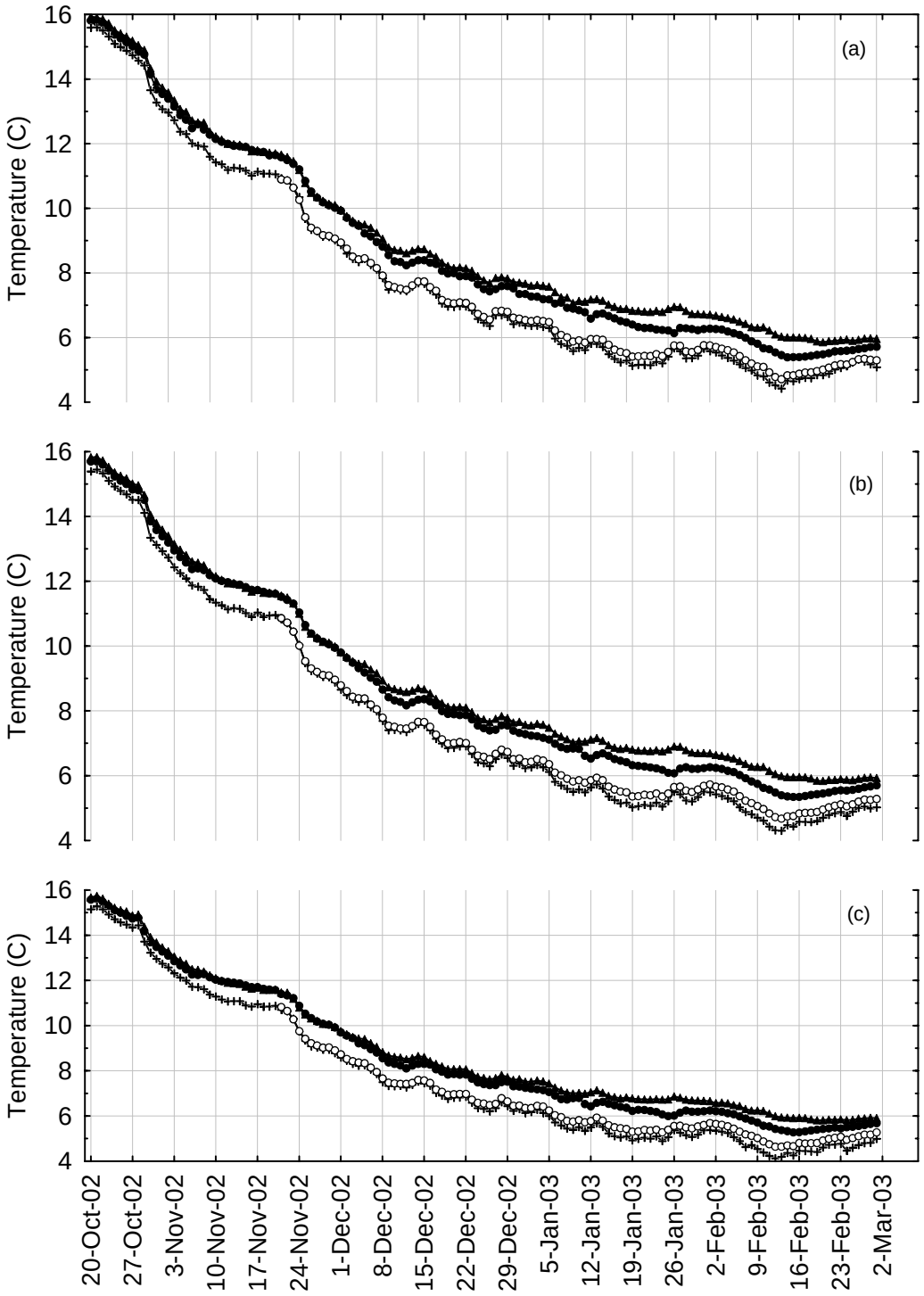

Appendix Figure 53. Daily maximum (a), average (b), and minimum (c) temperature of the river (+), egg pocket (○), shallow hyporheic (●) and deep hyporheic (▲) zones at site 222.7.

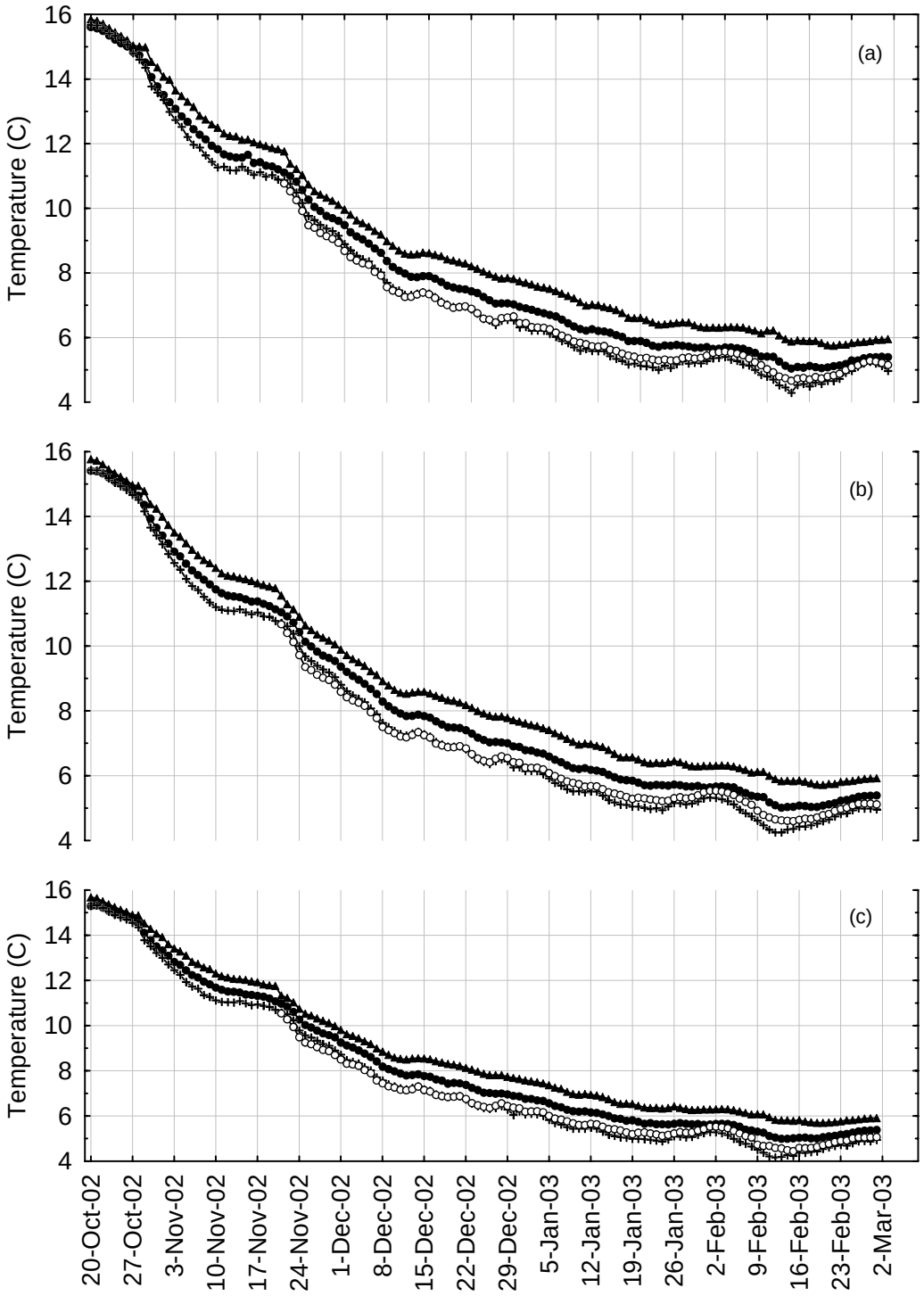

Appendix Figure 54. Daily maximum (a), average (b), and minimum (c) temperature of the river (+), egg pocket (○), shallow hyporheic (●) and deep hyporheic (▲) zones at site 238.6.

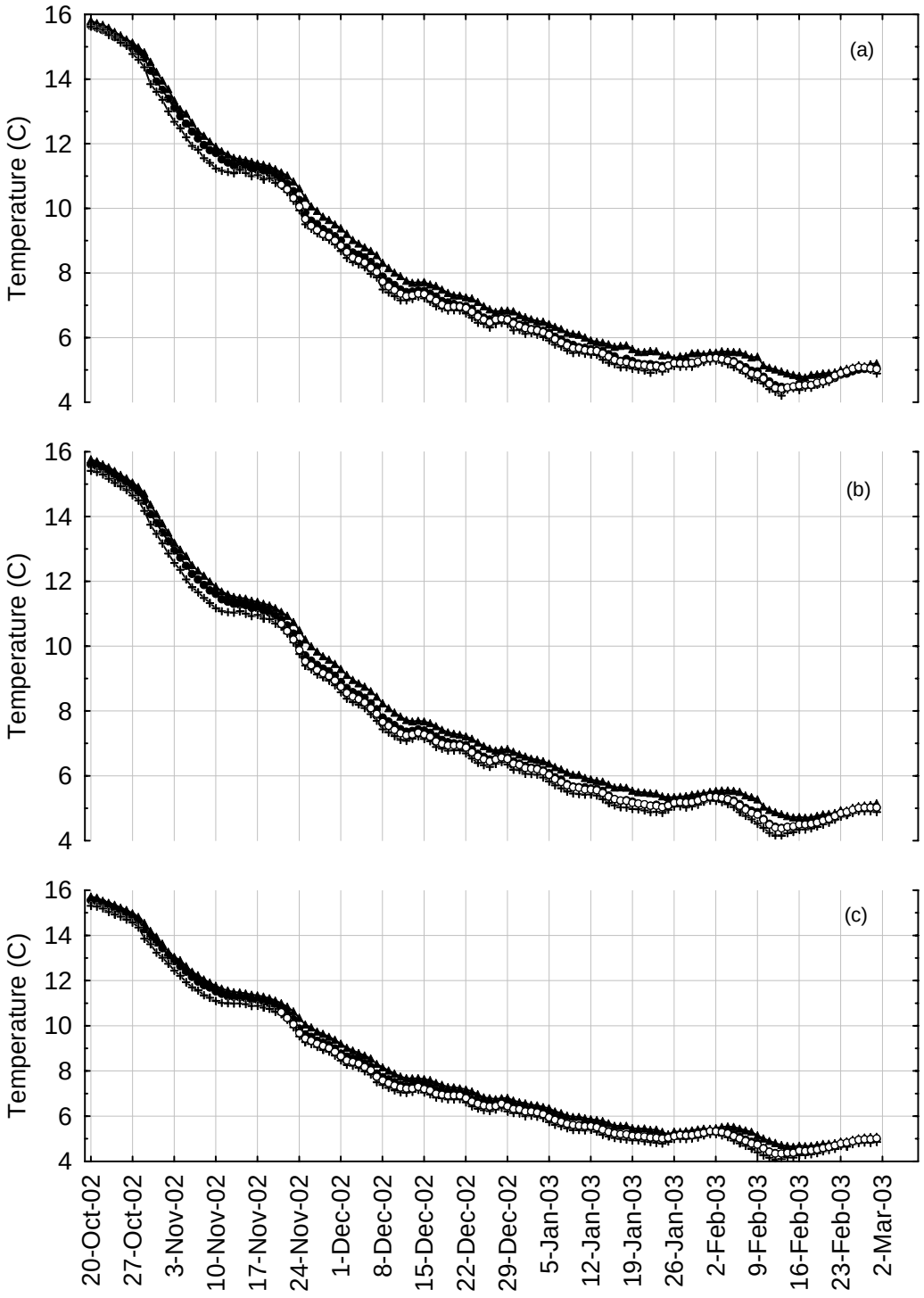

Appendix Figure 55. Daily maximum (a), average (b), and minimum (c) temperature of the river (+), egg pocket (○), shallow hyporheic (●) and deep hyporheic (▲) zones at site 240.6.

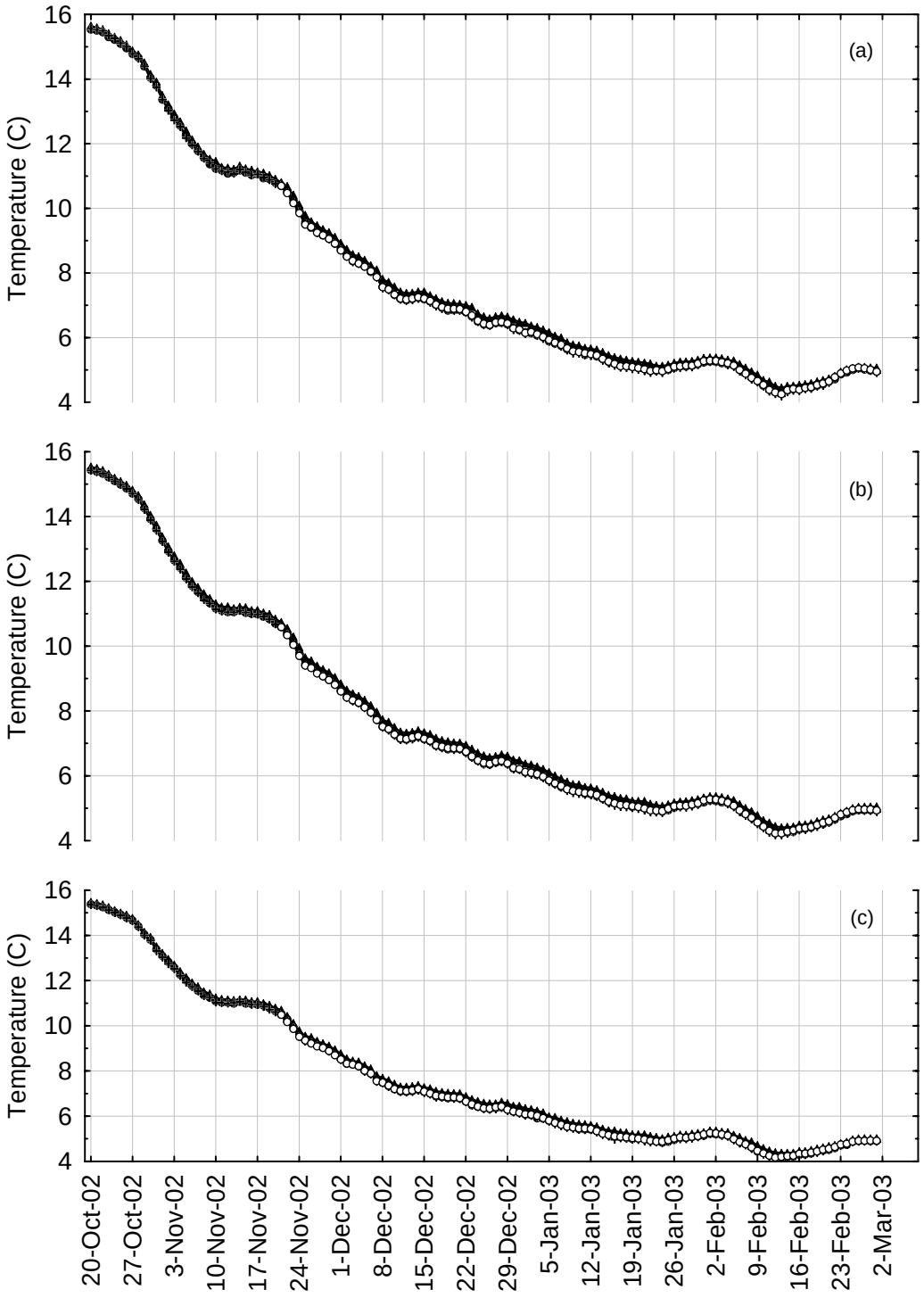

Appendix Figure 56. Daily maximum (a), average (b), and minimum (c) temperature of the river (+), egg pocket (○), shallow hyporheic (●) and deep hyporheic (▲) zones at site 244.5.

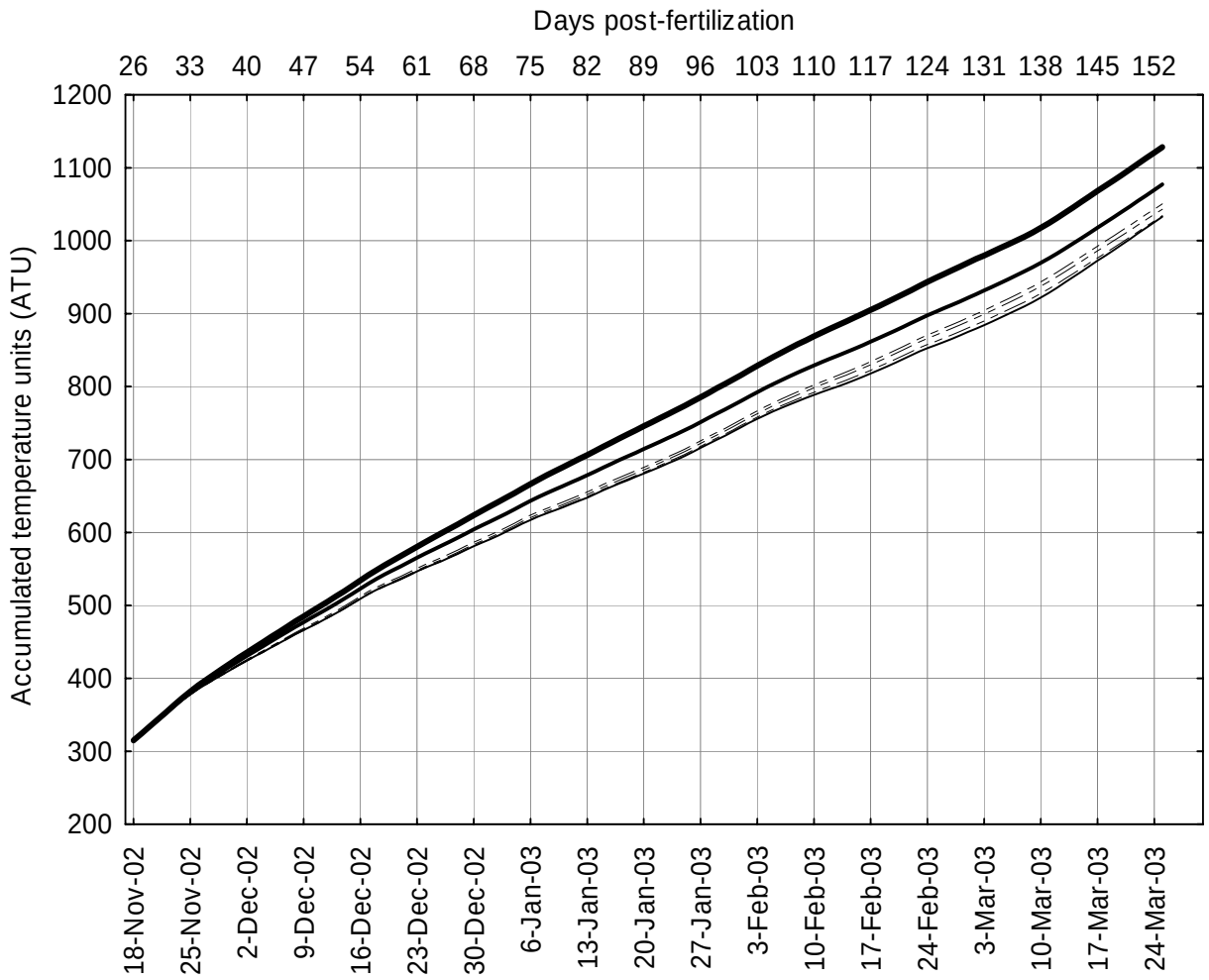

Appendix Figure 57. Accumulated temperature units (ATU) at site 148.5 based on temperatures from the river (_____), egg pockets (_ . _ . .), shallow hyporheic (▬▬), and deep hyporheic (▬▬) zones.

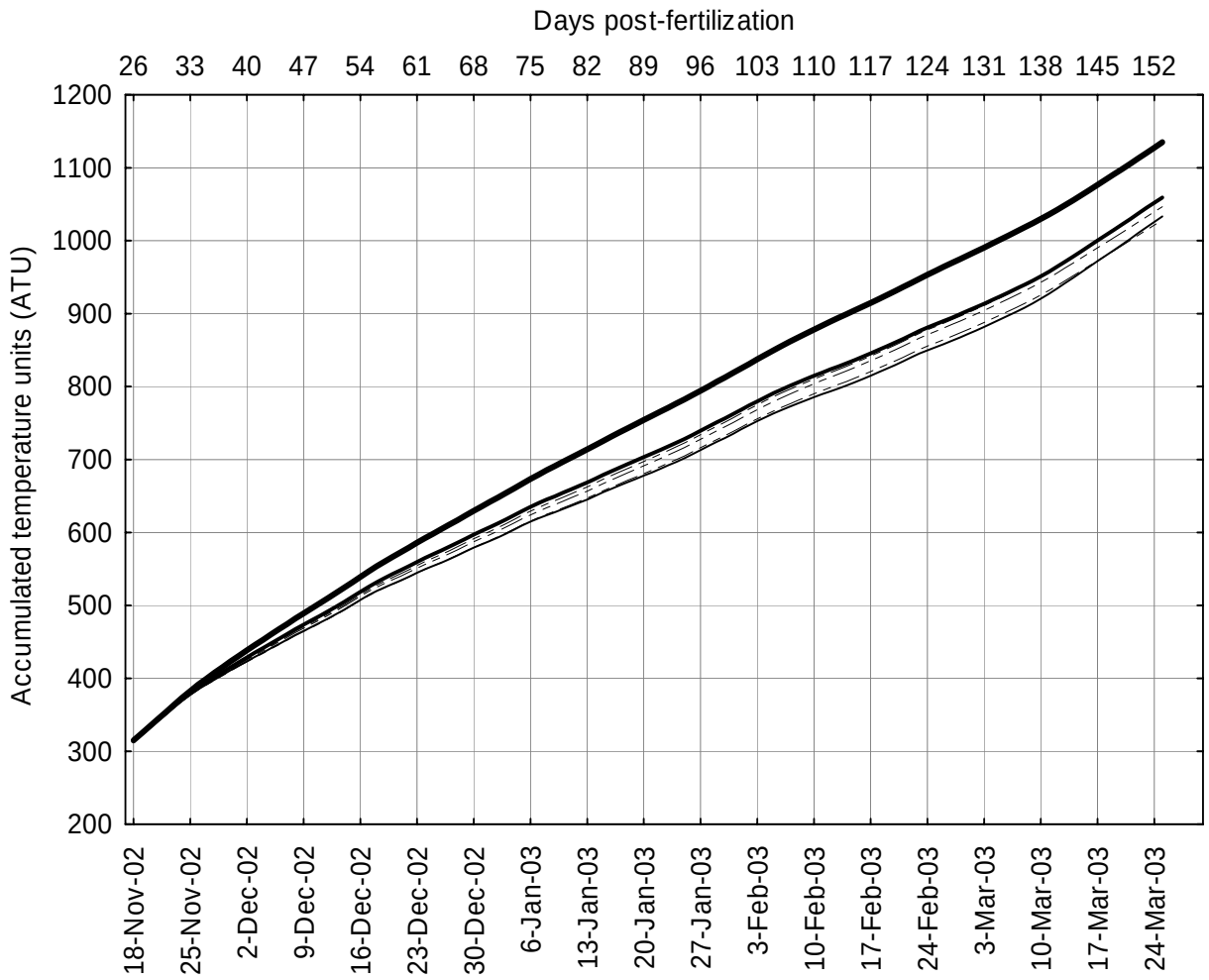

Appendix Figure 58. Accumulated temperature units (ATU) at site 149.2 based on temperatures from the river (_____), egg pockets (_ . _ . .), shallow hyporheic (▬▬), and deep hyporheic (▬▬) zones.

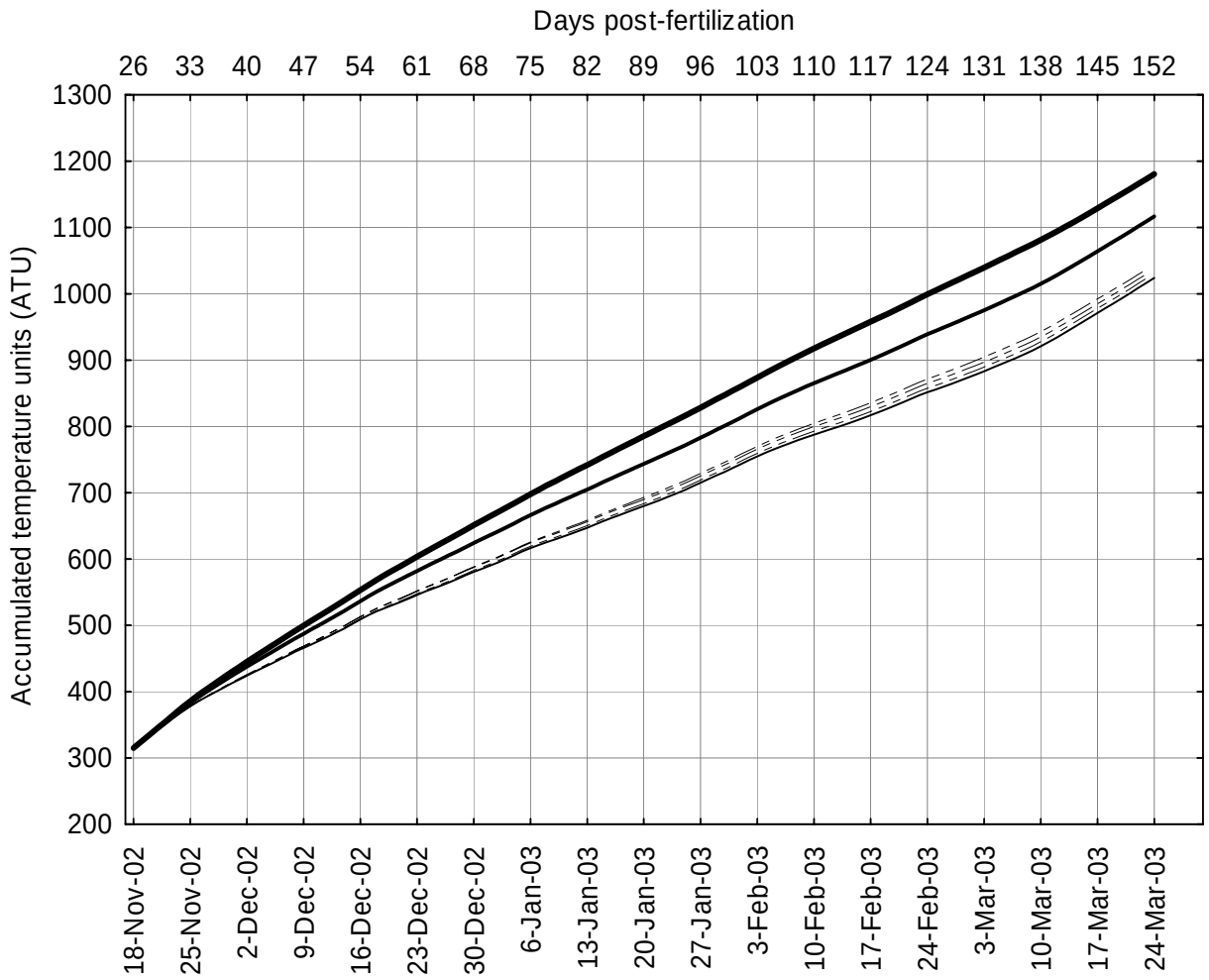

Appendix Figure 59. Accumulated temperature units (ATU) at site 152.3 based on temperatures from the river (_____), egg pockets (_ . _ . .), shallow hyporheic (▬▬), and deep hyporheic (▬▬) zones.

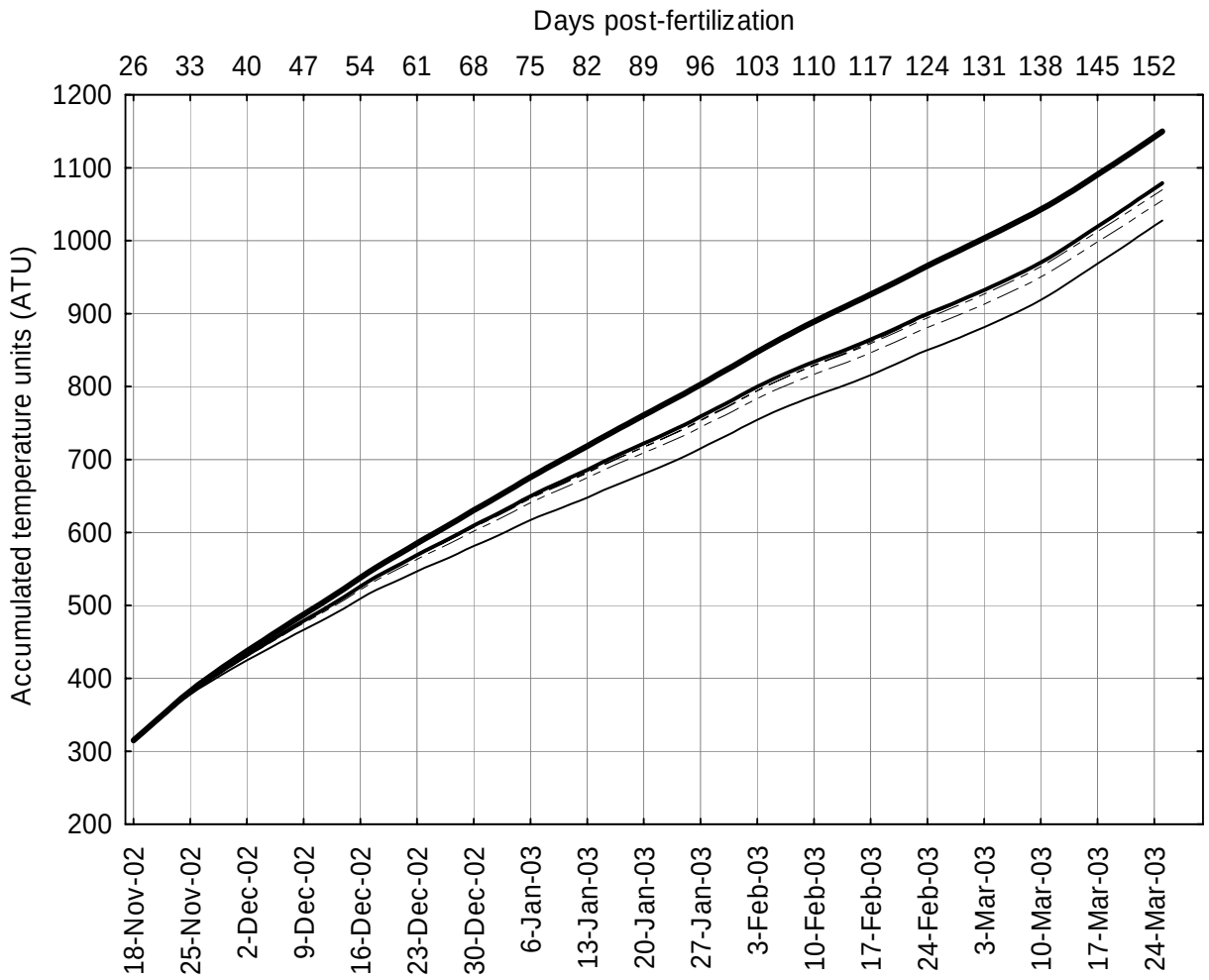

Appendix Figure 60. Accumulated temperature units (ATU) at site 156.8 based on temperatures from the river (——), egg pockets (– – –), shallow hyporheic (——), and deep hyporheic (▬▬) zones.

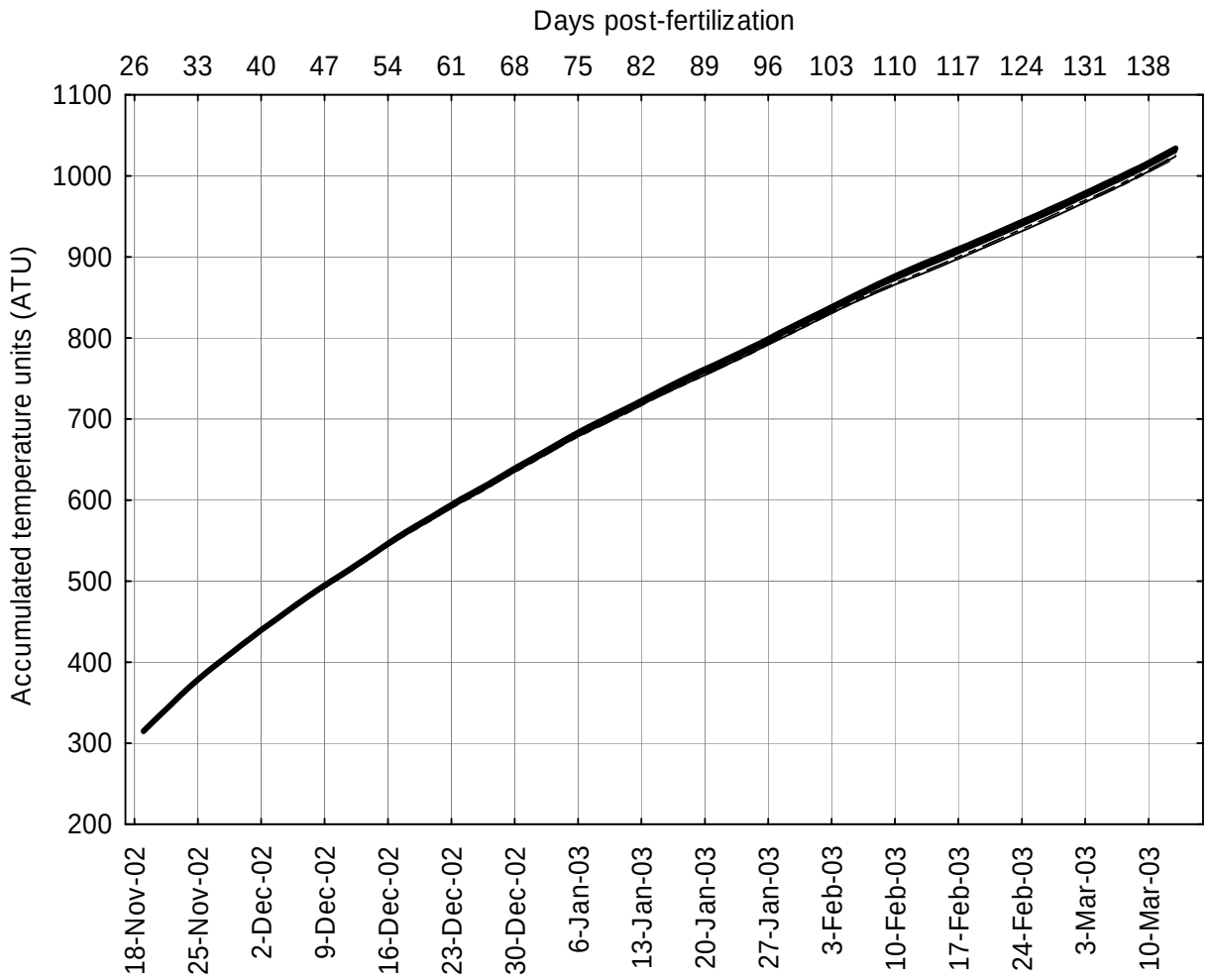

Appendix Figure 61. Accumulated temperature units (ATU) at site 196.0 based on temperatures from the river (_____), egg pockets (_ . _ . .), shallow hyporheic (_____), and deep hyporheic (_____) zones.

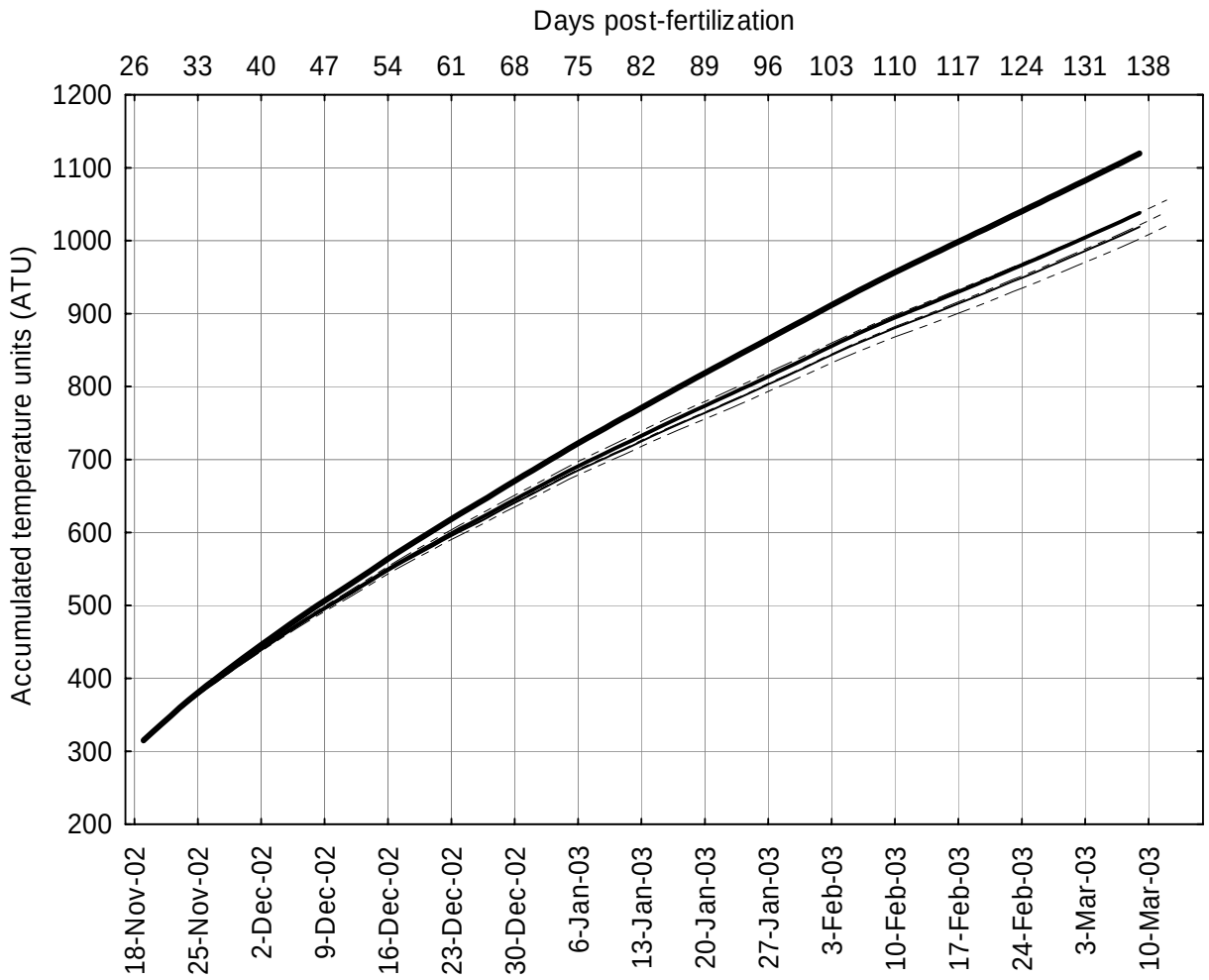

Appendix Figure 62. Accumulated temperature units (ATU) at site 198.2 based on temperatures from the river (_____), egg pockets (_ . _ . .), shallow hyporheic (▬▬), and deep hyporheic (▬▬) zones.

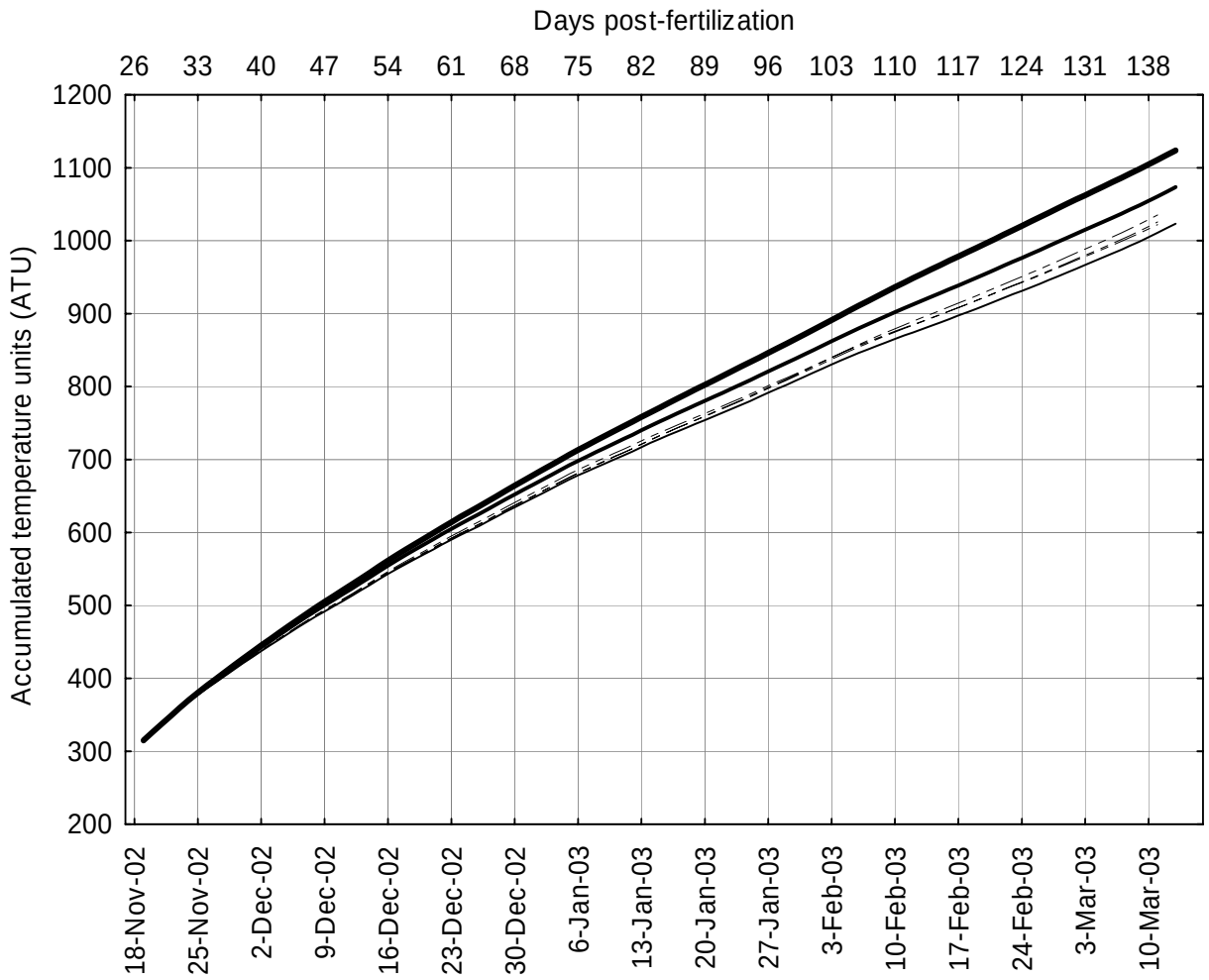

Appendix Figure 63. Accumulated temperature units (ATU) at site 198.8 based on temperatures from the river (_____), egg pockets (_ . _ . .), shallow hyporheic (_____), and deep hyporheic (▬▬) zones.

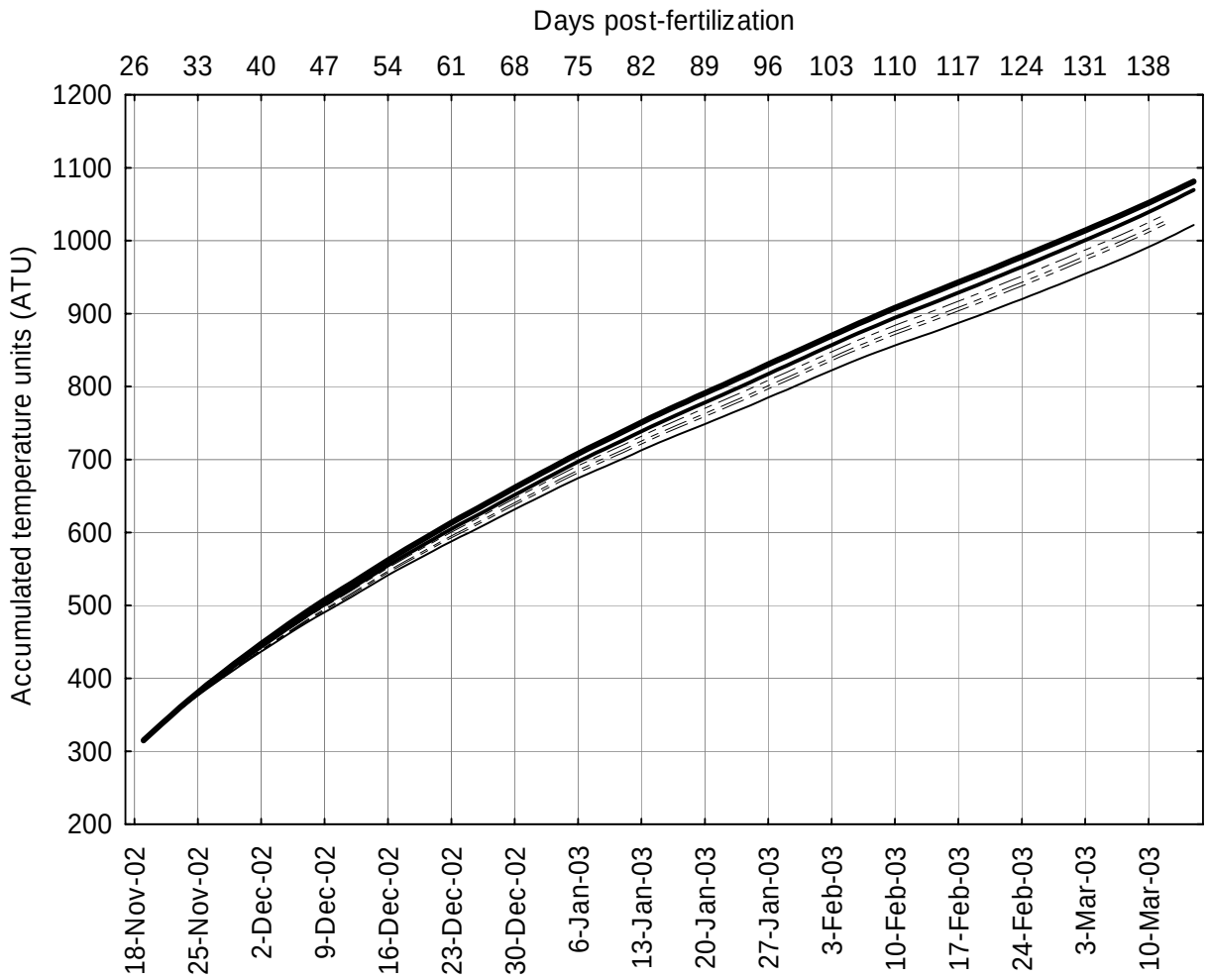

Appendix Figure 64. Accumulated temperature units (ATU) at site 211.9 based on temperatures from the river (_____), egg pockets (_ . _ . .), shallow hyporheic (_____), and deep hyporheic (▬▬) zones.

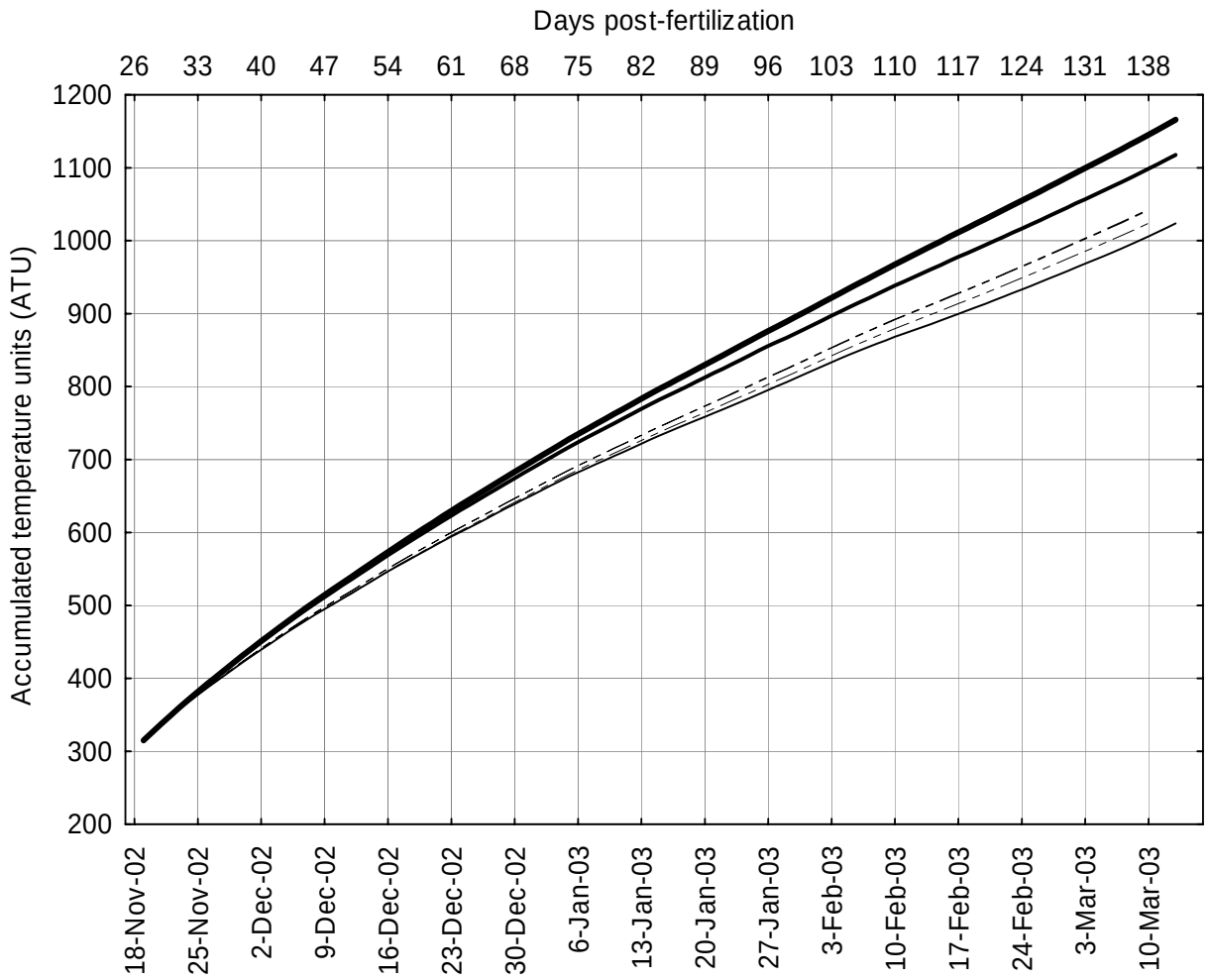

Appendix Figure 65. Accumulated temperature units (ATU) at site 218.7 based on temperatures from the river (_____), egg pockets (_ . _ . .), shallow hyporheic (_____), and deep hyporheic (▬▬) zones.

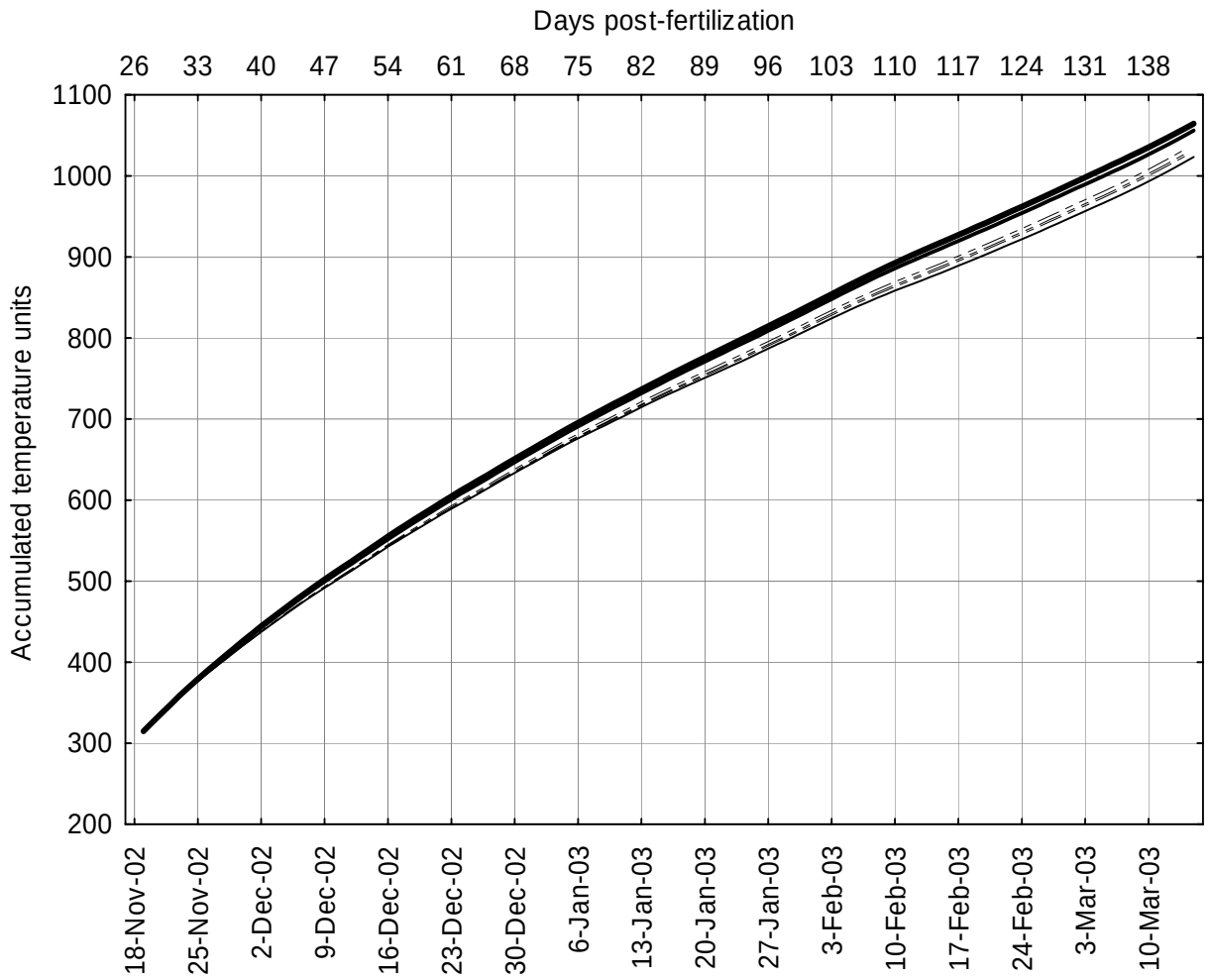

Appendix Figure 66. Accumulated temperature units (ATU) at site 219.3 based on temperatures from the river (_____), egg pockets (_ . _ . .), shallow hyporheic (_____), and deep hyporheic (▬▬) zones.

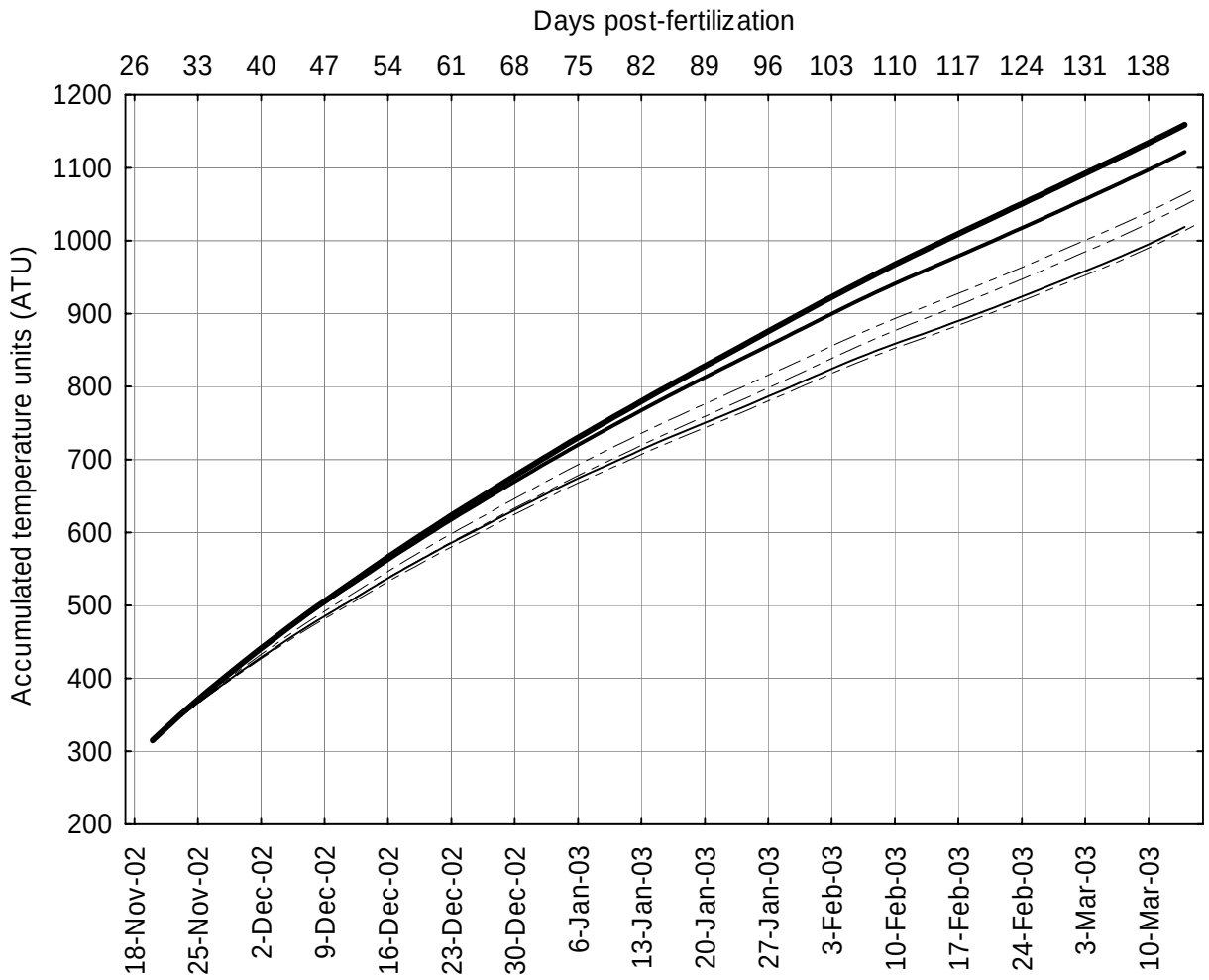

Appendix Figure 67. Accumulated temperature units (ATU) at site 222.7 based on temperatures from the river (_____), egg pockets (_ . _ . .), shallow hyporheic (▬▬), and deep hyporheic (▬▬) zones.

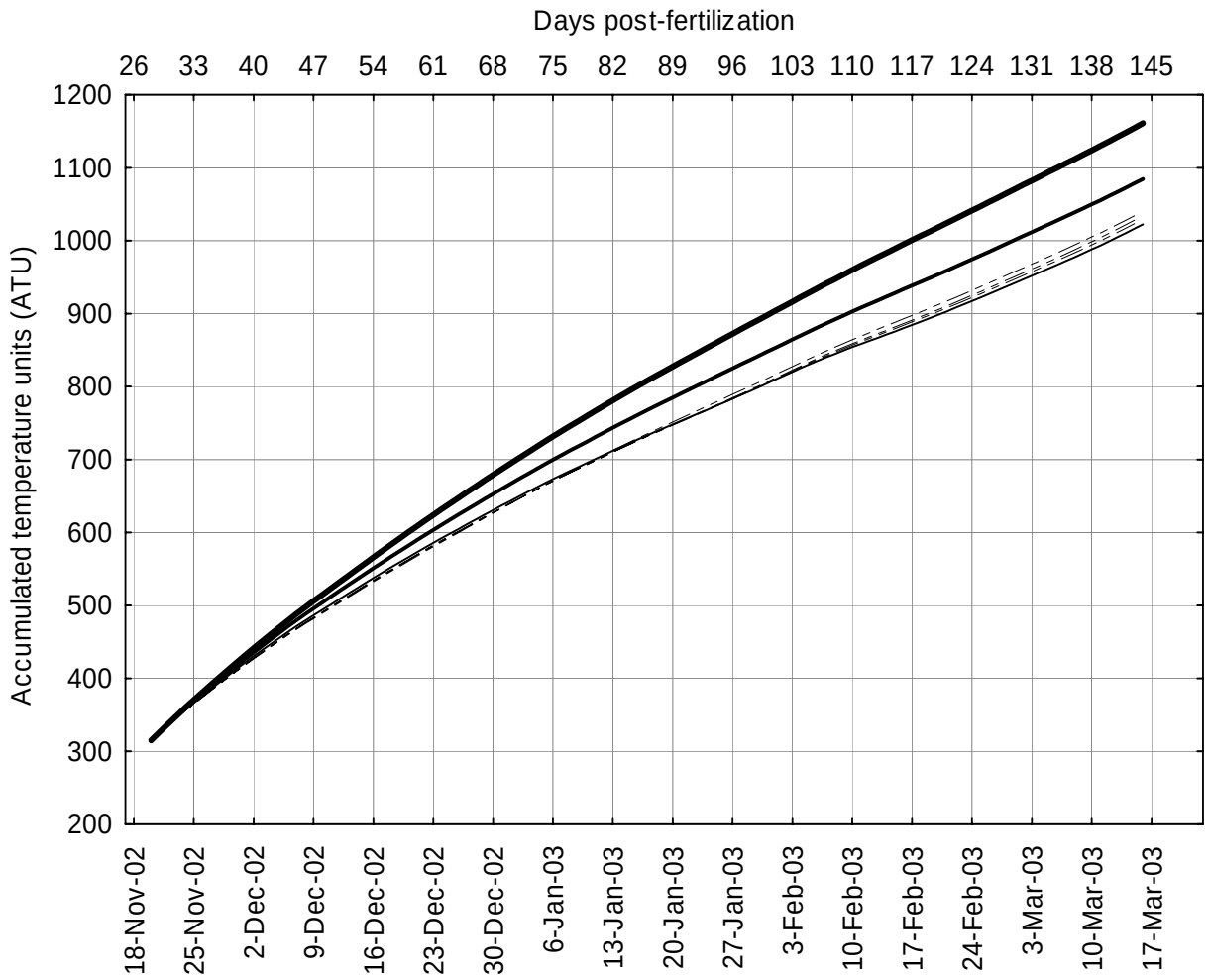

Appendix Figure 68. Accumulated temperature units (ATU) at site 238.6 based on temperatures from the river (_____), egg pockets (_ . _ . .), shallow hyporheic (▬▬), and deep hyporheic (▬▬) zones.

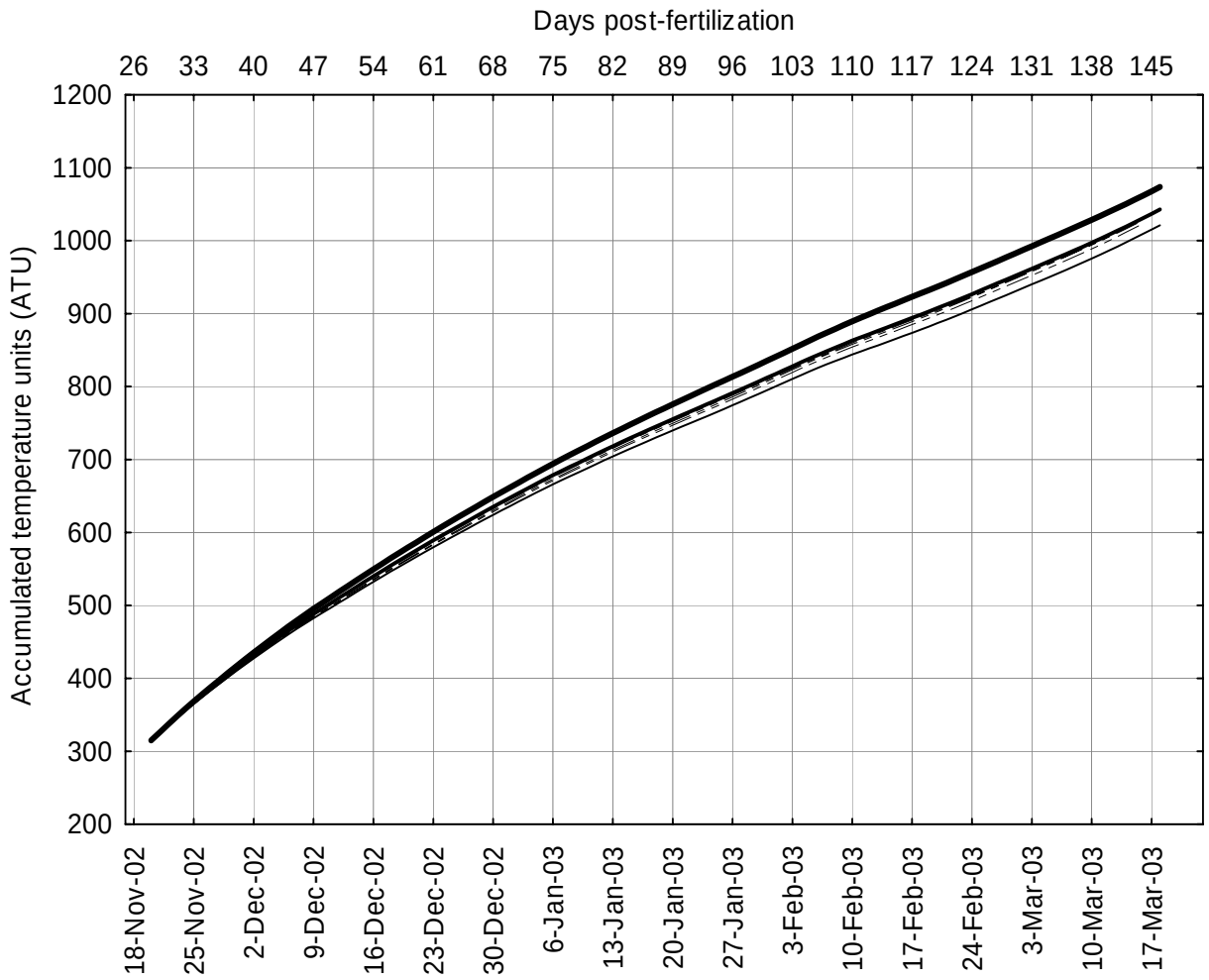

Appendix Figure 69. Accumulated temperature units (ATU) at site 240.6 based on temperatures from the river (_____), egg pockets (_ . _ . .), shallow hyporheic (▬▬), and deep hyporheic (▬▬) zones.

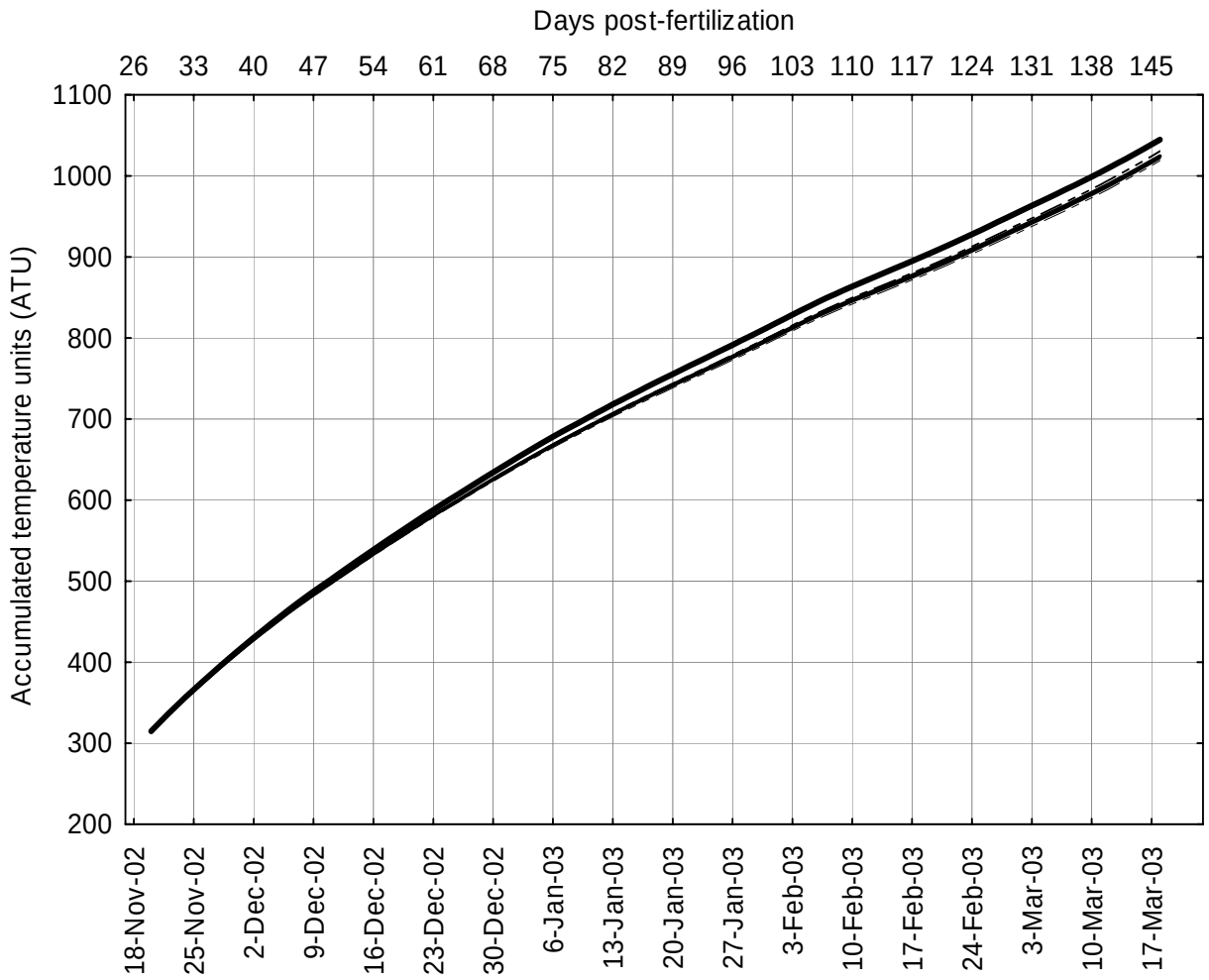

Appendix Figure 70. Accumulated temperature units (ATU) at site 244.5 based on temperatures from the river (——), egg pockets (– . – . .), shallow hyporheic (——), and deep hyporheic (▬▬) zones.

Distribution

No. of Copies

OFFSITE

Jim Chandler (5)
Idaho Power Company
1221 Idaho Street
Boise, ID 83707

Bill Maslen (5)
Bonneville Power Administration
KEWR-4
P.O. Box 3621
Portland, OR 97208-3621

Tracy Noice (5)
Bonneville Power Administration
KEWU-4
P.O. Box 3621
Portland, OR 97208-3621

No. of Copies

56 **Pacific Northwest National Laboratory**

C.S. Abernethy	K6-85
E. V. Arntzen	K6-85
C. A. Brandt	K6-85
D. D. Dauble (40)	K6-84
D. R. Geist	K6-85
T. P. Hanrahan (5)	K6-85
Information Release Office (7)	K1-06